



# D-instantons and String Field Theory

## Citation

Agmon, Nathan Benjamin. 2023. D-instantons and String Field Theory. Doctoral dissertation, Harvard University Graduate School of Arts and Sciences.

## Permanent link

<https://nrs.harvard.edu/URN-3:HUL.INSTREPOS:37375763>

## Terms of Use

This article was downloaded from Harvard University's DASH repository, and is made available under the terms and conditions applicable to Other Posted Material, as set forth at <http://nrs.harvard.edu/urn-3:HUL.InstRepos:dash.current.terms-of-use#LAA>

## Share Your Story

The Harvard community has made this article openly available.  
Please share how this access benefits you. [Submit a story](#).

[Accessibility](#)

HARVARD UNIVERSITY  
Graduate School of Arts and Sciences



DISSERTATION ACCEPTANCE CERTIFICATE

The undersigned, appointed by the  
Department of Physics  
have examined a dissertation entitled

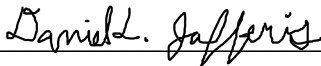
D-instantons and String Field Theory

presented by Nathan Benjamin Agmon

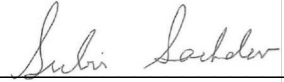
candidate for the degree of Doctor of Philosophy and hereby  
certify that it is worthy of acceptance.

Signature  \_\_\_\_\_

Typed name: Xi Yin, Chair

Signature  \_\_\_\_\_

Typed name: Professor Daniel Jafferis

Signature  \_\_\_\_\_

Typed name: Professor Subir Sachdev

Date: April 28, 2023



# D-instantons and String Field Theory

A DISSERTATION PRESENTED  
BY  
NATHAN BENJAMIN AGMON  
TO  
THE DEPARTMENT OF PHYSICS

IN PARTIAL FULFILLMENT OF THE REQUIREMENTS  
FOR THE DEGREE OF  
DOCTOR OF PHILOSOPHY  
IN THE SUBJECT OF  
PHYSICS

HARVARD UNIVERSITY  
CAMBRIDGE, MASSACHUSETTS  
APRIL 2023

©2023 – NATHAN BENJAMIN AGMON  
ALL RIGHTS RESERVED.

## D-instantons and String Field Theory

### ABSTRACT

In this thesis, we study D-instanton contributions to supergraviton scattering amplitudes in ten-dimensional type IIB superstring theory beyond the leading non-perturbative order. Our computation is based on the Neveu-Schwarz-Ramond (NSR) formalism with picture changing operators and vertical integration. In the first chapter, we determine the single D-instanton contribution to maximal R-symmetry violating (MRV) amplitudes with arbitrary momenta at the first subleading order in string coupling, as well as the effects of a D-/anti-D-instanton pair at leading nontrivial order in the momentum expansion. These results confirm a number of predictions of S-duality, and unveil some previously unknown pieces of type IIB string amplitudes.

The naive on-shell prescription for D-instanton mediated amplitudes, based on integration over the moduli space of worldsheet geometries as well as that of D-instanton boundary conditions, suffers from potential open string divergences and regularization ambiguities. In the second chapter, we employ the framework of open+closed superstring field theory (SFT) to address such issues. From this, we are able to unambiguously compute a part of the momentum-independent constant that appears at first subleading order in the string coupling, which serves as a highly nontrivial consistency check on spacetime supersymmetry and soft relations.

# Contents

TITLE PAGE	i
COPYRIGHT	ii
ABSTRACT	iii
TABLE OF CONTENTS	iv
AUTHOR LIST	v
LIST OF FIGURES	vi
ACKNOWLEDGEMENTS	x
0 INTRODUCTION	1
1 ON-SHELL METHODS	6
1.1 Introduction	6
1.2 Effects of a single D-instanton	17
1.3 Higher-point MRV amplitudes	42
1.4 Effects of a D-instanton/anti-D-instanton pair	50
1.5 A test of non-perturbative unitarity	60
1.6 Discussion	65
2 STRING FIELD THEORETIC EFFECTS	68
2.1 Introduction	68
2.2 Results and discussion	84
2.3 Disc 2-point amplitude	105
2.4 Annulus 1-point amplitude	110
2.5 $\delta\tau, \chi, \chi^*, \zeta^2$ disc amplitude	124
2.6 $\delta\tau, \delta\tau, \phi$ disc amplitude	140
2.7 $\delta\tau, \lambda, \theta_\alpha$ disc amplitude	148
A APPENDIX	156
A.1 Conventions	156
A.2 Modular forms and $SL(2, \mathbb{Z})$ covariance	172
A.3 Annulus 1-point diagram	175
A.4 Open string background independence and Sen gauge	179
REFERENCES	189

# Author List

The following authors contributed to this dissertation: Bruno Balthazar, Minjae Cho, Victor A. Rodriguez, Xi Yin.



# Listing of figures

1.1	The two-punctured disc represented as the upper half plane with global coordinate $z$ . One vertex operator $V_{\delta\tau(p)}$ is fixed at position $z = i$ while the second vertex operator $V_{\delta\tau(k)}$ is fixed at position $z = iy$ , integrating over the modulus $y \in [0, 1]$ . The $b$ ghost contour $B_y$ surrounds the integrated vertex operator as drawn. . . . .	31
1.2	The limit $y \rightarrow 0$ , where the 2-punctured disc degenerates into two 1-punctured discs glued together by an infinitely long strip. . . . .	36
1.3	Spacetime Feynman diagram that contributes to the unitarity cut. After cutting the internal propagators to put the intermediate particles on-shell, the vertices are given by either the D-instanton or anti-D-instanton mediated contributions to $R^4$ . Ingoing arrows denote $\delta\tau$ and outgoing arrows denote $\delta\bar{\tau}$ . . . . .	63
2.1	Diagrams contributing to the D-instanton amplitude for $N$ closed strings at order $g_s$ . Each comes with an arbitrary number of insertions of open string field collective modes $\Phi_o^m$ as represented by the blue boundaries. Black crosses are linear combinations of closed string vertex operators for $\delta\tau$ and $\delta\bar{\tau}$ , while red crosses are vertex operators for $\delta\tau$ . $\Delta B$ is a momentum-independent constant that depends on the string field theory parameters. All the diagrams are at the D-instanton location $x^\mu$ . . . . .	77
2.2	Disc 3-point vertex for open strings, described by the UHP with complex coordinate $z$ . The three open string punctures are located at $z = 0, 1, \infty$ , where they reside at the origin of their respective local coordinate patches $w_i$ . The vertex is defined such that a half-disc of radius 1 in the $w_i$ coordinate corresponds to a half-disc of radius $O(\alpha^{-1})$ in $z$ . There is also a PCO in the bulk at $z = p_{ooo}$ . . . . .	85
2.3	Open-closed disc vertex, described by the UHP with complex coordinate $z$ . The closed string puncture is located at $z = i$ together with the PCO, the latter of which is averaged over a contour surrounding the closed string. The open string puncture, which sits at $z = 0$ , is equipped with local coordinate $w$ . The vertex is defined such that a half-disc of radius 1 in the $w$ coordinate corresponds to a half-disc of radius $\lambda^{-1}$ in $z$ . . . . .	86
2.4	Feynman diagrams and the corresponding moduli domains for the disc with two NSNS insertions. Dotted circles correspond to averaged PCO insertions. On the worldsheet represented as the UHP, the closed strings (indicated by crosses) are inserted at $z = i$ and $z = iy$ . In the moduli space parameterized by $y$ , the domain $(0, \lambda^{-2})$ is the propagator region (red region), while $(\lambda^{-2}, 1)$ is the vertex region (blue region). . . . .	87

- 2.5 Feynman diagrams and the corresponding moduli domains for the annulus with one NSNS insertion. Here, a cross indicates a closed string puncture, while a wavy line indicates an open string propagator with two open string punctures at the endpoints. Dotted circles are PCO insertions averaged over a small contour enclosing the closed string. The worldsheet is given by the annulus, represented as a strip  $w \in (0, \pi) \times i\mathbb{R}$  with  $w \sim w + 2\pi it$  and  $v = e^{-2\pi t}$ , with the closed string located at  $w = u$ . The vertex region is shaded blue. Vertical integration is required along the walls  $u = \tilde{\lambda}^{-1}, \pi - \tilde{\lambda}^{-1}$  for  $v \in (0, 1)$ . . . 91
- 2.6 Feynman diagrams for the disc with one NSNS insertion and three NS insertions. The closed and open string punctures are represented by crosses. Black dots represent a PCO insertion in the bulk, while dotted (semi-)circles indicate a PCO averaged over a contour surrounding the (open) closed string puncture. Diagram (a) is the Feynman vertex corresponding to the vertex region of the 2d moduli space, while diagrams (b-d) each cover a propagator region. 94
- 2.7 Feynman diagrams and the corresponding moduli domains for the disc with two NSNS insertions and one NS insertion. Here, a cross indicates a closed/open string puncture, while a wavy line indicates an open string propagator with two open string punctures at the endpoints. Dotted circles are PCO insertions averaged over a small contour enclosing the closed string, while points are PCO insertions. The worldsheet is given by the disc, represented as the UHP, with the closed strings located at  $z = i$  and  $z = iy$ , and the open string at  $z = x$ . The vertex region is shaded blue. Vertical integration is required along each 1d segment separating adjacent diagrams. . . . . 96
- 2.8 Feynman diagrams and the corresponding moduli domains for the disc with an NSNS, NSR/RNS, and R insertion. Here, a cross indicates a closed/open string puncture, while a wavy line indicates an open string propagator with two open string punctures at the endpoints. Dotted circles are PCO insertions averaged over a small contour enclosing the closed string, while points are PCO insertions. The worldsheet is given by the disc, represented as the UHP, with the closed strings located at  $z = i$  and  $z = iy$ , and the open string at  $z = x$ . The vertex region is shaded blue. Vertical integration is indicated by the purple, teal, and orange segments. . . . . 99
- 2.9 A family of 1-punctured annuli, parametrized by the metric modulus  $0 < t < \frac{\ln \alpha^2}{2\pi}$  and antiholomorphic PCO location  $\bar{p}$ . On the  $w$  strip, the closed string is located at  $w = \tilde{\lambda}^{-1}$ , depicted by a black cross. The  $\tilde{\partial}\tilde{\xi}$  insertion at  $w = \bar{p}$  is represented by a purple cross. As  $\bar{p}$  varies, it traces out a purple “vertical segment” corresponding to vertical integration. . . . . 117
- 2.10 A family of open-closed 3-punctured discs, expressed in terms of the UHP with coordinate  $z$ , as parametrized by the modulus  $\beta \in ((2\tilde{\lambda})^{-1}, 2\tilde{\lambda})$ . There is one closed string puncture located at  $z = i$  corresponding to the black cross, while there are two open string punctures at  $z = \pm\beta$  corresponding to the blue crosses. The  $b$ -ghost contour  $B_\beta$  surrounds the two open string punctures, as represented by the dotted counterclockwise curves. As  $\beta$  varies, the blue crosses trace out the two blue segments, corresponding to moduli integration over the vertex region. . . . . 123

2.11	A family of discs with 1 bulk puncture and 3 boundary punctures parametrized by the modulus $\beta \in ((2\tilde{\lambda})^{-1}, 2\tilde{\lambda})$ and PCO coordinate $p_1$ ( $p_2$ ). On the UHP $z$ , the closed string is located at $z = i$ , shown by the black cross, and the open strings at $z = -\beta, \Delta_{-\beta}, \Delta_{+\beta}$ , represented by blue crosses. The $b$ -ghost insertion $B_\beta$ surrounds all three punctures, as indicated by the dotted counterclockwise contours. The $\partial\xi$ insertion is located at $\bar{p}_1$ ( $p_2$ ), as represented by the purple cross. As $\beta$ varies, the open string insertions trace out blue curves corresponding to moduli integration (none of the punctures collide, since $\Delta_\beta - \Delta_{-\beta} > \alpha^{-2}\tilde{\lambda}^{-1}$ ). Meanwhile as $\bar{p}_1$ ( $p_2$ ) varies, it traces out a purple “vertical segment” corresponding to vertical integration (VI). . . . .	135
2.12	A family of 4-punctured discs, expressed in terms of the UHP with coordinate $z$ , parametrized by the modulus $x \in \mathcal{R}_{\text{OOOO}}$ . The open string punctures at $z = 0, 1, \infty$ are indicated by black crosses, while the open string puncture at $z = x$ is represented by a blue cross. The contour of the $b$ -ghost insertion $B_x$ surrounds all four punctures, as indicated by the counterclockwise contours. As $x$ varies, the blue cross traces out three blue segments, corresponding to moduli integration over the vertex region. . . . .	138
2.13	A family of open-closed 3-punctured discs parametrized by the moduli $(x, y)$ . On the UHP, the closed strings are at $z = i, iy$ and the open string at $z = x$ , as indicated by the different crosses. The $b$ -ghost insertions $B_x$ and $B_y$ separately surround the open/closed string punctures, as indicated by the contours. As $x, y$ vary, the integrated vertex operators, represented by blue crosses, trace out two blue segments corresponding to the vertex region. . . . .	144
2.14	A family of discs with 2 closed string punctures and 1 open string puncture, parametrized by the modulus $ x  < \tilde{\lambda}^{-1}$ ( $ x  > \tilde{\lambda}^{-1}$ ) and PCO location $p$ . Representing the disc as the UHP $z$ , the closed strings are at $z = i$ and $z = iy_0$ , depicted by black crosses, and the open string puncture at $z = x$ , with a blue cross. The $b$ -ghost insertion $B_x$ surrounds the open string, as indicated by the dotted counterclockwise contour. The $\bar{\partial}\xi$ insertion at $z = p$ is represented by a purple cross. As $x$ varies, the open string insertion traces out a blue curve corresponding to moduli integration. Meanwhile as $p$ varies, $\bar{\partial}\xi$ traces out a purple “vertical segment” corresponding to vertical integration. . . .	146
2.15	Vertical integration along the boundary $x \in \mathbb{R}$ and $y_0 = \tilde{\lambda}^{-2}$ between the vertex and propagator regions of $(x, y)$ moduli space for the $\delta\tau(p)$ , $\lambda(k)$ , $\theta_\alpha$ amplitude on the disc. The fixed closed string punctures are depicted by black crosses. The integrated open string puncture is depicted by a blue cross, as surrounded by a $B_x$ ghost contour indicated by a dotted counterclockwise semi-circle. The operator $\bar{\partial}\xi$ , depicted by an orange cross, is integrated along the PCO direction $p$ , corresponding to the purple vertical segment, in order to fill in the gap. The blue segment corresponds to moduli integration in $x \in \mathbb{R}$ . . .	152
A.1	Properties of the basic holomorphic operators in the free worldsheet theory, where $n \in \mathbb{Z}$ . . . . .	161

A.2	The annulus $A^2(t)$ represented by a rectangle $w \in [0, \pi] \times [0, 2\pi it]$ with opposite sides $w \simeq w+2\pi it$ identified. There is a single closed string puncture at $w = u$ for $u \in \mathbb{R}$ , which has been drawn off the real axis for clarity. The $b$ ghost contour $B_u$ surrounds the (picture zero) integrated vertex operator $V_{\delta\tau(p)}^{(0)}$ , while $B_t$ runs along a horizontal line segment. . . . .	176
A.3	Plumbing configuration of the 4-point propagator region for a finite choice of the SFT parameter $\alpha$ . Vertex operator insertions are marked with black crosses, while PCO insertions are marked with blue dots. . . . .	183

# Acknowledgments

I would like to thank my advisor, Professor Xi Yin, for his infectious energy and passion for physics; for his encouragement to tackle hard problems; for the many invaluable conversations and advice; for his respect, treating me as an independent researcher and collaborator from the very beginning; and for his continued mentorship and support. I also would like to thank my committee members, Professors Daniel Jafferis and Subir Sachdev for their useful advice and interesting discussions; current and former members of Xi's research group, including Bruno Balthazar, Scott Collier, Minjae Cho, Barak Gabai, Victor Rodriguez, with whom I've made countless happy memories, especially through our many late nights and endless Zoom meetings; Professor Yifan Wang for serving as an unofficial advisor and mentor, who has greatly assisted me in becoming an independent researcher; Professor Silviu Pufu, my undergraduate advisor, whose teaching and encouragement led me to pursue high energy physics research; my other collaborators: Nick Agia, Shai Chester, and Andrea Dei, for their helpful comments and shared efforts; the high energy group for making Harvard such a welcoming place; members of my cohort for creating lifelong friendships; my parents and grandparents, whose many sacrifices enabled me to reach this point; my friends and family for their unwavering love and support; my fiancée, who has stood by my side from our early undergraduate days to the final ones of our doctoral studies, and whose companionship has brought great joy and meaning to my life.

# 0

## Introduction

Critical string theories are defined at the level of the perturbative spacetime S-matrix by a two-dimensional worldsheet conformal field theory with BRST-exact stress-energy tensor and a prescription for integration over the moduli space of punctured Riemann surfaces [1–3]. The worldsheet formalism is also known to capture certain non-perturbative effects, known as D-instantons, by including worldsheets with boundaries subject to suitable Dirichlet-type boundary conditions [4]. While D-instanton effects are fundamental to the dynamics of string theory [5, 6], and have been determined in some cases by a combination of on-shell worldsheet methods and string dualities [7–27], a systematic

framework for computing them has been lacking until recent work of Sen [28–33] based on open+closed string field theory [34].

The goal of this work is to apply the framework of D-instanton perturbation theory to compute D-instanton contributions to the S-matrix of type IIB superstring theory in ten-dimensional Minkowskian spacetime, beyond the leading order results of [7, 32]. There are two known types of non-perturbative effects in string theory: D-instanton effects of order  $e^{-1/g_s}$ , and gravitational (including NS brane) instanton effects of order  $e^{-1/g_s^2}$ . The latter are analogous to instantons in quantum field theory in the sense that they correspond to saddle points of the Euclidean functional integral based on an (effective) action of spacetime fields. The D-instantons, on the other hand, cannot be understood as saddle points of an action of closed string fields. Rather, they must be included as extra contributions to a scattering amplitude through worldsheets with boundaries, or “holes”, that are attached to the D-instanton.

As with any non-perturbative corrections, one can meaningfully speak of the D-instanton effects only if there is a way to distinguish them from the perturbative results, or if there is a prescription for summing up the perturbative expansion. In the 2D  $c = 1$  string theory analyzed in [24, 25], the perturbative series for closed string scattering amplitudes are Borel-summable (assuming the conjectured matrix model dual), and the D-instanton contributions were understood to be corrections on top of the Borel-resummed perturbative results. In the present work, we will focus on D-instanton effects in type IIB string theory that are either distinguished from the perturbative contributions in that the former violate certain perturbative global symmetries, or correct a perturbative expansion that is known to terminate at a finite order.

## THE GENERAL STRUCTURE OF D-INSTANTON PERTURBATION THEORY

Our working hypothesis is that with a suitable prescription for summing up the perturbative series, there is a well-defined contribution from each D-instanton sector, i.e. a family of BRST-invariant boundary conditions of Dirichlet type on the worldsheet.

The boundary conformal field theory of the D-instanton gives rise to the space of open string fields  $\mathcal{H}_o$  in the sense of Batalin-Vilkovisky (BV) formalism [34]. For type IIB string theory, states of  $\mathcal{H}_o$  are subject to GSO invariance and the usual restriction on picture number, namely  $(-1)$ -picture in the Neveu-Schwarz (NS) sector and  $(-\frac{1}{2})$ - and  $(-\frac{3}{2})$ -picture in the Ramond (R) sector.

Let  $\mathcal{H}_c$  be the space of closed string fields, as defined in [35]. We will denote by  $\Psi_c \in \mathcal{H}_c$  a closed string field and  $\Psi_o \in \mathcal{H}_o$  an open string field on the D-instanton. The space of string fields is equipped with a Grassmann-odd symplectic structure defined through the BV anti-bracket. In performing the functional integral over open string fields, one should restrict to a Lagrangian subspace  $L$  (i.e. a BV gauge condition).<sup>1</sup> The contribution from the D-instanton to the closed string field Euclidean 1PI effective action  $\Gamma[\Psi_c]$  takes the schematic form

$$e^{-\Gamma[\Psi_c]} \Big|_{\text{D-inst}} = e^{-\frac{C}{g_s}} \int D\Phi_o|_L \exp(-S_{oc}[\Psi_o, \Psi_c]). \quad (1)$$

Here we have separated the D-instanton action  $C/g_s$  from the rest of the open+closed

---

<sup>1</sup>For instance, one may split  $\Psi_o$  into the “regular” field  $\Phi_o$  and BV anti-field  $\Phi_o^\ddagger$  based on ghost number grading, and define the subspace  $L$  by the constraint  $\Phi_o^\ddagger = \frac{\delta V}{\delta \Phi_o}$  for some choice of functional  $V[\Phi_o]$ . Further details on the BV gauge condition for D-instanton perturbation theory are discussed in Section 2.1.2.



string field action  $S_{oc}[\Psi_o, \Psi_c]$ , defined “perturbatively” by integration over string vertices [34] that are 1PI with respect to the closed string fields and Wilsonian with respect to the open string fields.

To perform the functional integral of (1), one separates the open string modes into two types: the “massive” modes with non-degenerate kinetic terms, and the “massless” modes with degenerate kinetic terms. The massive modes can be integrated out perturbatively, giving rise to Feynman diagrams with open string loops. Note that the worldsheet configuration corresponding to a Feynman diagram need not be connected, but rather should be “connected modulo boundary” (e.g. in (1.1)).

The integration over massless open string modes, on the other hand, cannot be treated perturbatively. This includes the collective modes  $\Phi_o^m$ , whose integration is analogous to integrating over the D-instanton moduli space, and a mode that corresponds to the Faddeev-Popov ghost associated with fixing the  $U(1)$  gauge symmetry on the D-instanton. A consistent treatment of the integration over massless open string fields, as explained in [29], will be discussed in Chapter 2 for the type IIB string amplitudes of interest.

Open+closed string field theory provides a framework for computing D-instanton effects on the closed string amplitude, at the level of perturbation theory around a D-instanton configuration. Such a perturbation theory may break down when open string modes on the D-instantons become tachyonic. The latter occurs for the ZZ-instantons in  $c = 1$  string theory [24, 25, 30], where a Wick rotation prescription for the integration contour in the open string tachyon field has been proposed, as is anticipated from the general prescription for summing over saddle point contributions based on steepest descent contours. In type IIB superstring theory, a pair consisting of a D-instanton and an anti-D-instanton

that are sufficiently nearby one another gives rise to tachyonic open string modes. It is unclear whether the string field theory formalism provides an unambiguous result in this situation, as there may be intrinsic ambiguities in such D-instanton contributions that are tied to the resummation prescription for string perturbation theory.

# 1

## On-shell methods

### 1.1 INTRODUCTION

Working explicitly with all components of the open string field on the D-instanton can be exceedingly tedious. It is often possible to take a shortcut, in which one extends the rules of on-shell string perturbation theory, based on integrating correlators of BRST-closed string vertex operators over the moduli space of Riemann surfaces, to include worldsheets with boundaries ending on the D-instanton. As was pointed out in [4, 7], such an on-shell prescription is subject to ambiguities due to divergences where the worldsheet degener-

ates. In this chapter, we view the on-shell prescription as nothing more than a computational shortcut for obtaining partial results that could be in principle recovered from string field theory. The remaining “regularization ambiguity” may either be determined by consideration of symmetries that are not manifest in the on-shell prescription, such as spacetime supersymmetry (as will be the case for the results presented in this work), or a genuine string field theoretic computation (part of which is performed in Chapter 2).

### 1.1.1 THE (SOMEWHAT NAIVE) ON-SHELL PRESCRIPTION

For type IIB superstring theory in ten-dimensional Minkowskian spacetime, the known D-instantons include both the “BPS” D-instanton that carries unit charge with respect to the Ramond-Ramond axion (0-form potential), and the corresponding anti-D-instanton that carries the opposite RR charge. One expects any closed string amplitude to receive contributions from arbitrary configurations of  $n$  D-instantons and  $m$  anti-D-instantons,<sup>1</sup> given schematically by

$$\mathcal{A}_{(n,m)} = \int_{\widetilde{\mathcal{M}}_{n,m}} d\tilde{\mu} \exp \left( \text{[diagrams]} \right) \times \left[ \text{[diagrams]} \right] \quad (1.1)$$

The diagrams in the equation represent various instanton configurations. The first part of the exponential is a sum of four diagrams: a solid grey circle, a grey circle with a white center, a grey circle with a white center and a horizontal line through it, and a grey circle with two white centers. The second part is a sum of four diagrams inside square brackets: a grey circle with an 'x' inside, a grey circle with an 'x' inside and a white center, a grey circle with an 'x' inside and a white center, and a grey circle with an 'x' inside and a white center.

in the on-shell prescription. Here,  $\widetilde{\mathcal{M}}_{n,m}$  is the super-moduli space of the  $(n, m)$  D-instanton boundary conditions, whose bosonic and fermionic collective coordinates are in correspondence with the massless open string BRST cohomology in the Neveu-Schwarz and Ra-

<sup>1</sup>Here we focus only on D(-1) branes in Minkowski spacetime. Both the string field theory and on-shell approaches generalize to D-instantons appearing in other backgrounds, such as Euclidean  $Dp$ -branes wrapping non-contractible cycles in the type II string theories (see e.g. [36, 37]).

mond sectors, respectively. The measure  $d\tilde{\mu}$ , without including any of the empty disconnected diagrams, is the natural one determined by the Zamolodchikov metric of boundary deformations (flat in the present example), up to a constant normalization to be specified later. The integrand meanwhile takes the form of a sum over the topologies of (generally disconnected) Riemann surfaces  $\Sigma$ , whose connected components all share the same D-instanton boundary condition, with a given number of vertex operator insertions that correspond to closed string asymptotic states. Each diagram comes with the string coupling dependence  $g_s^{-\chi(\Sigma)}$ , where  $\chi$  is the Euler characteristic (including  $-1$  from each puncture/vertex operator). Of note is the sum over empty discs, each of which evaluates to minus the D-instanton action  $-(n+m)\frac{C}{g_s}$ , that exponentiates to give the prefactor  $e^{-(n+m)\frac{C}{g_s}}$  in (1). The sum over remaining topologies is then interpreted as a perturbative series in the  $(n, m)$  type D-instanton background.

A general deformation of the D-instanton along its super-moduli space is formally characterized by a boundary deformation of the worldsheet action, which takes the form

$$\Delta S_{\text{WS}} = \int_{\partial\Sigma} dx U_{\text{NS},m}^{(0)}(x) + \int_{\partial\Sigma} dx \mathbf{P}_{\frac{1}{2}} U_{\text{R}}^{(-\frac{1}{2})}(x). \quad (1.2)$$

Here  $U_{\text{NS},m}^{(0)}$  is a pictured-raised unfixed vertex operator in the NS sector, constructed purely from the matter sector of the worldsheet CFT, that is BRST invariant modulo total derivatives.  $U_{\text{R}}^{(-\frac{1}{2})}$  meanwhile is an unfixed Ramond sector vertex operator in the  $(-\frac{1}{2})$ -picture, which necessarily involves the ghost fields. To ensure that the deformation has picture number 0, one introduces a formal “ $\frac{1}{2}$ -picture raising” operator  $\mathbf{P}_{\frac{1}{2}}$  [38, 39], defined in such a way that a pair of  $\mathbf{P}_{\frac{1}{2}}$  insertions amounts to that of a single picture-

changing operator  $\mathcal{X}$  (PCO). For instance, one may propose to replace (1.2) with the insertion of [40]<sup>2</sup>

$$e^{-\Delta S_{\text{ws}}} \equiv \exp \left( - \int_{\partial\Sigma} dx U_{\text{NS},m}^{(0)}(x) \right) \times \sum_{j=0}^{\infty} \frac{1}{(2j)!} \left[ \int_{\partial\Sigma} dx U_{\text{R}}^{(+\frac{1}{2})}(x) \right]^j \left[ \int_{\partial\Sigma} dx U_{\text{R}}^{(-\frac{1}{2})}(x) \right]^j, \quad (1.3)$$

into worldsheet correlators, where  $U_{\text{R}}^{(+\frac{1}{2})}$  is the picture-raised version of  $U_{\text{R}}^{(-\frac{1}{2})}$ , in the  $(+\frac{1}{2})$ -picture. Note that such a deformation leads to a non-local boundary CFT.

The deformation operators appearing on the RHS of (1.2) can be expanded in a basis of local boundary operators, with Grassmann even coefficients  $x$  in the NS sector and Grassmann odd coefficients  $\theta$  in the R sector. Together,  $(x, \theta)$  comprise the collective coordinates on a patch of the super-moduli space of the D-instanton, whose origin corresponds to the undeformed boundary CFT. In the case of  $(n, m)$  D-instanton in flat space-time, the supermoduli space  $\widetilde{\mathcal{M}}_{(n,m)}$  is parameterized by  $10(n+m)$  bosonic and  $16(n+m)$  fermionic collective coordinates, at least when the D-instantons and anti-D-instantons are sufficiently far separated so that all modes of the open strings stretched between them are “massive,” or off-shell.

Starting from the string field theory for the D-instantons, one may integrate out the massive open string modes perturbatively, leaving only integration over the massless open string modes. One might expect the physical massless open string degrees of freedom to be in correspondence with the moduli of the D-instanton, and that the quantum effec-

---

<sup>2</sup>Note that (1.3) amounts to expanding the exponential R deformation in (1.2), and keeping only even powers of the R sector deformation, with half of them in picture  $-\frac{1}{2}$  and the other half in picture  $+\frac{1}{2}$  through  $\mathbf{P}_{\frac{1}{2}}^2 = \mathcal{X}$ . This new insertion is not a local deformation of the worldsheet CFT, but can be justified by consistent factorization of string amplitudes.

tive action for massless open string modes to be roughly equivalent to the diagrammatic expansion appearing on the RHS of (1.1). However, this expectation fails to hold in two important ways.

First, the diagrammatic expansion (1.1) suffers from logarithmic divergences due to the propagation of massless open string modes<sup>3</sup> along a thin strip that pinches near the boundary of the moduli space of the worldsheet geometry. One may regularize such divergences by cutting off near the boundary of the moduli space; indeed, the leading divergences cancel between different diagrams that contribute to on-shell closed string amplitudes mediated by the D-instanton [4]. Such a prescription leaves a finite regulator-dependent ambiguity whose resolution generally requires string field theory. Nonetheless, the on-shell prescription can still capture a meaningful part of the D-instanton amplitude, as will be explained later in this work.

Second, not all massless, or on-shell, modes of the open string field correspond to moduli of the D-instanton. This occurs for the multi-D-instanton, say of type  $(n, 0)$  where  $n \geq 2$ , where the open string fields carry  $u(n)$  Chan-Paton factors, whereas the moduli space is  $\text{Sym}^n(\mathbb{R}^{10|16})$ . In this case, the integrand appearing on the RHS (1.1) is singular along the loci where D-instantons collide, and the naive on-shell open string perturbation theory breaks down. This is already apparent in the low energy limit, where for suitable observables, the open string field theory reduces to the IKKT matrix model [33, 41, 42], which does not admit a perturbative expansion [43–45].

---

<sup>3</sup>This should be contrasted with open strings on a  $Dp$ -brane for  $p \geq 0$  that generically carry nonzero momenta along the worldvolume of the brane.

### 1.1.2 SUPERGRAVITON AMPLITUDES IN TYPE IIB STRING THEORY

A fundamental observable of type IIB string theory is the S-matrix in asymptotically ten-dimensional Minkowskian spacetime. At the non-perturbative level, the S-matrix elements are expected to be well-defined for asymptotic states spanned by the Fock space of supergravitons. The simplest nontrivial S-matrix element is that of  $2 \rightarrow 2$  supergraviton scattering, well known to be constrained by supersymmetry to be of the form [46]

$$\mathcal{A}_{2 \rightarrow 2} = \mathcal{A}_{2 \rightarrow 2}^{SUGRA} M(s, t; \tau, \bar{\tau}), \quad (1.4)$$

where  $\mathcal{A}_{2 \rightarrow 2}^{SUGRA}$  is the corresponding amplitude in tree-level (two-derivative) type IIB supergravity, and  $M(s, t; \tau, \bar{\tau})$  is a single function that approaches 1 in the low energy limit  $s, t \rightarrow 0$ . Here  $s$  and  $t$  are Mandelstam variables, and  $\tau = \tau_1 + i\tau_2$  ( $\tau_2 = 1/g_s$ ) is the axion-dilaton expectation value parameterizing type IIB vacua, on which the low-energy accidental  $SL(2, \mathbb{R})$  symmetry acts by Möbius transformation.

Note that the full function  $M(s, t; \tau, \bar{\tau})$  is exceedingly complicated, as it encapsulates all possible resonances that are produced by scattering a pair of gravitons, including black hole states. It can be organized in two different expansions: in energy/momentum, or in string coupling. The momentum expansion takes the form

$$M(s, t; \tau, \bar{\tau}) = \underline{stu} \left[ \frac{1}{\underline{stu}} + f_0(\tau, \bar{\tau}) + H_2(\underline{s}, \underline{t}) + f_4(\tau, \bar{\tau})(\underline{s}^2 + \underline{t}^2 + \underline{u}^2) + f_6(\tau, \bar{\tau})(\underline{s}^3 + \underline{t}^3 + \underline{u}^3) + f_8(\tau, \bar{\tau})(\underline{s}^4 + \underline{t}^4 + \underline{u}^4) + f_0(\tau, \bar{\tau})H_8(\underline{s}, \underline{t}) + \dots \right] \quad (1.5)$$

where the underlined notation  $\underline{s}, \underline{t}, \underline{u}$  stands for the Mandelstam variables in units of the



ten-dimensional Planck mass. The momentum-independent coefficients  $f_0, f_4, f_6, f_8, \dots$  are commonly referred to as the coefficients of  $R^4, D^4 R^4, D^6 R^4, D^8 R^4, \dots$  terms in the quantum effective action of type IIB string theory. The function  $H_2(\underline{s}, \underline{t})$ , which is independent of the moduli  $\tau$ , scales like two powers of momenta with logarithmic branch cuts extending to zero momentum, and is determined by the supergravity 1-loop amplitude. The function  $H_8(\underline{s}, \underline{t})$  similarly scales like eight powers of momenta with non-analyticity at zero momentum, and whose discontinuity factorizes into a supergravity tree amplitude and an  $R^4$  vertex.

The coefficients  $f_0, f_4, f_6$  are known to be constrained by supersymmetry [47, 48] to satisfied second-order differential equations on the moduli space of IIB vacua. For instance,  $f_0(\tau, \bar{\tau})$  obeys the equation

$$\left( \tau_2^2 \partial_\tau \partial_{\bar{\tau}} - \frac{3}{16} \right) f_0(\tau, \bar{\tau}) = 0. \quad (1.6)$$

Such equations dictate that the perturbative string contributions to  $f_0, f_4, f_6$  truncates at a finite loop order, and the combination of perturbative results together with the assumption of S-duality invariance fixes these functions completely.  $f_8$ , on the other hand, is not known to be constrained by supersymmetry, and is not even known in perturbation theory starting at 3-loop order.

The string coupling expansion of  $M(s, t; \tau, \bar{\tau})$ , on the other hand, is expected to take

the form

$$\tau_2^{-2} M(s, t; \tau, \bar{\tau}) = \sum_{h=0}^{\infty} \tau_2^{-2-2h} M_h(\alpha' s, \alpha' t) + \sum_{n,m} e^{2\pi i(n\tau - m\bar{\tau})} M^{(n,m)}(\alpha' s, \alpha' t; \tau_2) + \dots . \quad (1.7)$$

Here  $M_h$  stands for the genus  $h$  perturbative string amplitude,  $M^{(n,m)}$  stands for the contribution from  $n$  D-instantons and  $m$  anti-D-instantons, and  $\dots$  stands for possible gravitational instanton effects. Note that the relation between the string tension and Planck mass is such that  $\alpha' s = \tau_2^{\frac{1}{2}} \underline{s}$ . As already alluded to, the instanton corrections are unambiguously defined only if there is a prescription for summing up the perturbative series, or if the perturbative contributions of certain momentum and/or coupling dependence are absent.

In the naive on-shell prescription, each D-instanton sector contribution  $M^{(n,m)}$  is given by a sum over worldsheet diagrams with D-instanton boundary conditions, integrated over the moduli space of the D- and anti-D-instantons, with the structure

$$M^{(n,m)}(\alpha' s, \alpha' t; \tau_2) = \tau_2^{-\frac{7}{2}(n+m)} \sum_{L=0}^{\infty} \tau_2^{-L} M_L^{(n,m)}(\alpha' s, \alpha' t), \quad (1.8)$$

where the “open string loop order”  $L$  is minus the Euler characteristic of the worldsheet diagram (with closed string insertions as punctures). The overall factor  $\tau_2^{-\frac{7}{2}(n+m)}$  comes from the normalization of the measure on the D-instanton moduli space. (1.8) is expected to hold when the D-instanton moduli integration is non-singular, as will be the case for the contributions explicitly computed in this work, including  $M^{(1,0)}$  and certain terms in  $M^{(1,1)}$ . On the other hand, it is known to fail when there are singularities in the D-

instanton moduli space, which occurs in  $M^{(n,0)}$  for  $n \geq 2$ . Such singularities are due to the appearance of new “massless” open string modes, and may be resolved in the open+closed string field theory approach [33].

### 1.1.3 SUMMARY OF RESULTS

The leading one-D-instanton contribution to the four-graviton amplitude, namely  $M_0^{(1,0)}$  in the notation of (1.7), (1.8) (and similarly  $M_0^{(0,1)}$  for the anti-D-instanton), was studied in [7] and shown to be  $stu$  times a constant. This constant is determined to be

$$\frac{1}{\alpha'^3 stu} M_0^{(1,0)}(\alpha' s, \alpha' t) = \frac{\pi}{16} \quad (1.9)$$

by S-duality and consideration of supersymmetry [47, 48], and was reproduced from a first principles string field theoretic computation recently in [32].

In Section 1.2, we present the first main result of this chapter: the next-to-leading order single D-instanton contribution,

$$\frac{1}{\alpha'^3 stu} M_1^{(1,0)}(\alpha' s, \alpha' t) = C_1 + \sum_{p=2}^{\infty} \frac{\zeta(p)}{2^{2p+3}} \alpha'^p (s^p + t^p + u^p), \quad \text{where } C_1 = \frac{3}{256}. \quad (1.10)$$

The momentum dependent terms on the RHS of (1.10) come from the worldsheet diagram consisting of three discs with boundary on the D-instanton, where one of the discs contains two closed string vertex operators, while the other two each contain one closed string insertion. The constant term  $C_1$  appearing on the RHS of (1.10) cannot be computed directly in the on-shell approach due to ambiguities in the regularization scheme.

In fact, we are not aware of any simple regularization scheme based on cutting off the worldsheet moduli integral that produces the correct answer. On the other hand,  $C_1$  has been argued in [48] to be fixed by consideration of supersymmetry Ward identities for 6-point amplitudes and a soft relation between the 6- and 4-point amplitudes, giving the result of (1.10).

It is illuminating to consider a generalization of  $C_1$ , namely the coefficient of the  $N$ -point “maximal R-symmetry violating” (MRV) coupling of the schematic form  $(\delta\tau)^{N-4}R^4$  at order  $e^{2\pi i\tau}\tau_2^{-1}$ , which is fixed by consideration of supersymmetry and soft limits in Section 1.3.1 to be (see also [49])

$$C_1^{(N)} \equiv \frac{N(N-1)}{2}a_0 + Na_1 + a_2 = \frac{3}{256} - \frac{(N-4)(N-5)}{64}. \quad (1.11)$$

From the SFT perspective,  $a_0$  comes entirely from the worldsheet diagram that involves a disc with two closed string insertions, whereas  $a_1$  includes contributions from an annulus with one closed string insertion, and the Jacobian factor due to the change of integration variables from open string collective modes to the D-instanton moduli. The constant  $a_2$ , having the most complicated origin, includes contributions from worldsheet diagrams of the topology of a 3-holed sphere or a 1-holed torus.

In Section 1.3, we apply our results on certain connected worldsheet diagrams (with boundary) appearing in D-instanton perturbation theory to analyze the single D-instanton contribution to  $N$ -point MRV amplitudes. In particular, we obtain the leading-order contribution and the full momentum dependence of the next-to-leading order contribution. This includes the 6-point 14-derivative order MRV amplitude considered in [49], pinning

down a previously unknown coefficient.<sup>4</sup>

In Section 1.4, we analyze the contribution from a D-instanton/anti-D-instanton pair, at leading order in the open string expansion, namely  $M_0^{(1,1)}$  in (1.7). The main new idea here is the nontrivial measure on the instanton moduli space, as determined from the annulus diagram with two boundary components on the D- and anti-D-instanton respectively. We will see that the moduli space integrand is singular at finite distance from the origin, and that the on-shell computation of  $M_0^{(1,1)}$  is ill-defined. This is perhaps unsurprising given that the precise definition of  $M_0^{(1,1)}$  requires a (as of yet unknown) prescription for summing up the perturbative closed string amplitudes. Nonetheless, we will argue that the leading term in the momentum expansion of  $M_0^{(1,1)}$  is unambiguously determined by the integration over the instanton moduli space at asymptotically large separation between the D- and anti-D-instanton, giving the result

$$\frac{1}{\alpha'^3 stu} M_0^{(1,1)}(\alpha' s, \alpha' t) = -2^{-11} \alpha'^3 (s^3 + t^3 + u^3) + \mathcal{O}(\alpha'^4). \quad (1.12)$$

This confirms, in a highly nontrivial manner, a prediction of S-duality for the  $D^6 R^4$  effective coupling [50].

Furthermore, in Section 1.5, we perform a check of non-perturbative unitarity for D-instanton scattering amplitudes. In particular, we demonstrate that certain terms in the low energy expansion of  $M_0^{(1,1)}$  have non-analytic dependence on the momenta, and are related to amplitudes mediated by a single D-instanton or anti-D-instanton, namely  $M_0^{(1,0)}$  or  $M_0^{(0,1)}$ , through unitarity cuts.

---

<sup>4</sup>This coefficient is  $c_1$  in the notation of [49], section 6.

## 1.2 EFFECTS OF A SINGLE D-INSTANTON

Before we begin, let us outline our conventions for superamplitudes in type IIB string theory following the spinor helicity formalism of [51]. Given a massless external particle  $i$ , its momentum  $p_i$  can be expressed in terms of auxiliary spinor helicity variables  $\lambda_{ia}^\alpha$  according to

$$p_i^\mu (\gamma_\mu)^{\alpha\beta} = \lambda_{ia}^\alpha \lambda_i^{\beta a}, \quad (1.13)$$

where  $\alpha$  denotes an  $SO(1,9)$  16-dimensional chiral spinor index, and  $a$  denotes an  $SO(8)$  little group index. Using these variables, we can also construct the supermomenta

$$q_{i+}^\alpha = \lambda_{ia}^\alpha \eta_i^a, \quad q_{i-}^\alpha = \lambda_i^{\alpha a} \frac{\partial}{\partial \eta_i^a}, \quad (1.14)$$

where  $\eta_i^a$  is a Grassmann odd object satisfying  $\{\eta_i^a, \frac{\partial}{\partial \eta_i^b}\} = \delta_b^a$ . From this, it follows that the supercharges

$$Q_+^\alpha = \sum_i q_{i+}^\alpha, \quad Q_-^\alpha = \sum_i q_{i-}^\alpha, \quad (1.15)$$

satisfy the  $\mathcal{N} = (2,0)$  super-Poincaré algebra

$$\{Q_+^\alpha, Q_-^\beta\} = -(\gamma_\mu)^{\alpha\beta} P^\mu, \quad (1.16)$$

where  $P^\mu = \sum_i p_i^\mu$  is the total momentum.

The  $2^8 = 256$  one-particle states of the supergraviton multiplet can be embedded into a superstate

$$\Phi_i = \Phi_i^{(0)} + \eta_i^a \Phi_{ia}^{(1)} + \frac{1}{2!} \eta_i^a \eta_i^b \Phi_{iab}^{(2)} + \cdots + \frac{1}{8!} \eta_i^{a_1} \cdots \eta_i^{a_8} \Phi_{ia_1 \cdots a_8}^{(8)}. \quad (1.17)$$

Each of the components is assigned a definite weight  $q_R$  under the  $U(1)_R$  that acts as an outer-automorphism of the supersymmetry algebra in (1.16), which also appears as an accidental R-symmetry in the low energy limit. We shall take  $\Phi_i$  to have weight  $q_R = -1$  and  $\eta$  to have weight  $q_R = -\frac{1}{4}$ , which fixes the weights of the rest of the components. Of particular interest are the axion-dilaton  $\delta\tau$  and its complex-conjugate  $\delta\bar{\tau}$ , which appear at the ends of the multiplet as

$$\Phi_i^{(0)} = |\delta\tau, p_i\rangle, \quad \Phi_{ia_1\dots a_8}^{(8)} = \epsilon_{a_1\dots a_8} |\delta\bar{\tau}, p_i\rangle, \quad (1.18)$$

where  $|\delta\tau, p_i\rangle$  and  $|\delta\bar{\tau}, p_i\rangle$  are the associated 1-particle states. From this it follows that  $\delta\tau$  transforms with weight  $q_R = -1$  and  $\delta\bar{\tau}$  with weight  $q_R = +1$ .

Given a set of external superstates, it is meaningful to talk about the superamplitude  $\mathcal{A}(\Phi_i)$ , which generically takes the form

$$\mathcal{A}(\Phi_i) = i(2\pi)^{10} \delta^{10}(P) Q_+^{16} \mathcal{F}(\lambda_i, \eta_i), \quad (1.19)$$

where  $Q_{\pm}^{16}$  is defined as

$$Q_{\pm}^{16} = \frac{1}{16!} \epsilon_{\alpha_1\dots\alpha_{16}} Q_{\pm}^{\alpha_1} \dots Q_{\pm}^{\alpha_{16}}. \quad (1.20)$$

The superamplitude is constrained by supersymmetry to obey various Ward identities, which can be conveniently packaged into the expression

$$\delta^{10}(P) Q_+^{16} Q_-^{\alpha} \mathcal{F}(\lambda_i, \eta_i) = 0. \quad (1.21)$$

Now consider the case of  $2 \rightarrow 2$  supergraviton scattering. Here, supersymmetry constrains the superamplitude to take the form

$$\mathcal{A}_{2 \rightarrow 2}(\Phi_i) = i(2\pi)^{10} \delta^{10}(P) Q_+^{16} F(s, t), \quad (1.22)$$

where  $F(s, t)$  is a single function of the Mandelstam variables

$$s = -(p_1 + p_2)^2, \quad t = -(p_1 + p_3)^2, \quad u = -(p_1 + p_4)^2. \quad (1.23)$$

### 1.2.1 DIAGRAMMATIC EXPANSION

In the on-shell approach, we define the contribution of a single D-instanton to the  $2 \rightarrow 2$  supergraviton scattering amplitude as<sup>5</sup>

$$\mathcal{A}_{2 \rightarrow 2}^{(1,0)} = \mathcal{N}_D e^{2\pi i \tau} \int d^{10}x d^{16}\theta \sum_{L=0}^{\infty} \tau_2^{-L} A_{2 \rightarrow 2}^{(L)}(x, \theta), \quad (1.24)$$

where the superscript  $(n, m) = (1, 0)$  labels the number of D-instantons  $n$  and number of anti-D-instantons  $m$ . The super-moduli space  $\widetilde{\mathcal{M}}_{1,0} = \mathbb{R}^{10|16}$  is parameterized by ten bosonic collective coordinates  $x^\mu$  and sixteen fermionic collective coordinates  $\theta_\alpha$ .  $\tau$  is the vacuum expectation value of the axion-dilaton field, defined in such a way that it transforms in the Möbius form with respect to the low energy  $SL(2, \mathbb{R})$  symmetry. The overall normalization of the measure on super-moduli space, namely the factor  $\mathcal{N}_D$ , a priori depends on  $\tau$  and is not fixed by consideration of unitarity alone. Note that it can be determined either in the on-shell formalism with the assumption of S-duality [7], or from first

---

<sup>5</sup>For a summary of our worldsheet conventions, see Appendix A.1.



principles in the string field theory formalism [31, 32].

The integrand on the RHS of (1.24) takes the form of a sum over worldsheet diagrams with four insertions of the supergraviton vertex operators. The  $e^{2\pi i\tau}$  factor comes from the exponentiated empty disc diagram.<sup>6</sup> The sum over empty annuli exponentiates to some constant of order  $\tau_2^0$ , which has been absorbed into the overall normalization  $\mathcal{N}_D$ . The function  $A_{2 \rightarrow 2}^{(L)}(x, \theta)$  captures the contribution from the remaining components of the worldsheet diagrams with Euler characteristic  $-L$  (taking into account  $-1$  from each puncture), including empty connected components with negative Euler characteristic.

The leading-order term of (1.24) receives contributions from four disconnected discs, each with a single puncture:

$$\mathcal{A}_{2 \rightarrow 2}^{(1,0)} \Big|_{\text{LO}} = \mathcal{N}_D e^{2\pi i\tau} \int d^{10}x d^{16}\theta \text{ (x) (x) (x) (x) } . \quad (1.25)$$

Here, a black cross denotes the vertex operator associated to a general state of the supergraviton multiplet. The worldsheet diagrams have boundary conditions set by the  $(1, 0)$  D-instanton, as represented by the blue boundary. In particular, the bosonic worldsheet matter fields satisfy  $X^\mu|_{\partial\Sigma} = x^\mu$ . The dependence on the fermionic collective coordinates is introduced through the insertion of the R sector boundary deformation

$$e^{-\Delta S_{\text{WS,R}}(\theta)} \equiv \sum_{j=0}^{\infty} \frac{1}{(2j)!} \left[ \theta_\alpha (\gamma^\mu)^{\alpha\beta} \int_{\partial\Sigma} dx i\partial X_\mu(x) e^{+\frac{1}{2}\phi} S_\beta \right]^j \left[ \theta_\alpha \int_{\partial\Sigma} dx e^{-\frac{1}{2}\phi} S^\alpha(x) \right]^j . \quad (1.26)$$

---

<sup>6</sup>The worldsheet computation is performed for  $\tau_1 = 0$ , whose result generalizes straightforwardly to nonzero  $\tau_1$ .

At next-to-leading order in  $\tau_2^{-1}$ , the D-instanton now contributes as

$$\mathcal{A}_{2 \rightarrow 2}^{(1,0)} \Big|_{\text{NLO}} = \mathcal{N}_D e^{2\pi i \tau} \int d^{10} x d^{16} \theta \left\{ \begin{array}{l} \text{Diagram 1} + \text{Diagram 2} \\ \text{Diagram 3} + \text{Diagram 4} \end{array} \right\}, \quad (1.27)$$

which includes several new topologies, including the 2-punctured disc, the 1-punctured annulus, and several empty diagrams; namely, the 1-holed torus and the 3-holed sphere. Contributions from the empty diagrams can be interpreted as order  $\tau_2^{-1}$  corrections to the D-instanton action  $-2\pi i \tau$ . However, spacetime supersymmetry implies that the action is not renormalized, and so we expect all higher-order empty diagrams to vanish.

### 1.2.2 INTEGRATION OVER THE D-INSTANTON MODULI

For the case of the single D-instanton, it is possible to handle integration over the moduli before computing any worldsheet diagrams. Let us first turn tackle the effects of the bosonic moduli  $x^\mu$ . Each of the closed string vertex operators depends on the zero mode of  $X^\mu$  as  $e^{ip_i \cdot x}$ , and so  $A_{2 \rightarrow 2}^{(L)}(x, \theta)$  necessarily takes the form  $e^{iP \cdot x} f(\theta)$ , where  $f(\theta)$  is independent of  $x^\mu$ . Integrating over  $x^\mu$  thus gives  $f(\theta)$  multiplied by a momentum-conserving delta function  $i(2\pi)^{10} \delta^{10}(P)$ , where the factor of  $i$  arises from Wick rotation to Lorentzian signature. In this way, integration over the bosonic moduli restores the target space translation symmetry.

Next let us turn our attention to the fermionic moduli. Performing the Berezin integral over  $\theta_\alpha$  gives

$$\int d^{16} \theta e^{-\Delta S_{\text{WS,R}}(\theta)} = \pi^{16} \widehat{Q}_-^{16}, \quad (1.28)$$

where the operator  $\widehat{Q}_-^{16}$  is given by a formal product over the broken supercharges

$$\widehat{Q}_\pm^{16} \equiv \frac{1}{16!} \epsilon_{\alpha_1 \dots \alpha_{16}} \widehat{Q}_{(+\frac{1}{2}), \pm}^{\alpha_1} \widehat{Q}_{(-\frac{1}{2}), \pm}^{\alpha_2} \dots \widehat{Q}_{(+\frac{1}{2}), \pm}^{\alpha_{15}} \widehat{Q}_{(-\frac{1}{2}), \pm}^{\alpha_{16}}, \quad (1.29)$$

with  $\widehat{Q}_{(\pm\frac{1}{2}), \pm}^\alpha$  taking the form of an integrated picture- $(\pm\frac{1}{2})$  supercurrent along the boundary  $\partial\Sigma$ , as defined in Appendix A.1.2. (For brevity we shall drop picture subscript whenever both choices apply.) The RHS of (1.29) is ill-defined due to divergences arising from operator collisions on the boundary. It can be rendered well-defined by separately deforming each of the contours into the bulk, while keeping them away from one another as well as any closed string vertex operators.<sup>7</sup> The expression in (1.29) should thus be interpreted as an ordered product of contours in the bulk, with the contour of a given operator surrounding those of its neighbors on the right, and in turn being surrounded by those of its neighbors on the left. Note that while  $\widehat{Q}_\pm^{16}$  requires a choice of ordering to be well-defined, the individual supercharges anti-commute, and so the operator is ultimately free of possible ordering ambiguities.

Similar to the bosonic moduli, integration over the fermionic moduli is generally expected to restore spacetime supersymmetry. This can be observed in practice by shrinking the contours of  $\widehat{Q}_-^{16}$  on the vertex operators and determining the supersymmetry transformation of the 1-particle states. For simplicity, we shall restrict our attention to the  $\eta_1^8 \eta_3^8$  component of the superamplitude, which corresponds to the axion-dilaton scat-

---

<sup>7</sup>To be precise, in deforming the contour of  $\widehat{Q}_-^\alpha$  from the boundary into the bulk, the operator becomes a generic linear combination of the form  $\widehat{Q}_-^\alpha + a\widehat{Q}_+^\alpha$  with  $a \in \mathbb{C}$ . This is related to the fact that the  $\widehat{Q}_+^\alpha$  uniquely correspond to the supercharges preserved (annihilated) by the D-instanton boundary condition, whereas the “broken supercharges” are a priori ambiguous. We shall find it convenient to set  $a = 0$ , referring to  $\widehat{Q}_-^\alpha$  as the broken supercharges.

tering process  $\delta\bar{\tau}(p_1)\delta\tau(p_2) \rightarrow \delta\bar{\tau}(p_3)\delta\tau(p_4)$ . The action of the supercharge on the axion-dilaton vertex operators  $V_{\delta\tau/\delta\bar{\tau}(p)} \equiv \frac{1}{\sqrt{2}}(V_{\delta\tau_1(p)} \pm iV_{\delta\tau_2(p)})$  is given by

$$\widehat{Q}_{(-\frac{1}{2}),\mp}^\alpha V_{\delta\tau_1(p)} \pm i\widehat{Q}_{(+\frac{1}{2}),\mp}^\alpha V_{\delta\tau_2(p)} = Q_B \Lambda \quad (1.30)$$

for some vertex operator  $\Lambda$ . In other words, the preserved supercharges  $\widehat{Q}_+^\alpha$  annihilate  $V_{\delta\bar{\tau}(p)}$  and the broken supercharges  $\widehat{Q}_-^\alpha$  annihilate  $V_{\delta\tau(p)}$ , up to the addition of BRST-exact terms. (Such terms do not contribute to the unambiguous part of this amplitude, and so we shall ignore them in the following discussion.) Consequently, the non-vanishing configurations are given by eight of the broken supercharges acting on  $V_{\delta\bar{\tau}(p_1)}$  and the other eight on  $V_{\delta\bar{\tau}(p_3)}$ , which converts each of them to  $V_{\delta\tau(p_i)}$  for  $p_i = 1, 3$  together with an overall kinematic factor proportional to  $(p_1 \cdot p_3)^4$ .

In order to determine its precise value, it is simplest to work in the center-of-mass (COM) frame where the momenta of the closed strings are

$$\begin{aligned} p_1^\mu &= E(1, 0, \dots, 0, 1)^\mu, \\ p_2^\mu &= E(1, 0, \dots, 0, -1)^\mu, \\ p_3^\mu &= E(-1, 0, \dots, \sin\theta, \cos\theta)^\mu, \\ p_4^\mu &= E(-1, 0, \dots, -\sin\theta, -\cos\theta)^\mu, \end{aligned} \quad (1.31)$$

where  $2E$  is the COM energy and  $\theta$  is the scattering angle. In this frame, the action of

the super-Poincaré algebra for  $\delta\bar{\tau}(p_1)$  reduces to

$$\{\widehat{Q}_{(\pm\frac{1}{2}),-}^{\alpha}, \widehat{Q}_{(\mp\frac{1}{2}),-}^{\beta}\} V_{\delta\bar{\tau}(p_1)} = 2E \begin{pmatrix} 0_{8\times 8} & 0_{8\times 8} \\ 0_{8\times 8} & 1_{8\times 8} \end{pmatrix}^{\alpha\beta} V_{\delta\bar{\tau}(p_1)}. \quad (1.32)$$

From this, we observe that  $\widehat{Q}_{-}^{9,\dots,16}$  act as lowering operators on the supergraviton multiplet associated to  $\delta\bar{\tau}(p_1)$ , whereas  $\widehat{Q}_{-}^{1,\dots,8}$  annihilate the entire multiplet. This implies that there is a unique nontrivial configuration of supercharges in the COM frame, with  $\widehat{Q}_{-}^{9,\dots,16}$  acting on  $V_{\delta\bar{\tau}(p_1)}$  and  $\widehat{Q}_{-}^{1,\dots,8}$  on  $V_{\delta\bar{\tau}(p_3)}$ , both of which are proportional to  $V_{\delta\tau(p_1)}$ . Using (1.32), we find

$$\widehat{Q}_{(+\frac{1}{2}),-}^9 \widehat{Q}_{(-\frac{1}{2}),-}^{10} \cdots \widehat{Q}_{(+\frac{1}{2}),-}^{15} \widehat{Q}_{(-\frac{1}{2}),-}^{16} V_{\delta\bar{\tau}(p_1)} = 16E^4 V_{\delta\tau(p_1)}. \quad (1.33)$$

In order to determine the action of the broken supercharges on  $V_{\delta\bar{\tau}(p_3)}$ , we perform a  $\theta$  clockwise rotation in the 89 plane combined with a time reversal such that  $p_3^{\mu} \rightarrow p_3^{\mu'} = p_1^{\mu}$ . As chiral spinors, the supercharges transform under this rotation as

$$\begin{pmatrix} \widehat{Q}_{(\pm\frac{1}{2}),-}^{\alpha} \\ \widehat{Q}_{(\pm\frac{1}{2}),-}^{\alpha+8} \end{pmatrix} \rightarrow \begin{pmatrix} \widehat{Q}_{(\pm\frac{1}{2}),-}^{\alpha'} \\ \widehat{Q}_{(\pm\frac{1}{2}),-}^{\alpha'+8} \end{pmatrix} = \begin{pmatrix} \cos(\frac{\theta}{2}) & -\sin(\frac{\theta}{2}) \\ \sin(\frac{\theta}{2}) & \cos(\frac{\theta}{2}) \end{pmatrix} \begin{pmatrix} \widehat{Q}_{(\pm\frac{1}{2}),-}^{\alpha} \\ \widehat{Q}_{(\pm\frac{1}{2}),-}^{\alpha+8} \end{pmatrix}, \quad \alpha = 1, \dots, 8. \quad (1.34)$$

The supercharges in the rotated frame obey the same commutation relations as in (1.32) up to an irrelevant factor of  $i$ , with  $\delta\bar{\tau}(p_1)$  replaced by  $\delta\bar{\tau}(p_3)$ . This implies that the rotated supercharges  $\widehat{Q}_{-}^{\alpha'=9,\dots,16}$  act as lowering operators on  $\delta\bar{\tau}(p_3)$ , while  $\widehat{Q}_{-}^{\alpha'=1,\dots,8}$  annihilate it. The original supercharges are given by linear combinations of the rotated ones,

and so using (the inverse of) (1.34) we have

$$\widehat{Q}_{(+\frac{1}{2}),-}^1 \widehat{Q}_{(-\frac{1}{2}),-}^2 \cdots \widehat{Q}_{(+\frac{1}{2}),-}^7 \widehat{Q}_{(-\frac{1}{2}),-}^8 V_{\delta\bar{\tau}(p_3)} = 16E^4 \cos^8\left(\frac{\theta}{2}\right) V_{\delta\tau(p_3)}. \quad (1.35)$$

Using (1.32) and (1.34), we find the desired result for the action of  $\widehat{Q}_-^{16}$  on the vertex operators, namely

$$\widehat{Q}_-^{16} (V_{\delta\bar{\tau}(p_1)} V_{\delta\tau(p_2)} V_{\delta\bar{\tau}(p_3)} V_{\delta\tau(p_4)}) = t^4 V_{\delta\tau(p_1)} V_{\delta\tau(p_2)} V_{\delta\tau(p_3)} V_{\delta\tau(p_4)}, \quad (1.36)$$

where  $256E^8 \cos^8(\frac{\theta}{2})^8$  has been replaced by the manifestly Lorentz-invariant quantity  $t^4 = (p_1 + p_3)^8$ . In arriving at this expression, we have exploited the fact that our argument does not rely on the ordering of the supercharges; consequently, the different orderings contribute a factor of  $16!$  that cancels a similar factor in the numerator of (1.29). We can identify the  $t^4$  factor in (1.36) as precisely the  $\eta_1^8 \eta_3^8$  component of the superamplitude contained in the supersymmetry factor

$$Q_+^{16} = \eta_1^8 \eta_2^8 s^4 + \eta_1^8 \eta_3^8 t^4 + \eta_1^8 \eta_4^8 u^4 + \cdots, \quad (1.37)$$

where  $\cdots$  captures contributions from other states in the multiplet and

$$\eta_i^8 \equiv \epsilon_{a_1 \cdots a_8} \eta_i^{a_1} \cdots \eta_i^{a_8}. \quad (1.38)$$

Generalizing our results from integration over the bosonic moduli and fermionic moduli in (1.36), we find that the D-instanton contribution to the superamplitude in (1.24)

reduces to<sup>8</sup>

$$\mathcal{A}_{2 \rightarrow 2}^{(1,0)} = i(2\pi)^{10} \delta^{10}(P) Q_+^{16} \pi^{16} \mathcal{N}_D e^{2\pi i \tau} \sum_{L=0}^{\infty} \tau_2^{-L} A_{2 \rightarrow 2}^{(L)}. \quad (1.39)$$

Here,  $A_{2 \rightarrow 2}^{(L)}$  captures D-instanton contributions to the *axion-dilaton* amplitude from world-sheet diagrams with Euler characteristic  $-L$  (with the empty disc and annulus excluded), and with fixed boundary conditions for  $X^\mu$  such that  $x^\mu = 0$ . In other words, the D-instanton contribution to the entire superamplitude is captured by diagrams involving only the axion-dilaton states  $\delta\tau(p_i)$  with vertex operators  $V_{\delta\tau(p_i)}$ , supplemented by the momentum-conserving delta function  $i(2\pi)^{10} \delta^{10}(P)$  as well as an overall kinematic factor  $Q_+^{16}$  corresponding to conservation of super-momentum.

### 1.2.3 LEADING ORDER CONTRIBUTION

We now compute the leading order contribution from a single D-instanton to the  $2 \rightarrow 2$  scattering amplitude. Unless otherwise specified, we work in units where  $\alpha' = 1$ . Following (1.39) with  $L = 0$ , it is given by

$$\mathcal{A}_{2 \rightarrow 2}^{(1,0)} \Big|_{\text{LO}} = i(2\pi)^{10} \delta^{10}(P) Q_+^{16} e^{2\pi i \tau} \mathcal{N}_D \begin{array}{c} \textcircled{\times} \textcircled{\times} \textcircled{\times} \textcircled{\times} \end{array}. \quad (1.40)$$

Consider the disc 1-point amplitude  $\mathcal{A}_{\delta\tau}^{D^2}$  for  $\delta\tau$  with boundary lying on the D-instanton.

The  $PSL(2, \mathbb{R})$  gauge redundancy can be used to fix the closed string puncture to  $z = i$ .

Without any additional closed/open string insertions, there is a residual  $U(1)$  that rotates

---

<sup>8</sup>We emphasize that although this result was derived for a specific component of the 4-point superamplitude, the appearance of  $\widehat{Q}_-^{16}$  indicates that the same type of argument should hold for any choice of asymptotic states. That is, all of the vertex operators are converted to  $V_{\delta\tau(p_i)}$ , with the kinematic factor  $t^4$  corresponding to the  $\eta_1^8 \eta_3^8$  component replaced by the analogous quantity in  $Q_+^{16}$  (1.37).

$D^2$  around its origin, i.e. leaves the closed string puncture at  $z = i$  invariant. It can be accounted for by dividing by the volume of the gauge group  $\text{Vol}(U(1)) = 2\pi$ , whose normalization is unambiguous with respect to the open-closed disc 2-point amplitude. It is also necessary to insert  $c_0$  to soak up the remaining zero mode of  $c(z)$  in the  $bc$  path integral. Finally, due to the picture anomaly of the disc, the open/closed insertions must have a total picture of  $-2$  (holomorphic and antiholomorphic picture are not separately conserved).

First consider the contribution of the dilaton. We shall work with the NSNS vertex operator in picture  $(-1, -1)$ . Using the doubling trick, we can replace all of the antiholomorphic operators in the upper half plane with their holomorphic counterparts at the reflected point in the lower half plane. In doing so, we must also include any phase factors present in the boundary conditions relating the holomorphic and antiholomorphic operators. For the NSNS vertex operator, this gives an overall factor of  $-1$  from the replacement  $\tilde{\psi}^\mu(-i) \rightarrow -\psi^\mu(-i)$ . It follows that disc diagram is

$$-\frac{g_c C_{D^2}}{2\pi} e_{\mu\nu}(p) \left\langle \partial c c e^{-\phi} \psi^\mu e^{ip \cdot X_L}(i) c e^{-\phi} \psi^\nu e^{-ip \cdot X_L}(-i) \right\rangle_{\text{chiral}} = \frac{\sqrt{2} g_c C_{D^2}}{\pi}, \quad (1.41)$$

where  $g_c$  is the closed string coupling, and  $C_{D^2}$  is a constant multiplying all disc correlators that cannot be fixed purely from CFT considerations. Here,  $\langle \cdot \rangle_{\text{chiral}}$  stands for the  $S^2$  correlator evaluated in the chiral sector of the CFT, i.e. only for holomorphic operators.

It is normalized such that

$$\langle c(z_1) c(z_2) c(z_3) e^{-2\phi}(z) \rangle_{\text{chiral}} = z_{12} z_{13} z_{23}. \quad (1.42)$$



where  $X_L^\mu$  is defined as the holomorphic part of  $X^\mu$  with the zero mode removed. In writing the above expression, we have used  $\eta^{\mu\nu}e_{\mu\nu}(p) = 2\sqrt{2}$ , which follows from our normalization conventions for the dilaton polarization tensor in (A.28).

Next we turn our attention to the contribution of the axion. Strictly speaking, it is ill-defined since the RR vertex operator appears in the  $(-\frac{1}{2}, -\frac{1}{2})$  picture; even so, there are various ways to assign it a definitive value. For instance, in certain circumstances one can define an “inverse” PCO that carries picture  $-1$ . We shall take a more natural approach from the on-shell perspective as follows. Consider the disc 2-point diagram for one closed string insertion with momentum  $p^\mu$  as well as a bosonic collective coordinate  $\delta x^\mu$ . The vertex operator for  $\delta x^\mu$  is proportional to  $c\partial X^\mu$  in the 0-picture, and so the 2-point diagram necessarily factorizes into a product of the closed string 1-point diagram together with a universal kinematic factor proportional to  $p^\mu$ . The axion 1-point diagram can then be *defined* as the 2-point diagram for  $\delta\tau_1(p)$  divided by this factor.

For instance, consider the 2-point diagram for  $\delta\tau_2(p)$ . The results do not depend on the choice of picture, and so we work with the NSNS vertex operator in the  $(0, -1)$  picture and  $\delta x^\mu$  in the  $(-1)$ -picture, given by  $ce^{-\phi}\psi^\mu$ . The residual  $PSL(2, \mathbb{R})$  gauge redundancy can be used to fix the closed string vertex operator to  $z = i$  and the open string vertex operator to  $z = 0$ . The doubling trick in this case gives the same factor of  $-1$  from the antiholomorphic fermion. It follows that the diagram reads

$$\begin{aligned} & \sqrt{2}g_c C_{D^2} e_{\sigma\rho}(p) \left\langle ce^{-\phi}\psi^\mu(0) c(i\partial X_L^\sigma + \frac{1}{2}p \cdot \psi\psi^\sigma)e^{ip \cdot X_L}(i) ce^{-\phi}\psi^\rho e^{-ip \cdot X_L}(-i) \right\rangle_{\text{chiral}} \\ & = 2g_c C_{D^2} p^\mu. \end{aligned} \quad (1.43)$$

In evaluating the correlator, we made use of the fact that transversality  $p^\mu e_{\mu\nu}(p) = 0$  together with the mass-shell constraint  $p^2 = 0$  imply that the  $X^\mu$  CFT does not contribute. Comparing this to 1-point diagram in (1.41), we find that the kinematic factor is

$$\sqrt{2\pi}p^\mu. \quad (1.44)$$

Now let us return to the case of the axion, which we take to be in the  $(-\frac{1}{2}, -\frac{1}{2})$ -picture. The vertex operator insertions are arranged in the same fashion as before. Here, the doubling trick gives a factor of  $-i$  from the replacement  $\tilde{S}^\beta(i) \rightarrow -iS^\beta(-i)$ , and so the diagram yields

$$\begin{aligned} ig_c C_{D^2} f_{\alpha\beta}(p) \left\langle ce^{-\phi} \psi^\mu(0) ce^{-\frac{1}{2}\phi} S^\alpha e^{ip \cdot X_L}(i) ce^{-\frac{1}{2}\phi} S^\beta e^{-ip \cdot X_L}(-i) \right\rangle_{\text{chiral}} \\ = 2ig_c C_{D^2} p^\mu. \end{aligned} \quad (1.45)$$

Note that the axion polarization tensor contributes through  $\text{tr}(\not{p}\gamma^\mu) = 16p^\mu$ . From this, we can divide by  $\sqrt{2\pi}p^\mu$  to extract the desired disc 1-point diagram

$$i \frac{\sqrt{2}g_c C_{D^2}}{\pi}. \quad (1.46)$$

The disc 1-point diagram for the axion-dilaton can be determined from  $V_{\delta\tau} = \frac{1}{\sqrt{2}}(V_{\delta\tau_1} + iV_{\delta\tau_2})$ . Using the disc 1-point results from (1.41) and (1.46), we find that the diagram takes the form

$$\mathcal{A}_{\delta\tau}^{D^2} = i \frac{2\sqrt{2}g_c C_{D^2}}{\pi}. \quad (1.47)$$

The leading contribution of a single D-instanton to the 4-point amplitude follows from

a straightforward application of (1.39) together with four copies of the disc 1-point diagram (1.47). This involves several constants, which can be related to Newton's coupling  $\kappa$  as well as the dilaton expectation value  $\tau_2^{-1}$ . The disc constant  $C_{D^2}$ , which is proportional to the tension of the D-instanton, can be fixed by unitarity of the perturbative string S-matrix. In our conventions, it reads [3, 52]

$$C_{D^2} = 4\pi^3 \tau_2. \quad (1.48)$$

Meanwhile, Newton's constant and the dilaton VEV are related to the closed string coupling by [52]

$$\kappa^2 = (2\pi g_c)^2 = \frac{1}{2} (2\pi)^7 \alpha'^4 \tau_2^{-2}. \quad (1.49)$$

Finally, we need the value of the moduli space measure

$$\mathcal{N}_D = 2^{-18} \pi^{-26} \alpha'^{-1} \tau_2^{-\frac{7}{2}}, \quad (1.50)$$

as formally determined by the exponential of the empty annulus diagram. While inaccessible to the on-shell approach, it can be derived from first principles in the string field theory formalism. (This was first done in [32] and was shown to be consistent with the expectation from S-duality.) It follows that the contribution to the 2→2 amplitude is

$$\mathcal{A}_{2 \rightarrow 2}^{(1,0)} \Big|_{\text{LO}} = i(2\pi)^{10} \delta^{10}(P) Q_+^{16} \frac{\pi \alpha'^3 \kappa^2}{16} e^{2\pi i \tau} \tau_2^{-\frac{3}{2}}. \quad (1.51)$$

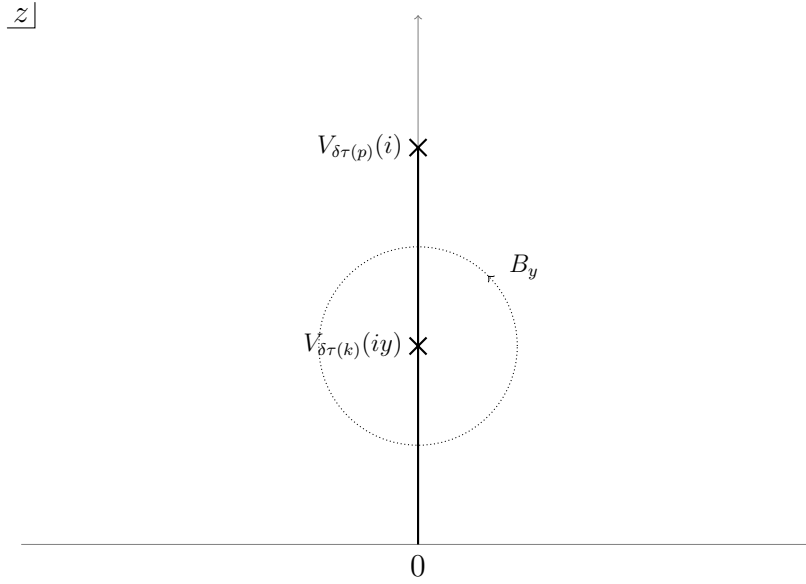


**Figure 1.1:** The two-punctured disc represented as the upper half plane with global coordinate  $z$ . One vertex operator  $V_{\delta\tau(p)}$  is fixed at position  $z = i$  while the second vertex operator  $V_{\delta\tau(k)}$  is fixed at position  $z = iy$ , integrating over the modulus  $y \in [0, 1]$ . The  $b$  ghost contour  $B_y$  surrounds the integrated vertex operator as drawn.

#### 1.2.4 NEXT-TO-LEADING ORDER CONTRIBUTION

The next-to-leading order contribution from a single D-instanton to the  $2 \rightarrow 2$  scattering amplitude consists of the following worldsheet diagrams,

$$\mathcal{A}_{2 \rightarrow 2}^{(1,0)} \Big|_{\text{NLO}} = i(2\pi)^{10} \delta^{10}(P) Q_+^{16} e^{2\pi i\tau} \mathcal{N}_D \left\{ \begin{array}{l} \text{Diagram 1} + \text{Diagram 2} \\ \text{Diagram 3} + \text{Diagram 4} \end{array} \right\}, \quad (1.52)$$

which includes a sum over distinct permutations of the on-shell closed string vertex operator insertions  $V_{\delta\tau(p_i)}$  with  $i = 1, \dots, 4$ . Out of these new topologies, only the disc 2-point diagram  $\mathcal{A}_{\delta\tau\delta\tau}^{D^2}$  gives nonvanishing contribution. (This is demonstrated explicitly for the annulus 1-point diagram in Appendix A.3).

Consider the disc diagram containing two insertions of  $\delta\tau$ . The residual  $PSL(2, \mathbb{R})$

gauge redundancy can be used to fix one closed string puncture to  $z = i$  and the other to  $z = iy$  with  $0 \leq y \leq 1$ , as shown in Figure 1.1. Under this choice, the diagram reads

$$\mathcal{A}_{\delta\tau(p)\delta\tau(k)}^{D^2} = \int_0^1 dy \left\langle B_y V_{\delta\tau(p)}^{(-1)}(i, -i) V_{\delta\tau(k)}^{(-1)}(iy, -iy) \right\rangle_{x^\mu=0}^{D^2}. \quad (1.53)$$

where each vertex operator is taken to have total picture  $-1$ . In particular, we work with the NSNS vertex operator in picture  $(0, -1)$  and the RR vertex operator in picture  $(-\frac{1}{2}, -\frac{1}{2})$ . The  $b$  ghost insertion  $B_y$  accompanying the modulus  $y$  takes the form

$$B_y = \frac{1}{2\pi} \oint_{C_{iy}} \left( dz b(z) + d\bar{z} \tilde{b}(\bar{z}) \right), \quad (1.54)$$

where the contour  $C_{iy}$  surrounds the puncture at  $z = iy$ . Each vertex operator takes the form  $V_{\delta\tau(p)} = c\tilde{c}U_{\delta\tau(p)}$  plus terms with nonzero  $\eta, \xi$  charge that do not contribute to the amplitude. It follows that the contribution of the  $b, c$  ghost system is

$$\langle B_y c\tilde{c}(i, -i) c\tilde{c}(iy, -iy) \rangle_0^{D^2} = -4(1 - y^2), \quad (1.55)$$

and so the amplitude reduces to

$$\mathcal{A}_{\delta\tau(p)\delta\tau(k)}^{D^2} = -4 \int_0^1 dy (1 - y^2) \langle c_{-1}c_0c_1 U_{\delta\tau}(i, -i) U_{\delta\tau}(iy, -iy) \rangle_{x^\mu=0}^{D^2}, \quad (1.56)$$

where the inclusion of  $c_{-1}c_0c_1$  ensures that the correlator evaluated in the full matter+ghost CFT is nonzero.

We first evaluate the amplitude for two axions, which contribute to (1.56) as

$$4g_c^2 f_{\alpha\beta}^{(0)}(p) f_{\gamma\delta}^{(0)}(k) \int_0^1 dy (1-y^2) \left\langle c_{-1} c_0 c_1 e^{-\frac{1}{2}\phi} S^\alpha e^{ip \cdot X_L(i)} e^{-\frac{1}{2}\phi} S^\beta e^{-ip \cdot X_L(-i)} e^{-\frac{1}{2}\phi} S^\gamma e^{ik \cdot X_L(iy)} e^{-\frac{1}{2}\phi} S^\delta e^{-ik \cdot X_L(-iy)} \right\rangle_{\text{chiral}}, \quad (1.57)$$

where the doubling trick provides an overall factor of  $-1$  from the two antiholomorphic spin fields (A.42). This correlator can be evaluated using (A.53) together with Wick contractions for the free fields in the  $X^\mu$  CFT, which gives

$$-\frac{1}{2} g_c^2 C_{D^2} \int_0^1 dy \left( \frac{1-y}{1+y} \right)^{p \cdot k} \left[ \frac{\text{tr} \{f(p) \gamma^\mu\} \text{tr} \{f^{(0)}(k) \gamma_\mu\}}{y} + \frac{2 \text{tr} \{f^{(0)}(p) \gamma^\mu [f^{(0)}(k) + f^{(0)}(k)^T] \gamma_\mu\}}{y(1-y^2)} + \frac{2 \text{tr} \{f^{(0)}(p) \gamma^\mu [f^{(0)}(k) - f^{(0)}(k)^T] \gamma_\mu\}}{(1-y^2)} \right]. \quad (1.58)$$

After specializing to the axion polarization tensor (A.29), we are left with

$$-\frac{1}{64} g_c^2 C_{D^2} \int_0^1 dy \left( \frac{1-y}{1+y} \right)^{p \cdot k} \left( \frac{4 \text{tr} (\not{p} \gamma^\mu \not{k} \gamma_\mu)}{y(1-y^2)} + \frac{\text{tr} (\not{p} \gamma^\mu) \text{tr} (\not{k} \gamma_\mu)}{y} \right) = 4g_c^2 C_{D^2} I(p \cdot k), \quad (1.59)$$

where we have introduced the worldsheet integral

$$I(s) \equiv s \int_0^1 dy \frac{(1+y^2)(1-y)^{s-1}}{y(1+y)^{s+1}}. \quad (1.60)$$

Next consider the contribution from one axion and one dilaton to (1.56), as given by

$$4\sqrt{2}g_c^2 C_{D^2} e_{\mu\nu}(p) f_{\alpha\beta}^{(0)}(k) \int_0^1 dy (1-y)^2 \left\langle c_{-1} c_0 c_1 \left( i\partial X_L^\mu + \frac{1}{2} p \cdot \psi \psi^\mu \right) e^{ip \cdot X_L(i)} \right. \\ \left. \times e^{-\phi} \psi^\nu e^{-ip \cdot X_L(-i)} e^{-\frac{1}{2}\phi} S^\alpha e^{ik \cdot X_L(iy)} e^{-\frac{1}{2}\phi} S^\beta e^{-ik \cdot X_L(-iy)} \right\rangle_{\text{chiral}}. \quad (1.61)$$

The correlator can be simplified by applying the Ward identities for the translation current  $\partial X_L^\mu$  and the Lorentz current  $\psi^\mu \psi^\nu$ , which give

$$4\sqrt{2}g_c^2 C_{D^2} e_{\mu\nu}(p) f_{\alpha\beta}^{(0)}(k) \int_0^1 dy (1-y)^2 \left( M_\sigma^{\mu\nu} \delta_\gamma^\alpha \delta_\delta^\beta + \delta_\sigma^\nu N_{\gamma\delta}^{\mu;\alpha\beta} \right) \\ \times \left\langle c_{-1} c_0 c_1 e^{ip \cdot X_L(i)} e^{-\phi} \psi^\sigma e^{-ip \cdot X_L(-i)} \right. \\ \left. e^{-\frac{1}{2}\phi} S^\gamma e^{ik \cdot X_L(iy)} e^{-\frac{1}{2}\phi} S^\delta e^{-ik \cdot X_L(-iy)} \right\rangle_{\text{chiral}}, \quad (1.62)$$

where  $M$  and  $N$  are  $c$ -number tensor structures arising from the Poincaré algebra,

$$M_\sigma^{\mu\nu} = \frac{1}{2} \left( \frac{k^\mu \delta_\sigma^\nu}{i-iy} + \frac{-k^\mu \delta_\sigma^\nu}{i+iy} + \frac{\eta^{\mu\nu} p_\sigma - p^\nu \delta_\sigma^\mu}{2i} \right), \\ N_{\gamma\delta}^{\mu;\alpha\beta} = -\frac{1}{4} \left( \frac{p_\sigma (\gamma^{\sigma\mu})^\alpha_\gamma \delta_\delta^\beta}{i-iy} + \frac{p_\sigma (\gamma^{\sigma\mu})^\beta_\delta \delta_\gamma^\alpha}{i+iy} \right). \quad (1.63)$$

The resulting correlator in (1.62) is readily evaluated using (A.52), from which it follows

that the tensor structures simply to give

$$2\sqrt{2}g_c^2 C_{D^2} e_{\mu\nu}(p) f_{\alpha\beta}^{(0)}(k) \int_0^1 dy \left( \frac{1-y}{1+y} \right)^{p \cdot k} \left( \not{p}^{\alpha\beta} \eta^{\mu\nu} \frac{1+y^2}{y-y^3} - 4k^\mu (\gamma^\nu)^{\alpha\beta} \frac{1}{1-y^2} \right). \quad (1.64)$$

Specializing to the axion and dilaton polarization tensors, we are left with

$$4g_c^2 C_{D^2} \left( I(p \cdot k) - \frac{e_{\mu\nu}(p)k^\mu k^\nu}{\sqrt{2}p \cdot k} \right). \quad (1.65)$$

Lastly, consider the contribution of two dilatons to (1.56)

$$\begin{aligned} & -8g_c^2 C_{D^2} e_{\mu\nu}(p) e_{\sigma\rho}(k) \\ & \times \int_0^1 dy (1-y)^2 \left\langle c_{-1} c_0 c_1 (i\partial X_L^\mu + \frac{1}{2}p \cdot \psi \psi^\mu) e^{ip \cdot X_L}(i) e^{-\phi} \psi^\nu e^{-ip \cdot X_L}(-i) \right. \\ & \left. (i\partial X_L^\rho + \frac{1}{2}k \cdot \psi \psi^\rho) e^{ik \cdot X_L}(iy) e^{-\phi} \psi^\sigma e^{-ik \cdot X_L}(-iy) \right\rangle_{\text{chiral}}. \end{aligned} \quad (1.66)$$

Carrying out the appropriate Wick contractions gives

$$\begin{aligned} & -4g_c^2 C_{D^2} (p \cdot k) \int_0^1 dy \frac{1}{y} \left( \frac{1-y}{1+y} \right)^{p \cdot k - 1} \\ & + 4\sqrt{2}g_c^2 C_{D^2} (e_{\mu\nu}(p)k^\mu k^\nu + e_{\sigma\rho}(k)p^\sigma p^\rho) \int_0^1 dy \frac{(1-y)^{p \cdot k - 1}}{(1+y)^{p \cdot k + 1}} \\ & + 4g_c^2 C_{D^2} e_{\mu\nu}(p) e^{\mu\nu}(k) \int_0^1 dy \frac{\partial}{\partial y} \left( \frac{y(1+y)^{p \cdot k - 2}}{(1-y)^{p \cdot k}} \right). \end{aligned} \quad (1.67)$$

The form of the integral in the first line can be massaged to give  $I(p \cdot k) + 1$ , while the other integrals can be evaluated directly, with the one in the third line vanishing altogether. After specializing to the dilaton polarization tensor, the contribution reduces to

$$-4g_c^2 C_{D^2} \left( I(p \cdot k) + 1 - \frac{e_{\sigma\rho}(p)k^\sigma k^\rho + e_{\sigma\rho}(k)p^\sigma p^\rho}{\sqrt{2}p \cdot k} \right). \quad (1.68)$$

Using (1.59), (1.68), and (1.65), it follows that the axion-dilaton disc 2-point amplitude



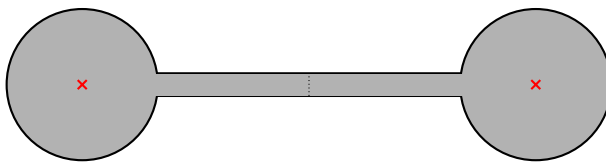


**Figure 1.2:** The limit  $y \rightarrow 0$ , where the 2-punctured disc degenerates into two 1-punctured discs glued together by an infinitely long strip.

is

$$\mathcal{A}_{\delta\tau(p)\delta\tau(k)}^{D^2} = 2g_c^2 C_{D^2} \left( 4I(p \cdot k) + 1 - 2 \frac{e_{\sigma\rho}(p)k^\sigma k^\rho + e_{\sigma\rho}(k)p^\sigma p^\rho}{\sqrt{2}p \cdot k} \right). \quad (1.69)$$

The integral  $I(p \cdot k)$  as defined in (1.60) diverges logarithmically near the boundary of moduli space  $y = 0$  as

$$p \cdot k \int_0 \frac{dy}{y}, \quad (1.70)$$

which occurs when the disc with two bulk punctures degenerates into two separate discs, each with a single bulk puncture, connected via an infinitely long strip, as shown in Figure 1.2. As mentioned in the Introduction, this limit corresponds to intermediate “massless” open string states with  $L_0 = 0$ , which formally contribute  $\infty$  to the amplitude. In the SFT approach, such massless states are forbidden from propagating, and so the amplitude is manifestly finite. In the naive on-shell prescription, such divergences can be tamed by implementing a cutoff  $\epsilon > 0$ . The regularized integral then evaluates to

$$\begin{aligned} I(p \cdot k) &\rightarrow p \cdot k \int_\epsilon^1 dy \frac{(1+y^2)(1-y)^{p \cdot k - 1}}{y(1+y)^{p \cdot k + 1}} \\ &= -p \cdot k \left( \psi\left(1 + \frac{1}{2}p \cdot k\right) + \gamma + \log(4\epsilon) \right) + 1, \end{aligned} \quad (1.71)$$

where  $\gamma = 0.577\dots$  is the Euler–Mascheroni constant and  $\psi(z) = \partial_z \log \Gamma(z)$  is the

digamma function. From this, it follows that the disc 2-point amplitude is

$$\mathcal{A}_{\delta\tau(p)\delta\tau(k)}^{D^2} = 2g_c^2 C_{D^2} \left[ 5 - \sqrt{2} \frac{e_{\sigma\rho}(p)k^\sigma k^\rho + e_{\sigma\rho}(k)p^\sigma p^\rho}{p \cdot k} - 4\alpha'(p \cdot k) \left( \psi(1 + \frac{1}{2}p \cdot k) + \gamma + \log(4\epsilon) \right) \right]. \quad (1.72)$$

We now have all the ingredients necessary to assemble the next-to-leading order D-instanton contribution to the 4-point amplitude. To find the contribution of the disc 2-point diagram, we are instructed to sum over distinct pairs of vertex operators  $V_{\delta\tau(p_i)}V_{\delta\tau(p_j)}$  with  $1 \leq i < j \leq 4$  and multiply the result by two copies of the disc 1-point diagram (1.47). Using momentum conservation, it follows that

$$\sum_{1 \leq i < j \leq 4} p_i \cdot p_j = 0, \quad (1.73)$$

$$\sum_{1 \leq i < j \leq 4} \frac{e_{\mu\nu}(p_i)p_j^\mu p_j^\nu + e_{\mu\nu}(p_j)p_i^\mu p_i^\nu}{p_i \cdot p_j} = \sqrt{8}.$$

and so the final amplitude is independent of the dilaton polarization tensor, as expected.

The annulus 1-point diagram vanishes, as do the contributions from the 1-holed torus and 3-holed sphere. Consequently, the 4-point amplitude is given by

$$\mathcal{A}_{2 \rightarrow 2}^{(1,0)} \Big|_{\text{NLO}} = i(2\pi)^{10} \delta^{10}(P) Q_+^{16} \frac{\alpha'^3 \kappa^2}{32} F(\alpha' s, \alpha' t) e^{2\pi i \tau} \tau_2^{-\frac{5}{2}}, \quad (1.74)$$

where

$$F(\alpha' s, \alpha' t) \equiv 32C_1 - \alpha' s \psi(1 - \frac{\alpha' s}{4}) - \alpha' t \psi(1 - \frac{\alpha' t}{4}) - \alpha' u \psi(1 - \frac{\alpha' u}{4}). \quad (1.75)$$

In writing this result, we have grouped the constant terms which contribute at leading order in the momentum expansion into  $32C_1$ . As we will discuss in the next section, such terms are ambiguous in the on-shell approach.

### 1.2.5 AN AMBIGUITY AND ITS TENSION WITH SUPERSYMMETRY

In general, D-instanton amplitudes as computed from the on-shell prescription suffer from ambiguities related to the choice of regularization scheme. This is to be contrasted with perturbative string amplitudes for on-shell external states which, barring any spurious singularities, are independent of such data. For our choice of regularization scheme, these ambiguities partially manifest themselves in the choice of PCO locations. Normally, amplitudes with different arrangement of PCOs can differ by at most a boundary term in the worldsheet moduli space. However, it is precisely these types of boundary terms which are divergent in the naive formulation of D-instanton perturbation theory, and so can lead to regulator-dependent discrepancies.

For the specific amplitudes under consideration, this ambiguity manifests itself as an unknown momentum-independent constant at next-to-leading order in  $\tau_2^{-1}$ , as denoted by  $C_1$ . As we shall soon see, this ambiguity is in tension with spacetime supersymmetry. One approach to mend this issue is to abandon the on-shell prescription altogether, as string field theory is free of such ambiguities. Instead of computing any off-shell quantities directly, we shall take a slightly more modest approach and simply demand that the physical amplitude respects supersymmetry. This turns out to be sufficient to pin down the exact value of  $C_1$ .

The relevant object of study here is the coefficient  $f_0(\tau, \bar{\tau})$  multiplying the  $R^4$  vertex.<sup>9</sup> As mentioned in the Introduction, this coefficient, as well as those of  $D^4 R^4$  and  $D^6 R^4$ , is constrained by supersymmetry to obey a second order differential equation on the moduli space of vacua. A particularly elegant method of deriving these constraints can be found in [48], whose logic we briefly summarize as follows. The basic idea is to analyze the constraints imposed by supersymmetry and unitarity on the factorization of supergraviton scattering amplitudes. For the  $R^4$  coefficient, the relevant object of study is the 6-point amplitude. Dimensional analysis implies that it can only factorize through a single  $R^4$  vertex and a pair of cubic supergravity vertices. The  $\delta\tau\delta\bar{\tau}R^4$  coupling can then be extracted by taking the soft limit where the momenta of  $\delta\tau$  and  $\delta\bar{\tau}$  are taken to zero. From this it follows that the coupling is necessarily proportional to  $\tau_2^2\partial_\tau\partial_{\bar{\tau}}f_0$ , where the factor of  $\tau_2^2$  arises from the normalization of the axion-dilaton kinetic term. Supersymmetry dictates that there is no independent  $\delta\tau\delta\bar{\tau}R^4$  coupling, and so it must be proportional to  $f_0$  itself. The constant of proportionality can then be fixed by comparing with the  $R^4$  coupling in any supersymmetric theory, such as type IIB string theory, which results in the differential equation [48]

$$\left(\tau_2^2\partial_\tau\partial_{\bar{\tau}} - \frac{3}{16}\right)f_0(\tau, \bar{\tau}) = 0. \quad (1.76)$$

In order to understand the implications of (1.76) for our D-instanton results, it is first necessary to recast the amplitudes in a manifestly  $SL(2, \mathbb{Z})$  invariant form, which can be

---

<sup>9</sup>Recall that  $f_i(\tau, \bar{\tau})$  enter into the expansion of  $M(s, t; \tau, \bar{\tau})$ , defined as the ratio of  $\mathcal{A}_{2\rightarrow 2}$  to the supergravity contribution  $\mathcal{A}_{2\rightarrow 2}^{\text{SUGRA}}$ .

accomplished by factoring out the type IIB supergravity contribution

$$\mathcal{A}_{2 \rightarrow 2}^{\text{SUGRA}} = i(2\pi)^{10} \delta^{10}(P) Q_+^{16} \frac{\kappa^2}{stu} \tau_2^{-\frac{3}{2}} \quad (1.77)$$

and working with the Mandelstam variables in units of the ten-dimensional Planck mass

$$\alpha' s = \underline{s} \tau_2^{\frac{1}{2}}, \quad \alpha' t = \underline{t} \tau_2^{\frac{1}{2}}, \quad \alpha' u = \underline{u} \tau_2^{\frac{1}{2}}. \quad (1.78)$$

Upon inspecting (1.51), we find that the leading-order contribution of a single D-instanton is

$$\frac{1}{\alpha'^3 stu} e^{2\pi i \tau} M_0^{(1,0)}(\alpha' s, \alpha' t) = \frac{\pi}{16}. \quad (1.79)$$

Similarly, from (1.74) we have that the next-to-leading order contribution is given by

$$\frac{1}{\alpha'^3 stu} M_1^{(1,0)}(\alpha' s, \alpha' t) = \frac{1}{32} F(\alpha' s, \alpha' t). \quad (1.80)$$

Together, the D-instanton amplitudes contribute to  $f_0$  via the momentum-independent terms in (1.79) and (1.80), i.e.

$$e^{2\pi i \tau} \left( \frac{\pi}{16} + C_1 \tau_2^{-1} \right). \quad (1.81)$$

Plugging this into (1.76) then fixes the value of the constant to

$$C_1 = \frac{3}{256}. \quad (1.82)$$

## COMPARISON AGAINST S-DUALITY

The next-to-leading D-instanton amplitude in (1.80) admits an expansion in powers of momenta given by

$$\frac{1}{\alpha'^3 stu} M_1^{(1,0)}(\alpha' s, \alpha' t) = \frac{3}{256} + \sum_{p=2}^{\infty} \frac{\zeta(p)}{2^{3+2p}} \tau_2^{\frac{p}{2}} (\underline{s}^p + \underline{t}^p + \underline{u}^p), \quad (1.83)$$

where we have used the value of  $C_1 = \frac{3}{256}$ , as determined by supersymmetry. Unlike the constant term, the momentum-dependent terms in the sum are unambiguous and represent the leading-order single D-instanton contribution to higher-order vertices of the form  $D^{2p}R^4$ , thus serving as a nontrivial test of S-duality. We can carry out such a test explicitly for the supersymmetry-protected terms, namely  $D^4R^4$  and  $D^6R^4$ , whose coefficients admit weak-coupling expansions of the form

$$\begin{aligned} 2^{11} f_4(\tau, \bar{\tau}) &= 2\zeta(5)\tau_2^{\frac{3}{2}} + \frac{4\pi^4}{135}\tau_2^{-\frac{3}{2}} + (e^{2\pi i\tau} + e^{-2\pi i\tau}) (16\zeta(2) + O(\tau_2^{-1})) + O(e^{-4\pi\tau_2}), \\ 2^{12} f_6(\tau, \bar{\tau}) &= \frac{2\zeta(3)^2}{3}\tau_2^3 + \frac{4\zeta(2)\zeta(3)}{3}\tau_2 + \frac{8\zeta(2)^2}{5}\tau_2^{-1} + \frac{4\zeta(6)}{28}\tau_2^{-3} \\ &\quad + (e^{2\pi i\tau} + e^{-2\pi i\tau})(8\zeta(3)\tau_2^{\frac{1}{2}} + O(1)) - e^{-4\pi\tau_2} (2\tau_2^{-2} + O(\tau_2^{-3})) \\ &\quad + O(e^{-6\pi\tau_2}). \end{aligned} \quad (1.84)$$

The leading order D-instanton contribution to these vertices, which arises at next-to-leading order in the open string loop expansion, can be identified as the leading terms multiplying  $e^{2\pi i\tau}$ , i.e.

$$f_4^{(1,0)}(\tau, \bar{\tau}) \Big|_{\text{NLO}} = \frac{\zeta(2)}{128} e^{2\pi i\tau}, \quad f_6^{(1,0)}(\tau, \bar{\tau}) \Big|_{\text{NLO}} = \frac{\zeta(3)}{512} e^{2\pi i\tau} \tau_2^{\frac{1}{2}}. \quad (1.85)$$

which precisely match with our results in (1.83) for  $p = 2, 3!$

### 1.3 HIGHER-POINT MRV AMPLITUDES

In this section, we generalize our results for the  $2 \rightarrow 2$  scattering amplitude in Section 1.2 to higher-point supergraviton amplitudes. Recall that each component of the multiplet has a definite weight  $q_R$  under the  $U(1)_R$  outer-automorphism group of the supersymmetry algebra, which serves as an accidental global symmetry in the low energy limit. Even though this symmetry is broken explicitly by superstring amplitudes, the degree to which it is violated is controlled by supersymmetric Ward identities. In particular, a given  $N$ -point amplitude is non-vanishing only if its net charge lies in the range  $|q_R| \leq |N - 4|$  [53]. We shall restrict our attention to the so-called “maximal R-symmetry violating” (MRV) amplitudes that saturate this bound with  $q_R = 4 - N$ , since these share the most similarities with the 4-point amplitude. In particular, they are constrained by supersymmetry to take the form

$$\mathcal{R}_N(\Phi_i) = i(2\pi)^{10} \delta^{10}(P) Q_+^{16} R_N(\alpha' s_{ij}), \quad (1.86)$$

where  $R(\alpha' s_{ij})$  is a single function of the Mandelstam variables  $s_{ij} \equiv -(p_i + p_j)^2$ . We have labeled the amplitude by  $\mathcal{R}$  instead of  $\mathcal{A}$  to distinguish it from more general R-charge assignments. Note that the  $\eta_i^{\delta} \eta_j^{\delta}$  component of  $\mathcal{R}_N$ , which corresponds to  $(N - 2) \delta\tau$  particles and two  $\delta\bar{\tau}$  particles, can be related to the same component of  $\mathcal{R}_{N-k}$  in the soft limit where  $k$  copies of  $\delta\tau$  are taken to have vanishing momentum. Consequently, these

amplitudes admit a low energy expansion of the schematic form

$$\begin{aligned}
R_N(\alpha' s_{ij}) &= r_0^{(N)}(\tau, \bar{\tau}) + r_4^{(N)}(\tau, \bar{\tau}) \sum_{1 \leq i < j \leq N} \underline{s}_{ij}^2 \\
&+ r_6^{(N)}(\tau, \bar{\tau}) \sum_{1 \leq i < j \leq N} \underline{s}_{ij}^3 + O(\underline{s}_{ij}^4),
\end{aligned} \tag{1.87}$$

Here, the coefficient  $r_{2p}^{(N)}(\tau, \bar{\tau})$  is a weight  $(N - 4, 4 - N)$  non-holomorphic modular form under the  $SL(2, \mathbb{Z})$  duality group that multiplies the  $(\delta\tau)^{N-4} D^{2p} R^4$  vertex in the quantum effective action. To be precise, there can be several such coefficients for each value of  $p$ , which corresponds to the set of independent kinematic structures at each order in the momentum expansion. Due to the aforementioned soft theorems, the coefficients for a given value of  $p$  but different  $N$  are then related by certain differential equations in  $\tau$ . [49].<sup>10</sup>

### 1.3.1 D-INSTANTON EFFECTS

Consider the contribution of a single D-instanton to the  $N$ -point MRV amplitude. For a single D-instanton, the diagrammatics of the  $N$ -point case mirror those of the 4-point amplitude in Section 1.2.1, with

$$\mathcal{R}_N^{(1,0)} = \mathcal{N}_D e^{2\pi i \tau} \int d^{10}x d^{16}\theta \sum_{L=0}^{\infty} \tau_2^{-L} R_N^{(L)}(x, \theta), \tag{1.88}$$

---

<sup>10</sup>As a minor note of caution,  $f_{2p}$  is not strictly the same as  $r_{2p}^{(N)}$  for  $N=4$ , since the former is defined as a coefficient in the low energy expansion of  $M(s, t; \tau, \bar{\tau})$ , with the supergravity piece factored out, whereas the latter appears in that of the full amplitude  $R_4(s, t)$ .



where  $R_N^{(L)}(x, \theta)$  captures the contributions of worldsheet diagrams of Euler characteristic  $-L$  with D-instanton boundary conditions  $(x, \theta)$ . The factor of  $\mathcal{N}_D$  as well as the moduli  $(x, \theta)$  are identical to the 4-point case since they are universal to any process mediated by a single D-instanton. It follows that integration over the  $x^\mu$  restores momentum conservation via  $i(2\pi)^{10}\delta^{10}(P)$ . Similarly, integration over the  $\theta_\alpha$  acts to replace  $\delta\bar{\tau}(p_i)\delta\bar{\tau}(p_j)$  by  $\delta\tau(p_i)\delta\tau(p_j)$  while picking up an overall kinematic factor proportional to  $s_{ij}^2$ . This can be explained by the fact that the  $\delta\tau$  insertions, as the lowest components of the supergraviton multiplet, are blind to the broken supercharges  $\widehat{Q}_-$ . The net result is that the amplitude takes on a familiar form

$$\mathcal{R}_N^{(1,0)} = i(2\pi)^{10}\delta^{10}(P) Q_+^{16} \pi^{16} \mathcal{N}_D e^{2\pi i\tau} \sum_{L=0}^{\infty} \tau_2^{-L} R_N^{(L)}, \quad (1.89)$$

where  $R_N^{(L)}$  is a sum over worldsheet diagrams of Euler characteristic  $-L$  with fixed boundary conditions  $x^\mu = 0$ , and with  $N$  insertions of  $\delta\tau$ .

At leading order, the superamplitude is given by

$$\begin{aligned} \mathcal{R}_N^{(1,0)} \Big|_{\text{LO}} &= i(2\pi)^{10}\delta^{10}(P) Q_+^{16} e^{2\pi i\tau} \mathcal{N}_D \textcircled{\times} \cdots \textcircled{\times} \\ &= i(2\pi)^{10}\delta^{10}(P) Q_+^{16} i^N \frac{\pi}{16} (4\pi)^{N-4} \alpha'^3 \kappa^{N-2} e^{2\pi i\tau} \tau_2^{N-\frac{11}{2}}, \end{aligned} \quad (1.90)$$

which consists of  $N$  copies of the disc 1-point diagram for  $\delta\tau$  (1.47).

At next-to-leading order, the amplitude receives contributions from

$$\begin{aligned}
\mathcal{R}_N^{(1,0)} \Big|_{\text{NLO}} &= i(2\pi)^{10} \delta^{10}(P) Q_+^{16} e^{2\pi i \tau} \mathcal{N}_D \left\{ \begin{array}{l} \text{---} \textcircled{\times} \textcircled{\times} \cdots \textcircled{\times} \textcircled{\times} \text{---} + \textcircled{\times} \textcircled{\circ} \textcircled{\times} \cdots \textcircled{\times} \\ + \textcircled{\circ} \textcircled{\circ} \textcircled{\times} \cdots \textcircled{\times} + \textcircled{\circ} \textcircled{\circ} \textcircled{\times} \cdots \textcircled{\times} \end{array} \right\} \\
&= -i(2\pi)^{10} \delta^{10}(P) Q_+^{16} i^N \frac{1}{32} (4\pi)^{N-4} \alpha'^3 \kappa^{N-2} G(\alpha' s_{ij}) e^{2\pi i \tau} \tau_2^{N-\frac{13}{2}}
\end{aligned} \tag{1.91}$$

which includes the disc 2-point diagram and the annulus 1-point diagram, as well as the 3-holed sphere and 1-holed torus. Recall that only the disc 2-point diagram is non-vanishing. Its contribution has been determined by summing over  $1 \leq i < j \leq N$  in (1.72) and multiplying the result by  $N - 2$  copies of the disc 1-point diagram (1.47). In the above expression, we have also introduced

$$G(\alpha' s_{ij}) = 32C_1(N) - \sum_{1 \leq i < j \leq N} \alpha' s_{ij} \psi\left(1 - \frac{\alpha'}{4} s_{ij}\right), \tag{1.92}$$

where  $C_1(N)$  is a momentum-independent constant that is ambiguous in the on-shell approach. It is related to the unknown constant in the 4-point amplitude by  $C_1(4) = C_1$ . In the low energy expansion, the amplitude (1.91) decomposes as

$$\begin{aligned}
\mathcal{R}_N^{(1,0)} \Big|_{\text{NLO}} &= i(2\pi)^{10} \delta^{10}(P) Q_+^{16} i^N \frac{1}{32} (4\pi)^{N-4} \alpha'^3 \kappa^{N-2} e^{2\pi i \tau} \tau_2^{N-\frac{13}{2}} \\
&\quad \times \left[ 32C_1(N) + \sum_{p=2}^{\infty} \frac{\zeta(p) \tau_2^{\frac{p}{2}}}{2^{2p-3}} \mathcal{O}_N^{(p)} \right],
\end{aligned} \tag{1.93}$$

where we have introduced the kinematic structures

$$\mathcal{O}_N^{(p)} \equiv \frac{1}{2} \sum_{1 \leq i < j \leq N} s_{ij}^p. \tag{1.94}$$

For the case of 4-point scattering, they reduce to the familiar structures  $\mathcal{O}_4^{(p)} = \underline{s}^p + \underline{t}^p + \underline{u}^p$ .

## CONSEQUENCES OF SOFT RELATIONS

Amplitudes in type IIB string theory have well-known soft behavior that relates amplitudes in the limit where the momenta of several of the external particles are taken to zero [54–56]. For instance, the  $(N + 1)$ -point MRV amplitude with a soft  $\delta\tau(p_i)$  is related to the  $N$ -point MRV amplitude without this particle by

$$\mathcal{R}_{N+1}(X, \delta\tau(p_i))|_{p_i \rightarrow 0} = -2i\kappa \mathcal{D}_{N-4} \mathcal{R}_N(X), \quad (1.95)$$

where  $\mathcal{D}_w$  is the modular covariant derivative that takes modular forms of weight  $(w, \tilde{w})$  to those of weight  $(w+1, \tilde{w}-1)$ , as defined in Appendix A.2, and  $X$  denotes the remaining  $N$  particles with finite momenta. Given the leading-order (1.90) and next-to-leading order (1.93) D-instanton contributions, the soft theorem implies that the unknown constant satisfies a recursion relation given by

$$C_1(N+1) = C_1(N) + \frac{4-N}{32}. \quad (1.96)$$

By inputting the boundary value  $C_1(4) = C_1$  in (1.10), as fixed by supersymmetry, we find the solution

$$C_1(N) = \frac{3}{256} - \frac{(N-4)(N-5)}{64}. \quad (1.97)$$

### 1.3.2 IMPLICATIONS FOR HIGHER-POINT EFFECTIVE COUPLINGS

In the previous section, we found that D-instanton amplitudes have relatively simple dependence on the momenta, at least for low orders in the open string loop expansion. For instance, the leading-order contribution, which consists of a product of disc 1-point diagrams, has no momentum dependence whatsoever. Similarly, at next-to-leading order the disc 2-point diagram, which involves the kinematic structures  $\mathcal{O}_N^{(p)}$ , entirely captures the momentum dependence at this order. The fact that only a few kinematic structures enter at low orders can be seen as a consequence of the diagrammatics of D-instanton perturbation theory, i.e. that disconnected diagrams contribute to the connected amplitude. The structure of the diagrammatics in turn has implications for the higher-point effective couplings, ruling out D-instanton contributions to certain kinematic structures.

For instance, consider the 6-point MRV amplitude. Using (1.86), the tree-level contribution to the low-energy expansion of the amplitude takes the form [49]<sup>11</sup>

$$N_6^{-1} R_6^{\text{tree}}(s_{ij}) = \frac{15\zeta(3)}{2} \tau_3^{\frac{3}{2}} + \frac{35\zeta(5)}{64} \tau_2^{\frac{5}{2}} \mathcal{O}_6^{(2)} + \frac{\zeta(3)^2}{512} \tau_2^3 \mathcal{O}_{6,1}^{(3)} + \dots, \quad (1.98)$$

where the overall normalization  $N_6$  of the amplitude is irrelevant for the following analysis. In the above expression, the kinematic structure  $\mathcal{O}_{6,1}^{(3)}$  is given by

$$\mathcal{O}_{6,1}^{(3)} \equiv \frac{1}{32} \left( 10 \sum_{1 \leq i < j \leq 6} \underline{s}_{ij}^3 + 3 \sum_{1 \leq i < j < k \leq 6} \underline{s}_{ijk}^3 \right), \quad (1.99)$$

where  $s_{ijk} = -(p_i + p_j + p_k)^2$ , with the underlined quantities written in Planck units.

---

<sup>11</sup>Our conventions for Newton's constant are related to the ones in [49] by  $\kappa_{\text{ours}} = 16\kappa_{\text{theirs}}$ .

Similar to the 4-point case, the first few terms in the momentum expansion of the 6-point amplitude are protected by supersymmetry and can be determined by  $SL(2, \mathbb{Z})$  covariance [49]. That is, the momentum expansion of the 6-point amplitude takes the form

$$N_6^{-1} R_6(s_{ij})|_{\text{analytic}} = r_0^{(6)}(\tau, \bar{\tau}) + r_4^{(6)}(\tau, \bar{\tau}) \mathcal{O}_6^{(2)} + r_{6,1}^{(6)}(\tau, \bar{\tau}) \mathcal{O}_{6,1}^{(3)} + r_{6,2}^{(6)}(\tau, \bar{\tau}) \mathcal{O}_{6,2}^{(3)} + \dots, \quad (1.100)$$

where  $r_0^{(6)}, r_4^{(6)}, r_{6,1}^{(6)}, r_{6,2}^{(6)}, \dots$  are weight  $(2, -2)$  modular forms which multiply the  $\delta\tau^2 R^4$ ,  $\delta\tau^2 D^4 R^4$ ,  $\delta\tau^2 D^6 R^4, \dots$  terms in the quantum effective action (see Appendix A.2 for more details). To be precise, there are two kinematic structures  $\mathcal{O}_{6,i}^{(3)}$  with  $i = 1, 2$  that appear in the six-point amplitude, which we refer to as  $(\delta\tau)^2 D_i^6 R^4$ . The structure with  $i = 1$  is given by (1.99), while the structure with  $i = 2$  takes the form

$$\mathcal{O}_{6,2}^{(3)} \equiv 2 \sum_{1 \leq i < j \leq 6} \underline{s}_{ij}^3 - \sum_{1 \leq i < j < k \leq 6} \underline{s}_{ijk}^3. \quad (1.101)$$

Note that the functional form of  $r_{6,2}^{(6)}(\tau, \bar{\tau})$  is only determined up to an overall multiplicative constant  $c_1$  which cannot be fixed by the tree-level contribution and  $SL(2, \mathbb{Z})$ -covariance alone.

The unknown constant can be determined using the D-instanton diagrammatics, as discussed in the previous section, *without* appealing to the precise value of the amplitude. According to (1.100) and (A.68), the single D-instanton is expected to contribute up to

eighth order in the momentum expansion, and up to next-to-leading order in  $\tau_2^{-1}$  as

$$\begin{aligned}
N_6^{-1} R_6^{(1,0)}(s_{ij}) = e^{2\pi i \tau} & \left[ \pi^3 \tau_2^2 - \frac{5\pi^2}{16} \tau_2 + O(1) \right. \\
& + \left( \frac{\pi^2 \zeta(2)}{8} \tau_2^2 + O(\tau_2) \right) \mathcal{O}_6^{(2)} \\
& + \frac{\pi^2 \zeta(3)}{32} \tau_2^{\frac{5}{2}} \mathcal{O}_{6,1}^{(3)} + \frac{\pi^2 \zeta(3) c_1}{96} \tau_2^{\frac{5}{2}} \mathcal{O}_{6,2}^{(3)} + O(\tau_2^{\frac{3}{2}}) \\
& \left. + O(\underline{s}_{ij}^4) \right].
\end{aligned} \tag{1.102}$$

The disc 2-point diagram is solely responsible for the nontrivial momentum dependence at these orders, and so  $\mathcal{O}_6^{(p)} = \frac{1}{2} \sum_{i < j} \underline{s}_{ij}^p$  is the only kinematic structure which can appear in the expression above. The two kinematic structures  $\sum_{i < j} \underline{s}_{ij}^3$  and  $\sum_{i < j < k} \underline{s}_{ijk}^3$  that enter into  $\mathcal{O}_{6,i}^{(3)}$  are linearly independent, and thus the coefficient of the latter in (1.102) is necessarily zero. This immediately implies

$$c_1 = \frac{9}{32}. \tag{1.103}$$

Note that this result does not rely on the specific value of the disc 2-point diagram, nor any other diagrams which enter at this order. Nevertheless, as a consistency check we can substitute in this value in (1.102), which yields a prediction that agrees with our D-instanton calculations in (1.90) and (1.91) for  $N = 6$ . Furthermore, it was mentioned in [49] that  $c_1$  is independently determined by the one-loop amplitude, which would serve as a nontrivial test of the D-instanton diagrammatics.

## 1.4 EFFECTS OF A D-INSTANTON/ANTI-D-INSTANTON PAIR

In this section we analyze the contribution of a D-instanton and an anti-D-instanton pair, or D- $\bar{D}$  pair for short, to the 4-point supergraviton scattering amplitude, at leading order in both the open string loop and low energy expansions. The final result is presented in (1.124) and matches precisely with the coefficient of  $D^6 R^4$ , as expected from supersymmetry and S-duality.

### 1.4.1 DIAGRAMMATIC EXPANSION

The contribution of a D- $\bar{D}$  pair to the  $2 \rightarrow 2$  supergraviton scattering amplitude is given by the formal expression

$$\mathcal{A}_{2 \rightarrow 2}^{(1,1)} = \mathcal{N}_D \mathcal{N}_{\bar{D}} e^{-4\pi\tau_2} \int d^{10}x_1 d^{16}\theta_1 d^{10}x_2 d^{16}\theta_2 \sum_{L=0}^{\infty} \tau_2^{-L} A_{2 \rightarrow 2}^{(L)}(x_1, x_2, \theta_1, \theta_2), \quad (1.104)$$

where the supermoduli space  $\widetilde{\mathcal{M}}_{1,1} = \mathbb{R}^{20|32}$  is parameterized by 10+16 collective coordinates  $(x_1^\mu, \theta_{1\alpha})$  for the D-instanton and 10+16 collective coordinates  $(x_2^\mu, \theta_{2\alpha})$  for the anti-D-instanton. The notation here follows that of Section 1.2, with the sum over  $L$  denoting the open string loop expansion. The normalization of the supermoduli space measure factorizes into a product  $\mathcal{N}_D \mathcal{N}_{\bar{D}}$ , where  $\mathcal{N}_{\bar{D}} = \mathcal{N}_D$  is the normalization for that of the anti-D-instanton.

The integrand on the RHS takes the form of a sum over (disconnected) worldsheet diagrams with boundary ending on either the D-instanton or anti-D-instanton. The empty disc diagrams, which come in pairs with net zero  $\tau_1$  charge, exponentiate to give an over-

all factor of  $e^{-4\pi\tau_2}$ . The contributions from empty annuli with both ends on the same (anti-)D-instanton have been absorbed into the overall normalization  $(\mathcal{N}_{\bar{D}}) \mathcal{N}_D$ .

A new feature of scattering amplitudes mediated by the D- $\bar{D}$  pair is the contribution from empty annuli whose boundaries lie on different D-instantons. In particular, we denote the annulus diagram with one boundary on the D-instanton and the other on the anti-D-instanton by  $C_{D_1\bar{D}_2}$ . In the sum over Riemann surfaces, such diagrams exponentiate to give an overall factor of  $e^{2C_{D_1\bar{D}_2}}$ , thereby providing a nontrivial measure on  $\widetilde{\mathcal{M}}_{1,1}$ <sup>12</sup>. While in principle there are other empty diagrams which can correct the super-moduli space measure, these appear at subleading orders in  $\tau_2^{-1}$  and hence will not be considered in our analysis.

As in (1.26), the fermionic moduli contribute through an insertion of the form

$$e^{-\Delta S_{\text{WS,R}}(\theta_1) - \Delta S_{\text{WS,R}}(\theta_2)}, \quad (1.105)$$

where the R-sector vertex operators in  $S_{\text{WS,R}}(\theta_1)$  correspond to open strings with endpoints on the D-instanton, and analogously for  $S_{\text{WS,R}}(\theta_2)$  and the anti-D-instanton.

The leading order contribution  $A_{2 \rightarrow 2}^{(0)}(x_1, x_2, \theta_1, \theta_2)$  comes from the diagram consisting of four disconnected discs, each with one bulk puncture, together with the exponentiated annulus diagram for the D- $\bar{D}$  pair. It contributes to the amplitude as

$$\begin{aligned} \mathcal{A}_{2 \rightarrow 2}^{(1,1)}|_{\text{LO}} = & \mathcal{N}_D \mathcal{N}_{\bar{D}} e^{-4\pi\tau_2} \int d^{10}x_1 d^{10}x_2 d^{16}\theta_1 d^{16}\theta_2 \exp \left( \text{Diagram} \right) \\ & \times \left( \text{Diagram 1} + \text{Diagram 2} + \dots \right), \end{aligned} \quad (1.106)$$

---

<sup>12</sup>The factor of 2 accounts for the two opposite orientations of open strings stretched between the D- $\bar{D}$  pair.



where  $\dots$  includes the other distinct ways to color the boundary. Here, a blue boundary corresponds to the D-instanton at position  $x_1$  with fermionic insertion  $e^{-\Delta S_{\text{WS,R}}(\theta_1)}$ , while a red boundary corresponds to the anti-D-instanton at position  $x_2$  with  $e^{-\Delta S_{\text{WS,R}}(\theta_2)}$ . As before, the black crosses indicate supergraviton states represented on the worldsheet as vertex operators.

#### 1.4.2 INTEGRATION OVER THE FERMIONIC MODULI

We shall first discuss how to perform the integral over the  $\theta_i$  coordinates. The Berezin integral on the RHS of (1.106) gives

$$\int d^{16}\theta_1 d^{16}\theta_2 e^{-\Delta S_{\text{WS,R}}(\theta_1) - \Delta S_{\text{WS,R}}(\theta_2)} = \pi^{32} \widehat{Q}_+^{16} \widehat{Q}_-^{16}, \quad (1.107)$$

where the supercharge operators are given in (1.29). We identify  $\widehat{Q}_s^\alpha$  as the spacetime supercharges broken by the D-instanton ( $s = -1$ ) and anti-D-instanton ( $s = +1$ ), respectively, which as before are defined modulo additive contributions from the preserved supercharges. They are topological in the sense that they can be deformed in a worldsheet diagram so long as they do not cross any bulk closed string insertions.

We proceed to evaluate the amplitude using the approach of Section 1.2, where the supercharge contours are taken to surround the closed string vertex operators, acting as supersymmetry transformations on the 1-particle states. As was the case for the single D-instanton, after restricting to the  $\eta_1^8 \eta_3^8$  component of the superamplitude, the supercharges  $\widehat{Q}_\pm^{16}$  act only on the  $V_{\delta\bar{\tau}(p_i)}$ , converting the two vertex operators to  $V_{\delta\tau(p_i)}$  with an overall factor of  $t^4$ . What remains are four  $V_{\delta\tau(p_i)}$  insertions surrounded by the sixteen

supercharges broken by the anti-D-instanton, namely  $\widehat{Q}_+^{16}$ . Here we need to appeal to the details of the D-instanton/anti-D-instanton boundary conditions. In particular, the disc 1-point diagram vanishes for all massless insertions except for  $\delta\tau$  and  $\delta\bar{\tau}$ . Consequently, the only nontrivial configurations are given by two  $\delta\tau$  insertions and two  $\delta\bar{\tau}$  insertions, where the latter correspond to eight supercharges acting on  $V_{\delta\tau(p_i)}$ . Using the same type of argument in the COM frame, it is straightforward to show that the remaining supercharges convert  $V_{\delta\tau(p_i)}, V_{\delta\tau(p_j)}$  into  $V_{\delta\bar{\tau}(p_i)}, V_{\delta\bar{\tau}(p_j)}$  with an overall factor of  $(p_i + p_j)^8$ . There are a total of  $6 = \binom{4}{2}$  such configurations, which naturally decompose into  $s, t, u$  channels corresponding to which particles are paired. Overall, we find that the leading-order D- $\bar{D}$  contribution takes the form

$$\mathcal{A}_{2 \rightarrow 2}^{(1,1)} \Big|_{\text{LO}} = Q_+^{16} 2\pi^{32} \mathcal{N}_D \mathcal{N}_{\bar{D}} e^{-4\pi\tau_2} \left[ s^4 A_{2 \rightarrow 2}^{(0),s} + t^4 A_{2 \rightarrow 2}^{(0),t} + u^4 A_{2 \rightarrow 2}^{(0),u} \right], \quad (1.108)$$

where the contribution from each of the three channels is given by

$$\begin{aligned} A_{2 \rightarrow 2}^{(0),s} &= \int d^{10}x_1 d^{10}x_2 e^{2C_{D_1, \bar{D}_2}} \langle c_0 V_{\delta\bar{\tau}(p_1)} \rangle_{x_2}^{D^2} \langle c_0 V_{\delta\bar{\tau}(p_2)} \rangle_{x_2}^{D^2} \langle c_0 V_{\delta\tau(p_3)} \rangle_{x_1}^{D^2} \langle c_0 V_{\delta\tau(p_4)} \rangle_{x_1}^{D^2}, \\ A_{2 \rightarrow 2}^{(0),t} &= \int d^{10}x_1 d^{10}x_2 e^{2C_{D_1, \bar{D}_2}} \langle c_0 V_{\delta\bar{\tau}(p_1)} \rangle_{x_2}^{D^2} \langle c_0 V_{\delta\tau(p_2)} \rangle_{x_1}^{D^2} \langle c_0 V_{\delta\bar{\tau}(p_3)} \rangle_{x_2}^{D^2} \langle c_0 V_{\delta\tau(p_4)} \rangle_{x_1}^{D^2}, \\ A_{2 \rightarrow 2}^{(0),u} &= \int d^{10}x_1 d^{10}x_2 e^{2C_{D_1, \bar{D}_2}} \langle c_0 V_{\delta\bar{\tau}(p_1)} \rangle_{x_2}^{D^2} \langle c_0 V_{\delta\tau(p_2)} \rangle_{x_1}^{D^2} \langle c_0 V_{\delta\tau(p_3)} \rangle_{x_1}^{D^2} \langle c_0 V_{\delta\bar{\tau}(p_4)} \rangle_{x_2}^{D^2}. \end{aligned} \quad (1.109)$$

which consists of the exponentiated annulus diagram with mixed boundary conditions  $C_{D_1, \bar{D}_2}$ , together with four 1-punctured discs, where the vertex operators are distributed such that the discs with D-instanton boundary conditions contain  $V_{\delta\tau(p_i)}$ , while those with anti-D-instanton boundary conditions contain  $V_{\delta\bar{\tau}(p_j)}$ . For the disc topology the anti-

D-instanton boundary conditions are identical to those of the D-instanton other than a sign flip relating the spin fields, and so the disc 1-point diagrams are given by

$$\begin{aligned} \langle c_0 V_{\delta\tau(p)} \rangle_{x_1}^{D^2} &= \mathcal{A}_{\delta\tau}^{D^2} e^{ip \cdot x_1}, & \langle c_0 V_{\delta\tau} \rangle_{x_2}^{D^2} &= 0, \\ \langle c_0 V_{\delta\bar{\tau}(p)} \rangle_{x_1}^{D^2} &= 0, & \langle c_0 V_{\delta\bar{\tau}(p)} \rangle_{x_2}^{D^2} &= \mathcal{A}_{\delta\tau}^{D^2} e^{ip \cdot x_2}, \end{aligned} \tag{1.110}$$

where  $x_1$  denotes the boundary condition for the D-instanton at  $x_1$ , and similarly for the anti-D-instanton at  $x_2$ . Here,  $\mathcal{A}_{\delta\tau}^{D^2}$  is given by the  $\delta\tau$  disc 1-point diagram (1.47) with boundary condition  $x^\mu = 0$ .

### 1.4.3 THE MEASURE ON MODULI SPACE

We now discuss how to compute the annulus diagram  $C_{D_1\bar{D}_2}$ , which contributes nontrivially to the measure on the moduli space for the D- $\bar{D}$  pair.

The boundary conditions for the D-instanton with bosonic modulus  $x$  can be embedded in a GSO-even boundary state of the form

$$|D_x\rangle = \frac{1}{\sqrt{2}} (|\text{NSNS}; x\rangle + |\text{RR}; x\rangle), \tag{1.111}$$

where  $|\text{NSNS}; x\rangle$  and  $|\text{RR}; x\rangle$  denote the contribution to the boundary state coming from closed strings in the NSNS and RR sectors, respectively. For simplicity, we have set the fermionic modulus  $\theta = 0$ . The anti-D-instanton has opposite charge with respect to the RR axion field, and therefore its boundary state is given by

$$|\bar{D}_x\rangle = \frac{1}{\sqrt{2}} (|\text{NSNS}; x\rangle - |\text{RR}; x\rangle). \tag{1.112}$$

Let us first consider the cylinder diagram between two D-instantons with bosonic collective coordinates  $x_1, x_2$ . In the closed string channel, this is given by the overlap of two D-instanton boundary states, which takes the form<sup>13</sup>

$$Z_{D_1 D_2}(t) = \langle D_1 | e^{-\frac{\pi}{t}(L_0 + \tilde{L}_0)} b_0 c_0 | D_2 \rangle, \quad (1.113)$$

where  $D_i$  labels the D-instanton with collective coordinate  $x_i$ . In (1.113), we are working with a cylinder of length  $1/(2t)$  and circumference  $2\pi$ . The ghost insertion  $b_0 c_0$  is required for a nonzero result, acting as the projector onto the ghost ground state annihilated by  $b_0$ . Here,  $L_0$  ( $\tilde{L}_0$ ) denotes the zero Fourier mode of the stress tensor  $T$  ( $\tilde{T}$ ). Under a modular transformation of the cylinder, (1.113) is related to the open string partition function for a cylinder of length  $\pi$  and circumference  $2\pi t$ , i.e.

$$Z_{D_1 D_2}(t) = \left( \text{Tr}_{\mathcal{H}_0^{\text{NS}}} - \text{Tr}_{\mathcal{H}_0^{\text{R}}} \right) \frac{1 + (-1)^F}{2} (-)^{N_{bc} + N_{\beta\gamma}} b_0 c_0 e^{-2\pi t L_0}. \quad (1.114)$$

In the above expression, the trace is taken with respect to the NS and R sectors of the Hilbert space of open strings stretched between two D-instantons at positions  $x_1, x_2$ , and the factor  $(1 + (-1)^F)/2$  implements the type IIB GSO projection. The minus sign in front of the Ramond sector contribution has the usual interpretation of spacetime fermions running in the loop. The insertion  $(-)^{N_{bc} + N_{\beta\gamma}} b_0 c_0$  projects onto the ghost ground state, and is needed to obtain a non-zero result.

In (1.114), the terms with the  $(-)^F$  insertion map under the inverse modular trans-

---

<sup>13</sup>We take the RR sector component of the D-instanton boundary state  $|D_i\rangle$  to have picture number  $(-\frac{1}{2}, -\frac{3}{2})$ , while its bra  $\langle D_i|$  has picture number  $(-\frac{3}{2}, -\frac{1}{2})$ . This ensures that the overlap (1.113) has total picture number  $(-2, -2)$ , as required for a non-zero result [32].

formation to closed string states with periodic boundary conditions along the circle, and therefore correspond to the RR sector contributions to the boundary state (1.111). On the other hand, the terms without the  $(-)^F$  insertion map to closed string states in the NSNS component of the boundary state.

For now, we focus on the contribution coming from the exchange of closed strings in the NSNS sector, which corresponds to open strings with anti-periodic boundary condition in the time direction. The ghosts give a contribution that cancel one pair of oscillators as usual. It follows that [57]

$$\begin{aligned} Z_{D_1 D_2}^{\text{NS}}(t) &= \frac{1}{2} \left( \text{Tr}_{\mathcal{H}_0^{\text{NS}}} - \text{Tr}_{\mathcal{H}_0^{\text{R}}} \right) (-)^{N_{bc} + N_{\beta\gamma}} b_0 c_0 e^{-2\pi\tau L_0} \\ &= \frac{1}{2} e^{-t \frac{(x_{12})^2}{2\pi}} (\eta(it))^{-8} \left( \left[ \frac{\vartheta_3(it)}{\eta(it)} \right]^4 - \left[ \frac{\vartheta_2(it)}{\eta(it)} \right]^4 \right), \end{aligned} \quad (1.115)$$

where  $x_{12} \equiv x_1 - x_2$  is the relative position between the D-instantons. Note that there is no overall factor of  $i$  since each D-instanton is localized in Euclidean target space. Overall, we find the NSNS contribution to the amplitude between two D-instantons is

$$\begin{aligned} C_{D_1 D_2}^{\text{NS}} &= \int_0^\infty \frac{dt}{2t} Z_{D_1, D_2}^{\text{NS}}(t) \\ &= \int_0^\infty \frac{dt}{4t} e^{-t \frac{(x_{12})^2}{2\pi}} (\eta(it))^{-8} \left( \left[ \frac{\vartheta_3(it)}{\eta(it)} \right]^4 - \left[ \frac{\vartheta_2(it)}{\eta(it)} \right]^4 \right). \\ &= \frac{1}{4} \int_0^\infty dt t^3 e^{-t \frac{(x_{12})^2}{2\pi}} \left[ 16 + \mathcal{O} \left( e^{-\frac{2\pi}{t}} \right) \right] \\ &= \frac{24(2\pi)^4}{(x_{12})^8} + \mathcal{O} \left( \frac{e^{-2|x_{12}|}}{(x_{12})^4} \right). \end{aligned} \quad (1.116)$$

In the second line we performed a modular transformation of the cylinder on (1.114). The first term in the last line of (1.116) gives the contribution to the amplitude due to mass-

less closed strings in the NSNS sector. The other terms are exponentially suppressed at large  $x_{12}$  and can be interpreted as the contribution of massive closed strings. As we will see, it is only the massless exchange which is relevant for our analysis.

The contribution to (1.114) coming from the RR closed strings must cancel that of the NSNS closed strings, since the potential between the D-instantons vanishes by supersymmetry, and so

$$C_{D_1 D_2}^{\text{NS}} + C_{D_1 D_2}^{\text{R}} = 0. \quad (1.117)$$

The anti-D-instanton boundary state differs from the D-instanton boundary state by a minus sign multiplying the RR component, which implies that the annulus amplitude for the D- $\bar{D}$  pair is given by twice the NSNS contribution (1.116), i.e.

$$\begin{aligned} C_{D_1 \bar{D}_2} &= 2 \int_0^\infty \frac{dt}{4t} e^{-t \frac{(x_{12})^2}{2\pi}} (\eta(it))^{-8} \left( \left[ \frac{\vartheta_3(it)}{\eta(it)} \right]^4 - \left[ \frac{\vartheta_2(it)}{\eta(it)} \right]^4 \right) \\ &= \frac{48(2\pi)^4}{(x_{12})^8} + \mathcal{O} \left( \frac{e^{-2|x_{12}|}}{(x_{12})^4} \right). \end{aligned} \quad (1.118)$$

The measure on moduli space is given by the exponential of this diagram, which thus takes the form

$$\exp \left[ \frac{96(2\pi)^4}{(x_{12})^8} + \mathcal{O} \left( \frac{e^{-2|x_{12}|}}{(x_{12})^4} \right) \right] = \sum_{n=1}^{\infty} \frac{1}{n!} \left[ \frac{96(2\pi)^4}{(x_{12})^8} \right]^n + \mathcal{O} \left( \frac{e^{-2|x_{12}|}}{(x_{12})^4} \right), \quad (1.119)$$

where we continue to ignore the contribution of massive closed strings.

#### 1.4.4 INTEGRATION OVER THE BOSONIC MODULI

At leading order in  $\tau_2^{-1}$ , the moduli space measure is given by the exponentiated annulus diagram  $e^{2C_{D_1\bar{D}_2}}$ , where  $C_{D_1\bar{D}_2}$  is given by (1.118). From (1.118), we observe that the integral over  $t$  develops a logarithmic divergence when the D- $\bar{D}$  pair is separated by a distance

$$(x_{12})^2 = 2\pi^2. \quad (1.120)$$

This has the interpretation of an open string stretched between the D- $\bar{D}$  pair going on-shell. Furthermore, this divergent behavior becomes tachyonic for  $(x_{12})^2 < 2\pi^2$ . Thus, the integration over the full range of  $x_1, x_2$  in (1.109) is only well-defined for a choice of contour avoiding these singularities.

Instead of worrying about the choice of contour, we shall focus only on the part of (1.118) corresponding to asymptotic separation of the D- $\bar{D}$  pair. As we shall see, such contributions are unambiguous. Using (1.119), we find that the contribution of massless closed string states to the  $s$ -channel amplitude is given by

$$A_{2 \rightarrow 2}^{(0),s} = (A_{\delta\tau}^{D^2})^4 \int_{|x_{12}| > a} d^{10}x_1 d^{10}x_2 \sum_{n=0}^{\infty} \frac{1}{n!} \left[ \frac{96(2\pi)^4}{(x_{12})^8} \right]^n e^{i(p_1+p_2)\cdot x_2 + i(p_3+p_4)\cdot x_1}, \quad (1.121)$$

where we have cut out a finite domain of the moduli space. In the above expression, higher-order terms in the sum over  $n$  contribute only to the higher-order terms in the low energy expansion of the scattering amplitude. The lowest order term,  $n = 0$ , contributes only to the disconnected part of the amplitude, and can be neglected.

The next term in the sum,  $n = 1$ , is given by

$$\begin{aligned}
i(2\pi)^{10}\delta^{10}(P)\int_{|x_{12}|>a}d^{10}x_{12}\frac{96(2\pi)^4}{(x_{12})^8}e^{-ix_{12}\cdot(p_1+p_2)} \\
= -i(2\pi)^{10}\delta^{10}(P)\left[\frac{2^{10}\pi^9}{s} + \text{analytic}\right],
\end{aligned}
\tag{1.122}$$

where on the LHS we have integrated over the center-of-mass collective coordinates  $x_1 + x_2$ , which restores momentum conservation. On the RHS, we omitted terms that are analytic in momenta at  $s = 0$ , which is part of the “analytic ambiguity” of the amplitude that involves the integration over a finite domain of the moduli space with a yet unspecified contour prescription. Meanwhile, the  $s^{-1}$  term captures the contribution of massless closed string exchange at large relative separation  $x_{12}$  of the D- $\bar{D}$  pair. Crucially, it is independent of  $a$ , and so this contribution [58], at leading order in both the open string loop expansion and low energy expansion, is unambiguously defined.

A similar analysis in the  $t$ - and  $u$ -channels yields analogous results, with  $s$  replaced by  $t$  and  $u$ , respectively. Using (1.121) and (1.122), we find that the leading contribution (both in the open string loop expansion, and in momentum) from the D- $\bar{D}$  pair to the superamplitude is

$$\mathcal{A}_{2\rightarrow 2}^{(1,1)}\Big|_{\text{LO}} = -i(2\pi)^{10}\delta^{10}(P)Q_+^{16}2^{-11}\alpha'^3\kappa^2e^{-4\pi\tau_2}\tau_2^{-5}\left[\alpha'^3(s^3+t^3+u^3)+\mathcal{O}(\alpha'^4)\right],
\tag{1.123}$$

where we have used our results for  $\mathcal{A}_{\delta\tau}^{D^2}$  in (1.47) and  $\mathcal{N}_D$  in (1.50), and have restored the value of  $\alpha'$ .



### 1.4.5 COMPARISON AGAINST S-DUALITY

We now test our results for the D- $\bar{D}$  amplitude in (1.123) against the  $D^6R^4$  coefficient  $f_6(\tau, \bar{\tau})$  expected from supersymmetry and S-duality. Extracting the SUGRA piece of the former gives

$$\frac{1}{\alpha'^3 stu} M_0^{(1,1)}(\alpha' s, \alpha' t) = -2^{-11} \alpha'^3 (s^3 + t^3 + u^3) + O(\alpha'^4). \quad (1.124)$$

The D- $\bar{D}$  contributions to the latter can be identified as the as the terms multiplying  $e^{-4\pi\tau_2}$  in (1.84), which at leading-order reads

$$f_6^{(1,1)}(\tau, \bar{\tau}) = -2^{-11} e^{-4\pi\tau_2} \tau_2^{-2} + O(e^{-4\pi\tau_2} \tau_2^{-3}). \quad (1.125)$$

This matches precisely with our results in (1.124)! Before moving on, we note that in retrospect it seems somewhat surprising that the  $D^6R^4$  vertex, which is protected by supersymmetry by virtue of being  $\frac{1}{8}$ -BPS, receives contributions from the non-supersymmetric D- $\bar{D}$  instanton configuration.

### 1.5 A TEST OF NON-PERTURBATIVE UNITARITY

As discussed in Section 1.4, the measure on the supermoduli space is singular due to open strings going on-shell, which in turn implies that the integration over the bosonic moduli suffers from ambiguities. So far, we have investigated D- $\bar{D}$  contributions to the  $2 \rightarrow 2$  scattering amplitude which are insensitive to these ambiguities, which were found to be consistent with supersymmetry and  $SL(2, \mathbb{Z})$  duality.

This leads us to ask whether there are other D- $\bar{D}$  contributions which are unambiguous in the on-shell approach. From the expression in (1.119) for the moduli space measure, and following the steps leading to (1.123), it is clear that arbitrarily massive closed strings will contribute to the scattering amplitude at higher orders in the low energy expansion. Although this would seem to suggest that all such higher order terms are ambiguous, it turns out that certain contributions are unambiguous owing to the fact that they have non-polynomial dependence on the external momenta. This is related to the idea that such amplitudes can be obtained from lower-point amplitudes by unitarity cuts. In this section, we analyze the simplest example of this phenomenon from the worldsheet perspective, thereby providing a nontrivial check of non-perturbative unitarity in type IIB scattering amplitudes.

### 1.5.1 A DISCONTINUITY IN THE D- $\bar{D}$ AMPLITUDE

We begin by returning to the D- $\bar{D}$  contribution to the  $2 \rightarrow 2$  amplitude coming from the next term in the expansion of (1.121), i.e. the term with  $n = 2$ . This corresponds to two copies of the annulus diagram (or more precisely, of the contribution from the massless closed strings to the annulus diagram). In the  $s$ -channel, this can be written as

$$\begin{aligned}
A_{2 \rightarrow 2}^{(0),s} &\supset \frac{1}{2} (A_{\delta\tau}^{D^2})^4 \alpha'^8 \int_{|x_{12}| > a} d^{10}x_{12} \frac{[96(2\pi)^4]^2}{(x_{12})^{16}} e^{-ix_{12} \cdot (p_1 + p_2)} \\
&= 9 \cdot 2^{17} \pi^8 S_8 (A_{\delta\tau}^{D^2})^4 \alpha'^8 \int_a^\infty dr r^9 \int_0^\pi d\theta \sin^8 \theta \frac{1}{r^{16}} e^{ipr \cos \theta},
\end{aligned} \tag{1.126}$$

where  $r = -|x_{12}|$ ,  $p = |p_1 + p_2|$ , and  $S_8 = \frac{32\pi^4}{105}$  is the area of the 8-sphere. We can directly evaluate the regularized expression in (1.126), with the understanding that the

terms analytic in  $s$  are ambiguous, as they are sensitive to the cutoff  $a$ . The non-analytic piece receives contributions from

$$\int_a^\infty dr r^9 \int_0^\pi d\theta \sin^8 \theta \frac{1}{r^{16}} e^{ipr \cos \theta} = \frac{\pi s^3 \ln(-s)}{9 \cdot 2^{16}} + \dots, \quad (1.127)$$

where  $\dots$  indicates terms analytic in  $s = -(p_1 + p_2)^2$ . It follows that the leading-order contribution from the D- $\bar{D}$  pair to the non-analytic part of the amplitude goes like

$$\mathcal{A}_{2 \rightarrow 2}^{(1,1)} \Big|_{\text{LO}}^{\text{non-analytic}} = -i(2\pi)^{10} \delta^{10}(P) Q_+^{16} 2^{-26} \pi^{-7} S_8 \alpha'^6 \kappa^4 e^{-4\pi\tau_2} \tau_2^{-3} H(s, t). \quad (1.128)$$

The momentum dependence has been relegated to the function

$$H(s, t) = s^7 \ln(-s) + t^7 \ln(-t) + u^7 \ln(-u), \quad (1.129)$$

where the extra terms come from a similar analysis in the  $t$ - and  $u$ -channels.

Let  $T_{2 \rightarrow 2}^{(n,m)}$  be the  $(n, m)$  D-instanton contribution to the  $\eta_1^8 \eta_2^8$  component of the reduced amplitude with the delta function stripped away, such that

$$\tilde{\mathcal{A}}_{2 \rightarrow 2}^{(n,m)} \Big|_{\eta_1^8 \eta_2^8} = i(2\pi)^{10} \delta(P) T_{2 \rightarrow 2}^{(n,m)}. \quad (1.130)$$

In each of the  $s, t, u$  channels, the logarithmic dependence gives rise to a branch cut in the corresponding complex plane. For instance, the discontinuity across the  $s$ -cut is given by

$$2\text{Re} \left( T_{2 \rightarrow 2}^{(1,1)} \Big|_{\text{LO}}^s \right) = 2^{-25} \pi^{-6} S_8 \alpha'^6 \kappa^4 \tau_2^{-3} e^{-4\pi\tau_2} s^{11}, \quad (1.131)$$

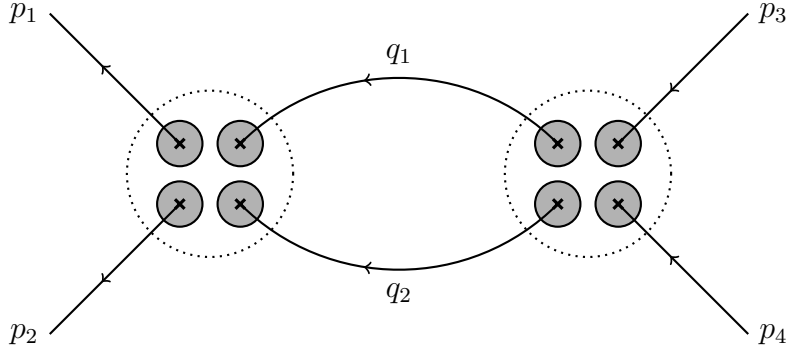


**Figure 1.3:** Spacetime Feynman diagram that contributes to the unitarity cut. After cutting the internal propagators to put the intermediate particles on-shell, the vertices are given by either the D-instanton or anti-D-instanton mediated contributions to  $R^4$ . Ingoing arrows denote  $\delta\tau$  and outgoing arrows denote  $\delta\bar{\tau}$ .

where the superscript  $s$  indicates that we keep the terms multiplying the  $s$ -channel contribution  $A_{2\rightarrow 2}^{(0),s}$  in (1.108). Furthermore, we are ignoring contributions from higher particle cuts to  $A_{2\rightarrow 2}^{(0),s}$  (e.g. 3-particle cuts or higher), which come from higher order terms in the expansion of (1.121) (i.e.  $n \geq 3$ ). The discontinuity across the branch cut in (1.131) has the interpretation of massless closed strings exchanged between the D-instanton and anti D-instanton being on-shell. In the next subsection, we shall verify this explicitly through a worldsheet calculation that relies only on scattering amplitudes mediated by a single D-instanton. This provides a nontrivial check of (1.131) and verifies that (1.128) is insensitive to the analytic ambiguities present in the bosonic moduli integration.

## 1.5.2 VERIFICATION OF UNITARITY

In search of unitarity, we will focus on the  $s$ -channel cut contribution to the  $2 \rightarrow 2$  axion-dilaton scattering amplitude, as represented by the diagram in Figure 1.3. Note that to extract the original axion-dilaton amplitude from the new one, we must make the replacement  $t \rightarrow s$  in (1.131). In principle, there are also  $t$ - and  $u$ -channel cuts, which can be

obtained in an analogous fashion.

We now proceed to evaluate the contribution from the diagram in Figure 1.3 with the internal lines cut, as given by<sup>14</sup>

$$\begin{aligned}
-2\text{Re} \left( T_{2 \rightarrow 2}^{(1,1)} \Big|_{\text{LO}}^s \right) &= \frac{1}{2} \int \frac{d^{10}q_1}{(2\pi)^{10}} \frac{d^{10}q_2}{(2\pi)^{10}} (-2\pi i)^2 \delta(q_1^2) \delta(q_2^2) \\
&\times \left[ T_{2 \rightarrow 2}^{(1,0)} \Big|_{\text{LO}}(p_1, p_2, q_1, q_2) T_{2 \rightarrow 2}^{(0,1)} \Big|_{\text{LO}}(q_1, q_2, p_3, p_4) + (p_i \leftrightarrow q_i) \right],
\end{aligned} \tag{1.132}$$

The subscript LO reminds us that the D-instanton and anti-D-instanton contributions to the  $R^4$  vertex appear at leading order in the open string loop expansion. The quantity  $T_{2 \rightarrow 2}^{(0,1)}$  in the above expression captures the anti-D-instanton contributions to the scattering amplitude, which at leading order agrees with that of the D-instanton, i.e.

$$e^{-2\pi i \tau} T_{2 \rightarrow 2}^{(0,1)} \Big|_{\text{LO}} = e^{2\pi i \bar{\tau}} T_{2 \rightarrow 2}^{(1,0)} \Big|_{\text{LO}} . \tag{1.133}$$

Using our results for these amplitudes as presented in (1.51), we find

$$\begin{aligned}
2\text{Re} \left( T_{2 \rightarrow 2}^{(1,1)} \Big|_{\text{LO}}^s \right) &= \\
&\pi^{12} \alpha'^6 \kappa^4 e^{-4\pi\tau_2} \tau_2^{-3} s^8 \int \frac{d^9 \vec{q}_1}{(2\pi)^9} \frac{d^9 \vec{q}_2}{(2\pi)^9} \frac{1}{|\vec{q}_1| |\vec{q}_2|} \delta^{10}(p_1 + p_2 + q_1 + q_2),
\end{aligned} \tag{1.134}$$

where we have stripped off an overall factor of  $i(2\pi)^{10} \delta(P)$  from the RHS of (1.132). To

---

<sup>14</sup>The  $\delta\tau\delta\bar{\tau}$  propagator at momentum  $p^\mu$  is given by  $\frac{i}{-p^2+i\epsilon}$ .

evaluate this integral, we find it helpful to work in the COM frame (1.31), where we find

$$\begin{aligned}
& \int \frac{d^9 \vec{q}_1}{(2\pi)^9} \frac{d^9 \vec{q}_2}{(2\pi)^9} \frac{1}{|\vec{q}_1| |\vec{q}_2|} \delta^{(10)}(p_1 + p_2 + q_1 + q_2) \\
&= \frac{1}{(2\pi)^{18}} \int \frac{d^9 \vec{q}_1}{|\vec{q}_1|^2} \delta(2E - 2|\vec{q}_1|) \\
&= \frac{S_8}{2^{25} \pi^{18}} s^3,
\end{aligned} \tag{1.135}$$

In the first line of the above expression, we used the  $\delta$ -functions to set  $\vec{q}_2 = -\vec{q}_1$ , and in the second we substituted out  $E$  using  $s = 4E^2$ . Plugging (1.135) into (1.134), we immediately find

$$2\text{Im} \left( T_{2 \rightarrow 2}^{(1,1)} \Big|_{\text{LO}}^s \right) = 2^{-25} \pi^{-6} S_8 \alpha'^6 \kappa^4 e^{-4\pi\tau_2} \tau_2^{-3} s^{11}, \tag{1.136}$$

which exactly reproduces the discontinuity found in the worldsheet calculation, after replacing  $t \rightarrow s$  in (1.131). This is a non-trivial test of the interpretation of the discontinuity in the D-instanton/anti-D-instanton mediated scattering amplitude, and of unitarity of non-perturbative scattering amplitudes in type IIB string theory.

## 1.6 DISCUSSION

Let us recap the logic of the determination of D-instanton effects in this chapter. Our working assumption has been that D-instanton contributions to closed string scattering amplitudes should be computed by the SFT of bulk closed strings and open strings on the D-instanton, to the extent in which the D-instanton effects are unambiguously defined. Certain aspects of the SFT formulation of D-instanton perturbation theory are

analogous to that of the naive on-shell formulation. For instance, the integration over D-instanton moduli space is taken into account in SFT as part of the functional integration over open string fields. A priori, the on-shell approach to D-instanton amplitudes is subject to open string divergences and regularization ambiguities, which are resolved in SFT. On the other hand, the naive on-shell computation often captures the SFT result up to ambiguities of a simple form, which may be fixed by either indirect arguments or genuine SFT computations.

Indeed, most of our explicit computations, particularly concerning MRV amplitudes, are carried out in the naive on-shell formalism. As we will see in the next chapter, the naive on-shell results necessarily agree with the string field theoretic computation up to terms that can be fixed indirectly by considerations of spacetime supersymmetry and soft theorems concerning moduli of type IIB string vacua. This has allowed us to obtain unambiguous D-instanton contributions to MRV amplitudes.

Nonetheless, there is value in carrying out a first-principles SFT computation of the amplitudes considered in this work, specifically the constant coefficients  $a_0, a_1, a_2$  (1.11) appearing in the NLO one-D-instanton contribution to the  $N$ -point MRV amplitude. This would serve to verify that the closed string vacuum preserves Poincaré supersymmetry, which is certainly expected for the Minkowskian vacuum of type IIB string theory at the non-perturbative level, but is not at all manifest in the string field theoretic formulation of D-instanton perturbation theory.

A few other comments are in order. From the on-shell perspective, the moduli space of multiple D-instantons typically admits singularities where new massless open string modes appear. This difficulty was evaded in the analyses of [25, 27] in  $c = 1$  and type

0B string theory due to the simplicity of the moduli space of ZZ-instantons. In the setting of the D-instanton/anti-D-instanton pair analyzed in Section 1.4, it so happens that the contribution to the  $D^6 R^4$  effective coupling comes from only the integration over the asymptotic region of the moduli space, which is well-defined. Generally, the integral over multi-D-instanton moduli spaces is expected to be singular, and should be replaced by an integral over non-Abelian open string fields in the SFT framework. This was carried out to leading order in D-instanton perturbation theory in [33], and it would be very interesting to extend the analysis to subleading orders.

Finally, let us remark that the D-instanton amplitudes of the sort computed in this work may provide useful input for the program of bootstrapping the non-perturbative string S-matrix [59, 60].



# 2

## String field theoretic effects

### 2.1 INTRODUCTION

It has been emphasized recently that closed SFT is a rigorous framework for string perturbation theory. In particular, it provides a fully consistent regularization of possible divergences near the boundary of the moduli space in the on-shell worldsheet formulation of scattering amplitudes [61]. The situation is more dramatic in D-instanton perturbation theory, where the open+closed SFT is necessary to fix ambiguities of the naive on-shell formalism [28–33, 36, 37, 61, 62]. In this chapter, we carry out (most of) the full string

field theoretic computation of (1.10). The main purpose here is to explain why such a computation is free of divergences, and that it agrees with the naive on-shell computation apart from the constant term appearing on the RHS of (1.10). We also demonstrate explicitly how SFT unambiguously computes  $C_1$  in (1.11). Whether SFT in fact produces the correct value of  $C_1$  amounts to the dynamical question of whether the super-Poincaré symmetry is preserved by the Minkowskian vacua of type IIB string theory at the non-perturbative level. While the latter is certainly expected, it is not manifest in the SFT formulation of D-instanton perturbation theory, where the closed string field vacuum is determined by extremizing the quantum effective action  $\Gamma[\Psi_c]$  with all open string fields integrated out. A similar problem in the context of the  $c < 1$  and  $c = 1$  string theories was examined in detail in [28–30, 62]. The extension of this analysis to type IIB string theory requires taking into account the additional ingredients of PCOs and vertical integration [63].

### 2.1.1 GENERAL STRATEGY OF THE STRING FIELD THEORETIC COMPUTATION

The amplitudes of interest are extracted from the path integral (1) over the open string fields, while the closed string fields are taken to be on-shell. The open+closed SFT action  $S_{oc}[\Psi_o, \Psi_c]$  consists of the kinetic terms for open string fields and the string vertices for open+closed string fields. Here we briefly recap the logic of how this action is constructed.

In SFT, the worldsheet moduli space is divided into domains that correspond to distinct Feynman diagrams, each of which is formed by gluing string vertices with propagators. To specify the string vertices further requires choosing local coordinates around each

of the punctures on the worldsheet surface where the string fields are inserted, as well as the loci of PCO insertions. As the closed string field insertions are on-shell in D-instanton perturbation theory, one only needs to keep track of the local coordinates around the boundary points of the worldsheet where the open string fields are inserted.

A propagator amounts to the plumbing construction that identifies the neighborhoods of a pair of punctures, on either one or two connected surfaces in the vertex region. The moduli domain corresponding to a Feynman diagram with a single propagator, referred to as the ‘propagator region,’ meets the vertex region along a codimension 1 wall in the moduli space where the propagator shrinks to zero length. It is important that at the wall separating the propagator and vertex regions, the choices of coordinate charts around the punctures on the worldsheet, as well as the PCO locations (possibly with vertical integration), agree with one another. This requirement amounts to the so-called geometric master equation, which ensures that the SFT action constructed from the string vertices is gauge invariant. The explicit construction of the relevant string vertices in the bosonic string case is described for example in section 4 of [30]. For the case of the superstring D-instanton, we will need to extend their definition to include the placement of PCOs.

The vertex region, by design, resides away from the boundary of the moduli space where the worldsheet surface degenerates, and thus the moduli integration over the vertex region is finite, modulo potential spurious singularities in the PCO locations which can be circumvented through the vertical integration prescription of [63]. A string vertex  $\mathcal{V}[\Psi_o, \Psi_c]$  is a term in the SFT action obtained by integrating a worldsheet correlator with  $\Psi_o, \Psi_c$  insertions over the corresponding vertex region of the moduli space. A propagator region, on the other hand, corresponds to a Feynman diagram in which the string

vertices are connected through the string field propagator.

### 2.1.2 BV GAUGE CONDITION AND MASSLESS OPEN STRING MODES

The open SFT path integral (1) is defined subject to a choice of the BV gauge condition  $L$ . It is important to make sure that this gauge condition is non-singular. As was pointed out in [29], the commonly adopted Siegel gauge, in which the open string fields are annihilated by  $b_0$ , is singular for D-instantons and must be modified.

To see this, we begin by inspecting the kinetic terms in the action and their corresponding propagators. The propagator for an open string field  $\Psi_o$  in NS sector is obtained by inverting its kinetic term  $\frac{1}{2}\langle\Psi_o|Q_B|\Psi_o\rangle$ . In the Siegel gauge, this propagator is  $\frac{b_0}{L_0}$ , where  $L_0$  is proportional to the “mass squared” of the open string field. A similar propagator that involves picture changing can be derived in the R sector. The massive open string fields have well-defined propagators; they can be integrated out perturbatively, and their propagators appear in Feynman diagrams. The massless open string fields do not have well-defined propagators in the Siegel gauge, and require special treatment.

One class of massless open string fields correspond to the collective coordinates of the D-instanton. Namely, there are ten bosonic modes  $\phi^\mu$  associated with the vertex operators  $ce^{-\phi}\psi_\mu$ , and sixteen fermionic modes  $\theta_\alpha$  associated with the vertex operators  $ce^{-\frac{\phi}{2}}S^\alpha$ . The integration over these modes amounts to the integration over the D-instanton (super) moduli space. However, there is a subtle but important difference between these open string fields and the deformation parameters for D-instanton boundary conditions in the worldsheet CFT, which we discuss in Sections 2.1.5 and 2.1.6.

There is another class of massless open string fields that cannot be interpreted as collective coordinates, of the form

$$\varkappa^1 \beta_{-1/2} c_0 c_1 | - 1 \rangle + \zeta^2 \beta_{-1/2} c_1 | - 1 \rangle + \zeta_1 \gamma_{-1/2} c_1 | - 1 \rangle + \varkappa_2 \gamma_{-1/2} c_0 c_1 | - 1 \rangle, \quad (2.1)$$

where  $| - 1 \rangle$  stands for the state corresponding to the vertex operator  $e^{-\phi}$ . The coefficients  $\varkappa^1$  and  $\varkappa_2$  are Grassmann even, whereas  $\zeta_1$  and  $\zeta^2$  are Grassmann odd. They will be referred to as “ghost zero modes.” In Siegel gauge,  $\varkappa^1$  and  $\varkappa_2$  are set to zero, while the propagating modes  $\zeta_1$  and  $\zeta^2$  have vanishing kinetic term. The latter leads to a vanishing path integral, which seems problematic. However, it was pointed out in [29] that this indicates not the breakdown of D-instanton perturbation theory, but rather that the Siegel gauge condition is singular.

Instead, [29] adopts a different BV gauge condition for the ghost zero mode sector, which we refer to as Sen gauge, defined by setting  $\zeta_1$  and  $\varkappa_2$  to zero. In this gauge, the propagator for  $\varkappa^1$  is finite. We can see this explicitly by analyzing the kinetic term

$$\frac{1}{2} \langle \varkappa^1 | Q_B | \varkappa^1 \rangle = -(\varkappa^1)^2, \quad (2.2)$$

where  $|\varkappa^1 \rangle$  has been defined as the first term of (2.1). By inverting this expression, we can read off the propagator for  $\varkappa^1$ ,<sup>1</sup>

$$P_{\varkappa^1} = \frac{1}{2}. \quad (2.3)$$

The propagator for  $\zeta^2$  is still ill-defined. Naively, consideration of ghost number symme-

---

<sup>1</sup>A highly nontrivial consistency check of the propagation of  $\varkappa^1$  is seen in the computation of the effective potential for the bosonic open string collective modes in Appendix A.4.

try indicates that  $\zeta^2$  decouples from the effective action of massless open string fields, and if one simply omits the integration over  $\zeta^2$ , the open string path integral would appear to be well-defined. However,  $\zeta^2$  in fact has the interpretation of the Faddeev-Popov ghost associated with fixing the  $U(1)$  gauge symmetry on the D-instanton, and would be coupled to non-Abelian open string modes in the presence of other D-instantons. Integrating out  $\zeta^2$  would then lead to a correction to the measure in the open string fields, which is present even in the absence of other D-instantons. This extremely subtle analysis is discussed in Section 2.1.4.

Following [29], we will work in Siegel gauge for all sectors except for the ghost zero modes (2.1), where we impose Sen gauge instead. Among the open string fields, we denote by  $\Psi_o^f$  the modes with finite propagators, namely  $\varkappa^1$  in addition to all the massive modes. The remaining open string field components that require special treatment are the collective modes  $\phi^\mu, \theta_\alpha$ , and  $\zeta^2$ . This leads us to consider the path integral (1) in the form

$$e^{-\Gamma[\Psi_c]} \Big|_{\text{D-inst}} = \mathcal{N}_D e^{-\frac{2\pi}{g_s}} \int d^{10}\phi d^{16}\theta d\zeta^2 \exp(W_f[\phi^\mu, \theta_\alpha, \zeta^2, \Psi_c]) . \quad (2.4)$$

Here, the overall normalization  $\mathcal{N}_D$ , which recall arises from the exponential of the empty annulus, has been set to the value in (1.50). It can be derived from the SFT of open string modes, as was done in [32]. The factor  $e^{-2\pi\tau_2}$ , meanwhile, comes from the exponential of the empty disc. From the perspective of SFT, it is a factor we must add by hand.

The remaining term on the RHS involves the effective action  $W_f$ , defined by

$$\exp(W_f[\phi^\mu, \theta_\alpha, \zeta^2, \Psi_c]) = \int D\Psi_o^f \exp\left(-S_{oc}[\phi^\mu, \theta_\alpha, \zeta^2, \Psi_o^f, \Psi_c]\right) , \quad (2.5)$$

which can be calculated perturbatively by Feynman diagrams with well-defined propagators.

### 2.1.3 VALIDITY AND EXTENSION OF THE ON-SHELL RESULTS

Of concern to the amplitudes considered in this work are the order  $g_s$  terms in  $W_f$ . These involve worldsheets of the following topologies: a disc with two closed string insertions, an annulus with one closed string insertion, a sphere with three holes, and a torus with one hole, as already described in (1.52). Each worldsheet topology corresponds to several SFT Feynman diagrams, which are manifestly finite by design.

Except for the disc with two closed string insertions, the remaining worldsheet topologies mentioned above involve either one or fewer closed string insertions. As the closed string field is taken to be that of an on-shell axion-dilaton state, the corresponding SFT Feynman diagrams evaluate to constants, independent of the closed string momentum, as a simple consequence of Lorentz invariance. In other words, nontrivial momentum dependence arises only from the disc with two closed string insertions. As we show in the main text, the SFT Feynman diagrams contributing to this amplitude disagree with the on-shell results by at most a constant, or a total derivative that vanishes once momentum conservation is restored.

In addition to the Feynman diagrams for  $W_f$ , we must also integrate over the zero modes  $\phi^\mu$ ,  $\theta_\alpha$ , and  $\zeta^2$ . As shown in the following sections, these only contribute to the constant  $C_1$ , which implies that the on-shell analysis of the previous chapter completely determines the momentum-dependence of the amplitude at order  $g_s$ . It should be noted that this is a fortunate coincidence which will no longer apply at higher orders, where

even the momentum-dependent terms will suffer from ambiguities in the on-shell prescription.

#### 2.1.4 INTEGRATION OVER $\zeta^2$

We shall now spend some time discussing the integration over the open string zero modes. The Grassmann-odd ghost zero mode  $\zeta^2$ , as already mentioned, has the interpretation as the Faddeev-Popov ghost associated with gauge fixing the  $U(1)$  symmetry on the D-instanton. However, there are no charged open strings on a single D-instanton, and so  $\zeta^2$  is absent in the effective action  $W_f$  (2.5). Formally, the integration over  $\zeta^2$  in (2.4) gives zero, and one may be tempted to simply drop the  $\zeta^2$ -integral, but this leaves an ambiguous (possibly background field dependent) normalization.

A more careful treatment that fixes the normalization requires introducing a spectator D-instanton [29] (which we refer to as the  $D^s$ -instanton), so that there are charged open string modes with respect to the  $U(1)$  gauge symmetry on the original D-instanton. At leading order in  $g_s$ ,  $W_f$  now contains couplings between  $\zeta^2$ , D- $D^s$  open string fields  $\chi$ , and  $D^s$ -D open string fields  $\chi^*$ , of the form

$$\mathcal{A}_{\zeta^2\chi\chi^*}^{D^2} \zeta^2 \chi \chi^* \tag{2.6}$$

as computed by the  $\chi, \chi^*, \zeta^2$  disc amplitude  $\mathcal{A}_{\zeta^2\chi\chi^*}^{D^2}$ . One can then calculate the  $\zeta^2$ -integral, which is now nonzero, and move the spectator  $D^s$ -instanton to infinity in the end.<sup>2</sup>

At the first subleading order in  $g_s$ , there is a contribution to  $W_f$  from the analogous

---

<sup>2</sup>In [29], the integration over  $\zeta^2$  is interpreted as the division by the volume of the  $U(1)$  gauge group.



disc diagram with an extra closed string field insertion. Such a coupling that is relevant to the amplitude considered in this work is of the form

$$g_s \mathcal{A}_{\delta\tau\zeta^2\chi\chi^*}^{D^2} \zeta^2 \chi \chi^* \left[ \delta\tau(x) + \dots \right], \quad (2.7)$$

where  $\mathcal{A}_{\delta\tau\zeta^2\chi\chi^*}^{D^2}$  is a momentum-independent constant, as computed from the disc amplitude for  $\delta\tau$ ,  $\zeta^2$ ,  $\chi$ , and  $\chi^*$ , that depends on the string field theoretic parameters that enter into the definition of the string vertices. In the above expression,  $\delta\tau(x)$  is the axion-dilaton field at the D-instanton location  $x^\mu$ , and  $\dots$  represents terms involving  $\theta_\alpha$  and other components of the supergraviton multiplet. As we will discuss in Section 2.1.6, to leading order in  $g_s$ , the insertion of a fermionic open string field  $\theta_\alpha$  on the boundary can be replaced by that of a supercharge  $\widehat{Q}_{(\pm\frac{1}{2}),-}^\alpha$ . In the axion-dilaton background, the linear combination of  $\delta\tau$  and  $\delta\bar{\tau}$  that appear in (2.7) is determined by the nonlinearly realized super-Poincaré symmetry to be  $(e^{i\theta_\alpha \mathcal{Q}_-^\alpha} \delta\tau)(x)$ , which contains a term of order  $\theta^8$  that involves  $\delta\bar{\tau}$ . Here,  $\mathcal{Q}_-^\alpha$  is the supercharge acting as a raising operator on the spacetime fields, which can be regarded as a dual of the supercharge  $\widehat{Q}_-^\alpha$  acting as a lowering operator on the one-particle states. As we will see, the computation of  $Y$  is nontrivial and requires considering contributions from multiple Feynman diagrams.

After integrating over  $\chi$  and  $\chi^*$ , the remaining  $\zeta^2$  integral is now nonzero. Performing the integration corrects (2.4) by the factor

$$\sum_\chi \mathcal{A}_{\zeta^2\chi\chi^*}^{D^2} \left[ 1 + g_s Y \left( e^{i\theta_\alpha \mathcal{Q}_-^\alpha} \delta\tau \right) (x) \right], \quad Y = \mathcal{A}_{\delta\tau\zeta^2\chi\chi^*} (\mathcal{A}_{\zeta^2\chi\chi^*}^{D^2})^{-1}, \quad (2.8)$$

$$\begin{aligned}
& \int d\Phi_o^m \left[ \begin{array}{c} \text{Diagram 1: } \text{blue circle with } \times \times \cdots \times + \text{blue circle with } \circ \times \cdots \times \\ \text{Diagram 2: } \text{blue circle with } \circ \circ \cdots \times + \text{blue circle with } \circ \text{ and a loop} \cdots \times \end{array} \right] \\
& = \int d^{10}x \left[ \begin{array}{c} \text{Diagram 3: } \text{grey circle with } \times \times \cdots \times + \left( \text{grey circle with } \circ \times + g_s \Delta B \right) \cdots \times \\ \text{Diagram 4: } \text{grey circle with } \circ \circ \cdots \times + \text{grey circle with } \circ \text{ and a loop} \cdots \times \end{array} \right]
\end{aligned}$$

**Figure 2.1:** Diagrams contributing to the D-instanton amplitude for  $N$  closed strings at order  $g_s$ . Each comes with an arbitrary number of insertions of open string field collective modes  $\Phi_o^m$  as represented by the blue boundaries. Black crosses are linear combinations of closed string vertex operators for  $\delta\tau$  and  $\delta\bar{\tau}$ , while red crosses are vertex operators for  $\delta\tau$ .  $\Delta B$  is a momentum-independent constant that depends on the string field theory parameters. All the diagrams are at the D-instanton location  $x^\mu$ .

where the sum is taken over all of the open string fields  $\chi$  stretched between D and  $D^s$ .

The subleading coefficient  $Y$  is universal in the sense that it takes the same value for all choices of  $\chi$ . Consequently, the sum takes on a factorized form, and so we can choose to absorb  $\sum_\chi \mathcal{A}_{\zeta^2 \chi \chi^*}^{D^2}$  into the overall normalization of the D-instanton path integral, for which (2.8) reduces to

$$1 + g_s Y \left( e^{i\theta_\alpha Q_\alpha} \delta\tau \right) (x). \quad (2.9)$$

### 2.1.5 INTEGRATION OVER $\phi^\mu$

After integrating out  $\zeta^2$  in (2.4) according to the prescription in the previous subsection, we are left with

$$e^{2\pi i \tau} \int d^{10} \phi d^{16} \theta e^{W[\phi, \theta, x; \Psi_c]}, \quad (2.10)$$

where we have indicated the explicit dependence of the integrand on the D-instanton moduli  $x^\mu$ .  $W[\phi, \theta, x; \Psi_c]$  includes diagrams with an arbitrary number of  $\phi^\mu$  and  $\theta_\alpha$  insertions even at a given order in  $g_s$  (Figure 2.1). Even though the integration over  $\theta_\alpha$  picks out only the terms proportional to  $\theta^{16}$  in  $W[\phi, \theta, x; \Psi_c]$ , they still include arbitrarily many powers of  $\phi^\mu$ . In this section, we discuss how to carry out the sum over infinitely many such terms by an appropriate change of variables for  $\phi^\mu$ . We then discuss the effects of  $\theta_\alpha$  insertions in the next section.

Heuristically, the integration in  $\phi$  should be equivalent to an integration over the D-instanton moduli space. One way to understand their relation is through the background independence of SFT [64–66]: a deformation of the boundary moduli  $\delta x^\mu$  can be absorbed by an open string field redefinition  $(\phi^\mu, \theta_\alpha) \rightarrow (\phi^\mu + \delta\phi^\mu, \theta_\alpha + \delta\theta_\alpha)$ , where

$$\delta\phi^\mu = \delta x^\nu f^\mu{}_\nu[\phi, \theta, x; \Psi_c], \quad \delta\theta_\alpha = \delta x^\nu g_{\alpha\nu}[\phi, \theta, x; \Psi_c]. \quad (2.11)$$

In other words, different points on a hypersurface obtained by integrating the equation (2.11) represent equivalent string field configurations. Transporting along this hypersurface from  $x$  to  $x'$ ,  $(\phi, \theta)$  turn into  $(\phi', \theta')$ , while the integration measure (2.10) is invariant, namely

$$d^{10}\phi d^{16}\theta e^{W[\phi, \theta, x; \Psi_c]} = d^{10}\phi' d^{16}\theta' e^{W[\phi', \theta', x'; \Psi_c]}. \quad (2.12)$$

Now we can transport along the hypersurface to  $\phi = 0$ , and write the integral in (2.10) equivalently as

$$\int d^{10}\phi d^{16}\theta e^{W[\phi, \theta, x; \Psi_c]} = \int d^{10}x d^{16}\theta \det\left(f^\mu{}_\nu[0, \theta, x; \Psi_c]\right) e^{W[0, \theta, x; \Psi_c]}. \quad (2.13)$$

where the dependence on the bosonic open string field has now been eliminated from the integrand on the RHS.<sup>3</sup>

For the purpose of extracting the Jacobian factor  $\det f$  to first order in  $g_s$ , we can replace  $\theta_\alpha$  insertions with that of the supercharges, which amounts to viewing  $\theta$  as fermionic moduli rather than open string fields. This eliminates the need for considering the shift  $\delta\theta$  in (2.11). Expanding

$$f[0, \theta, x; \Psi_c] = 1 + g_s f_1[\theta, x; \Psi_c], \quad (2.14)$$

we expect the  $\theta$ -dependence of  $f_1$  to be dictated by the nonlinearly realized super-Poincaré symmetry, similar to (2.9). We can determine  $f_1[0, x; \Psi_c]$  from the equation<sup>4</sup>

$$\left( f^\mu{}_\nu[0, 0, x; \Psi_c] \frac{\partial}{\partial \phi^\mu} - \frac{\partial}{\partial x^\nu} \right) W[\phi, 0, x; \Psi_c] \Big|_{\phi=0} = 0. \quad (2.15)$$

Expanding  $W = \sum_{n=0}^{\infty} g_s^n W^{(n)}$ , we have at order  $g_s$  the relation

$$(f_1)^\mu{}_\nu[0, x; \Psi_c] \frac{\partial}{\partial \phi^\mu} W^{(0)}[\phi, 0, x; \Psi_c] \Big|_{\phi=0} = \frac{\partial}{\partial x^\nu} W^{(1)}[0, 0, x; \Psi_c] - \frac{\partial}{\partial \phi^\nu} W^{(1)}[\phi, 0, x; \Psi_c] \Big|_{\phi=0}. \quad (2.16)$$

In a closed string background where only supergraviton modes are turned on, the order  $g_s^0$  term in the effective action is expected to give

$$W^{(0)}[\phi, 0, x; \Psi_c] = \mathcal{A}_{\delta\tau}^{D^2} \delta\tau(x + \phi). \quad (2.17)$$

---

<sup>3</sup>This in particular implies that  $W[\phi, \theta, x; \Psi_c]$  does not include terms consisting of only  $\phi^\mu$ 's. In Appendix A.4, we perform an explicit computation of the  $\phi^4$  term in  $W[\phi, \theta, x; \Psi_c]$  and show that it is indeed zero.

<sup>4</sup>This is a special case of the analog of (4.12) of [65] for open string field theory, restricted to  $\phi = 0$ . Here we also assumed  $\partial_\phi f^\mu{}_\nu|_{\phi=0} = 0$ , which follows from the general construction of [65].

To be precise, the dependence on  $\phi$  will come multiplied by a factor  $\mathcal{N}_\phi$  corresponding to the normalization of  $\phi_\mu c e^{-\phi} \psi^\mu$ . For instance, such a factor enters into the amplitude for  $\delta\tau$  with one insertion of  $\phi$ ,

$$\mathcal{A}_{\delta\tau(p)\phi^\mu}^{D^2} = ip^\mu \mathcal{N}_\phi \mathcal{A}_{\delta\tau}^{D^2}. \quad (2.18)$$

In order to arrive at (2.17), we must first perform a field redefinition  $\phi \mapsto \mathcal{N}_\phi^{-1} \phi$ .

At first order in  $g_s$ , the effective action now receives contributions from the disc amplitude for two axion-dilatons together with  $\phi^\mu$ , of the form

$$\begin{aligned} & \left. \frac{\partial}{\partial x^\nu} W^{(1)}[0, 0, x; \Psi_c] - \frac{\partial}{\partial \phi^\nu} W^{(1)}[\phi, 0, x; \Psi_c] \right|_{\phi=0} \\ &= \mathcal{A}_{\delta\tau}^{D^2} \left[ \Delta U \delta\tau(x) \partial_\nu \delta\tau(x) + \Delta U' \partial^\mu \delta\tau(x) \partial_\mu \partial_\nu \delta\tau(x) + \Delta U'' \partial^\mu \delta\tau(x) D_{\mu\nu} \delta\tau(x) \right] \end{aligned} \quad (2.19)$$

where  $\Delta U$ ,  $\Delta U'$ , and  $\Delta U''$  are constants that depend on SFT parameters. Here,  $D_{\mu\nu} \delta\tau(x)$  is a nonlocal term in the effective action. In momentum space it takes the form

$$D_{\mu\nu} \delta\tau(x) = \int d^{10}p e^{ipx} e_{\mu\nu}(p) \widetilde{\delta\tau}(p), \quad (2.20)$$

where  $e_{\mu\nu}$  is a symmetric polarization tensor obeying  $p^\mu e_{\mu\nu} = 0$  with  $e^\mu{}_\mu = 1$ . Such a term is an artifact from working with the closed string fields in Siegel gauge. Indeed, there exist other suitable gauge choices where  $\Delta U'' = 0$ . The fact that the analysis is sensitive to the gauge reflects the fact that  $W$  and  $W_f$  are not gauge invariant objects, as compared to  $\Gamma$ . Regardless, such nonlocal terms do not pose any serious conceptual issues,

and from (2.16) we solve

$$(f_1)^\mu{}_\nu[0, x; \Psi_c] = \Delta U \delta^\mu_\nu \delta\tau(x) + \Delta U' \partial^\mu \partial_\nu \delta\tau(x) + \Delta U'' D^\mu{}_\nu \delta\tau(x), \quad (2.21)$$

where we have included the effect of renormalizing  $\phi$ . After restoring the  $\theta$ -dependence by super-Poincaré symmetry, we obtain the Jacobian factor

$$\det f[0, \theta, x, \Psi_c] = 1 + g_s (10\Delta U + \Delta U'') \left( e^{i\theta_\alpha \mathcal{Q}_-^\alpha} \delta\tau \right) (x) \quad (2.22)$$

that appears on the RHS of (2.13). Note that  $\Delta U'$  drops out due to the on-shell condition of the background field  $\delta\tau(x)$ . Furthermore, the above expression only involves the local, gauge-invariant operator  $D^\mu{}_\mu = 1$ . Similar to the correction factor (2.9), the Jacobian factor (2.22) contributes only to the constant term in (1.83).

### 2.1.6 INTEGRATION OVER $\theta_\alpha$

In this section, we shall integrate over the fermionic open string collective modes  $\theta_\alpha$ . As previously mentioned, this is similar to inserting the spacetime supercharge  $\widehat{Q}_{(\pm\frac{1}{2}),-}^\alpha$  represented as a contour integral of the spin field along the boundary of the worldsheet, but they are not the same beyond leading order in  $g_s$ . In particular, while the former is unambiguously defined in SFT, the latter is subject to an ambiguity in the location of the PCOs that accompany the supercharge insertion, as already encountered in the on-shell computation of Section 1.2.

The goal of this section is to find some field redefinition of  $\theta$ , say  $\hat{\theta}$ , whose integration

implements the associated supersymmetry transformations, at least to first order in  $g_s$ .

Under an infinitesimal change of variables

$$\delta\theta_\alpha^\beta = h_\alpha^\beta[\phi, x; \Psi_c] \delta\hat{\theta}_\beta \quad (2.23)$$

the integral in (2.10) becomes

$$\int d^{10}x d^{16}\theta e^{W[\phi, \theta, x; \Psi_c]} = \int d^{10}\phi d^{16}\hat{\theta} \det \left( h_\alpha[\phi, x; \Psi_c] \right)^{-1} e^{\hat{W}[\phi, \hat{\theta}, x; \Psi_c]}, \quad (2.24)$$

where the effective action  $\hat{W}$  is defined as mentioned above. Since we are only after first order corrections in  $g_s$ , we can safely set  $\phi = 0$  and work with the expansion

$$h[0, x; \Psi_c] = \hat{\theta}_\alpha + g_s h_1[x; \Psi_c] + O(g_s^2). \quad (2.25)$$

We can determine  $h$  from the analogue of (2.15),

$$h_\alpha^\beta[0, x; \Psi_c] \frac{\partial}{\partial\theta_\alpha} W[0, \theta, x; \Psi_c] \Big|_{\theta=\hat{\theta}} - \frac{\partial}{\partial\hat{\theta}_\beta} W[0, \hat{\theta}, x; \Psi_c] = 0. \quad (2.26)$$

Expanding to first order in  $g_s$  gives

$$\begin{aligned} & (h_1)_\alpha^\beta[x; \Psi_c] \frac{\partial}{\partial\theta_\alpha} W^{(0)}[0, \theta, x; \Psi_c] \Big|_{\theta=\hat{\theta}} \\ &= \frac{\partial}{\partial\hat{\theta}_\beta} \widehat{W}^{(1)}[0, \hat{\theta}, x; \Psi_c] \Big|_{\theta=\hat{\theta}} - \frac{\partial}{\partial\theta_\beta} W^{(1)}[0, \theta, x; \Psi_c] \Big|_{\theta=\hat{\theta}}. \end{aligned} \quad (2.27)$$

At leading order in  $g_s$ ,  $W$  contains an effective string vertex that couples  $\theta$  to the di-

latino  $\lambda$ . Restoring  $\theta$  dependence in (2.17) gives

$$W^{(0)}[0, \theta, x; \Psi_c] = \mathcal{A}_{\delta\tau}^{D^2} \delta\tau(x) + \mathcal{N}_\theta \mathcal{A}_{\delta\tau}^{D^2} \theta_\alpha \lambda^\alpha(x) + O(\theta^2), \quad (2.28)$$

where the coefficient of the second term, computed by the disc amplitude for the dilatino together with  $\theta$ , is equal to the axion-dilaton disc amplitude up to a multiplicative constant  $\mathcal{N}_\theta$  that similarly reflects the normalization of  $\theta_\alpha e^{-\frac{1}{2}\phi} S^\alpha$ .

At the next order in  $g_s$ , the effective action receives contributions from several Feynman diagrams leading to

$$\begin{aligned} & \frac{\partial}{\partial \hat{\theta}_\beta} \widehat{W}^{(1)}[0, \hat{\theta}, x; \Psi_c] \Big|_{\theta=\hat{\theta}} - \frac{\partial}{\partial \theta_\beta} W^{(1)}[0, \theta, x; \Psi_c] \Big|_{\theta=\hat{\theta}} \\ & = \mathcal{N}_\theta \mathcal{A}_{\delta\tau}^{D^2} \left[ \Delta V \lambda^\beta(x) \delta\tau(x) + \Delta V' \partial_\mu \lambda^\beta(x) \partial^\mu \delta\tau(x) \right] + O(\theta). \end{aligned} \quad (2.29)$$

Similar to the bosonic case, the coefficients  $\Delta V, \Delta V'$  are constants depending on the SFT parameters that represent the mismatch between  $\theta$  and the SUSY parameter  $\hat{\theta}$ . They can be determined from the disc amplitude for an axion-dilaton, dilatino, and fermionic collective coordinate after subtracting off the contribution from the axion-dilaton two-point amplitude.

Plugging (2.28) and (2.29) into (2.27) gives

$$(h_1)_\alpha{}^\beta[x; \Psi_c] = \delta_\alpha{}^\beta \Delta V \delta\tau(x) + \delta_\alpha{}^\beta \Delta V' \partial^\mu \partial_\mu \delta\tau(x). \quad (2.30)$$

The term containing  $\Delta V'$  is proportional to the equation of motion for  $\delta\tau$ . Since the closed string fields are on-shell, it vanishes in the effective action. This leads to the Ja-



cobian factor

$$\det \left( h_\alpha^\beta[0, x; \Psi_c] \right)^{-1} = 1 + 16g_s \Delta V \delta\tau(x) + O(g_s^2). \quad (2.31)$$

At leading order in  $g_s$ , this does not mix with the factors arising from integration over  $\zeta^2$  and  $\phi^\mu$ , and so (2.4) reduces to the desired form

$$e^{-\Gamma[\Psi_c]} \Big|_{\text{D-inst}} = \mathcal{N}_D e^{-\frac{2\pi}{g_s}} \int d^{10}x d^{16}\hat{\theta} \left\{ 1 + g_s Z \left( e^{i\hat{\theta}_\alpha \mathcal{Q}^\alpha} \delta\tau \right) (x) \right\} e^{\widehat{W}_f[\hat{\theta}, x; \Psi_c]}. \quad (2.32)$$

In this expression, the coefficient

$$Z = Y + 10\Delta U + \Delta U'' + \Delta V \quad (2.33)$$

represents integration over the open string zero modes, save for  $\hat{\theta}$ , which implements the standard SUSY transformation. The effective action  $\widehat{W}_f$  on the RHS involves only Feynman diagrams with massive open string propagators.

## 2.2 RESULTS AND DISCUSSION

In this section, we present our results for the Feynman diagrams that contribute to the RHS of (2.32), delegating their construction and computation to subsequent sections in the chapter. Using (2.32), we find that the single D-instanton contribution to the MRV

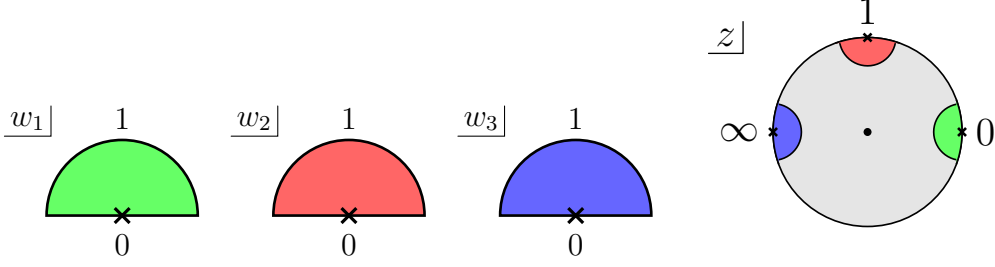


**Figure 2.2:** Disc 3-point vertex for open strings, described by the UHP with complex coordinate  $z$ . The three open string punctures are located at  $z = 0, 1, \infty$ , where they reside at the origin of their respective local coordinate patches  $w_i$ . The vertex is defined such that a half-disc of radius 1 in the  $w_i$  coordinate corresponds to a half-disc of radius  $O(\alpha^{-1})$  in  $z$ . There is also a PCO in the bulk at  $z = p_{\text{ooo}}$ .

supergraviton amplitude at NLO reads

$$\begin{aligned}
\mathcal{R}_N^{(1,0)} \Big|_{\text{NLO}} &= i(2\pi)^{10} \delta^{10}(P) Q_+^{16} \pi^{16} \mathcal{N}_D g_c^N C_{D^2}^{N-1} e^{2\pi i \tau} \\
&\times \left\{ (\mathcal{A}_{\delta\tau}^{D^2})^{N-2} \sum_{i < j}^N \mathcal{A}_{\delta\tau(p_i)\delta\tau(p_j)}^{D^2} \right. \\
&\quad + N (\mathcal{A}_{\delta\tau}^{D^2})^{N-1} \left( \mathcal{A}_{\delta\tau}^{A^2} + Y + 10\Delta U + \Delta U'' + \Delta V \right) \\
&\quad \left. + C_{D^2} (\mathcal{A}_{\delta\tau}^{D^2})^N (\mathcal{A}^{\Sigma_{1,1}} + \mathcal{A}^{\Sigma_{0,3}}) \right\}.
\end{aligned} \tag{2.34}$$

Note that we have pulled out a factor of  $g_c$  from each vertex operator as well as  $C_{D^2}$  from the disc, in order to simplify the calculations in this chapter. We have also rescaled the terms arising from integration over the massless open string fields by a factor of  $g_s^{-1}$ . Other than the corrections from integration over the massless open string modes, this expression involves the same topologies as the on-shell amplitude. However, it is important to remember that these amplitudes are defined in terms of SFT Feynman diagrams. Unlike those computed in the on-shell approach, these are manifestly finite and free from ambiguities. The price we pay is that they will generally depend on the definition of the

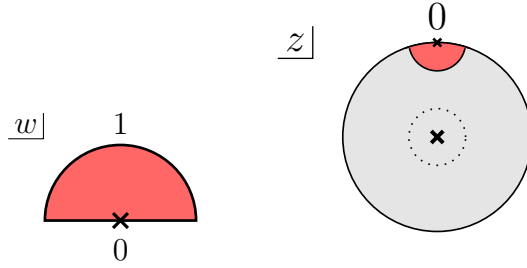


**Figure 2.3:** Open-closed disc vertex, described by the UHP with complex coordinate  $z$ . The closed string puncture is located at  $z = i$  together with the PCO, the latter of which is averaged over a contour surrounding the closed string. The open string puncture, which sits at  $z = 0$ , is equipped with local coordinate  $w$ . The vertex is defined such that a half-disc of radius 1 in the  $w$  coordinate corresponds to a half-disc of radius  $\lambda^{-1}$  in  $z$ .

Feynman vertices, which amounts to the choice of local coordinates for the open string punctures as well the PCO loci. This boils down to a functional dependence on the SFT parameters, the two most prominent of which are  $\alpha$  and  $\lambda$ . The former is associated with the open string disc 3-point vertex, shown in Figure 2.2, and the latter with the open-closed disc vertex, in Figure 2.3. Both roughly translate to the inverse radii for the local coordinate patches surrounding each of the open string punctures.

In order to simplify the Feynman diagram computations, we shall take the SFT parameters  $\alpha$  and  $\lambda$  to be arbitrarily large, say by rescaling the local coordinates. As a consequence, all of the open string modes in  $\Psi_o^f$ , save for  $\varkappa^1$ , will become infinitely massive and no longer contribute to the propagator regions. To be precise, a mode of conformal weight  $h > 0$  will have a propagator proportional to  $\lambda^{-h}$  or  $\alpha^{-h}$  which vanishes in the limit  $\lambda, \alpha \rightarrow \infty$ . On the other hand, the  $\varkappa^1$  propagator is independent of the SFT parameters since its associated vertex operator  $c\partial c e^{-2\phi} \partial \xi$  is a weight zero conformal primary.

With these points in mind, we shall provide a term-by-term analysis of the MRV amplitude in (2.34). Along the way, we shall determine the values of  $a_0$  and  $a_1$  in (1.11).

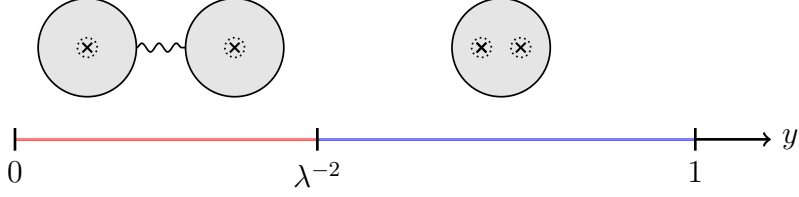


**Figure 2.4:** Feynman diagrams and the corresponding moduli domains for the disc with two NSNS insertions. Dotted circles correspond to averaged PCO insertions. On the worldsheet represented as the UHP, the closed strings (indicated by crosses) are inserted at  $z = i$  and  $z = iy$ . In the moduli space parameterized by  $y$ , the domain  $(0, \lambda^{-2})$  is the propagator region (red region), while  $(\lambda^{-2}, 1)$  is the vertex region (blue region).

### 2.2.1 DETERMINATION OF $a_0$

We first direct our efforts towards determining the disc 2-point amplitude  $\mathcal{A}_{\delta\tau(p)\delta\tau(k)}^{D^2}$ , as computed from SFT Feynman diagrams in Section 2.3. This consists of two  $\delta\tau$  insertions on the worldsheet, located at  $z = i$  and  $z = iy$  on the UHP, whose moduli space is parameterized by  $y \in (0, 1)$ . The amplitude decomposes into two types of Feynman diagrams, as as depicted in Figure 2.4. In the limit  $\lambda \rightarrow \infty$ , there are two such diagrams, namely

$$\mathcal{A}_{\delta\tau(p)\delta\tau(k)}^{D^2}(\lambda) = A_{\delta\tau(p)\delta\tau(k)}^{D^2} + A_{\delta\tau\chi^1}^{D^2} P_{\chi^1} A_{\delta\tau\chi^1}^{D^2}. \quad (2.35)$$

The LHS of the above expression emphasizes the expected dependence of the amplitude on  $\lambda$ . In other words, it will contain terms that do not vanish in the large  $\lambda$  limit. Here and throughout the rest of the chapter, the label  $A$  is reserved for a vertex entering into the Feynman rules as opposed to the associated term  $\mathcal{V}$  in the effective action, although the two are always related by a possible symmetry factor. Note that for well-defined quantities in the on-shell formalism,  $A$  exactly agrees with the full amplitude in the limit where certain SFT parameters are taken to be large.

The first diagram in (2.35) is the Feynman 2-point closed string vertex, which consists of moduli integration over the vertex region  $y \in (\lambda^{-2}, 1)$ . As the integrand exactly matches that of the on-shell computation, the diagram assumes a similar form

$$A_{\delta\tau(p)\delta\tau(k)}^{D^2} = 10 - 2\sqrt{2} \frac{e_{\sigma\rho}(p)k^\sigma k^\rho + e_{\sigma\rho}(k)p^\sigma p^\rho}{p \cdot k} - 8\alpha'(p \cdot k) \left( \psi\left(1 + \frac{\alpha' p \cdot k}{2}\right) + \gamma + \log(4\lambda^{-2}) \right). \quad (2.36)$$

Notice that the ad hoc cutoff  $\epsilon$  of the on-shell amplitude has been replaced by an unambiguous expression involving  $\lambda$ . Coincidentally, this  $\lambda$  dependence will drop out of the full  $N$ -point scattering amplitude once we sum over different permutations of the external states and momentum conservation is restored. This should not be so surprising, since this fact is a part of what allows us to trust the results for the momentum dependence of amplitude computed in the naive approach.

Importantly, in Sen gauge, SFT prescribes an additional contribution, namely the propagation of the ghost zero mode  $\varkappa^1$  in the second Feynman diagram of (2.35). This involves two open-closed string vertices  $A_{\delta\tau\varkappa^1}^{D^2}$  contracted by an open string propagator. Each takes the form of a disc with one  $\delta\tau$  insertion and one  $\varkappa^1$  insertion. The resulting Feynman diagram reads

$$A_{\delta\tau\varkappa^1}^{D^2} P_{\varkappa^1} A_{\delta\tau\varkappa^1}^{D^2} = -2, \quad (2.37)$$

and so  $\varkappa^1$  exchange contributes a nontrivial constant to the scattering amplitude.

Together, the two Feynman diagrams give rise to the SFT disc 2-point amplitude

$$\begin{aligned} \mathcal{A}_{\delta\tau(p)\delta\tau(k)}^{D^2}(\lambda) &= 8 - 2\sqrt{2} \frac{e_{\sigma\rho}(p)k^\sigma k^\rho + e_{\sigma\rho}(k)p^\sigma p^\rho}{p \cdot k} \\ &\quad - 8\alpha'(p \cdot k) \left( \psi\left(1 + \frac{\alpha' p \cdot k}{2}\right) + \gamma + \log(4\lambda^{-2}) \right), \end{aligned} \quad (2.38)$$

where the constant “8” in the first line differs with the factor of “10” appearing in the the Feynman vertex (as well as the on-shell amplitude). Multiplying this by  $(N - 2)$  copies of disc 1-point amplitude (1.47) and summing over distinct permutations of the momenta, we find this topology contributes to the constant  $C_1^{(N)}$  in the  $N$ -point MRV amplitude as

$$-\frac{1}{256} \sum_{1 \leq i < j \leq N} (8 + 2\ell_i \cdot p_j + \ell_j \cdot p_i) = -\frac{1}{32} \cdot \frac{N(N-1)}{2} + \frac{1}{128} \cdot N. \quad (2.39)$$

Here, the vector  $\ell_i$ , which appears in the polarization tensor  $e_{\mu\nu}(p_i)$  as in (A.28), satisfies  $\ell_i \cdot p_i = 1$ . In the above expression, we have also used momentum conservation to replace  $\sum_{j \neq i} p_j^\mu$  with  $-p_i^\mu$ . As already mentioned, while  $C_1^{(N)}$  also receives contributions from other worldsheet topologies as well as from the corrections that arise in the integration over the open string zero modes, (2.39) is solely responsible for the  $N^2$  term in  $C_1^{(N)}$ .

This unambiguously determines

$$a_0 = -\frac{1}{32} \quad (2.40)$$

in (1.11), in perfect agreement with the expected result (1.97)! We emphasize that the inclusion of the Feynman diagram where  $\mathcal{Z}^1$  propagates was essential in obtaining the correct result, which would not have been possible in the naive on-shell approach.

### 2.2.2 DETERMINATION OF $a_1$

We now focus on the constant  $a_1$ , which receives contributions from the disc 2-point amplitude as well as the annulus 1-point amplitude. It also depends on several new topologies arising from integration over the open string collective modes.

#### ANNULUS 1-POINT AMPLITUDE

In Section 2.4, we shall employ the SFT framework to recompute the annulus 1-point amplitude  $\mathcal{A}_{\delta\tau}^{A^2}$ . Recall that the amplitude corresponds to a family of worldsheets depending on the location of the closed string puncture  $w = u$  on the annulus together with its modulus  $t$ , and so there is a 2d moduli space parametrized by  $(2\pi t, u) \in \mathbb{R} \times (0, \pi)$ . Each worldsheet can also take on one of four spin structures  $\nu$ . The amplitude receives contributions from multiple Feynman diagrams, as shown in Figure 2.5. These depend on several different SFT parameters, including both  $\lambda$  and  $\alpha$ . In the large  $\lambda$  and  $\alpha$  limits, the amplitude takes the form

$$\begin{aligned} \mathcal{A}_{\delta\tau}^{A^2}(\alpha, \lambda) &= A_{\delta\tau}^{A^2} + A_{\delta\tau}^{D^2} P_{\varkappa^1} A_{\varkappa^1}^{A^2} + \frac{1}{2} A_{\delta\tau \varkappa^1 \varkappa^1}^{D^2} P_{\varkappa^1} \\ &+ \frac{1}{2} A_{\delta\tau \varkappa^1}^{D^2} P_{\varkappa^1} A_{\varkappa^1 \varkappa^1 \varkappa^1}^{D^2} P_{\varkappa^1}. \end{aligned} \tag{2.41}$$

The first term in (2.41) is the annulus 1-point vertex for the axion-dilaton. It is computed in part by moduli integration over the vertex region, indicated by the blue region in Figure 2.5. For our choice of PCO locations, the integrand is identical to that of the on-shell computation, and so gives zero once we sum over the spin structures. This is not the end of the story, since there is a mismatch in the PCO locations along the wall sepa-

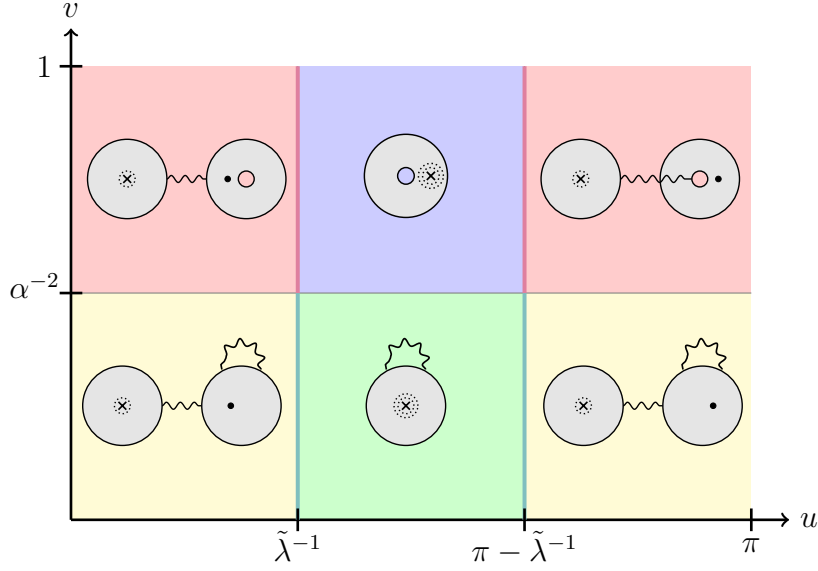


**Figure 2.5:** Feynman diagrams and the corresponding moduli domains for the annulus with one NSNS insertion. Here, a cross indicates a closed string puncture, while a wavy line indicates an open string propagator with two open string punctures at the endpoints. Dotted circles are PCO insertions averaged over a small contour enclosing the closed string. The worldsheet is given by the annulus, represented as a strip  $w \in (0, \pi) \times i\mathbb{R}$  with  $w \sim w + 2\pi it$  and  $v = e^{-2\pi t}$ , with the closed string located at  $w = u$ . The vertex region is shaded blue. Vertical integration is required along the walls  $u = \tilde{\lambda}^{-1}, \pi - \tilde{\lambda}^{-1}$  for  $v \in (0, 1)$ .

rating the vertex region and the red propagator region, corresponding to the purple segments in the figure. In order to close the gap, we must perform vertical integration along these segments, which yields a rather nontrivial expression of the form

$$A_{\delta\tau}^{A^2} = -2\pi \sum_{\nu=2}^4 (-)^{\nu} \int_0^{\ln(\alpha^2)/2\pi} dt \frac{\vartheta_{\nu}(it)^4}{\eta(it)^{12}} \frac{\partial}{\partial p_o} \log \vartheta_{\nu}(p_o|it). \quad (2.42)$$

Here,  $p_o$  is the (fixed) location of the PCO for an annulus 1-point vertex with an *open* string insertion.

The second term in (2.41), is given by the Feynman diagram consisting of an open-closed disc vertex  $A_{\delta\tau\kappa^1}^{D^2}$  contracted with the annulus 1-point vertex  $A_{\kappa^1}^{A^2}$  for  $\kappa^1$ . This diagram corresponds to the red propagator region in Figure 2.5. The annulus 1-point vertex



can be computed by integrating the correlation function involving a  $\varkappa^1$  insertion on the boundary over the vertex region  $t \in (\ln \alpha^2, \infty)$  of the 1d moduli space. Including the closed-open vertex and the open string propagator then gives the Feynman diagram

$$A_{\delta\tau}^{D^2} P_{\varkappa^1} A_{\varkappa^1}^{A^2} = 2\pi \sum_{\nu=2}^4 (-)^{\nu} \int_0^{\ln(\alpha^2)/2\pi} dt \frac{\vartheta_{\nu}(it)^4}{\eta(it)^{12}} \frac{\partial}{\partial p_o} \log \vartheta_{\nu}(p_o|it), \quad (2.43)$$

which exactly cancels with the contribution of the closed string annulus vertex in (2.42), ensuring that the final amplitude is independent of  $\alpha$  and  $p_o$ ! This exemplifies the delicate interplay between vertical integration and  $\varkappa^1$  propagation in string field theory.

The third term in (2.41) is a Feynman loop diagram consisting of the open-closed disc vertex  $A_{\delta\tau(p)\varkappa^1\varkappa^1}^{D^2}$  with the two open string punctures contracted, as depicted by the green propagator region in Figure 2.5. The associated disc amplitude corresponds to a family of worldsheets with a closed string at  $z = i$  together with two open strings at  $z = \pm\beta$ , and so has a 1d moduli space parametrized by  $\beta \in (0, \infty)$ . The disc vertex is then defined as moduli integration over the vertex region  $((2\tilde{\lambda})^{-1}, 2\tilde{\lambda})$ , where  $\tilde{\lambda} = \lambda\alpha$ . Including the ghost propagator as well as the symmetry factor of  $\frac{1}{2}$  common to all loop diagrams yields

$$\frac{1}{2} A_{\delta\tau\varkappa^1\varkappa^1}^{D^2} P_{\varkappa^1} = -\pi + 2\tilde{\lambda}. \quad (2.44)$$

The last Feynman diagram of (2.41) consists of vertices  $A_{\delta\tau\varkappa^1}^{D^2}$  and  $A_{\varkappa^1\varkappa^1\varkappa^1}^{D^2}$  with all of the open strings contracted. This corresponds to the yellow propagator region of Figure 2.5. Due to the ghost structure of  $\varkappa^1$ , the 3-point vertex vanishes and so the diagram does not contribute. Summing all the Feynman diagrams, it follows that the annulus am-

plitude is

$$\mathcal{A}_{\delta\tau}^{A^2} = -\pi + 2\tilde{\lambda}. \quad (2.45)$$

Notice that unlike the naive on-shell amplitude, which is zero, the SFT amplitude receives a constant,  $\tilde{\lambda}$ -dependent correction that contributes to the value of  $a_1$ .

### INTEGRATION OVER $\zeta^2$

We now focus on the SFT corrections which result from integration over the open string zero modes. First, let us consider the constant  $Y$  corresponding to integration in  $\zeta^2$ . Its value can be determined by computing the disc amplitude with a  $\delta\tau$  insertion together with the open string insertions  $\chi$ ,  $\chi^*$ , and  $\zeta^2$ . In Section 2.5, we compute this amplitude with  $\chi$  and  $\chi^*$  chosen such that their vertex operators agree with those of  $\zeta^2$  and  $\varkappa_2$  other than the Chan-Patton factors. On the UHP, we shall take the closed string position to be  $z = i$ , while the open string insertions reside on the real line at  $z = z_i$  for  $i = 1, 2, 3$ . Since all three open string states belong to different Hilbert spaces, the amplitude involves only a single cyclic ordering of  $z_1, z_2, z_3$ , which itself corresponds to three linear orderings given by  $z_1 < z_2 < z_3$ ,  $z_2 < z_3 < z_1$ , and  $z_3 < z_1 < z_2$ . Fixing one of the open string positions, say  $z_1 = 0$ , parametrizes the 2d moduli space in terms of  $(z_2, z_3)$ . In the large  $\lambda, \alpha$  limits, the amplitude receives contributions from only a finite number of Feynman diagrams, namely

$$\begin{aligned} \mathcal{A}_{\delta\tau\chi\chi^*\zeta^2} &= A_{\delta\tau\chi\chi^*\zeta^2}^{D^2} + A_{\delta\tau\varkappa^1}^{D^2} P_{\varkappa^1} A_{\varkappa^1\chi\chi^*\zeta^2}^{D^2} + A_{\delta\tau\chi\varkappa^1}^{D^2} P_{\varkappa^1} A_{\varkappa^1\chi^*\zeta^2}^{D^2} \\ &+ A_{\delta\tau\varkappa^1}^{D^2} P_{\varkappa^1} A_{\varkappa^1\chi\varkappa^1}^{D^2} P_{\varkappa^1} A_{\varkappa^1\chi^*\zeta^2}^{D^2} + \text{cyclic perm.} \end{aligned} \quad (2.46)$$

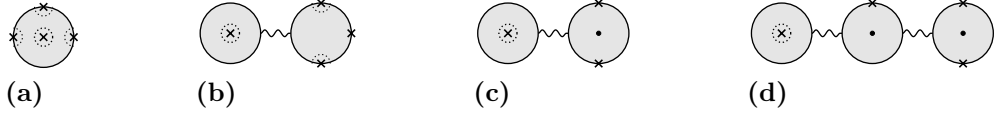


**Figure 2.6:** Feynman diagrams for the disc with one NSNS insertion and three NS insertions. The closed and open string punctures are represented by crosses. Black dots represent a PCO insertion in the bulk, while dotted (semi-)circles indicate a PCO averaged over a contour surrounding the (open) closed string puncture. Diagram (a) is the Feynman vertex corresponding to the vertex region of the 2d moduli space, while diagrams (b-d) each cover a propagator region.

The first diagram of (2.46) is given by the Feynman disc vertex  $A_{\delta\tau\chi\chi^*\zeta^2}^{D^2}$ , as shown in Figure 2.6(a). It receives contributions from moduli integration over the vertex region together with vertical integration at the 1d wall that meets with the propagator region corresponding to the Feynman diagram in Figure 2.6(c). For our choice of PCO loci, the former vanishes, and so we never need to explicitly integrate over any regions of the 2d moduli space. Meanwhile the later gives

$$A_{\delta\tau\chi\chi^*\zeta^2}^{D^2} = -2\tilde{\lambda}. \quad (2.47)$$

The second Feynman diagram in (2.46) corresponds to  $\varkappa^1$  exchange. It is given by an open-closed vertex  $A_{\delta\tau\varkappa^1}^{D^2}$  contracted with a 4-point vertex  $A_{\chi\chi^*\zeta^2\varkappa^1}^{D^2}$ , as shown in Figure 2.6(b). Consider the disc 4-point amplitude, which can be computed by inserting all three external open strings together with  $\varkappa^1$  on the disc. We fix the location of the vertex operators to  $z = 0, 1, \infty$  for the external states and take  $\varkappa^1$  to be at  $z = x$ . The 1d moduli space is completely covered by  $x \in \mathbb{R}$  since we must keep the cyclic ordering of the external states fixed. The Feynman 4-point vertex  $A_{\chi\chi^*\zeta^2\varkappa^1}^{D^2}$ , which contributes to this amplitude, corresponds to moduli integration over the vertex region  $x \in \mathcal{R}_{\text{O}000}$ , the details of which we postpone to Section 2.5. (In this case, vertical integration does not

contribute due to the ghost structures of the vertex operators). Together with the other vertex and the ghost propagator, it gives

$$A_{\delta\tau\kappa^1}^{D^2} P_{\kappa^1} A_{\chi\chi^*\zeta^2\kappa^1}^{D^2} = -2\pi. \quad (2.48)$$

The remaining Feynman diagrams in (2.46) all involve 3-point disc vertices of the open string fields including  $\kappa^1$ , corresponding to Figures 2.6(c-d). In practice, we find that these all vanish due to their ghost structures, and so the Feynman diagrams do not contribute.

Summing all the Feynman diagrams in (2.46) leads to the amplitude

$$\mathcal{A}_{\delta\tau\chi\chi^*\zeta^2}^{D^2}(\tilde{\lambda}) = -2\pi - 2\tilde{\lambda}. \quad (2.49)$$

In order to extract the value of  $Y$ , we must also compute the normalization factor in (2.8). This is given by the disc amplitude for the open strings, which we determine to be

$$\mathcal{A}_{\chi\chi^*\zeta^2}^{D^2} = -1. \quad (2.50)$$

Using (2.8) then gives

$$Y = 2\pi + 2\tilde{\lambda}. \quad (2.51)$$

#### INTEGRATION OVER $\phi^\mu$

We now determine the corrections  $\Delta U$  and  $\Delta U''$  arising from integration in  $\phi^\mu$ . These can be extracted from the disc amplitude with two  $\delta\tau$  insertions and one  $\phi^\mu$  insertion, the

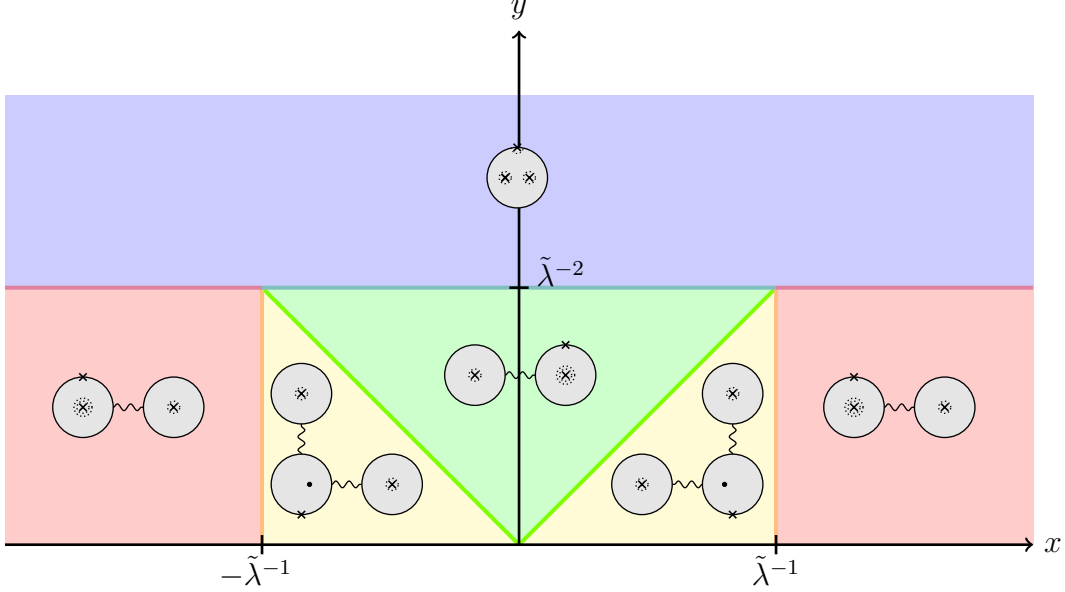


**Figure 2.7:** Feynman diagrams and the corresponding moduli domains for the disc with two NSNS insertions and one NS insertion. Here, a cross indicates a closed/open string puncture, while a wavy line indicates an open string propagator with two open string punctures at the endpoints. Dotted circles are PCO insertions averaged over a small contour enclosing the closed string, while points are PCO insertions. The worldsheet is given by the disc, represented as the UHP, with the closed strings located at  $z = i$  and  $z = iy$ , and the open string at  $z = x$ . The vertex region is shaded blue. Vertical integration is required along each 1d segment separating adjacent diagrams.

computation of which is carried out in Section 2.6. On the UHP, the closed strings are placed at  $z = i$  and  $z = iy$ , respectively, while the open string is located at  $z = x$ , leading to a 2d moduli space parametrized by  $(x, y) \in \mathbb{R} \times (0, 1)$ . The amplitude decomposes into Feynman diagrams according to Figure 2.7. In the large  $\tilde{\lambda}$  limit, the only contributions are

$$\begin{aligned}
\mathcal{A}_{\delta\tau(p)\delta\tau(k)\phi^\mu}^{D^2}(\tilde{\lambda}) &= A_{\delta\tau(p)\delta\tau(k)\phi^\mu}^{D^2} + A_{\delta\tau(p)\mathcal{X}^1}^{D^2} P_{\mathcal{X}^1} A_{\delta\tau(k)\mathcal{X}^1\phi^\mu}^{D^2} \\
&+ A_{\delta\tau(k)\mathcal{X}^1}^{D^2} P_{\mathcal{X}^1} A_{\delta\tau(p)\mathcal{X}^1\phi^\mu}^{D^2} + A_{\delta\tau(p)\mathcal{X}^1}^{D^2} P_{\mathcal{X}^1} A_{\mathcal{X}^1\mathcal{X}^1\phi^\mu}^{D^2} P_{\mathcal{X}^1} A_{\delta\tau(k)\mathcal{X}^1}^{D^2},
\end{aligned} \tag{2.52}$$

The first diagram in (2.52) is the Feynman vertex  $A_{\delta\tau(p)\mathcal{X}^1}^{D^2}$  itself, which corresponds to

integration over the vertex region  $\mathbb{R} \times (\tilde{\lambda}^{-2}, 1)$ , displayed in blue in Figure 2.7. Vertical integration is also necessary at  $y = \tilde{\lambda}^{-1}$ , indicated by the purple and teal segments, which corresponds to the boundary meeting two separate propagator regions (red and green). Together, the moduli and vertical integration contribute

$$\begin{aligned}
A_{\delta\tau(p)\delta\tau(k)\phi^\mu}^{D^2} &= \sqrt{2}\pi A_{\delta\tau(p)\delta\tau(k)}^{D^2}(\tilde{\lambda})(ip^\mu + ik^\mu) - 4\sqrt{2}(\frac{1}{2}\pi + \tilde{\lambda})(ip^\mu + ik^\mu) \\
&\quad + 4\pi(ip_\nu e^{\mu\nu}(k) + ik_\nu e^{\mu\nu}(p)).
\end{aligned} \tag{2.53}$$

Here  $A_{\delta\tau(p)\delta\tau(k)}^{D^2}(\tilde{\lambda})$  is the 2-point vertex in (2.36) with  $\lambda$  replaced by  $\tilde{\lambda}$ .

The next two Feynman vertices in (2.52) consist of a 2-point vertex  $A_{\delta\tau(p)\varkappa^1}^{D^2}$  contracted with a 3-point vertex  $A_{\delta\tau(p)\varkappa^1\phi^\mu}^{D^2}$ , including exchanging the closed string states. The diagrams separately correspond to the red and green propagator regions of Figure 2.7. They contribute as

$$A_{\delta\tau(p)\varkappa^1}^{D^2} P_{\varkappa^1} A_{\delta\tau(k)\varkappa^1\phi^\mu}^{D^2} = -2\sqrt{2}\pi(ip^\mu + ik^\mu) \tag{2.54}$$

and similarly for  $p \leftrightarrow k$ .

The last Feynman diagram in (2.52) involves two open-closed vertices as well as an open 3-point vertex, depicted by the yellow propagator region in Figure 2.7. The 3-point vertex  $A_{\varkappa^1\varkappa^1\phi^\mu}^{D^2} = 0$ , and so does the diagram does not contribute to the amplitude.

In total, the Feynman diagrams in (2.52) give

$$\begin{aligned}
\mathcal{A}_{\delta\tau(p)\delta\tau(k)\phi^\mu}^{D^2} &= \sqrt{2}\pi \mathcal{A}_{\delta\tau(p)\delta\tau(k)}^{D^2}(\tilde{\lambda})(ip^\mu + ik^\mu) - 4\sqrt{2}(\pi + \tilde{\lambda})(ip^\mu + ik^\mu) \\
&\quad + 4\pi(ip_\nu e^{\mu\nu}(k) + ik_\nu e^{\mu\nu}(p)),
\end{aligned} \tag{2.55}$$

where this expression has been written in terms of the full 2-point amplitude in (2.38)

with  $\lambda$  replaced by  $\tilde{\lambda}$ . Recall the definition of  $\Delta U$ ,  $\Delta U'$  and  $\Delta U''$  in the SFT effective action. From (2.19), it follows that the coefficients enter into the amplitude as

$$\begin{aligned} \mathcal{A}_{\delta\tau(p)\delta\tau(k)\phi^\mu}^{D^2}(\tilde{\lambda}) = \mathcal{N}_\phi \mathcal{A}_{\delta\tau}^{D^2} \left\{ (\mathcal{A}_{\delta\tau}^{D^2})^{-1} \mathcal{A}_{\delta\tau(p)\delta\tau(k)}^{D^2} (ip^\mu + ik^\mu) - 2\Delta U(ip^\mu + ik^\mu) \right. \\ \left. - 2\Delta U'(ip \cdot ik)(ip^\mu + ik^\mu) - 2\sqrt{2}\Delta U''(ip_\nu e^{\mu\nu}(k) + ik_\nu e^{\mu\nu}(p)) \right\}. \end{aligned} \quad (2.56)$$

The coefficients  $\Delta U$  and  $\Delta U'$  come multiplied by a symmetry factor of 2 corresponding to the two copies of  $\delta\tau$  in the effective action. Note that  $e_{\mu\nu}$  in this expression satisfies  $e_{\mu\nu}(p)e^{\mu\nu}(p) = 1$ . The normalization factor for  $\phi^\mu$  is given by

$$\mathcal{N}_\phi \mathcal{A}_{\delta\tau}^{D^2} = -2\sqrt{2}, \quad (2.57)$$

as computed from the disc amplitude with one insertion of  $\delta\tau$  and  $\phi^\mu$  each. Comparing (2.56) with (2.55) thus determines

$$10\Delta U + \Delta U'' = -\pi - 10\tilde{\lambda}. \quad (2.58)$$

#### INTEGRATION OVER $\theta_\alpha$

Finally, we determine the correction  $\Delta V$  that arises from integration over  $\theta_\alpha$ . This involves computing the amplitude for a  $\delta\tau$  insertion together with a dilatino  $\lambda$  and fermionic zero mode  $\theta_\alpha$ , whose details can be found in Section 2.7. The vertex operators are arranged on the UHP such that  $\delta\tau$  is at  $z = i$ ,  $\lambda$  at  $z = iy$ , and  $\theta_\alpha$  at  $z = x$ . In line with the closed-closed-open amplitude of the previous section, the moduli space is parameterized by  $(x, y) \in \mathbb{R} \times (0, 1)$ , with the amplitude admitting a similar Feynman diagram

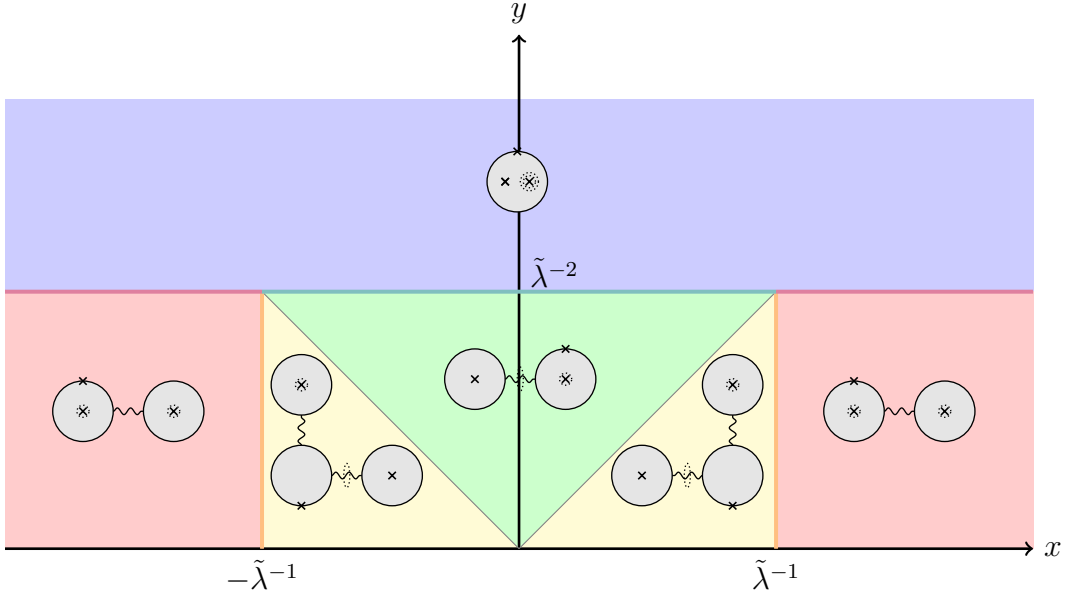


**Figure 2.8:** Feynman diagrams and the corresponding moduli domains for the disc with an NSNS, NSR/RNS, and R insertion. Here, a cross indicates a closed/open string puncture, while a wavy line indicates an open string propagator with two open string punctures at the endpoints. Dotted circles are PCO insertions averaged over a small contour enclosing the closed string, while points are PCO insertions. The worldsheet is given by the disc, represented as the UHP, with the closed strings located at  $z = i$  and  $z = iy$ , and the open string at  $z = x$ . The vertex region is shaded blue. Vertical integration is indicated by the purple, teal, and orange segments.

decomposition, as shown in Figure 2.7. One key difference is that the external states belong to different spacetime sectors, which in turn affects the PCO structure. In particular, in the  $\tilde{\lambda}$  limit, only two diagrams contribute, namely

$$\mathcal{A}_{\delta\tau(p)\lambda(k)\theta_\alpha}^{D^2}(\tilde{\lambda}) = A_{\delta\tau(p)\delta\tau(k)\theta_\alpha}^{D^2} + A_{\delta\tau(p)\varkappa^1}^{D^2} P_{\varkappa^1} A_{\lambda(k)\varkappa^1\theta_\alpha}^{D^2}. \quad (2.59)$$

The first diagram in (2.59) is the Feynman vertex  $A_{\delta\tau(p)\delta\tau(k)\theta_\alpha}^{D^2}$ , corresponding to the blue region in Figure 2.7. In addition to moduli integration, it receives contributions from vertical integration at the boundary  $y = \tilde{\lambda}^{-1}$ , indicated by the teal and purple segments.



Together, the two forms of integration contribute

$$A_{\delta\tau(p)\lambda(k)\theta_\alpha}^{D^2} = -i\pi u^\alpha(k) \left\{ \mathcal{A}_{\delta\tau(p)\delta\tau(k)}^{D^2}(\tilde{\lambda}) + 2(p \cdot k) \right\}. \quad (2.60)$$

where  $u^\alpha$  is the polarization spinor of the dilatino. In writing this expression, we have used the 2-point amplitude in (2.38) with  $\tilde{\lambda}$  replacing  $\lambda$ . The second Feynman diagram in (2.59) consists of the vertices  $A_{\delta\tau(p)\not{x}^1}^{D^2}$  and  $A_{\lambda(k)\not{x}^1\theta_\alpha}^{D^2}$  contracted together, corresponding to the red propagator region in Figure 2.7. Computation of this diagram gives

$$A_{\lambda(p)\not{x}^1\theta_\alpha}^{D^2} P_{\not{x}^1} A_{\delta\tau(k)\not{x}^1}^{D^2} = i\pi u^\alpha. \quad (2.61)$$

The two Feynman diagrams in (2.59) sum together to yield

$$\mathcal{A}_{\delta\tau(p)\lambda(k)\theta_\alpha}^{D^2} = -i\pi u^\alpha(k) \left\{ \mathcal{A}_{\delta\tau(p)\delta\tau(k)}^{D^2}(\tilde{\lambda}) - 1 + 2(p \cdot k) \right\}. \quad (2.62)$$

From (2.29) it follows that the SFT coefficients  $\Delta V$  and  $\Delta V'$  enter into the amplitude as

$$\mathcal{A}_{\delta\tau(p)\lambda(k)\theta_\alpha}^{D^2} = \mathcal{N}_\theta \mathcal{A}_{\delta\tau}^{D^2} u^\alpha(k) \left\{ (\mathcal{A}_{\delta\tau}^{D^2})^{-1} \mathcal{A}_{\delta\tau(p)\delta\tau(k)}^{D^2} - \Delta V - \Delta V'(ip \cdot ik) \right\}. \quad (2.63)$$

The normalization coefficient can be read off from the  $\delta\tau, \theta_\alpha$  disc amplitude with  $u^\alpha$

stripped away. This gives

$$\mathcal{N}_\theta \mathcal{A}_{\delta\tau}^{D^2} = -i. \quad (2.64)$$

Comparing (2.62) with (2.63), we find that the correction to (2.34) from integration in  $\theta_\alpha$

is

$$16\Delta V = 16\pi. \quad (2.65)$$

We now have all the ingredients necessary to compute the  $a_1$ . Using (2.38), (2.45), (2.51), (2.58), and (2.65) gives

$$\mathcal{A}_{\delta\tau}^{A^2} + Y + 10\Delta U + \Delta U'' + 16\Delta V = 16\pi - 6\tilde{\lambda} \quad (2.66)$$

Multiplying this by  $N - 1$  copies of disc 1-point amplitude (1.47), we find that this contributes to  $C_1^{(N)}$  in the  $N$ -point MRV amplitude (2.34) as

$$\frac{1}{128} \left( 16 - 6\frac{\tilde{\lambda}}{\pi} \right). \quad (2.67)$$

Together with the result for the disc 2-point amplitude in (2.39), we find

$$a_1 = \frac{17}{128} - \frac{3}{64\pi}\tilde{\lambda}. \quad (2.68)$$

This comes very close to value  $\frac{1}{8}$  predicted by supersymmetry and the soft relations. However, it also depends on the SFT parameter  $\tilde{\lambda}$ .

### 2.2.3 DISCUSSION

In this chapter, we have employed the framework of open+closed string field theory in order to carry out a first principles computation of D-instanton effects in type IIB string theory. We have derived the single D-instanton contribution to the  $N$ -point MRV super-

graviton scattering amplitude at next-to-leading non-perturbative order in the string coupling.

Let us briefly review the logical components necessary for the computation. In a D-instanton background, closed string amplitudes are defined through an effective action that is 1PI with respect to the closed string fields and Wilsonian with respect to the open string fields. The action takes the form of an open string path integral, which receives contributions from “massless” strings corresponding to BRST-exact states in the open string Hilbert space, as well as “massive” open strings with finite propagator. We chose to work with Siegel gauge for modes of nonzero weight and Sen gauge for those of zero weight, since the former is singular. Doing so introduced a new massive open string field  $\varkappa^1$  whose vertex operator has zero weight but is not BRST-closed. The massive open string fields in the gauge-fixed path integral were handled perturbatively, where they enter as intermediate states in Feynman diagrams contributing to the different worldsheet topologies. Such diagrams are constructed from SFT vertices, given by correlators integrated over subdomains of the worldsheet moduli space of Riemann surfaces with boundary. Their definition necessitated the introduction of several string field theoretic parameters that are expected to drop out of on-shell amplitudes. On the other hand, perturbation theory breaks down for the massless open string fields. These consist of the D-instanton collective modes  $\phi^\mu$ ,  $\theta_\alpha$  as well as a fermionic field  $\zeta^2$  corresponding to the  $U(1)$  gauge symmetry on the D-instanton worldvolume. We carried out the full non-perturbative path integral for such fields, first performing a field redefinition involving the closed string fields, which reproduced integration over the D-instanton supermoduli space  $\mathbb{R}^{10|16}$ . As a consequence of the field redefinition, the effective action receives contribu-

tions from new Feynman diagrams that cannot be attributed to the standard sum over worldsheet topologies.

The first result of this work was to show that the naive on-shell formalism, which generally suffers from divergences and ambiguities, correctly captures the momentum dependence of the MRV amplitude to the desired order in the string coupling. This relied on an argument involving various worldsheet topologies, and in particular the SFT construction of the disc 2-point amplitude. This was shown to agree with the on-shell result up to a momentum-independent constant. The remaining topologies involve at most one open closed string, and so do not play a part in this analysis. Note that this behavior is not expected to generalize at higher orders, where now Feynman diagrams with open string propagation can contribute to the momentum-dependent terms.

We also studied the momentum-independent constant coefficients  $a_0, a_1, a_2$ , which are ambiguous from the perspective of the on-shell formalism. The computation for  $a_0$  involved the disc 2-point amplitude, which in the SFT approach included a Feynman diagram corresponding to  $\varkappa^1$  propagation. Its final value agrees with the expectation of supersymmetry and soft limits, and so serves as a highly nontrivial test of D-instanton perturbation theory within superstring field theory.

The SFT computation of  $a_1$  was more delicate, as it receives contributions from several Feynman diagrams spanning amplitudes of different topologies. Complicating the computation is the fact that it also depends on the corrections arising from integration over the massless open string fields. After evaluating all of the relevant Feynman diagrams, we found a value for  $a_1$  that is very close to the predicted value from supersymmetry and soft limits, but does not quite match. Even so, we have still laid out many of the logical

and computational ingredients necessary for determining the correct value of  $a_1$ . Furthermore, many of the amplitudes we computed pass various consistency checks, such as the fact that most of the SFT parameters entering into intermediate Feynman diagrams drop out of the final calculation.

A more serious issue is that our result for  $a_1$  still depends on a single SFT parameter, which implies that the amplitude is not field redefinition invariant at the level of the open string path integral. Whether this is due to a mistake in our calculations or a sign of some missing logical piece is at the present time unclear. This uncertainty can be attributed to the fact that our approach is somewhat piecemeal, which makes determining the source of the error difficult. One subtlety in our analysis, which could contribute to this issue, is that in performing the open string path integral over the collective modes, we had to rely on open string background independence in a somewhat indirect manner. It would therefore be very interesting to analyze the D-instanton path integral and its invariance under field redefinitions in a more systematic way. For now, we shall postpone this issue to future work.<sup>5</sup>

We also hope to report on the SFT computation of  $a_2$  in the near future, which depends on the disc 2-point amplitude as well as certain empty topologies we have not studied in this work. Due to spacetime supersymmetry, it is expected that the bosonic and fermionic open string contributions to the latter cancel pairwise except for those from the zero mode sector. Their computation is only somewhat more involved than that of this

---

<sup>5</sup>Previously, a next-to-leading order SFT D-instanton computation was performed in the context of  $c = 1$  string theory in [30]. While there was highly non-trivial agreement with predictions of the duality with the matrix model, a mismatch in a single constant coefficient was found, which was later fixed by a more careful analysis in [62]. This constant of concern in [30] is analogous to  $a_1$  in (1.11).

work, since these topologies have three-dimensional moduli spaces.

A more intriguing question is to what extent the SFT framework captures D-instanton and anti D-instanton contributions. In this case, there are regions of the moduli space where tachyonic open string modes appear, and the integration over open string fields may be ill-defined. In simple situations such as ZZ-instantons in  $c = 1$  string theory, this problem appears to be remedied by a Wick rotation prescription on the open string field integration contour [24, 28, 29]. In type IIB string theory, on the other hand, it is unclear whether the contribution from a D-instanton/anti-D-instanton pair to certain observables, such as the  $D^8 R^4$  effective coupling, is even well-defined, as we do not understand the asymptotic properties of the perturbative contribution to the  $D^8 R^4$  coupling nor how to separate it from the D-instanton effects. Furthermore, the understanding of open+closed SFT in the presence of both D-instantons and anti-D-instantons seems to be crucial in connecting D-instanton perturbation theory in different instanton charge sectors, which are thus far treated separately, via open string tachyon condensation [67].

### 2.3 DISC 2-POINT AMPLITUDE

In this section, we shall calculate the disc 2-point amplitude with two  $\delta\tau$  insertions, as constructed from SFT Feynman diagrams. In order to proceed, it is necessary to first specify the string vertices that contribute to such diagrams. We begin with the string vertex  $\mathcal{V}_{D^2}^{1NSNS,1NS}$  that corresponds to a disc with one NSNS dilaton and one NS open string field insertion. Representing the disc as the upper-half plane (UHP), we place the closed string at  $z = i$  and open string at  $z = 0$ . We must further specify a local coordinate  $w$  on the chart that contains the open string insertion, with the transition map  $f^{\text{CO}}(z)$ . We

shall take  $f^{\text{CO}}(z) = \lambda^{-1}w$  with inverse

$$w^{\text{CO}}(z) = \lambda z, \quad (2.69)$$

where  $\lambda \in \mathbb{R}_+$  is an SFT parameter. Moreover, we need to place one PCO at some point on the UHP. For convenience, we shall take the PCO to be holomorphic and coincident with the closed string.<sup>6</sup> These data completely determine  $\mathcal{V}_{D^2}^{1NSNS,1NS}$ , as shown in Figure 2.3.

Next, we contract a pair of the vertices  $\mathcal{V}_{D^2}^{1NSNS,1NS}$  with an NS open string propagator to form a Feynman diagram. The corresponding family of worldsheet configurations is constructed by gluing together a pair of discs, parameterized by  $z$  and  $z'$  respectively, and identifying a pair of annuli around each of the open string insertions with the plumbing map

$$w^{\text{CO}}(z)w^{\text{CO}}(z') = -q, \quad q \in (0, 1). \quad (2.70)$$

This results in a single disc with two dilaton insertions and two PCOs. Representing the latter as the UHP, up to a  $\text{PSL}(2, \mathbb{R})$  transformation, we can place one closed string at  $z = i$  and another at  $z = iy$  with  $0 < y < 1$ . The plumbing construction determines  $y = y(q)$  as a function of  $q$ , as well as the locations of the two PCOs,  $p_1(q)$  and  $p_2(q)$ . The family of configurations obtained via plumbing covers a domain  $(0, y(q = 1)) = (0, \lambda^{-2})$  of the moduli space parameterized by  $y \in (0, 1)$ , as displayed in Figure 2.4.

There is a second Feynman diagram that is the string vertex  $\mathcal{V}_{D^2}^{1NSNS,2NSNS}$  itself. The

---

<sup>6</sup>The D-instanton boundary does not separately conserve holomorphic or antiholomorphic picture, but rather their total. This allows us to freely interchange holomorphic and antiholomorphic PCOs, which satisfy  $\mathcal{X}(u) = \tilde{\mathcal{X}}(u)$  on the boundary parameterized by  $u$ .

corresponding worldsheet configurations are that of a disc with two NSNS closed string insertions as above, but with the modulus  $y$  restricted to the domain  $(\lambda^{-2}, 1)$ . In defining this string vertex, we must also choose the locations of the two PCOs such that they agree with  $p_1(q = 1)$  and  $p_2(q = 1)$  at the boundary of the vertex region, namely  $y = y(q = 1) = \lambda^{-2}$ . If we simply place one holomorphic PCO on top of each of the closed string insertions, then  $\mathcal{V}_{D^2}^{1NSNS, 2NSNS}$  is essentially what we computed in (1.66) where the lower cutoff for the integration over  $y$  is taken to be  $\lambda^{-2}$ , and the locations of the two PCOs are continuous at  $y = \lambda^{-2}$  so that there is no need for the vertical integration.

A similar analysis applies to the diagrams involving RR axions. Each additional RR insertion removes one PCO, and so all of the vertices can be defined by placing each PCO coincident with one NSNS insertion, should any be present.

### 2.3.1 VERTEX DIAGRAM

We shall first compute the Feynman vertex  $A_{\delta\tau(p)\delta\tau(k)}^{D^2}$ , where again note that this the vertex that enters into the Feynman rules as opposed to the associated term  $\mathcal{V}_{D^2}^{\delta\tau(p)\delta\tau(k)}$  in the string field effective action. It is given by

$$A_{\delta\tau(p)\delta\tau(k)}^{D^2} = \int_{\lambda^{-2}}^1 dy \left\langle B_y V_{\delta\tau(p)}^{(-1)}(i, -i) V_{\delta\tau(k)}^{(-1)}(iy, -iy) \right\rangle_{x^\mu=0}^{D^2}. \quad (2.71)$$

We are only concerned with terms that survive in the  $\lambda \rightarrow \infty$  limit, and so the diagram is given by (1.72) with the singular part replaced by a term proportional to

$$\int_{\lambda^{-2}}^1 \frac{dy}{y} = \log \lambda^2. \quad (2.72)$$



We stress that this computation is manifestly non-singular, since throughout the SFT calculation we work with finite  $\lambda$ , and only take  $\lambda \rightarrow \infty$  at the end, where it has presumably dropped out of the final result. In any case, it follows that the vertex diagram evaluates to

$$A_{\delta\tau(p)\delta\tau(k)}^{D^2} = 10 - 2\sqrt{2} \frac{e_{\sigma\rho}(p)k^\sigma k^\rho + e_{\sigma\rho}(k)p^\sigma p^\rho}{p \cdot k} - 8\alpha'(p \cdot k) \left[ \psi \left( 1 + \frac{\alpha' p \cdot k}{2} \right) + \gamma + \log(4\lambda^{-2}) \right]. \quad (2.73)$$

The RHS of this expression is given by the on-shell amplitude computed in (1.72) with the arbitrary cutoff  $\epsilon$  replaced by a constant that depends on the SFT parameters.

### 2.3.2 $\varkappa^1$ EXCHANGE DIAGRAM

Next we consider the effect of  $\varkappa^1$  exchange, which contributes to the propagator region.

This involves the open-closed vertex, which reads

$$A_{\delta\tau\varkappa^1}^{D^2} = \left\langle V_{\delta\tau}^{(-1)}(i, -i) V_{\varkappa^1}^{(-1)}(0) \right\rangle_{x^\mu=0}^{D^2}. \quad (2.74)$$

According to our definition of the vertex, the single holomorphic PCO is coincident with the closed string. In writing the above expression, we have also taken for granted that the local coordinates do not enter since both the closed string vertex operator and that of  $\varkappa^1$  are (boundary and bulk, respectively) conformal primaries of zero weight. Recall that the latter is given by

$$V_{\varkappa^1}^{(-1)}(z) = c\partial c e^{-2\phi} \partial\xi(z). \quad (2.75)$$

Due to the unusual ghost structure of (2.75), only the dilaton contributes. The relevant terms in its picture-raised vertex operator are

$$V_{\delta\tau_2}^{(0,-1)}(z, \bar{z}) = -e_{\mu\nu} \eta e^{\phi} \psi^\mu \tilde{c} e^{-\tilde{\phi}} \tilde{\psi}^\nu e^{ip \cdot X}(z, \bar{z}) + \dots, \quad (2.76)$$

where the omitted terms do not contribute to vertex. The resulting open-closed string vertex is

$$\begin{aligned} A_{\delta\tau\kappa^1}^{D^2} &= -\frac{i}{\sqrt{2}} e_{\mu\nu}(p) \left\langle \eta e^{\phi} \psi^\mu \tilde{c} e^{-\tilde{\phi}} \tilde{\psi}^\nu e^{ip \cdot X}(i, -i) e^{-2\phi} \partial\xi c \partial c(0) \right\rangle_{x^\mu=0}^{D^2} \\ &= 2i. \end{aligned} \quad (2.77)$$

Here, the doubling trick has contributed a factor of  $-1$  due to the antiholomorphic fermion.

The first Feynman diagram of Figure 2.4 with a  $\kappa^1$ -propagator thus evaluates to

$$A_{\delta\tau\kappa^1}^{D^2} P_{\kappa^1} A_{\delta\tau\kappa^1}^{D^2} = -2. \quad (2.78)$$

We now assemble the full disc 2-point amplitude, which for the large  $\lambda$  limit consists of the Feynman diagrams

$$\mathcal{A}_{\delta\tau(p)\delta\tau(k)}^{D^2} = A_{\delta\tau(p)\delta\tau(k)}^{D^2} + A_{\delta\tau\kappa^1}^{D^2} P_{\kappa^1} A_{\delta\tau\kappa^1}^{D^2}. \quad (2.79)$$

Plugging in our results for (2.73) and (2.78), we find

$$\begin{aligned} \mathcal{A}_{\delta\tau(p)\delta\tau(k)}^{D^2} &= 8 - 2\sqrt{2} \frac{e_{\sigma\rho}(p) k^\sigma k^\rho + e_{\sigma\rho}(k) p^\sigma p^\rho}{p \cdot k} \\ &\quad - 8(p \cdot k) \left[ \psi\left(1 + \frac{p \cdot k}{2}\right) + \gamma + \log(4\lambda^{-2}) \right]. \end{aligned} \quad (2.80)$$

## 2.4 ANNULUS 1-POINT AMPLITUDE

Next we consider the annulus with one closed string insertion. Although this amplitude is formally zero in the on-shell prescription, it receives nontrivial corrections in the SFT framework that depend on the string field theoretic parameters.

### 2.4.1 FEYNMAN DIAGRAMS

We begin by specifying several new vertices that enter into the Feynman diagrams associated with the propagator regions. Our definitions mostly agree with those of [29], except we must also specify the PCO loci. Consider the disc 3-point vertex  $\mathcal{V}_{D^2}^{1_{NS}, 2_{NS}, 3_{NS}}$  for open strings, as shown in Figure 2.2. We shall employ the set of transition maps given by

$$f_1^{\text{OOO}}(w_1) = \frac{2w_1}{2\alpha + w_1}, \quad f_2^{\text{OOO}}(w_2) = \frac{2\alpha + w_2}{2\alpha - w_2}, \quad f_3^{\text{OOO}}(w_3) = \frac{w_3 - 2\alpha}{2w_3}, \quad (2.81)$$

where  $w_i$  labels the coordinates on three half-discs corresponding to the open string punctures, and  $\alpha \in \mathbb{R}$  is an SFT parameter. These functions map  $w_i = 0$  to the points  $z = 0, 1, \infty$  on the UHP, and are cyclically permuted under  $z \rightarrow (1 - z)^{-1}$ . Their inverses are given by

$$w_1^{\text{OOO}}(z) = \frac{2\alpha z}{2 - z}, \quad w_2^{\text{OOO}}(z) = \frac{2\alpha(z - 1)}{z + 1}, \quad w_3^{\text{OOO}}(z) = \frac{2\alpha}{1 - 2z}. \quad (2.82)$$

With this choice of coordinates, we take the PCO to be located at the permutation-invariant point  $z = p_{\text{ooo}}$  with

$$p_{\text{ooo}} = e^{\pm \frac{i\pi}{3}}, \quad (2.83)$$

although the precise choice of sign does not matter. By doing so, we avoid having to average over the PCO location. However, the local coordinates are not symmetric under the full permutation symmetry generated by  $z \mapsto (1-z)^{-1}$  together with  $z \mapsto -1/z$ , and so we must include the other cyclic ordering, e.g.  $1 \leftrightarrow 2$  exchanged, while leaving the PCO location  $p_{\text{ooo}}$  fixed.

The next vertex we shall need is the disc vertex  $\mathcal{V}_{D^2}^{1NSNS,1NS,2NS}$  that corresponds to a disc with one NSNS insertion and two NS insertions. This vertex can be determined by first considering the Feynman diagram consisting of  $\mathcal{V}_{D^2}^{1NS,2NS,3NS}$  contracted with  $\mathcal{V}_{D^2}^{1NSNS,1NS}$ . The associated worldsheet family consists of two discs, parametrized by UHPs  $z$  and  $z'$  respectively, sewn together via

$$w^{\text{CO}}(z)w_1^{\text{OOO}}(z') = -q, \quad q \in (0,1). \quad (2.84)$$

The closed string puncture is located at  $z = i$  and external open string punctures at  $z = \pm\beta$ , where

$$\beta = \frac{q}{2\tilde{\lambda}}, \quad \tilde{\lambda} \equiv \alpha\lambda. \quad (2.85)$$

The plumbing construction thus covers the range  $\beta < (2\tilde{\lambda})^{-1}$  for one choice of cyclic ordering and  $\beta > 2\tilde{\lambda}$  for the other. According to the plumbing map, one PCO will be coincident with the closed string and the other located at  $z = p(\beta)$ , whose precise form is unnecessary for our computation.

Now let us return to the vertex  $\mathcal{V}_{D^2}^{1NSNS,1NS,2NS}$ . This covers the remainder of moduli space consisting of  $\beta \in ((2\tilde{\lambda})^{-1}, 2\tilde{\lambda})$ . We shall take the local coordinates around the open

string punctures to be

$$w_1^{\text{COO}}(z) = \frac{\alpha\tilde{\lambda}(z+\beta)}{(1-\beta z) - \tilde{\lambda}f(\beta)(z+\beta)}, \quad w_2^{\text{COO}}(z) = \frac{\alpha\tilde{\lambda}(z-\beta)}{(1+\beta z) + \tilde{\lambda}f(\beta)(z-\beta)}. \quad (2.86)$$

These must be compatible with those of the other Feynman diagram, which is to say that the two must agree at the boundary  $\beta = (2\tilde{\lambda})^{-1}$  separating the vertex and propagator regions of moduli space. For this to be the case, the function  $f(\beta)$  necessarily satisfies

$$f(-\beta) = f(1/\beta) = -f(\beta), \quad f(2\tilde{\lambda}) = \frac{3-4\tilde{\lambda}^2}{8\tilde{\lambda}^2}. \quad (2.87)$$

We shall take the PCOs to be separately holomorphic/antiholomorphic and coincident with the closed string. This choice disagrees with the locations of the PCOs for the Feynman diagram of the propagator region, and thus vertical integration will be required.

The next vertex we shall need is the annulus open vertex  $\mathcal{V}_{A^2}^{1NS}$  corresponding to an annulus with a single NS open string insertion. Take the annulus to be the strip with global coordinate  $w \in (0, \pi)$  identified under  $w \simeq w + 2\pi it$ , with the open string at  $w = 0$ . There is a single PCO, which we take holomorphic and located at  $w = p_o$ , independent of  $t$ .<sup>7</sup> The diagram covers the vertex region  $2\pi t \in (0, \ln \alpha^2)$  of the annulus open string amplitude. We must also sum over the spin structures  $\nu$ . In principle, it is also necessary to introduce local coordinates for the open string puncture that agrees with those of the Feynman diagram covering the propagator region, i.e.  $\mathcal{V}_{D^2}^{1NS, 2NS, 3NS}$ , at the boundary  $2\pi t = \ln \alpha^2$ .

Now that the elementary vertices have been specified, we turn our attention to the

---

<sup>7</sup>After performing the doubling trick, the now holomorphic PCO is located at  $w = y'_0$ .

Feynman diagrams that contribute to the propagator regions of the annulus amplitude.

In the discussion which follows, we shall not need the local coordinate data for the external open string punctures.<sup>8</sup>

### CO-O(OO) DIAGRAM

The first Feynman diagram of consideration consists of the vertices  $\mathcal{V}_{D^2}^{1NSNS,1NS}$  and  $\mathcal{V}_{D^2}^{1NS,2NS,3NS}$ , with both pairs of open strings contracted together. The associated family of worldsheet configurations is constructed by joining together a pair of discs, parametrized by  $z$  and  $z'$  respectively, via the plumbing maps

$$\begin{aligned} w^{\text{CO}}(z)w_1^{\text{OOO}}(z') &= -q_1, & q_1 &\in (0, 1), \\ w_2^{\text{OOO}}(z')w_3^{\text{OOO}}(z') &= -q_2, & q_2 &\in (0, 1). \end{aligned} \tag{2.88}$$

The first line corresponds to NS open string exchange, whereas the second corresponds to an NS open string loop. This leads to an annulus, represented by the strip, with a single closed string insertion and two PCOs. Up to a  $PSL(2, \mathbb{R})$  transformation, we can place the closed string at  $w = u$  with  $u$  real, where  $w = -i \ln z$ . The plumbing construction determines  $u = u(q_1, q_2)$  and  $t = t(q_1, q_2)$  as a function of the gluing parameters  $q_1, q_2$ . Such a construction also fixes the locations of the PCOs, with one coincident with the closed string and the one at  $z' = p_o$  now located at  $w = p(u, t; p_o)$ , which varies with the moduli. In determining the propagator region corresponding to the range of  $q_1, q_2$ , we must also sum over the two cyclically inequivalent permutations of the open string punctures.

---

<sup>8</sup>For the curious reader, detailed local coordinate data for the open strings punctures in the annulus 1-point amplitude can be found in [29].

tures. To leading order in the SFT parameters, it consists of two disconnected regions  $2\pi t \in (\ln \alpha^2, \infty)$  and  $u \in (0, \tilde{\lambda}^{-1}) \cup (\pi - \tilde{\lambda}^{-1}, \pi)$ , where each component corresponds to a separate boundary of the annulus, as shown in Figure 2.5. There is a similar construction for R-sector open string loops, corresponding to replacing the 3-point vertex with  $\mathcal{V}_{D^2}^{1NS,2R,3R}$ , that gives rise to different spin structures of the annulus.

### CO-(O) DIAGRAM

The next Feynman diagram of consideration consists of the closed-open vertex  $\mathcal{V}_{D^2}^{1NSNS,1NS}$  contracted with  $\mathcal{V}_{A^2}^{2NS}$ . Here, the worldsheet configurations correspond to a disc glued to an annulus of modulus  $t$ , parametrized by the UHP  $z$  and strip  $w$ , respectively, via the plumbing map

$$w_1^{\text{CO}}(z)w_1^{\text{O}}(w) = -q_1, \quad q_1 \in (0, 1) \quad (2.89)$$

This leads to the desired annulus with a single closed string and two PCOs. After performing the appropriate  $PSL(2, \mathbb{R})$  transformation, the closed string and PCO from the disc are located at  $w = u$  with  $u = u(q_1)$  real. The other PCO gets mapped to  $w = p(u; p_o)$  in the bulk, which at leading order in  $\tilde{\lambda}$  is given by  $p(u; p_o) = p_o$ . Furthermore, the corresponding propagator region is given by  $(2\pi t, u) \in (\ln \alpha^2, \infty) \times (\tilde{\lambda}^{-1}, \pi - \tilde{\lambda}^{-1})$ , as shown in Figure 2.5.

### C(OO) DIAGRAM

The third and final Feynman diagram contributing to a propagator region consists of  $\mathcal{V}_{D^2}^{1NSNS,1NS,2NS}$  with the two open strings contracted. Here, the worldsheet configurations

arise from a disc with UHP coordinate  $z$ , with the two open string punctures at  $z = \pm\beta$  glued together via

$$w_1^{\text{COO}}(z)w_2^{\text{COO}}(z) = -q_2, \quad q_2 \in (0,1). \quad (2.90)$$

Transforming to the strip coordinate  $w = -i \ln z$ , we can use the  $PSL(2, \mathbb{R})$  symmetry to place the closed string puncture at  $w = u$ , where both PCOs remain coincident with the closed string. Note that  $u = u(\beta)$  varies with the modulus  $\beta$ . The range  $(2\tilde{\lambda})^{-1} < \beta < 2\tilde{\lambda}$  together with that of the plumbing parameter fixes the subdomain of moduli space to take the form of two disconnected components, with

$$(2\pi t, u) \in (0, \ln \alpha^2) \times (0, \tilde{\lambda}^{-1}) \cup (\pi - \tilde{\lambda}^{-1}, \pi), \quad (2.91)$$

as shown in Figure 2.5. Vertical integration is required along the walls  $u = \tilde{\lambda}, \pi - \tilde{\lambda}$  separating the C(OO) propagator region from the CO-O(OO) propagator region. Once again, we can replace the vertex with  $\mathcal{V}_{D^2}^{1NSNS, 1R, 2R}$  and carry out the same sewing procedure to get the contributions of the other spin structures.

## VERTEX DIAGRAM

Finally, we are in a position to analyze the Feynman diagram that contributes to the vertex region, which is just the annulus vertex  $\mathcal{V}_{A^2}^{1NSNS}$  itself. As usual, we shall take the annulus with modulus  $t$  to be represented by the strip with coordinate  $w$ , and place the closed string puncture at  $w = u$ . Both PCOs, one holomorphic and the other antiholomorphic, are taken coincident with the closed string. The vertex region corresponds to range of  $u$  and  $t$  that covers the remainder of moduli space, i.e.  $(2\pi t, u) \in (0, \ln \alpha) \times (\tilde{\lambda}^{-1}, \pi -$



$\tilde{\lambda}^{-1}$ ), as shown in Figure 2.5. It is also necessary to sum over the spin structures  $\nu$ .

There is an analogous construction of Feynman diagrams for an RR-sector closed string. In practice, we find that all such Feynman diagrams vanish, and so we shall not discuss them here.

#### 2.4.2 VERTEX REGION

In this section we compute the closed string annulus 1-point vertex. The contribution of moduli integration over the vertex region is given by

$$\frac{1}{4} \sum_{\nu=1}^4 (-1)^\nu \int_0^{\ln(\alpha^2)/2\pi} dt \int_{\tilde{\lambda}^{-1}}^{\pi-\tilde{\lambda}^{-1}} du \left\langle B_t B_u V_{\delta\tau}^{(0)}(u) \right\rangle_{x^\mu=0}^{A^2(t),\nu}. \quad (2.92)$$

Here,  $B_{t,u}$  are the same  $b$ -ghost insertions as in (A.70). The integrand matches that of the on-shell calculation in (A.69), and so from (A.76) it is proportional to

$$\int_0^{\ln(\alpha^2)/2\pi} dt \sum_{\nu=1}^4 (-1)^\nu \frac{\vartheta_\nu(it)^4}{\eta(it)^{12}} \int_{\tilde{\lambda}^{-1}}^{\pi-\tilde{\lambda}^{-1}} du \frac{\partial^2}{\partial u^2} \vartheta_1(2u|it) = 0, \quad (2.93)$$

which vanishes by the Jacobi quartic identity.

Next we turn our attention to the contributions from vertical integration. The vertex region shares a boundary with several propagator regions. The PCO placement is identical for the vertex and propagator region corresponding to the C(OO) diagrams, where the PCOs are located at  $w = u$  and  $\bar{w} = u$ , respectively. However, for the propagator region corresponding to the CO-(O) diagram, one of the PCOs resides at  $w = p_o$ . From this we see that the two sets of PCO locations disagree along the walls  $u = \tilde{\lambda}^{-1}$ ,  $\pi - \tilde{\lambda}$  and

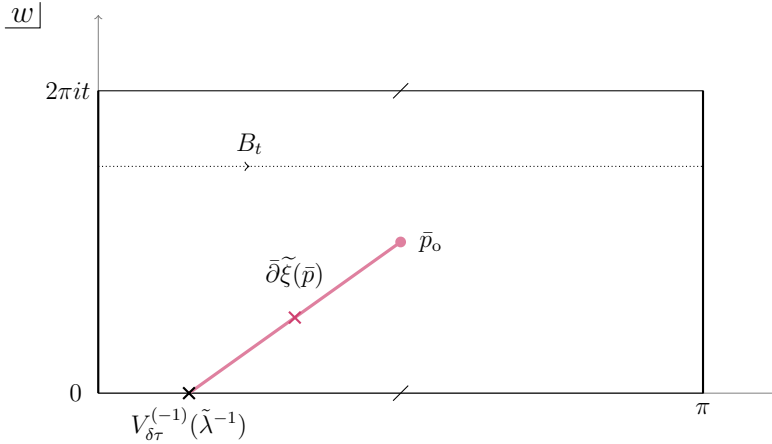


**Figure 2.9:** A family of 1-punctured annuli, parametrized by the metric modulus  $0 < t < \frac{\ln \alpha^2}{2\pi}$  and antiholomorphic PCO location  $\bar{p}$ . On the  $w$  strip, the closed string is located at  $w = \tilde{\lambda}^{-1}$ , depicted by a black cross. The  $\bar{\partial}\tilde{\xi}$  insertion at  $w = \bar{p}$  is represented by a purple cross. As  $\bar{p}$  varies, it traces out a purple “vertical segment” corresponding to vertical integration.

$2\pi t \in (0, \ln \alpha^2)$ , where vertical integration is necessary to close the gap. Carrying out the vertical integration in Figure 2.9 gives

$$\frac{1}{2} \sum_{\nu=1}^4 (-1)^\nu \int_0^{\ln(\alpha^2)/2\pi} dt \left\langle B_t \left( \tilde{\xi}(u_0) - \xi(p_o) \right) V_{\delta\tau}^{(-1)}(u_0) \right\rangle_{x^\mu=0}^{A^2(t), \nu}, \quad (2.94)$$

where we have used the symmetry  $u \mapsto \pi - u$  to write the expression in terms of a single boundary  $u_0 = \tilde{\lambda}^{-1}$ . Note that the holomorphic and antiholomorphic parts of the  $\eta$  factor takes into account first moving the antiholomorphic PCO from  $u_0$  to the boundary, where it is exchanged for a holomorphic PCO, and subsequently moved to  $p_o$ . Given that  $u_0$  is small, we can utilize the bulk-boundary OPE to write

$$V_{\delta\tau}^{(-1)}(u_0) = 2i c\eta(0) + \dots + O(u_0), \quad (2.95)$$

where  $\dots$  includes ghost structures that give vanishing contribution to (2.94). The contri-

bution of the  $b, c$  ghosts is

$$\langle B_t c(0) \rangle_{x^\mu=0}^{A^2(t), \nu} = 2\pi i \eta(it)^2, \quad (2.96)$$

whereas the fermionic ghosts give

$$\begin{aligned} & \left\langle \left( \tilde{\xi}(u_0) - \xi(p_o) \right) \eta(0) \right\rangle_{x^\mu=0}^{A^2(t), \nu} \\ &= \frac{1}{\eta(it)^9 \vartheta_\nu(it)} \left( 2\tilde{\lambda} + \frac{\partial}{\partial p_o} \log \vartheta_\nu(p_o|it) - \frac{\partial}{\partial p_o} \log E(p_o) \right) + O(\tilde{\lambda}^{-1}). \end{aligned} \quad (2.97)$$

In the above expression, we have introduced the function  $E(z|it) = \frac{\vartheta_1(z|it)}{\vartheta_1'(it)}$ . Including the  $\vartheta_\nu(it)^5/\eta(it)^5$  contribution of the free fermion CFT, we find

$$A_{\delta\tau}^{A^2} = -2\pi \sum_{\nu=2}^4 (-)^\nu \int_0^{\ln(\alpha^2)/2\pi} dt \frac{\vartheta_\nu(it)^4}{\eta(it)^{12}} \frac{\partial}{\partial p_o} \log \vartheta_\nu(p_o|it) + O(\tilde{\lambda}^{-1}), \quad (2.98)$$

where we have used the Jacobi quartic identity to discard any terms of the form  $\sum_\nu (-)^\nu \vartheta_\nu^4$ .

### 2.4.3 PROPAGATOR REGIONS

We now consider the the Feynman diagrams that contribute to the propagator regions of moduli space, where  $\alpha$  and  $\tilde{\lambda}$  are large such that only  $\varkappa^1$  propagates.

#### CO-O(OO) DIAGRAM

There is only a single CO-O(OO) diagram, which corresponds to contractions of the disc diagrams  $A_{\delta\tau\varkappa^1}^{D^2}$  and  $A_{\varkappa^1\varkappa^1\varkappa^1}^{D^2}$ . Due to the ghost structure of  $\varkappa^1$ , the 3-point vertex vanishes

$$A_{\varkappa^1\varkappa^1\varkappa^1}^{D^2} = 0 \quad (2.99)$$

and hence so does the CO-O(OO) diagram

$$\frac{1}{2} A_{\delta\tau\kappa^1}^{D^2} P_{\kappa^1} A_{\kappa^1\kappa^1\kappa^1}^{D^2} = 0, \quad (2.100)$$

where we have included a symmetry factor of  $1/2$  that accounts for contracting a pair of open strings on the same vertex.

### CO-(O) DIAGRAM

The relevant CO-(O) diagram consists of the vertices  $A_{\delta\tau\kappa^1}^{D^2}$  and  $A_{\kappa^1}^{A^2}$  contracted together.

The annulus 1-point vertex reads

$$A_{\kappa^1}^{A^2} = \frac{1}{2} \sum_{\nu=1}^4 (-1)^\nu \int_0^{\ln(\alpha^2)/2\pi} dt \left\langle B_t \mathcal{X}(p_o) V_{\kappa^1}^{(-1)}(0) \right\rangle_{x^\mu=0}^{A^2(t),\nu}, \quad (2.101)$$

where the details of the local coordinate chart are unimportant since  $V_{\kappa^1}$  is a weight zero conformal primary. As was the case for the annulus 1-point amplitude, the factor of  $\sum_\nu \frac{1}{2}(-)^\nu$  arises from the type IIB GSO projection.

In order to compute the diagram, we can consider the ghost and matter CFTs separately. In particular, there is a  $b, c$  contribution that involves two copies of each ghost field, which can be determined by one's favorite free field technique. Consider the ghost oscillators  $b_m$  and  $c_m$  for  $m \in \mathbb{Z}$  satisfying  $\{b_m, c_n\} = \delta_{m,n}$ . Writing the annulus correlator

as a trace over the strip Hilbert space gives

$$\begin{aligned}
\langle b(z)c(0)b_0c_0 \rangle^{A^2(t)} &= \text{Tr} \left[ (-)^{N_{bc}} v^{L_0 - c/24} b(z)c(0)b_0c_0 \right] \\
&= \sum_{r=-\infty}^{\infty} e^{irz} \text{Tr} \left[ (-)^{N_{bc}} v^{L_0 - c/24} b_r c_{-r} b_0 c_0 \right] \\
&= \eta(it)^2 \left[ \sum_{r=0}^{\infty} e^{irz} + \sum_{r=1}^{\infty} v^r \frac{e^{irz} - e^{-irz}}{1 - v^r} \right].
\end{aligned} \tag{2.102}$$

In the above expression,  $N_{bc}$  is the  $bc$  ghost number and  $v = e^{-2\pi t}$ . The third line follows from the fact that  $b_r c_{-r}$  ( $c_r b_{-r}$ ) for  $r > 0$  annihilates states containing  $c_{-r}$  ( $b_{-r}$ ) and gives 1 otherwise. Using the identities

$$\sum_{r=1}^{\infty} \frac{1}{r} x^r = -\log(1 - x), \quad \frac{x^r}{1 - v^r} = -\sum_{p=0}^{\infty} \log(1 - xv^p) \tag{2.103}$$

it follows that

$$\begin{aligned}
\langle b(z)c(0)b_0c_0 \rangle^{A^2(t)} &= \frac{1}{i} \eta(it)^2 \frac{\partial}{\partial z} \left[ \sum_{r=1}^{\infty} \frac{1}{r} e^{irz} + \sum_{r=1}^{\infty} \frac{v^r}{r} \frac{e^{irz} + e^{-irz}}{1 - v^r} \right] \\
&= i\eta(it)^2 \frac{\partial}{\partial z} \log \left[ (1 - e^{iz}) \prod_{p=1}^{\infty} (1 - v^p e^{irz})(1 - v^p e^{-irz}) \right] \\
&= i\eta(it)^2 \left[ \frac{i}{2} + \frac{\partial}{\partial z} \log E(z|it) \right],
\end{aligned} \tag{2.104}$$

where in going from the second to the third lines we have used

$$\frac{\partial}{\partial z} \log(1 - e^{-iz}) = \frac{\partial}{\partial z} \log \sin(z/2) + \frac{i}{2}. \tag{2.105}$$

Returning to the annulus amplitude of interest, we can use the above result to get

$$\left\langle B_t b(p_o) c \partial c(0) \right\rangle_{x^\mu=0}^{A^2(t),\nu} = 2\pi i \eta(it)^2 \frac{\partial^2}{\partial p_o^2} \ln E(p_o|it). \quad (2.106)$$

It follows that for all of the spin structures except  $\nu \neq 1$ , correlation function in the full matter+ghost CFT is

$$\begin{aligned} \left\langle B_t \left[ b \partial \eta e^{2\phi} + \partial(b \eta e^{2\phi}) \right] (p_o) c \partial c e^{-2\phi} \partial \xi(0) \right\rangle_{x^\mu=0}^{A^2(t),\nu} \\ = 2\pi i \frac{1}{\eta(it)^{12}} \frac{\vartheta_\nu(it)^6}{\vartheta_\nu(p_o|it)^2} E(p_o|it) \frac{\partial^3}{\partial p_o^3} \ln E(p_o|it), \end{aligned} \quad (2.107)$$

while it vanishes for  $\nu = 1$ . The annulus 1-point vertex thus gives

$$A_{\mathcal{Z}^1}^{A^2} = i\pi \sum_{\nu=2}^4 (-1)^\nu \int_0^{\ln(\alpha^2)/2\pi} dt \frac{\vartheta_\nu(it)^6}{\eta(it)^{12} \vartheta_\nu(p_o|it)^2} E(p_o|it) \frac{\partial^3}{\partial p_o^3} \ln E(p_o|it). \quad (2.108)$$

We can further simplify this expression using the following identity<sup>9</sup>

$$\sum_{\nu=2}^4 (-)^\nu \frac{\vartheta_\nu(it)^6}{\vartheta_\nu(w|it)^2} E(w|it) \frac{\partial^3}{\partial w^3} \ln E(w|it) = 2 \sum_{\nu=2}^4 (-)^\nu \vartheta_\nu(it)^4 \frac{\partial}{\partial w} \log \vartheta_\nu(w|it). \quad (2.109)$$

Multiplying by  $P_{\mathcal{Z}^1} = 1/2$  and  $A_{\mathcal{Z}^1 \delta\tau}^{D^2} = -2i$ , we find that the contribution of the CO-(O) diagram is

$$A_{\delta\tau \mathcal{Z}^1}^{D^2} P_{\mathcal{Z}^1} A_{\mathcal{Z}^1}^{A^2} = 2\pi \sum_{\nu=2}^4 (-1)^\nu \int_0^{\ln(\alpha^2)/2\pi} dt \frac{\vartheta_\nu(it)^4}{\eta(it)^{12}} \frac{\partial}{\partial p_o} \log \vartheta_\nu(p_o|it). \quad (2.110)$$

---

<sup>9</sup>The two modular forms share the same pole structure, and so their equivalence can be proved by equating terms order-by-order in a series expansion around  $v = e^{-2\pi t} = 0$ . Using Mathematica, we have verified that the equality holds to arbitrarily high order.

Comparing the with the 1-point vertex in (2.98), we find that the two exactly cancel such that

$$A_{\delta\tau}^{A^2} + A_{\delta\tau\kappa^1}^{D^2} P_{\kappa^1} A_{\kappa^1}^{A^2} = 0. \quad (2.111)$$

Crucially, this ensures that the final amplitude is independent of the PCO location  $p_o$  for the annulus open string vertex, which is to be expected since there are no other Feynman diagrams that involve this vertex. It also serves as a highly nontrivial consistency check for the SFT annulus amplitude.

### C(OO) DIAGRAM

The relevant C(OO) diagram consists of the disc vertex diagram  $A_{\delta\tau\kappa^1\kappa^1}^{D^2}$  stitched together by an open string propagator  $P_{\kappa^1}$ . The vertex is given by the moduli integral

$$A_{\delta\tau\kappa^1\kappa^1}^{D^2} = \int_{(2\tilde{\lambda})^{-1}}^{2\tilde{\lambda}} d\beta \left\langle B_\beta V_{\kappa^1}(-\beta) V_{\kappa^1}(\beta) V_{\delta\tau}^{(0)}(i, -i) \right\rangle_{x^\mu=0}^{D^2}, \quad (2.112)$$

as pictured in Figure 2.10. The form of the  $b$ -ghost insertion is fixed by the definition of the local coordinates in (2.86), namely

$$\begin{aligned} B_\beta &= -\frac{1}{1+\beta^2} \int_{S_{-\beta}} \frac{dz}{\pi i} \left[ \tilde{\lambda}(z+\beta)^2 f'(\beta) + z^2 + 1 \right] b(z) \\ &\quad + \frac{1}{1+\beta^2} \int_{S_\beta} \frac{dz}{\pi i} \left[ \tilde{\lambda}(z-\beta)^2 f'(\beta) + z^2 + 1 \right] b(z). \end{aligned} \quad (2.113)$$

Although vertical integration is in principle required, we find that it does not contribute in practice due to the ghost structure of the  $\kappa^1$ . A similar argument implies that the ax-

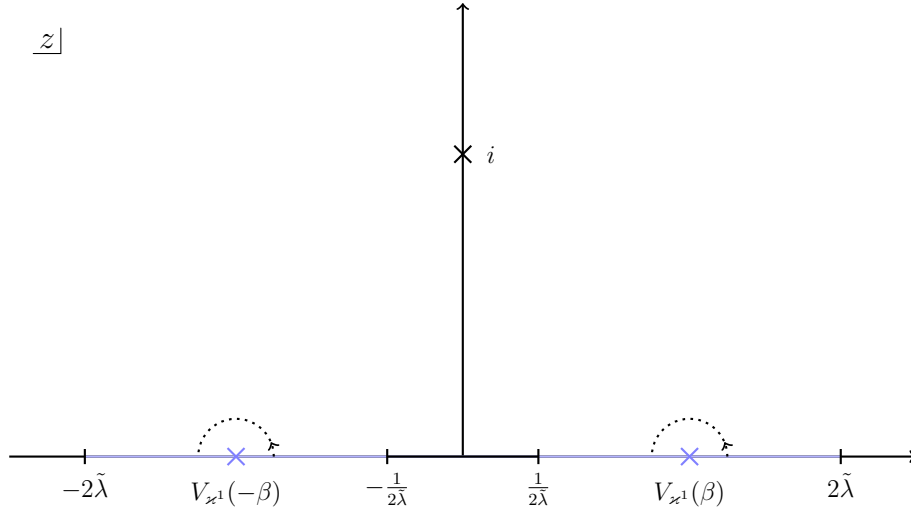


**Figure 2.10:** A family of open-closed 3-punctured discs, expressed in terms of the UHP with coordinate  $z$ , as parametrized by the modulus  $\beta \in ((2\tilde{\lambda})^{-1}, 2\tilde{\lambda})$ . There is one closed string puncture located at  $z = i$  corresponding to the black cross, while there are two open string punctures at  $z = \pm\beta$  corresponding to the blue crosses. The  $b$ -ghost contour  $B_\beta$  surrounds the two open string punctures, as represented by the dotted counterclockwise curves. As  $\beta$  varies, the blue crosses trace out the two blue segments, corresponding to moduli integration over the vertex region.

ion does not participate either. For the dilaton, we find

$$\begin{aligned}
A_{\delta\tau z^1 z^1}^{D^2} &= 2 \int_{(2\tilde{\lambda})^{-1}}^{2\tilde{\lambda}} d\beta \frac{(1 - \beta^2)^2}{\beta^2(1 + \beta^2)} \\
&= -4\pi + 8\tilde{\lambda} + O(\tilde{\lambda}^{-1})
\end{aligned} \tag{2.114}$$

and so the C(OO) diagram contributes as

$$\frac{1}{2} A_{\delta\tau z^1 z^1}^{D^2} P_{z^1} = -\pi + 2\tilde{\lambda}. \tag{2.115}$$

In the limit of large  $\tilde{\lambda}$ , the annulus 1-point amplitude is fully captured by the Feynman diagrams

$$\begin{aligned}
\mathcal{A}_{\delta\tau}^{A^2} &= A_{\delta\tau}^{A^2} + \frac{1}{2} A_{\delta\tau z^1}^{D^2} P_{z^1} A_{z^1 z^1 z^1}^{D^2} P_{z^1} \\
&\quad + A_{\delta\tau z^1}^{D^2} P_{z^1} A_{z^1}^{A^2} + \frac{1}{2} A_{\delta\tau z^1 z^1}^{D^2} P_{z^1}.
\end{aligned} \tag{2.116}$$



Plugging in (2.98), (2.100), (2.110), and (2.115), we find that all of the contributions vanish or cancel except for the C(OO) diagram,

$$\mathcal{A}_{\delta\tau}^{A^2} = -\pi + 2\tilde{\lambda}. \quad (2.117)$$

A few comments are in order. First and most important, unlike the naive on-shell result (A.76), we can see that the SFT annulus amplitude is nonzero, and so contributes to the constant  $a_1$ . Second, it also depends linearly on the SFT parameter  $\tilde{\lambda}$ , which suggests that other Feynman diagrams must come into play in order to guarantee a result for  $a_1$  free of SFT parameters. As we argued for previously, such diagrams arise from the integration over the open string collective modes, which we consider in the next few sections.

## 2.5 $\delta\tau$ , $\chi$ , $\chi^*$ , $\zeta^2$ DISC AMPLITUDE

In this section, we shall consider the disc amplitude an axion-dilaton together with  $\chi$ ,  $\chi^*$ , and  $\zeta^2$ . This amplitude determines the order  $g_s$  correction  $Y$  to the SFT effective action arising from integration over the  $U(1)$  ghost field  $\zeta^2$ .

### 2.5.1 FEYNMAN DIAGRAMS

We begin with a discussion of the Feynman diagrams that contribute to disc amplitudes with one NSNS insertion, one D-D<sup>s</sup> NS insertion, one D<sup>s</sup>-D NS insertion, and one D-D NS insertion. (The axion does not contribute due to its ghost structure).

## CO-OOO-OOO DIAGRAMS

The first Feynman diagram we shall consider, the CO-OO<sub>1</sub>O-OO<sub>2</sub>O<sub>3</sub> diagram, consists of three vertices contracted together, namely  $\mathcal{V}^{1NSNS,1NS}$  with two copies of  $\mathcal{V}^{1NS,2NS,3NS}$ , as shown in Figure 2.6(d). This corresponds to a family of worldsheets given by three discs, parametrized by UHP coordinates  $z, z', z''$  respectively, that are sewn together via

$$\begin{aligned} w^{\text{CO}}(z)w_1^{\text{OOO}}(z') &= -q_1, & q_1 &\in (0, 1), \\ w_1^{\text{OOO}}(z')w_3^{\text{OOO}}(z'') &= -q_2, & q_2 &\in (0, 1). \end{aligned} \tag{2.118}$$

The resulting topology is that of a disc, with the closed string puncture located at  $z = i$  and the open string punctures at  $z = z_a$  for  $z_a = z_a(q_1, q_2)$  and  $a = 1, 2, 3$ . One PCO is coincident with the closed string, while the two others at  $z' = p_{\text{ooo}}$  and  $z'' = p_{\text{ooo}}$  are located on the  $z$ -disc at  $z = p_1(q_1, q_2; p_{\text{ooo}})$  and  $z = p_2(q_1, q_2; p_{\text{ooo}})$ , respectively. Due to the different boundary conditions for the D- and D<sup>s</sup>-instantons, only a single cyclic ordering of the external open strings contributes to the Feynman diagrams. This corresponds to taking one cyclic ordering for the open string punctures on the  $z'$  disc, and the two cyclically inequivalent orderings for those of the  $z''$  disc, which together make up the CO-OO<sub>1</sub>O-OO<sub>2</sub>O<sub>3</sub> diagram. There are also two other Feynman diagrams that contribute to the amplitude, labeled by CO-OO<sub>3</sub>O-OO<sub>1</sub>O<sub>2</sub> and CO-OO<sub>2</sub>O-OO<sub>3</sub>O<sub>1</sub>, which consist of cyclically permuting the external open strings while leaving the PCO locations fixed. The three diagrams each separately cover a disjoint propagator region in the 2d moduli space.

## COO-OOO DIAGRAMS

The next Feynman diagram of interest appears in Figure 2.6(c). It consists of the vertices  $\mathcal{V}^{1NSNS,1NS,2NS}$  and  $\mathcal{V}^{1NS,2NS,3NS}$  contracted together, and will be referred to as the  $O_1O$ - $OO_2O_3$  diagram. The corresponding family of worldsheet configurations is given by two discs, parametrized by UHP coordinates  $z$  and  $z'$  respectively, sewn together via

$$w_1^{\text{COO}}(z)w_1^{\text{OOO}}(z') = -q_1, \quad q_1 \in (0, 1). \quad (2.119)$$

On the resulting  $z$  disc, the closed string puncture is located at  $z = i$  and the open string punctures at  $z = z_a(u, \beta)$  with

$$z_1 = \beta, \quad z_2 = -\beta, \quad z_3 = -\beta + \frac{u(1 + \beta^2)}{-1 + u\beta + u\tilde{\lambda}f(\beta)}. \quad (2.120)$$

Here,  $\beta$  is the modulus of the COO vertex, while  $u$  is a new parameter given by

$$u = \frac{2\tilde{\lambda}}{\alpha^2(1 + 4\tilde{\lambda}^2)}q_1. \quad (2.121)$$

From the plumbing construction, we find that this diagram covers a propagator region given by  $\beta \in ((2\tilde{\lambda})^{-1}, 2\tilde{\lambda})$  and  $u \in (0, u_0)$  with  $u_0 = u(q_1 = 1)$ . Furthermore, there is a holomorphic/antiholomorphic pair of PCOs coincident with the closed string at  $z = i$  as well as a third PCO located at  $z = p(\beta, u; p_{\text{ooo}})$  with

$$p = \beta + \left( \frac{p_{\text{ooo}} - 2}{p_{\text{ooo}}} \right) (1 + \beta^2)u + O(u^2). \quad (2.122)$$

To first subleading order in  $u$ , the transition maps for the open string punctures take the form

$$\begin{aligned}
f_1^{\text{CO}_1\text{O-OO}_2\text{O}_3}(w_1) &= -\beta + \frac{1 + \beta^2}{\alpha\tilde{\lambda}}w_1 + O(w_1^2), \\
f_2^{\text{CO}_1\text{O-OO}_2\text{O}_3}(w_2) &= \beta - (1 + \beta^2)u + \frac{2(1 + \beta^2)u}{\alpha}w_2 + O(w_2^2), \\
f_3^{\text{CO}_1\text{O-OO}_2\text{O}_3}(w_3) &= \beta + (1 + \beta^2)u + \frac{2(1 + \beta^2)u}{\alpha}w_3 + O(w_3^2),
\end{aligned} \tag{2.123}$$

where  $w_a$  are the coordinates of the respective local patches for the three open string punctures. Once again, the full  $\text{CO}_1\text{O-OO}_2\text{O}_3$  diagram consists of a *single* cyclic ordering of the open 3-point vertex. There are two other diagrams,  $\text{CO}_3\text{O-OO}_1\text{O}_2$  and  $\text{CO}_2\text{O-OO}_3\text{O}_1$ , which consist of permuting the external open strings and leaving the PCOs untouched.

#### CO-OO<sub>1</sub>O<sub>2</sub>O<sub>3</sub> DIAGRAM

Next we turn our attention to the Feynman diagram described by contracting the vertices  $\mathcal{V}^{1NSNS,1NS}$  and  $\mathcal{V}^{1NS,2NS,3NS,4NS}$ , displayed in Figure 2.6(b). We must first describe the details of the open 4-point vertex with three open strings taken to have fixed cyclic ordering. In order to do so, consider the Feynman diagram consisting of two vertices  $\mathcal{V}^{1NS,2NS,3NS}$  contracted together. The family of worldsheet configurations can be found by gluing together two discs, parametrized by UHP coordinates  $z'$  and  $z''$  respectively, via the map

$$w_2^{\text{OO}}(z')w_2^{\text{OO}}(z'') = -q_1, \quad q_1 \in (0, 1). \tag{2.124}$$

After performing an appropriate  $PSL(2, \mathbb{R})$  transformation  $z = z(z')$ , the resulting topology is that of a disc with four open string punctures located at  $z = 0, 1, \infty, x$  with

$x = x(q_1)$ . There are several such transformations, one of which takes the form

$$z = 1 - \frac{1}{z} \frac{4\alpha^2 - q_1}{4\alpha^2 + q_1}. \quad (2.125)$$

From the plumbing construction, this implies that the open string at  $z'' = 0$  now resides at  $z = x(q_1)$  with

$$x = \alpha^{-2}q_1 + \frac{1}{2}\alpha^{-4}q_1^2 + O(\alpha^{-6}). \quad (2.126)$$

The two PCOs meanwhile are located away from the real axis at  $z = p_1(x; p_{\text{ooo}})$  and  $z = p_2(x; p_{\text{ooo}})$ , respectively; the precise forms of  $p_1$  and  $p_2$  are irrelevant for our discussion. We must also take into account the other cyclic ordering of one of the 3-punctured discs (the other contains two of the external open strings, and so is left alone). This can be achieved by extending the range of  $q_1$  to  $(-1, 1)$ , which effectively maps  $x \mapsto -x$ . Together, the plumbing construction and its reflection cover  $x \in \mathcal{R}_s$  with  $\mathcal{R}_s = (-\alpha^{-2}, \alpha^{-2})$ . The subscript  $s$  refers to the fact that this diagram is often called the  $s$ -channel exchange diagram for 4-string scattering. For computational purposes, we only need the transition maps around the open string puncture at  $x$  as well as one other insertion, say the puncture at  $z = 1$ . Using the plumbing construction in (2.124) together with (2.125), we find that the two transition maps are given by

$$\begin{aligned} f_2^{(s)}(w_2) &= 1 + \frac{\sqrt{1-x}}{\alpha} w_2 + O(w_2^2), \\ f_4^{(s)}(w_4) &= x + \frac{x\sqrt{1-x}}{\alpha} w_4 + O(w_4^2), \end{aligned} \quad (2.127)$$

where  $w_2$  and  $w_4$  are the local coordinates for the punctures at  $z = 1$  and  $z = x$ , respectively.

There are two other diagrams, the  $t$ - and  $u$ -channel diagrams, that correspond to cyclically permuting the external open strings at  $z = 0, 1, \infty$  while leaving the PCOs at their original locations (“external” being from the perspective of the COOO amplitude). This can be accomplished via the map  $z \mapsto (1 - z)^{-1}$ . One application gives the  $t$ -channel diagram covering  $x \in \mathcal{R}_t$ , with  $\mathcal{R}_t = (1 - \alpha^{-2}, 1 + \alpha^{-2})$  and transition functions

$$\begin{aligned} f_2^{(t)}(w_2) &= 1 - \frac{w}{\sqrt{x}\alpha} + O(w_2^2), \\ f_4^{(t)}(w_4) &= x - \frac{\sqrt{x}}{\alpha}w_4 + O(w_4^2). \end{aligned} \tag{2.128}$$

Similarly, another application gives the  $u$ -channel diagram, which covers  $x \in \mathcal{R}_u$  with  $\mathcal{R}_u = (-\infty, -\alpha^2) \cup (\alpha^2, \infty)$  and transition functions

$$\begin{aligned} f_2^{(u)}(w_2) &= 1 - \frac{\sqrt{x^2 - x}}{x\alpha}w_2 + O(w_2^2), \\ f_4^{(u)}(w_4) &= x + \frac{\sqrt{x^2 - x}}{\alpha}w_4 + O(w_4^2). \end{aligned} \tag{2.129}$$

The 4-point vertex  $\mathcal{V}^{1NS,2NS,3NS,4NS}$  can now be defined in reference to the  $s, t, u$ -channel diagrams and the associated propagator regions of the 4-point amplitude, as described above. The open strings are taken to reside at the same locations, with  $x$  now assuming values in the vertex region  $\mathcal{R}_{\text{OOOO}} = \mathbb{R} \setminus (\mathcal{R}_s \cup \mathcal{R}_t \cup \mathcal{R}_u)$ . We arrange the two PCOs to be coincident with the two open strings at  $z = 0$  and  $z = \infty$ , which avoids spurious singular-

ities associated with PCO collision.<sup>10</sup> The transition functions will generally depend on the local coordinates  $w_a$  of the open string punctures as

$$f_a^{\text{OOOO}}(w_a) = z_a + g_a(x)w_a + O(w_a^2) \quad (2.130)$$

for  $z_a \in \{0, 1, x\}$ , with an analogous expression for the puncture  $z_a = \infty$ . They must agree at the wall separating the vertex region and the propagator region, which in turn imposes constraints on the boundary values of  $g_a$ . Comparing with (2.127), (2.128), (2.129), we find

$$\begin{aligned} \text{(s-channel)} \quad & g_2(-\alpha^{-2}) = \alpha^{-1}, & g_2(\alpha^{-2}) &= \alpha^{-1}, \\ & g_4(-\alpha^{-2}) = \alpha^{-3}, & g_4(\alpha^{-2}) &= \alpha^{-3}, \\ \text{(t-channel)} \quad & g_2(1 - \alpha^{-2}) = \alpha^{-3}, & g_2(1 + \alpha^{-2}) &= -\alpha^{-3}, \\ & g_4(1 - \alpha^{-2}) = \alpha^{-3}, & g_4(1 + \alpha^{-2}) &= -\alpha^{-3}, \\ \text{(u-channel)} \quad & g_2(-\alpha^2) = \alpha^{-1}, & g_4(\alpha^2) &= \alpha^{-1}, \\ & g_4(-\alpha^2) = \alpha, & g_4(\alpha^2) &= \alpha. \end{aligned} \quad (2.131)$$

Finally, we can return to the construction of the  $\text{CO-OO}_1\text{O}_2\text{O}_3$  diagram, which consists of  $\mathcal{V}^{1NSNS,1NS}$  contracted with  $\mathcal{V}^{1NS,2NS,3NS,4NS}$ . While this is not strictly speaking well-defined, we *can* define these diagrams in terms of the plumbing procedure. In particular, we take two discs, parametrized by UHP coordinates  $z$  and  $z'$  respectively, and sew them

---

<sup>10</sup>Due to the PCO placement, our definition of the 4-point vertex is not symmetric under cyclic permutations of the external open string punctures. This implies that we cannot assign it the usual Feynman vertex interpretation in the field theoretic sense. Even so, as long as we are cognizant of this point, we can use the 4-point vertex in building more complicated diagrams. These diagrams are not defined not in terms of contracting field theoretic vertices, but rather only as integration over a subdomain of moduli space. In terms of this definition, such diagrams and the resulting string amplitudes are unambiguous.

together via

$$w^{\text{CO}}(z)w_4^{\text{OOOO}}(z') = -q_2, \quad q_2 \in (0, 1). \quad (2.132)$$

This corresponds to a family of worldsheets parametrized by  $(r, x)$ , where  $r = \lambda^{-1}q_2$ , with the closed string at  $z = i$  and the open strings at  $z = z_a(r, x)$  for  $a = 1, 2, 3$ . (We do not need the explicit form of these functions, nor the transition maps). This ‘diagram’ thus corresponds to a part of the propagator region of moduli space given by  $x \in \mathcal{R}_{\text{OOOO}}$  and  $r \in (0, \lambda^{-1})$ . Regarding the PCO locations, one is coincident with the closed string at  $z = i$ , while the other two are separately coincident with the open strings at  $z = z_1$  and  $z = z_3$ .

#### CO<sub>1</sub>O<sub>2</sub>O<sub>3</sub> DIAGRAM

The only remaining diagram consists of the vertex  $\mathcal{V}^{1NSNS,1NS,2NS,3NS}$  with one closed string and three open strings, as shown in Figure 2.6(a). On the disc parametrized by the UHP  $z$ , we take closed string to reside at  $z = i$  and the open strings at  $z = z_a$ , where  $z_a = z_a(t_1, t_2)$  depends on the two real moduli  $t_1, t_2$ , which generally differ from the moduli used for the propagator regions. For instance, one choice involves setting  $z_1 = 0$  and letting  $z_2$  and  $z_3$  parametrize the vertex region. This region covers the remainder of moduli space, which we denote by  $\mathcal{R}_{\text{COOO}}$ , although its explicit form is unnecessary for our purposes.

In order to have maximal agreement for PCO locations with the propagator region, we shall take one PCO coincident with the closed string and two PCOs coincident with open string punctures at  $z_1$  and  $z_3$ . While vertical integration is still needed, our choice of



PCOs renders it not too severe. Indeed, the only mismatch among PCO locations occurs at the wall separating the vertex region from the propagator regions corresponding to the COO-OOO diagrams.

With all of the requisite Feynman diagrams, we now set out to compute their contributions to the amplitude.

### 2.5.2 VERTEX DIAGRAM

In this section, we compute the Feynman vertex for the  $\chi$ ,  $\chi^*$ ,  $\zeta^2$ ,  $\delta\tau$  amplitude. The vertex operators for the strings stretching between the the D- and D<sup>s</sup>-instantons,  $\chi$  and  $\chi^*$ , are given by  $e_{12}V_{\zeta^2}$  and  $e_{21}V_{\zeta^2}$ , respectively. Here,  $e_{12}$  and  $e_{21}$  are the Chan-Patton factors mentioned previously, where  $e_{ij} = \delta_{ij}$  span  $\mathbb{C}^{2 \times 2}$ . The vertex operator for  $\zeta^2$ , which lives on the D-instanton, is  $e_{11}V_{\zeta^2}$ . It follows that the contribution of moduli integration over the vertex region takes the form<sup>11</sup>

$$\int_{\mathcal{R}_{\text{COOO}}} dt_1 dt_2 \left\langle B_{t_1} B_{t_2} V_{\zeta^2}^{(0)}(z_1) V_{\zeta^2}^{(-1)}(z_2) V_{\zeta^2}^{(0)}(z_3) V_{\delta\tau}^{(-1)}(i, -i) \right\rangle_{x^\mu=0}^{D^2}, \quad (2.133)$$

where the Chan-Patton factors give  $\text{tr}(e_{12}e_{21}e_{11}) = 1$ . Here,  $B_{t_1}$  and  $B_{t_2}$  are integrated  $b$ -ghost insertions whose precise forms are unnecessary for our purposes. As before, the transition maps do not play a role since the vertex operators are all weight zero conformal primaries. In order to avoid singularities, the picture-raised vertex operators for  $\chi$  and  $\zeta^2$

---

<sup>11</sup>Strictly speaking, there is an overall sign factor that depends on the orientation of  $dt^1 \wedge dt^2$  as compared with the global orientation of the moduli space.

are defined by averaging the PCO over a semicircle surrounding the open string, i.e.

$$V_{\zeta^2}^{(0)}(z) = \frac{1}{\pi i} \int_{S_z} \frac{dz'}{z' - z} \mathcal{X}(z') V_{z_1}^{(-1)}(z) = -1. \quad (2.134)$$

Note that this is equivalent to the conformal normal ordering procedure of throwing away all of the singular terms in the OPE before taking the coincident limit. From this, we find that (2.133) reduces to

$$\int_{\mathcal{R}_{\text{COOO}}} dt_1 dt_2 \left\langle B_{t_1} B_{t_2} \eta c \partial c(z_2) V_{\delta\tau}^{(-1)}(i, -i) \right\rangle_{x^\mu=0}^{D^2} = 0, \quad (2.135)$$

which vanishes since  $V_{\delta\tau}^{(-1)}(i, -i)$  does not contain any  $\xi$  ghosts to compensate for the  $\eta$  insertions. Thus, moduli integration does not contribute to the vertex diagram.

However, the vertex diagram does receive contributions from vertical integration due to the mismatch between the PCO placement in the vertex region as compared to the propagator regions corresponding to the COO-OOO diagrams, as discussed in the previous section. Consider the boundary between the vertex region and the CO<sub>1</sub>O-OO<sub>2</sub>O<sub>3</sub> propagator region. Here we are free to use the moduli  $(\beta, u)$  of the propagator region, where the boundary is described by  $u = u_0$  and  $\beta \in ((2\tilde{\lambda})^{-1}, 2\tilde{\lambda})$ . From the definition of the vertex, there is an antiholomorphic PCO located at  $\bar{p}_1 = z_1$  and a holomorphic one at  $p_2 = z_3$ . In the propagator region, they are instead located at  $\bar{p}_1 = -i$  and  $p_2 = p(\beta, u_0; p_{\text{ooo}})$ , as specified in (2.122). In order to fill in the gap, we must therefore perform vertical integration along the two PCO directions  $\bar{p}_1, p_2$ . The procedure to do this was outlined in [35], where we are instructed to simply integrate in one direction at a time. For each, vertical

integration consists of replacing the  $b$ -ghost insertion associated to  $u$  as well as the PCO at  $\bar{p}_1$  ( $p_2$ ) with a  $\xi$  insertion of the form  $\tilde{\xi}(\bar{z}_1) - \tilde{\xi}(-i)$ , and similarly for  $p_2$ .

We first consider vertical integration in the  $\bar{p}_1$  direction, as shown in Figure 2.11(a).

This is given by<sup>12</sup>

$$\int_{(2\tilde{\lambda})^{-1}}^{2\tilde{\lambda}} d\beta \left\langle B_\beta \left( \tilde{\xi}(z_1) - \tilde{\xi}(-i) \right) V_{\zeta^2}^{(-1)}(z_1) V_{z_2}^{(-1)}(z_2) V_{\zeta^2}^{(0)}(z_3) V_{\delta\tau}^{(-1)}(i, -i) \right\rangle_{x^\mu=0}^{D^2} \quad (2.136)$$

where the open strings positions  $z_a = z_a(\beta)$  can be found by setting  $w = 0$  and  $u = u_0$  in the transition maps found in (2.123). Doing so gives

$$z_1(\beta) = -\beta, \quad z_2(\beta) = \Delta_{-\beta}, \quad z_3(\beta) = \Delta_{+\beta} \quad (2.137)$$

where

$$\Delta_{\pm\beta} = \beta \pm (1 + \beta^2)u_0. \quad (2.138)$$

Following a similar vein of reasoning, the  $b$ -ghost insertion associated to  $\beta$  takes the form

$$\begin{aligned} B_\beta &= \sum_{a=1}^3 \frac{1}{\pi i} \int_{S_{z_a}} dz \frac{\partial f_a^{\text{CO}_1\text{O}-\text{OO}_2\text{O}_3}}{\partial \beta}(z) b(z) \\ &= - \int_{S_{z_1}} \frac{dz}{\pi i} \frac{1 + z^2 + (z + \beta)^2 \tilde{\lambda} f'(\beta)}{1 + \beta^2} + \int_{S_{z_2} \cup S_{z_3}} \frac{dz}{2\pi i} \frac{1 + z^2 + (z - \beta)^2 \tilde{\lambda} f'(\beta)}{1 + \beta^2}. \end{aligned} \quad (2.139)$$

After determining the correlation function and performing the contour integration in

(2.136), we are left with

$$- \frac{1}{2} \int_{(2\tilde{\lambda})^{-1}}^{2\tilde{\lambda}} d\beta \frac{1 + \beta^2}{\beta^2}. \quad (2.140)$$

---

<sup>12</sup>Strictly speaking, we should replace the expression  $\tilde{\xi}(z_1) V_{\zeta^2}^{(-1)}(z_1)$  with the regularized form  $\tilde{\xi}_0 V_{\zeta^2}^{(-1)}(z_1)$  inherited from the averaged PCO.

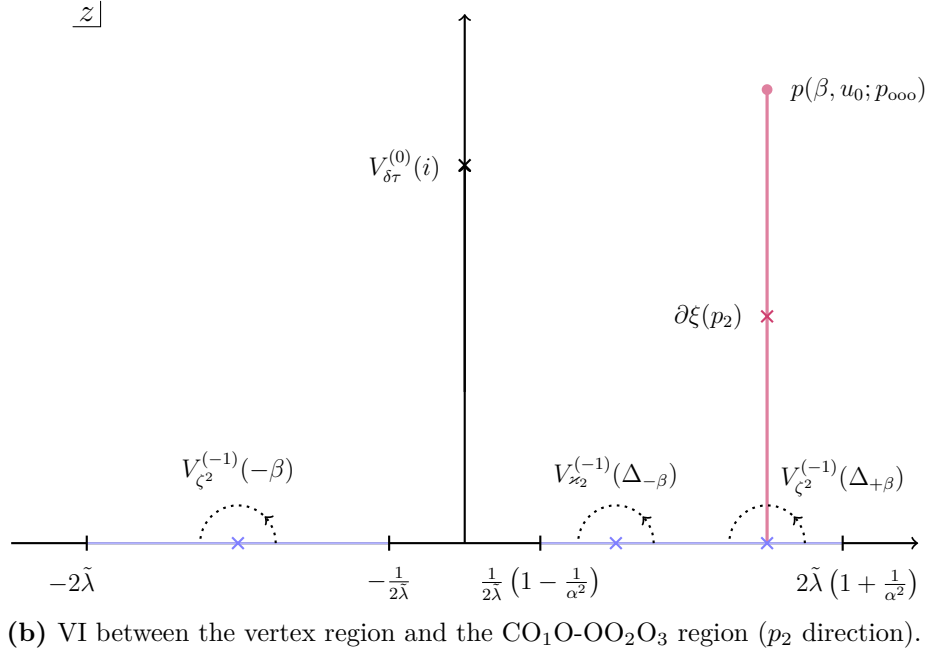
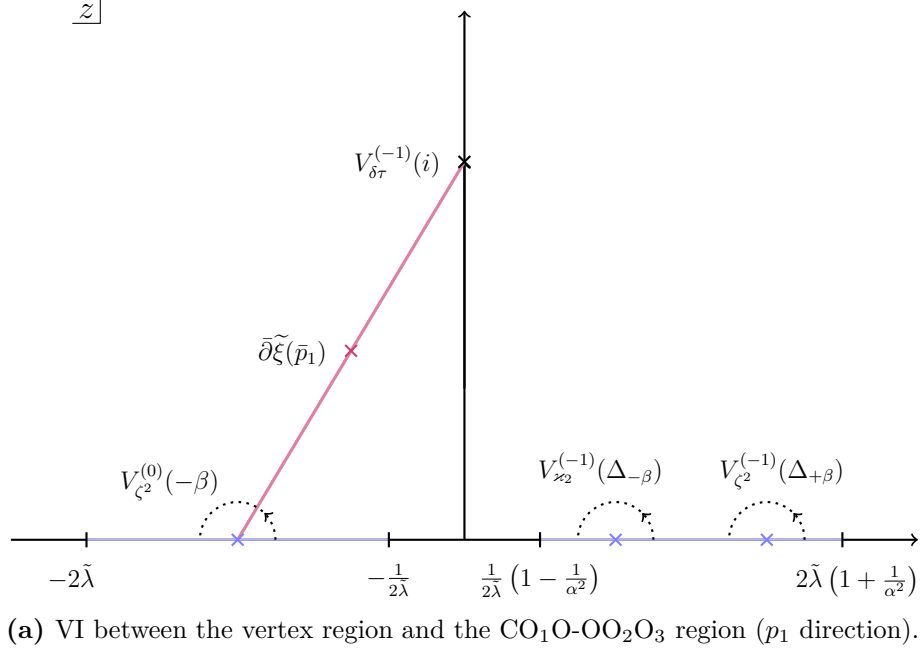


**Figure 2.11:** A family of discs with 1 bulk puncture and 3 boundary punctures parametrized by the modulus  $\beta \in ((2\tilde{\lambda})^{-1}, 2\tilde{\lambda})$  and PCO coordinate  $p_1$  ( $p_2$ ). On the UHP  $z$ , the closed string is located at  $z = i$ , shown by the black cross, and the open strings at  $z = -\beta, \Delta_{-\beta}, \Delta_{+\beta}$ , represented by blue crosses. The  $b$ -ghost insertion  $B_\beta$  surrounds all three punctures, as indicated by the dotted counterclockwise contours. The  $\partial\xi$  insertion is located at  $\tilde{p}_1$  ( $p_2$ ), as represented by the purple cross. As  $\beta$  varies, the open string insertions trace out blue curves corresponding to moduli integration (none of the punctures collide, since  $\Delta_\beta - \Delta_{-\beta} > \alpha^{-2}\tilde{\lambda}^{-1}$ ). Meanwhile as  $\tilde{p}_1$  ( $p_2$ ) varies, it traces out a purple “vertical segment” corresponding to vertical integration (VI).

Next consider vertical integration in the  $p_2$  direction. This is given by

$$\int_{(2\tilde{\lambda})^{-1}}^{2\tilde{\lambda}} d\beta \left\langle B_\beta \left( \xi(z_3) - \xi(p(\beta, u_0; p_{ooo})) \right) \right. \\ \left. V_{\zeta^2}^{(-1)}(z_1) V_{z_2}^{(-1)}(z_2) V_{\zeta^2}^{(-1)}(z_3) V_{\delta\tau}^{(0)}(i, -i) \right\rangle_{x^\mu=0}^{D^2} = O(\alpha^{-2}), \quad (2.141)$$

which we find to be subleading in  $\alpha^{-1}$ . Thus, vertical integration near the  $\text{CO}_1\text{O-OO}_2\text{O}_3$  region is simply given by (2.140).

Recall that there are three disconnected components of the boundary where vertical integration takes place, corresponding to  $\text{CO}_1\text{O-OO}_2\text{O}_3$  and its cyclic permutations. We shall handle these by assigning different cyclical permutations of the transition maps in (2.123) to the points  $z_1, z_2, z_3$ . From this perspective, the above expressions correspond to the identity permutation. Performing the vertical integration for the other two components proceeds in a similar fashion, giving

$$+ \frac{1}{2} \int_{(2\tilde{\lambda})^{-1}}^{2\tilde{\lambda}} d\beta \frac{1 + \beta^2}{\beta^2}, \quad -\frac{1}{2} \int_{(2\tilde{\lambda})^{-1}}^{2\tilde{\lambda}} d\beta \frac{1 + \beta^2}{\beta^2}. \quad (2.142)$$

Summing all three contributions in (2.140) and (2.142) together, we find that the disc vertex is thus

$$A_{\chi\chi^*\zeta^2\delta\tau}^{D^2} = -\frac{1}{2} \int_{(2\tilde{\lambda})^{-1}}^{2\tilde{\lambda}} d\beta \frac{1 + \beta^2}{\beta^2} = -2g_c C_{D^2} \tilde{\lambda}. \quad (2.143)$$

### 2.5.3 PROPAGATOR REGIONS

In this section, we discuss the contributions from the Feynman diagrams corresponding to the propagator regions. In the  $\tilde{\lambda}$  and  $\alpha$  limits, only the  $\varkappa^1$  propagator participates.

## CO-OOO-OOO DIAGRAMS

The CO-OO<sub>1</sub>O-OO<sub>2</sub>O<sub>3</sub> diagram consist of the Feynman vertices  $A_{\delta\tau\mathcal{Z}^1}^{D^2}$ ,  $A_{\mathcal{Z}^1\chi\mathcal{Z}^1}^{D^2}$ , and  $A_{\mathcal{Z}^1\chi^*\zeta^2}^{D^2}$  contracted together via two  $\mathcal{Z}^1$  propagators. The other diagrams CO-OO<sub>3</sub>O-OO<sub>1</sub>O<sub>2</sub> and CO-OO<sub>3</sub>O-OO<sub>3</sub>O<sub>1</sub> correspond to cyclically permuting the external open string fields. Due to the ghost structures of their vertex operators, all of the relevant 3-point vertices are zero. For instance, consider  $A_{\mathcal{Z}^1\chi^*\zeta^2}^{D^2}$ , which involves the vertex operators

$$c\partial c e^{-2\phi}\partial\xi, \quad c\partial c\eta, \quad c e^{-2\phi}\partial\xi \quad (2.144)$$

as well as a single PCO. The operators above contain a total of five copies of the  $c$  ghost, while the PCO can contribute at most one  $b$  ghost, and so the vertex vanishes.

## COO-OOO DIAGRAMS

The COO-OOO diagrams consist of Feynman vertices  $A_{\delta\tau\chi\mathcal{Z}^1}^{D^2}$  and  $A_{\mathcal{Z}^1\chi^*\zeta^2}^{D^2}$  contracted together, together with cyclic permutations of the external open strings. In the previous section, we noted that all the relevant 3-point vertices vanish, and so the COO-OOO diagrams do not contribute either.

## CO-OO<sub>1</sub>O<sub>2</sub>O<sub>3</sub> DIAGRAM

The only remaining Feynman diagram is given by the Feynman vertices  $A_{\delta\tau\mathcal{Z}^1}^{D^2}$  and  $A_{\mathcal{Z}^1\chi\chi^*\zeta^2}^{D^2}$  contracted together. We shall first compute the 4-point vertex, as depicted in Figure 2.12.

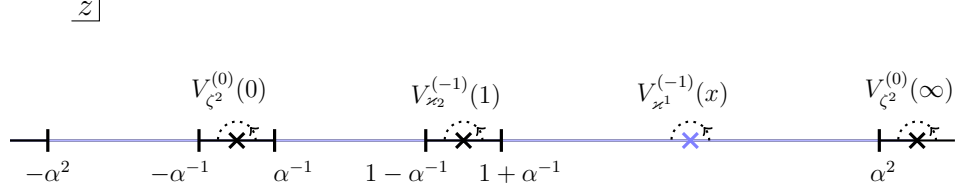


**Figure 2.12:** A family of 4-punctured discs, expressed in terms of the UHP with coordinate  $z$ , parametrized by the modulus  $x \in \mathcal{R}_{0000}$ . The open string punctures at  $z = 0, 1, \infty$  are indicated by black crosses, while the open string puncture at  $z = x$  is represented by a blue cross. The contour of the  $b$ -ghost insertion  $B_x$  surrounds all four punctures, as indicated by the counterclockwise contours. As  $x$  varies, the blue cross traces out three blue segments, corresponding to moduli integration over the vertex region.

Under our choice of local coordinates and PCO locations, it takes the form

$$A_{z^1 \chi \chi^* \zeta^2}^{D^2} = \int_{\mathcal{R}_{0000}} dx \left\langle B_x V_{\zeta^2}^{(0)}(0) V_{z^2}^{(-1)}(1) V_{\zeta^2}^{(0)}(\infty) V_{z^1}^{(-1)}(x) \right\rangle_{x^\mu=0}^{D^2}. \quad (2.145)$$

From (2.130) it follows that the  $b$ -ghost insertion is given by

$$B_x = \int_{S_1} \frac{dz}{\pi i} \frac{g_2'(x)}{g_2(x)} (z-x)b(z) + \int_{S_x} \frac{dz}{\pi i} \left( 1 + \frac{g_4'(x)}{g_4(x)}(z-x) \right) b(z) + \dots, \quad (2.146)$$

where we exclude terms that give vanishing contribution. Although vertical integration is in principle required, the  $\eta, \xi, \phi$  dependence of the vertex operators involved imply that it does contribute in practice. Shrinking the  $b$ -ghost contour on the second punctures gives

$$\int_{S_1} \frac{dz}{\pi i} \frac{g_2'(x)}{g_2(x)} (z-x)b(z) c \partial c \eta(1) = -\frac{g_2'(x)}{g_2(x)} c \eta(1), \quad (2.147)$$

and so it contributes to (2.145) as

$$\int_{\mathcal{R}_{0000}} dx \frac{g_2'(x)}{g_2(x)} \left\langle c \eta(1) c \partial c e^{-2\phi} \partial \xi(x) \right\rangle_{x^\mu=0}^{D^2} = \int_{\mathcal{R}_{0000}} dx \frac{g_2'(x)}{g_2(x)}. \quad (2.148)$$

Similarly,  $B_x$  acts on  $\varkappa^1$  to give

$$\int_{S_x} \frac{dz}{\pi i} \left( 1 + \frac{g_4'(x)}{g_4(x)}(z-x) \right) b(z) c \partial c e^{-2\phi} \partial \xi(x) = \left( \partial c(x) - \frac{g_4'(x)}{g_4(x)} c(x) \right) e^{-2\phi} \partial \xi(x), \quad (2.149)$$

which then contributes to (2.145) as

$$\begin{aligned} & - \int_{\mathcal{R}_{\text{OOOO}}} dx \left\langle c \partial c \eta(1) \left( \partial c(x) - \frac{g_4'(x)}{g_4(x)} c(x) \right) e^{-2\phi} \partial \xi(x) \right\rangle_{x^\mu=0}^{D^2} \\ & = \int_{\mathcal{R}_{\text{OOOO}}} dx \left( \frac{2}{1-x} + \frac{g_4'(x)}{g_4(x)} \right). \end{aligned} \quad (2.150)$$

Together, these sum to

$$\begin{aligned} A_{\varkappa^1 \chi \chi^* \zeta^2}^{D^2} & = \int_{\mathcal{R}_{\text{OOOO}}} dx \left( \frac{2}{1-x} + \frac{g_4'(x)}{g_4(x)} + \frac{g_2'(x)}{g_2(x)} \right) \\ & = (-2 \ln(x-1) + \ln g_4 + \ln g_2) \Big|_{\partial \mathcal{R}_{\text{OOOO}}}. \end{aligned} \quad (2.151)$$

This can be evaluated using the values  $x$  and  $g_a$  at the boundary of the vertex region, which recall are constrained by their values in the  $s, t, u$ -channel regions to (2.131). As usual, there is an additional minus sign if the outward direction of the boundary faces to the left. In total, the six boundary components yield

$$A_{\varkappa^1 \chi \chi^* \zeta^2}^{D^2} = -2\pi i. \quad (2.152)$$

From this, we find that the  $\text{CO-OO}_1\text{O}_2\text{O}_3$  Feynman diagram evaluates to

$$A_{\delta \tau \varkappa^1}^{D^2} P_{\varkappa^1} A_{\varkappa^1 \chi \chi^* \zeta^2}^{D^2} = -2\pi. \quad (2.153)$$



We now construct the full  $\delta\tau, \chi, \chi^*, \zeta^2$  amplitude, which is given by a sum over the Feynman diagrams

$$\begin{aligned} \mathcal{A}_{\delta\tau\chi\chi^*\zeta^2} &= A_{\delta\tau\chi\chi^*\zeta^2}^{D^2} + \left( A_{\delta\tau\chi^1}^{D^2} P_{\chi^1} A_{\chi^1\chi^2}^{D^2} P_{\chi^2} A_{\chi^2\chi^*\zeta^2}^{D^2} + \text{cyclic perm.} \right) \\ &+ \left( A_{\delta\tau\chi\chi^1}^{D^2} P_{\chi^1} A_{\chi^1\chi^*\zeta^2}^{D^2} + \text{cyclic perm.} \right) + A_{\delta\tau\chi^1}^{D^2} P_{\chi^1} A_{\chi^1\chi\chi^*\zeta^2}^{D^2}, \end{aligned} \quad (2.154)$$

including cyclic permutations of the external open strings. As we found in the previous sections, all of the Feynman diagrams vanish besides the vertex diagram as well as the CO-OO<sub>1</sub>O<sub>2</sub>O<sub>3</sub> diagram. Plugging in their values (2.153) and (2.153) gives

$$\mathcal{A}_{\delta\tau\zeta^2\chi^2\zeta^2}^{D^2} = -\pi - 2\tilde{\lambda}. \quad (2.155)$$

## 2.6 $\delta\tau, \delta\tau, \phi$ DISC AMPLITUDE

In this section, we compute the SFT disc amplitude with two  $\delta\tau$  insertions and one  $\phi^\mu$  insertion, which enters into the MRV amplitude due to integration over  $\phi^\mu$  in the effective action.

### 2.6.1 FEYNMAN DIAGRAMS

We begin by enumerating the Feynman diagrams that contribute to the propagator region. Since all of the external vertex operators are weight zero conformal primaries, we shall not need the explicit forms of the local coordinate charts.

The first Feynman diagram, referred to as the C<sub>1</sub>O-OOO-C<sub>2</sub>O diagram, consists of two open-closed vertices  $\mathcal{V}_{D^2}^{1NSNS,1NS}$  contracted with an open 3-point vertex  $\mathcal{V}_{D^2}^{1NS,2NS,3NS}$ .

The corresponding family of worldsheet configurations is constructed by joining together three discs, represented by UHPs parametrized by  $z, z', z'''$  respectively, via the plumbing maps

$$\begin{aligned} w^{\text{CO}}(z)w_1^{\text{OOO}}(z') &= -q_1, \quad q_1 \in (0, 1), \\ w_3^{\text{OOO}}(z')w^{\text{CO}}(z''') &= -q_2, \quad q_2 \in (0, 1). \end{aligned} \tag{2.156}$$

The resulting topology is that of a single disc with two open string punctures and one closed string puncture. Up to a  $PSL(2, \mathbb{R})$  transformation, the closed strings are taken to be located at  $z = i$  and  $z = iy$ , and the open string at  $z = x$ . Together, the two moduli are given by functions  $x = x(q_1, q_2)$  and  $y = y(q_1, q_2)$  of the plumbing parameters, whose explicit forms do not matter for the computation. From the sewing procedure, it follows that two PCOs are located coincident with each of the closed strings, and the remaining PCO resides at some generic location  $p = p(x, y; p_{\text{ooo}})$  depending on the moduli as well as its location  $p_{\text{ooo}}$  on the 3-punctured disc. Furthermore, the  $C_1\text{O-OOO-C}_2\text{O}$  diagram covers a propagator region in moduli space bounded by the curves  $y = 0$ ,  $x = \lambda^{-1}$ , and  $y = \tilde{\lambda}^{-1}x$ . It is also necessary to include the other cyclic ordering of the 3-point vertex, which corresponds to the reflected region  $x \mapsto -x$ . These two disjoint regions are shaded yellow in Figure 2.7.

The second Feynman diagram, referred to as the  $C_1\text{O-C}_2\text{OO}$  diagram, consists of the vertices  $\mathcal{V}_{D^2}^{1NSNS, 1NS}$  and  $\mathcal{V}_{D^2}^{1NSNS, 1NS, 2NS}$  contracted together. The associated worldsheet configurations are given by joining two discs, parametrized by UHPs  $z, z'$ , via

$$w^{\text{CO}}(z)w_1^{\text{COO}}(z') = -q_1, \quad q_1 \in (0, 1). \tag{2.157}$$

The plumbing parameter  $q_1$  matches that of the  $C_1O$ - $OOO$ - $C_2O$  diagram. Once again the closed strings can be placed at  $z = i, iy$  and the open string at  $z = x$ , where now the moduli are functions of  $q_1$  and  $\beta$ . Two of the three PCOs are coincident with the first closed string, while the third PCO is coincident with the second. Ranging over  $q_1 \in (0, 1)$  and  $\beta \in ((2\tilde{\lambda})^{-1}, 2\tilde{\lambda})$  corresponds to  $x \in (-\tilde{\lambda}^{-1}, \tilde{\lambda}^{-1})$  and  $|x| < y < \tilde{\lambda}^{-2}$ , given by the green propagator region in Figure 2.7. There is another Feynman diagram, referred to as the  $C_2O$ - $C_1OO$  diagram, which consists of exchanging the two closed string punctures. It covers  $|x| > \tilde{\lambda}^{-1}$  and  $0 < y < \tilde{\lambda}^{-2}$ , which corresponds to the red propagator region in Figure 2.7. There is a mismatch between the PCO locations at the walls separating both propagator regions from the  $C_1O$ - $OOO$ - $C_2O$  diagram, and so vertical integration is in principle required.

The last Feynman diagram is given by the 3-point vertex  $\mathcal{V}^{1NSNS, 2NSNS, 1NS}$ . The diagram covers the remainder of  $(x, y)$  moduli space, i.e. the blue vertex region in Figure 2.7, which consists of  $x \in \mathbb{R}$  and  $|y| > \tilde{\lambda}^{-2}$ . The PCOs are arranged such that each is coincident with one of the vertex operators. Vertical integration is needed at the two boundaries shared with the  $C_1O$ - $C_2OO$  and  $C_2O$ - $C_1OO$  propagator regions. There is also the prospect of vertical integration at the codimension 2 boundary involving the  $C_1O$ - $OOO$ - $C_2O$  region.

The elementary vertices are defined in a similar fashion for RR insertions, where for each RR insertion one PCO is removed.

## 2.6.2 VERTEX DIAGRAM

First consider the vertex diagram. The contribution of moduli integration takes the form

$$\int_{-\infty}^{\infty} dx \int_{\tilde{\lambda}^{-2}}^1 dy \left\langle B_x B_y V_{\phi^\mu}^{(0)}(x) V_{\delta\tau(p)}^{(-1)}(i, -i) V_{\delta\tau(k)}^{(-1)}(iy, -iy) \right\rangle_{x^\mu=0}^{D^2}, \quad (2.158)$$

as shown in Figure 2.13. The  $b$ -ghost insertions are given by

$$B_x = \int_{S_x} \frac{dz}{\pi i} b(z), \quad B_y = \oint_{C_{iy}} \frac{dz}{2\pi} \left( dz b(z) + d\bar{z} \tilde{b}(\bar{z}) \right). \quad (2.159)$$

Shrinking the contour of  $B_x$  around  $\phi^\mu$  gives

$$\int_{-\infty}^{\infty} dx \int_{S_x} \frac{dz}{\pi i} b(z) \left( \sqrt{2} ic \partial X^\mu(x) + \eta e^\phi \psi^\mu(x) \right) = \sqrt{2} \int_{-\infty}^{\infty} dx i \partial X^\mu(x). \quad (2.160)$$

In the above expression, there is an additional minus sign that comes from exchanging the ordering of  $B_x$  and  $B_y$ . Up to normalization, this operators acts as the translation charge on the closed strings. The moduli integral thus reduces to

$$\begin{aligned} & \pi \sqrt{2} (ip^\mu + ik^\mu) \int_{\tilde{\lambda}^{-2}}^1 dy \left\langle B_y V_{\delta\tau(p)}^{(-1)}(i, -i) V_{\delta\tau(k)}^{(-1)}(iy, -iy) \right\rangle_{x^\mu=0}^{D^2} \\ & = \pi \sqrt{2} (ip^\mu + ik^\mu) A_{\delta\tau(p)\delta\tau(k)}^{D^2}(\tilde{\lambda}), \end{aligned} \quad (2.161)$$

where  $A_{\delta\tau(p)\delta\tau(k)}^{D^2}(\tilde{\lambda})$  is given by the disc 2-point vertex in (2.73) with  $\lambda$  replaced by  $\tilde{\lambda}$ .

We next consider the effects of vertical integration. Since it does not contribute to the axion-axion amplitude, we shall first focus on the case of two dilatons. At the boundary  $y = y_0 = \tilde{\lambda}^{-2}$  of the vertex region there is a mismatch between PCO loci. In particular,

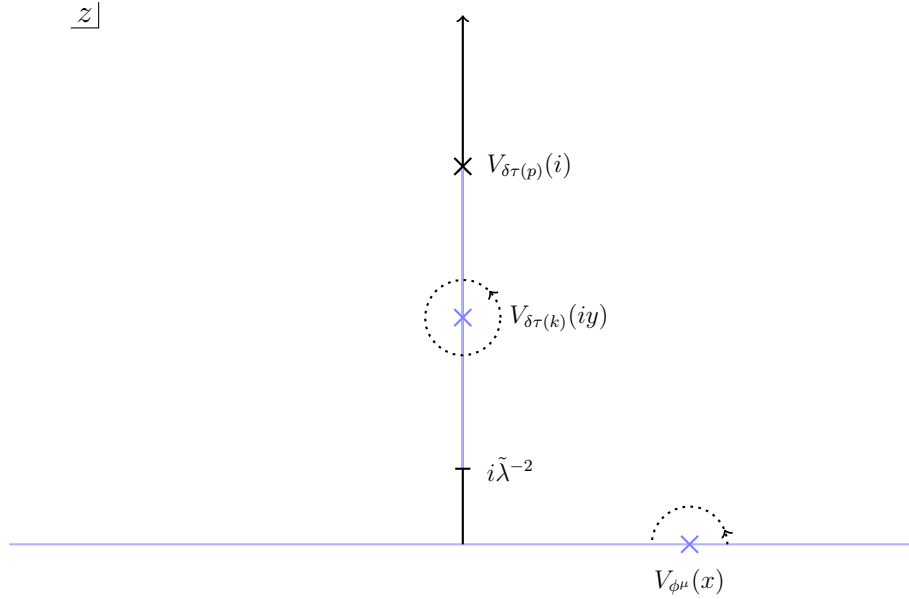


**Figure 2.13:** A family of open-closed 3-punctured discs parametrized by the moduli  $(x, y)$ . On the UHP, the closed strings are at  $z = i, iy$  and the open string at  $z = x$ , as indicated by the different crosses. The  $b$ -ghost insertions  $B_x$  and  $B_y$  separately surround the open/closed string punctures, as indicated by the contours. As  $x, y$  vary, the integrated vertex operators, represented by blue crosses, trace out two blue segments corresponding to the vertex region.

the PCO is coincident with  $\phi^\mu$  in the vertex region, while it is coincident with the dilaton at  $\bar{z} = -iy$  in the  $C_1O-C_2OO$  propagator region. In order to close the gap, we must vertically integrate along the PCO direction for  $|x| < \tilde{\lambda}^{-1}$ , as depicted by Figure 2.14(a), which gives

$$\begin{aligned} & \left(\frac{i}{\sqrt{2}}\right)^2 \int_{-\tilde{\lambda}^{-1}}^{\tilde{\lambda}^{-1}} dx \left\langle B_x \left[ \tilde{\xi}(x) - \tilde{\xi}(-iy_0) \right] V_{\phi^\mu}^{(-1)}(x) V_{\delta\tau_2(p)}^{(-1)}(i, -i) V_{\delta\tau_2(k)}^{(-1)}(iy_0, -iy_0) \right\rangle_{x^\mu=0}^{D^2} \\ & = -2\sqrt{2}(ip^\mu \tilde{\lambda} + \pi i k^\mu) + 4\pi e^{\mu\nu}(k)p_\nu. \end{aligned} \tag{2.162}$$

Similarly, the same PCO is coincident with the other NSNS insertion at  $\bar{z} = -i$  in the  $C_2O-C_1OO$  propagator region. Vertical integration is thus needed for  $|x| > \tilde{\lambda}^{-1}$ , as depicted in Figure 2.14(b). Due to the symmetry of the two closed strings, it can be found

by simply exchanging their momenta.<sup>13</sup> In total, vertical integration for two dilatons gives

$$-2\sqrt{2}(\tilde{\lambda} + \pi)(ip^\mu + ik^\mu) + 2\pi(e^{\mu\nu}(p)ik_\nu + e^{\mu\nu}(k)ip_\nu). \quad (2.163)$$

A similar story holds for one dilaton and one axion, where vertical integration contributes

$$-2\sqrt{2}\tilde{\lambda}(ip^\mu + ik^\mu) + 2\pi(e^{\mu\nu}(p)ik_\nu + e^{\mu\nu}(k)ip_\nu). \quad (2.164)$$

Together with moduli integration, the Feynman vertex is thus

$$\begin{aligned} A_{\delta\tau(p)\delta\tau(k)\phi^\mu}^{D^2} &= \pi\sqrt{2}(ip^\mu + ik^\mu)A_{\delta\tau(p)\delta\tau(k)}^{D^2}(\tilde{\lambda}) - 2\sqrt{2}(2\tilde{\lambda} + \pi)(ip^\mu + ik^\mu) \\ &\quad - 4\sqrt{2}(ik^\mu\tilde{\lambda} + ip^\mu) + 4\pi(e^{\mu\nu}(p)ik_\nu + e^{\mu\nu}(k)ip_\nu). \end{aligned} \quad (2.165)$$

### 2.6.3 PROPAGATOR REGIONS

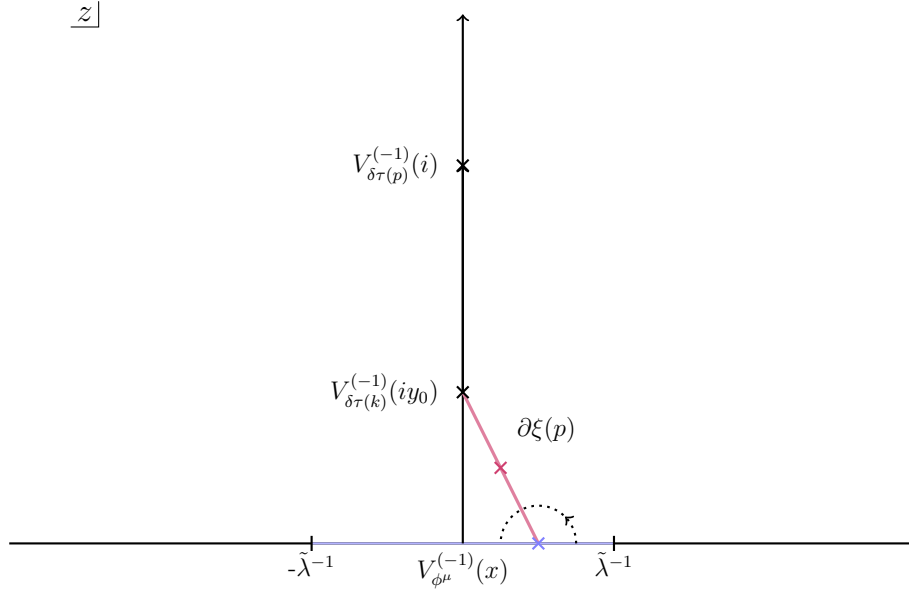
We now consider the Feynman diagrams corresponding to the propagator regions of moduli space. Recall that we are working in the large  $\tilde{\lambda}$  limit, and so only diagrams with intermediate  $\varkappa^1$  states can contribute.

#### C<sub>1</sub>O-OOO-C<sub>2</sub>O

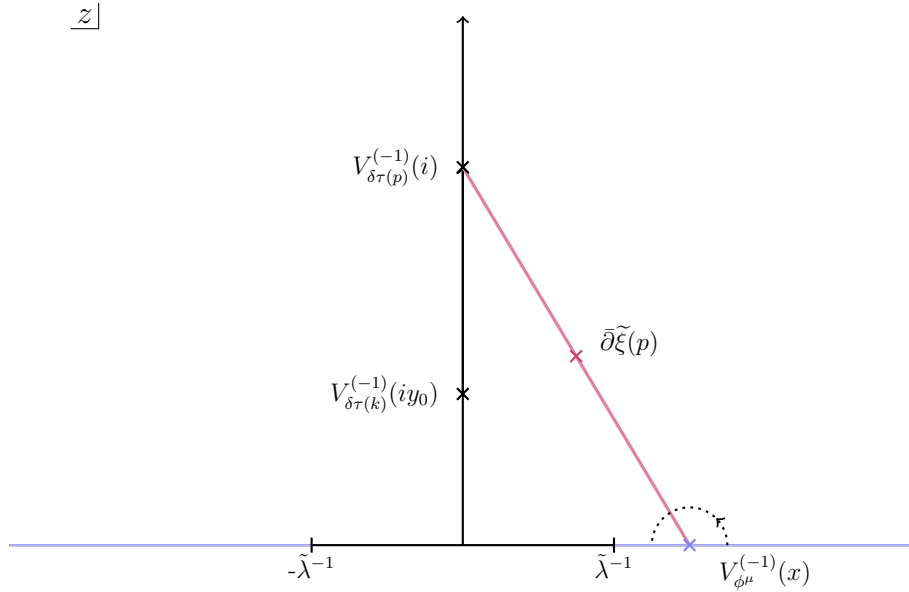
The relevant C<sub>1</sub>O-OOO-C<sub>2</sub>O diagram consists of the two copies of  $A_{\delta\tau\varkappa^1}^{D^2}$  together with  $A_{\varkappa^1\varkappa^1\phi^\mu}^{D^2}$  contracted together. The unusual ghost structure of  $\varkappa^1$  implies that the 3-point

---

<sup>13</sup>We have performed vertical integration explicitly for both regions and verified that this is true.



(a) VI between the vertex region and the  $C_1O$ - $C_2OO$  propagator region.



(b) VI between the vertex region and the  $C_2O$ - $C_1OO$  propagator region.

**Figure 2.14:** A family of discs with 2 closed string punctures and 1 open string puncture, parametrized by the modulus  $|x| < \tilde{\lambda}^{-1}$  ( $|x| > \tilde{\lambda}^{-1}$ ) and PCO location  $p$ . Representing the disc as the UHP  $z$ , the closed strings are at  $z = i$  and  $z = iy_0$ , depicted by black crosses, and the open string puncture at  $z = x$ , with a blue cross. The  $b$ -ghost insertion  $B_x$  surrounds the open string, as indicated by the dotted counterclockwise contour. The  $\partial\tilde{\xi}$  insertion at  $z = p$  is represented by a purple cross. As  $x$  varies, the open string insertion traces out a blue curve corresponding to moduli integration. Meanwhile as  $p$  varies,  $\partial\xi$  traces out a purple “vertical segment” corresponding to vertical integration.

vertex is zero, and so the Feynman diagram vanishes

$$A_{\delta\tau\kappa^1}^{D^2} P_{\kappa^1} A_{\kappa^1\kappa^1\phi^\mu}^{D^2} P_{\kappa^1} A_{\delta\tau\kappa^1}^{D^2} = 0. \quad (2.166)$$

## CO-COO DIAGRAMS

The  $C_1O$ - $C_2OO$  Feynman diagram consists of the vertex  $A_{\delta\tau\kappa^1}^{D^2}$  contracted with  $A_{\delta\tau(p)\kappa^1\phi^\mu}^{D^2}$  by an open string propagator  $P_{\kappa^1}$ . Consider first the open-closed 3-point vertex for the dilaton, as depicted in Figure 2.10. It gives

$$\begin{aligned} A_{\delta\tau_2(p)\kappa^1\phi^\mu}^{D^2} &= \int_{(2\tilde{\lambda})^{-1}}^{2\tilde{\lambda}} d\beta \left\langle B_\beta V_{\kappa^1}^{(-1)}(-\beta) V_{\phi^\mu}^{(-1)}(\beta) V_{\delta\tau_2(p)}^{(0)}(i, -i) \right\rangle_{x^\mu=0}^{D^2} \\ &= \sqrt{2}i p^\mu \int_{(2\tilde{\lambda})^{-1}}^{2\tilde{\lambda}} d\beta \left( \frac{\beta^2 - 1}{\beta + \beta^3} \right) \\ &= O(\tilde{\lambda}^{-2}), \end{aligned} \quad (2.167)$$

and so does not contribute in the large  $\tilde{\lambda}$  limit. While vertical integration is required in principle, it vanishes in practice due to the ghost structure of  $\kappa^1$ . On the other hand, the axion gives

$$\begin{aligned} A_{\delta\tau_1(p)\kappa^1\phi^\mu}^{D^2} &= \int_{(2\tilde{\lambda})^{-1}}^{2\tilde{\lambda}} d\beta \left\langle B_\beta V_{\kappa^1}^{(-1)}(-\beta) V_{\phi^\mu}^{(-1)}(\beta) V_{\delta\tau_1(p)}^{(0)}(i, -i) \right\rangle_{x^\mu=0}^{D^2} \\ &= 2\sqrt{2}i p^\mu \int_{(2\tilde{\lambda})^{-1}}^{2\tilde{\lambda}} d\beta \left( \frac{(\beta - i)^2}{\beta + \beta^3} \right) \\ &= 2\sqrt{2}\pi p^\mu. \end{aligned} \quad (2.168)$$



The same analysis applies for when the closed strings are exchanged. It follows that

$$A_{\delta\tau(p)\varkappa^1}^{D^2} P_{\varkappa^1} A_{\delta\tau(p)\varkappa^1\phi^\mu}^{D^2} + A_{\delta\tau(k)\varkappa^1}^{D^2} P_{\varkappa^1} A_{\delta\tau(p)\varkappa^1\phi^\mu}^{D^2} = -2\sqrt{2}\pi ip^\mu. \quad (2.169)$$

We are now in a position to assemble the full closed-closed-open amplitude, which decomposes into constituent Feynman diagrams as

$$\begin{aligned} \mathcal{A}_{\delta\tau(p)\delta\tau(k)\phi^\mu}^{D^2} &= A_{\delta\tau(p)\delta\tau(k)\phi^\mu}^{D^2} + 2A_{\delta\tau\varkappa^1}^{D^2} P_{\varkappa^1} A_{\varkappa^1\varkappa^1\phi^\mu}^{D^2} P_{\varkappa^1} A_{\delta\tau\varkappa^1}^{D^2} \\ &\quad + A_{\delta\tau(p)\varkappa^1}^{D^2} P_{\varkappa^1} A_{\delta\tau(p)\varkappa^1\phi^\mu}^{D^2} + A_{\delta\tau(k)\varkappa^1}^{D^2} P_{\varkappa^1} A_{\delta\tau(p)\varkappa^1\phi^\mu}^{D^2}. \end{aligned} \quad (2.170)$$

Plugging in (2.165), (2.166), and (2.169), we find

$$\begin{aligned} A_{\delta\tau(p)\delta\tau(k)\phi^\mu}^{D^2} &= \pi\sqrt{2}(ip^\mu + ik^\mu)A_{\delta\tau(p)\delta\tau(k)}^{D^2}(\tilde{\lambda}) - 4\sqrt{2}(\tilde{\lambda} + \pi)(ip^\mu + ik^\mu) \\ &\quad + 4\pi(e^{\mu\nu}(p)ik_\mu + e^{\mu\nu}(k)ip_\mu). \end{aligned} \quad (2.171)$$

Using (2.78), this can be massaged into the form

$$\begin{aligned} \mathcal{A}_{\delta\tau(p)\delta\tau(k)\phi^\mu}^{D^2} &= \pi\sqrt{2}(ip^\mu + ik^\mu)\mathcal{A}_{\delta\tau(p)\delta\tau(k)}^{D^2}(\tilde{\lambda}) - 4\sqrt{2}(\tilde{\lambda} + \frac{1}{2}\pi)(ip^\mu + ik^\mu) \\ &\quad + 4\pi(e^{\mu\nu}(p)ik_\mu + e^{\mu\nu}(k)ip_\mu). \end{aligned} \quad (2.172)$$

## 2.7 $\delta\tau$ , $\lambda$ , $\theta_\alpha$ DISC AMPLITUDE

In this section, we compute the  $\delta\tau$ ,  $\lambda$ ,  $\theta_\alpha$  disc amplitude, which corrects the MRV amplitude through integration over  $\theta_\alpha$ .

### 2.7.1 FEYNMAN DIAGRAMS

We begin with an overview of the Feynman diagrams that contribute the disc amplitude with one NSNS insertion, one NSR insertion, and one RR insertion. All of the diagrams share the same local coordinates and moduli with those of Section 2.6.1. A key difference between the two is that several diagrams now involve intermediate open strings in the R sector, which slightly modifies the PCO analysis. In particular, the R-sector propagator naturally comes paired with the PCO insertion

$$\mathcal{X}_0 = \frac{1}{\pi i} \int_{S_0} \frac{dw}{w} \mathcal{X}(w) = \frac{1}{\pi i} \int_{S_0} \frac{dw'}{w'} \mathcal{X}(w') \quad (2.173)$$

whose contour surrounds the sewn open string punctures, located at  $w, w' = 0$  on their respective local coordinate patches.

First consider the  $C_1O$ - $OOO$ - $C_2O$  diagram consisting of the vertices  $\mathcal{V}_{D^2}^{1NSNS,1NS}$ ,  $\mathcal{V}_{D^2}^{1NSR,1R}$ ,  $\mathcal{V}_{D^2}^{1NS,1R,2R}$  contracted together. Place the NSNS insertion at  $z = i$ , NSR insertion at  $z = iy$ , and the open string at  $z = x$ . The propagator region is the same as in Section 2.6.1, shaded yellow in Figure 2.7. There are two PCOs, both which are taken to be holomorphic. As prescribed by the plumbing procedure, one is coincident with the NSNS puncture, while the other is averaged over a contour whose details do not matter for our computation.

The next Feynman diagram, the  $C_1OO$ - $C_2O$  diagram, consists of the vertices  $\mathcal{V}_{D^2}^{1NSNS,1NS}$  and  $\mathcal{V}_{D^2}^{1NSR,1NS,1R}$  contracted together. As before, the moduli range over  $y < \tilde{\lambda}^{-2}$  and  $|x| < \tilde{\lambda}^{-1}$ . This corresponds to the red propagator region in Figure 2.7. The 3-point ver-

tex has a single PCO, taken to be holomorphic and coincident with the NSR insertion.

Both PCOs are thus separately coincident with the closed strings for the resulting Feynman diagram.

The last Feynman diagram contributing to a propagator region is the C<sub>2</sub>OO-C<sub>1</sub>O diagram, which consists of the vertices  $\mathcal{V}_{D^2}^{1NSR,1R}$  and  $\mathcal{V}_{D^2}^{1NSNS,1R,2R}$  contracted together, covering  $y < \tilde{\lambda}^{-2}$  and  $|x| > \tilde{\lambda}^{-1}$ , shown by the green propagator region in Figure 2.7. Note that it is not related to the C<sub>1</sub>OO-C<sub>2</sub>O diagram by closed string exchange, since it contains vertices involving different open string states. For the 3-point vertex at hand, we take the PCO to be coincident with the NSNS puncture. The R-sector propagator contributes an additional PCO. Following the plumbing procedure, it is averaged over a counterclockwise contour that surrounds only the NSR puncture. Shrinking the contour is thus equivalent to taking the PCO coincident with the NSR insertion.

Finally, consider the Feynman vertex  $\mathcal{V}_{D^2}^{1NSNS,1NSR,1R}$ , which covers  $x \in \mathbb{R}$  and  $y > \tilde{\lambda}^{-2}$ . This corresponds to the blue region of Figure 2.7. For ease of computation, both PCOs, which are separately holomorphic and antiholomorphic, are taken to be coincident with the NSNS insertion. This choice disagrees with the PCO locations at the boundary meeting the C<sub>1</sub>OO-C<sub>2</sub>O and C<sub>2</sub>OO-C<sub>1</sub>O propagator regions, and so vertical integration will be required.

The analysis for RNS and RR insertions proceeds in a similar fashion. For the former, we shall assume the same PCO placement as for the NSR insertion, but exchange holomorphic and antiholomorphic PCOs that are coincident with the RNS insertion. For the latter, the analysis is even simpler: there is only a single PCO, which is taken to be coincident with the NSR/RNS insertions, unless the sewing procedure indicates otherwise. It

follows that there is no vertical integration needed for the  $\mathcal{V}^{1RR,1NSR,1R}$  vertex.

## 2.7.2 VERTEX DIAGRAM

We shall now determine the vertex diagram as outlined in the previous section. First consider the contribution from moduli integration over the vertex region. Since the PCO placement differs for the NSNS and RR vertex operators, we shall consider their contributions separately. For the former, the two PCOs are coincident with the dilaton, which gives

$$\begin{aligned} & \frac{i}{\sqrt{2}} \int_{-\infty}^{\infty} dx \int_{\tilde{\lambda}^{-2}}^1 dy \left\langle B_x B_y V_{\theta_\alpha}^{(-\frac{1}{2})}(x) V_{\delta\tau_2(p)}^{(0,0)}(i, -i) V_{\lambda(k)}^{(-\frac{3}{2})}(iy, -iy) \right\rangle_{x^\mu=0}^{D^2} \\ &= i\pi u^\alpha(k) \int_{\tilde{\lambda}^{-2}}^1 dy \left( \frac{1-y}{1+y} \right)^{p \cdot k} \left( \frac{1-y^2}{y^2} + \frac{2\sqrt{2}}{1-y^2} e_{\mu\nu}(p) k^\mu k^\nu \right), \end{aligned} \quad (2.174)$$

where the vertex operator associated to  $\theta_\alpha$  is

$$V_{\theta_\alpha}^{(-\frac{1}{2})}(x) = ce^{-\frac{1}{2}\phi} S^\alpha. \quad (2.175)$$

Note that the  $b$ -ghost insertions  $B_x$  and  $B_y$  are identical to those in (2.159), and the factor of  $i/\sqrt{2}$  corresponds to our normalization for the 1-particle state. For the latter, we have that one PCO is coincident with the axion and the other with  $\lambda(k)$ . This contributes as

$$\begin{aligned} & \frac{1}{\sqrt{2}} \int_{-\infty}^{\infty} dx \int_{\tilde{\lambda}^{-2}}^1 dy \left\langle B_x B_y V_{\theta_\alpha}^{(-\frac{1}{2})}(x) V_{\delta\tau_1(p)}^{(-\frac{1}{2}, -\frac{1}{2})}(i, -i) V_{\lambda(k)}^{(-\frac{1}{2})}(iy, -iy) \right\rangle_{x^\mu=0}^{D^2} \\ &= -i\pi u^\alpha(k) (p \cdot k) \int_{\tilde{\lambda}^{-2}}^1 dy \left( \frac{1-y}{1+y} \right)^{p \cdot k} \left( \frac{2-y+2y^2}{y-y^3} \right). \end{aligned} \quad (2.176)$$

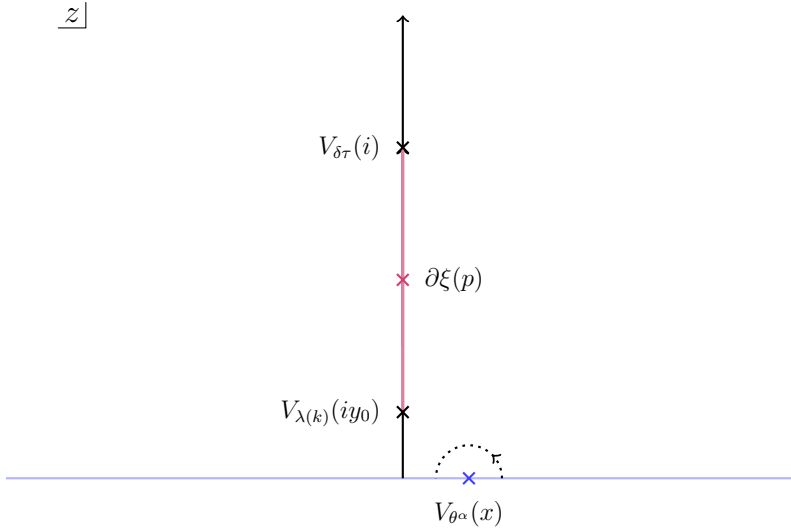


**Figure 2.15:** Vertical integration along the boundary  $x \in \mathbb{R}$  and  $y_0 = \tilde{\lambda}^{-2}$  between the vertex and propagator regions of  $(x, y)$  moduli space for the  $\delta\tau(p)$ ,  $\lambda(k)$ ,  $\theta_\alpha$  amplitude on the disc. The fixed closed string punctures are depicted by black crosses. The integrated open string puncture is depicted by a blue cross, as surrounded by a  $B_x$  ghost contour indicated by a dotted counter-clockwise semicircle. The operator  $\partial\xi$ , depicted by an orange cross, is integrated along the PCO direction  $p$ , corresponding to the purple vertical segment, in order to fill in the gap. The blue segment corresponds to moduli integration in  $x \in \mathbb{R}$ .

Integration over the vertex region thus gives

$$\begin{aligned}
I_{\delta\tau(p)\lambda(k)\theta_\alpha} &= -i\pi u^\alpha(k) \left\{ \tilde{\lambda}^2 - 2(p \cdot k) + 4(p \cdot k) \int_{\tilde{\lambda}^{-2}}^1 dy \frac{1+y^2}{y-y^3} \left( \frac{1-y}{1+y} \right)^{p \cdot k} \right. \\
&\quad \left. - \left( p \cdot k + 2\sqrt{2}e_{\mu\nu}(p)k^\mu k^\nu \right) \int_{\tilde{\lambda}^{-2}}^1 dy \frac{1}{1-y^2} \left( \frac{1-y}{1+y} \right)^{p \cdot k} \right\} \quad (2.177) \\
&= -i\pi u^\alpha(k) \left\{ \tilde{\lambda}^2 + 4I_{\tilde{\lambda}}(p \cdot k) - 1 - \sqrt{2} \frac{e_{\mu\nu}(p)k^\mu k^\nu}{p \cdot k} \right\},
\end{aligned}$$

where in writing the first line, we have performed an integration by parts on the divergent piece of the dilaton contribution. As was the case for the  $\delta\tau(p)\delta\tau(k)\phi^\mu$  amplitude, the integral  $I_{\tilde{\lambda}}(p \cdot k)$  is given by (1.71) with  $\epsilon$  replaced by  $\tilde{\lambda}^{-2}$ .

Now consider the effects of vertical integration, which takes place at the boundary  $y = y_0$ , as shown in Figure 2.15. Since the  $C_1\text{O}-C_2\text{OO}$  and  $C_2\text{O}-C_1\text{OO}$  diagrams both

share the same PCO placement, their contributions can be bundled together. In particular, in the vertex region the PCO is coincident with the NSNS puncture, while in the propagator region it is coincident with the NSR/RNS punctures. Strictly speaking, it is also important to take into account that it is antiholomorphic for the NSNS and RNS insertions, while it is holomorphic for the NSR insertion. The contribution of the former is

$$\begin{aligned} & \frac{i}{\sqrt{2}} \int_{-\infty}^{\infty} dx \left\langle B_x \left[ \tilde{\xi}(-i) - \tilde{\xi}(-iy_0) \right] V_{\theta_\alpha}^{(-\frac{1}{2})}(x) V_{\delta\tau(p)}^{(-1)}(i, -i) V_{\lambda_2(k)}^{(-\frac{1}{2}, -1)}(iy_0, -iy_0) \right\rangle_{x^\mu=0}^{D^2} \\ & = i\pi u^\alpha(k) \left( \frac{1}{2} \tilde{\lambda}^2 - (p \cdot k) \right) + O(\tilde{\lambda}^{-2}) \end{aligned} \quad (2.178)$$

while for the latter we have

$$\begin{aligned} & \frac{1}{\sqrt{2}} \int_{-\infty}^{\infty} dx \left\langle B_x \left[ \tilde{\xi}(-i) - \tilde{\xi}(-iy_0) \right] V_{\theta_\alpha}^{(-\frac{1}{2})}(x) V_{\delta\tau(p)}^{(-1)}(i, -i) V_{\lambda_1(k)}^{(-1, -\frac{1}{2})}(iy_0, -iy_0) \right\rangle_{x^\mu=0}^{D^2} \\ & = i\pi u^\alpha(k) \left( \frac{1}{2} \tilde{\lambda}^2 - (p \cdot k) - 1 \right) + O(\tilde{\lambda}^{-2}). \end{aligned} \quad (2.179)$$

In total, vertical integration contributes as

$$\text{VI}_{\delta\tau(p)\lambda(k)\theta_\alpha}^{D^2} = -i\pi u^\alpha(k) \left( -\tilde{\lambda}^2 + 2(p \cdot k) + 1 \right), \quad (2.180)$$

which, together with the moduli integration, implies that the disc vertex evaluates to

$$\begin{aligned} A_{\delta\tau(p)\lambda(k)\theta_\alpha}^{D^2} & = I_{\delta\tau(p)\lambda(k)\theta_\alpha}^{D^2} + \text{VI}_{\delta\tau(p)\lambda(k)\theta_\alpha}^{D^2} \\ & = -i\pi u^\alpha(k) \left\{ 4I_{\tilde{\lambda}}(p \cdot k) - \sqrt{2} \frac{e_{\mu\nu}(p) k^\mu k^\nu}{p \cdot k} + 2(p \cdot k) \right\}. \end{aligned} \quad (2.181)$$

### 2.7.3 PROPAGATOR REGIONS

Now consider the contributions of the propagator regions. In the large  $\tilde{\lambda}$  limit, only  $\varkappa^1$  exchange contributes. Only the C<sub>1</sub>O-C<sub>2</sub>OO diagram involves an NS-sector propagator, which consists of the Feynman vertices  $A_{\lambda(p)\varkappa^1\theta_\alpha}^{D^2}$  and  $A_{\delta\tau(k)\varkappa^1}^{D^2}$  contracted via  $P_{\varkappa^1}$ . The 3-point vertex is given by

$$\begin{aligned} A_{\lambda(p)\varkappa^1\theta_\alpha}^{D^2} &= \int_{(2\tilde{\lambda})^{-1}}^{2\tilde{\lambda}} d\beta \left\langle B_\beta V_{\varkappa^1}^{(-1)}(-\beta) V_{\theta_\alpha}^{(-\frac{1}{2})}(\beta) V_{\lambda(p)}^{(-\frac{1}{2})}(i, -i) \right\rangle_{x^\mu=0}^{D^2} \\ &= -2u^\alpha \int_{1/2\tilde{\lambda}}^{2\tilde{\lambda}} \frac{d\beta}{1+\beta^2} \\ &= -\pi u^\alpha + O(\tilde{\lambda}^{-1}) \end{aligned} \tag{2.182}$$

where we used the fact that  $B_\beta$  is identical to that of (2.113). Note that the picture-raised vertex operator for the dilatino is

$$V_\lambda^{(-\frac{1}{2})} = \frac{1}{\sqrt{2}} \left( V_{\lambda_1}^{(0, -\frac{1}{2})} + iV_{\lambda_2}^{(-\frac{1}{2}, 0)} \right). \tag{2.183}$$

Evaluating the remainder of the Feynman diagram gives

$$A_{\lambda(p)\varkappa^1\theta_\alpha}^{D^2} P_{\varkappa^1} A_{\delta\tau(k)\varkappa^1}^{D^2} = i\pi u^\alpha. \tag{2.184}$$

We now construct the full amplitude, which in the large  $\tilde{\lambda}$  limit receives consists only of the Feynman diagrams

$$\mathcal{A}_{\delta\tau(p)\lambda(k)\theta_\alpha} = A_{\delta\tau(p)\lambda(k)\theta_\alpha} + A_{\delta\tau(p)\varkappa^1}^{D^2} P_{\varkappa^1} A_{\lambda(p)\varkappa^1\theta_\alpha}^{D^2}. \tag{2.185}$$

Plugging in (2.181), (2.182), (2.184), we find

$$\mathcal{A}_{\delta\tau(p)\lambda(k)\theta_\alpha}^{D^2} = -i\pi u^\alpha(k) \left\{ 4I_{\tilde{\lambda}}(p \cdot k) - \sqrt{2} \frac{e_{\mu\nu}(p)k^\mu k^\nu}{p \cdot k} + 2(p \cdot k) - 1 \right\}. \quad (2.186)$$



# A

## Appendix

### A.1 CONVENTIONS

In this appendix, we lay out our conventions for calculating scattering amplitudes for the type IIB superstring.

### A.1.1 TARGET SPACE SPINORS

The  $SO(1, 9)$  gamma matrices  $\Gamma^\mu$  obey the Clifford algebra

$$\{\Gamma^\mu, \Gamma^\nu\} = 2\eta^{\mu\nu}. \quad (\text{A.1})$$

In Lorentzian signature, we can work with purely real matrices with the off-diagonal form

$$(\Gamma^\mu)_A{}^B = \begin{pmatrix} 0 & (\gamma^\mu)_{\alpha\beta} \\ (\gamma^\mu)^{\alpha\beta} & 0 \end{pmatrix}, \quad (\text{A.2})$$

where  $A, B = 1, \dots, 32$ , and  $\alpha, \beta = 1, \dots, 16$ . In this basis, the chirality matrix reads

$$(\Gamma)_A{}^B \equiv (\Gamma^0 \cdots \Gamma^9)_A{}^B = \begin{pmatrix} \delta_\beta^\alpha & 0 \\ 0 & -\delta_\beta^\alpha \end{pmatrix}. \quad (\text{A.3})$$

The chiral matrices  $(\gamma^\mu)_{\alpha\beta}$  and  $(\gamma^\mu)^{\alpha\beta}$  satisfy the Clifford algebra

$$\{\gamma^\mu, \gamma^\nu\} = 2\eta^{\mu\nu}, \quad (\text{A.4})$$

and have the following properties:

$$(\gamma^\mu)^{\alpha\beta} = (\gamma^\mu)^{\beta\alpha}, \quad (\gamma^i)^{\alpha\beta} = (\gamma^i)_{\alpha\beta}, \quad (\gamma^0)_{\alpha\beta} = -(\gamma^0)^{\alpha\beta} = \delta_{\alpha\beta}. \quad (\text{A.5})$$

Products of such matrices have a natural index structure, i.e.  $(\gamma^\mu \gamma^\nu)_\alpha{}^\beta = (\gamma^\mu)_{\alpha\delta} (\gamma^\nu)^{\delta\beta}$

and  $(\gamma^\mu \gamma^\nu)^\alpha{}_\beta = (\gamma^\mu)^{\alpha\delta} (\gamma^\nu)_{\delta\beta}$ .

In certain instances we will work with an explicit representation of the gamma matrices, where

$$(\gamma^0)^{\alpha\beta} = \begin{pmatrix} 1_{8\times 8} & 0_{8\times 8} \\ 0_{8\times 8} & 1_{8\times 8} \end{pmatrix}, \quad (\gamma^9)^{\alpha\beta} = \begin{pmatrix} 1_{8\times 8} & 0_{8\times 8} \\ 0_{8\times 8} & -1_{8\times 8} \end{pmatrix}. \quad (\text{A.6})$$

In Euclidean signature, we perform a Wick rotation and replace  $\gamma^0$  with  $i\gamma^0$  in all of the pertinent formulas. Note that in this case the spinors are now in general complex-valued.

### A.1.2 WORLDSHEET THEORY

The worldsheet of the type II superstring is described by a 2d  $\mathcal{N} = (1, 1)$  superconformal field theory (SCFT) with vanishing central charge  $c = 0$ , consisting of a unitary “matter” SCFT with  $c = 15$  that sets the background, together with a universal ghost SCFT consisting of the  $b, c$  diffeomorphism ghosts and their superpartners  $\beta, \gamma$ . The theory is invariant under a BRST symmetry generated by Grassmann odd operators  $Q_B$  and  $\tilde{Q}_B$ , with

$$Q_B = \oint \frac{dz}{2\pi i} \left[ cT_m - \frac{1}{2}c\partial\phi^2 - c\partial^2\phi - c\eta\partial\xi + \eta e^\phi G_m + bc\partial c - \eta\partial\eta b e^{2\phi} \right](z). \quad (\text{A.7})$$

The operators  $T_m$  and  $G_m$  are the stress tensor and supercurrent of the matter CFT, respectively. The  $\beta, \gamma$  ghosts meanwhile are expressed in their rebosonized forms

$$\gamma = \eta e^\phi, \quad \beta = e^{-\phi} \partial\xi, \quad (\text{A.8})$$

where the ghosts  $\eta$  and  $\xi$  are  $bc$ -like Grassmann odd fields, while  $\phi$  is a linear dilaton. In order to be consistent with the statistics of the  $\beta, \gamma$  ghosts,  $e^{q\phi}$  is taken to be Grassmann

even/odd for  $q$  even/odd. Furthermore, all products are taken to be conformally normal ordered with respect to the operator product expansion (OPE). The main OPEs of interest are

$$\begin{aligned} b(z)c(w) \sim c(z)b(w) \sim \frac{1}{z-w}, \quad \eta(z)\xi(w) \sim \xi(z)\eta(w) \sim \frac{1}{z-w} \\ \phi(z)\phi(w) \sim -\ln(z-w), \quad e^{q_1\phi(z)}e^{q_2\phi(w)} \sim (z-w)^{-q_1q_2} \end{aligned} \tag{A.9}$$

where  $\sim$  denotes the singular part of the OPE, and similarly for their antiholomorphic counterparts.

The full matter+ghost SCFT enjoys several global bosonic symmetries, including a  $U(1)_F$  fermion number symmetry, a  $U(1)_{\text{ghost}}$  ghost number symmetry, and a  $U(1)_{\text{picture}}$  picture number symmetry. The type IIB string is specified by the chiral GSO projection

$$(-1)^F = (-1)^{\tilde{F}} = +1, \tag{A.10}$$

where  $(-1)^F$  and  $(-1)^{\tilde{F}}$  are the holomorphic and antiholomorphic worldsheet fermion numbers, i.e. charges of  $U(1)_F$ .

In order to formulate string scattering amplitudes, it is necessary to introduce the so-called picture changing operator

$$\mathcal{X}(y) \equiv \{Q_B, \xi(z)\} = c\partial\xi + e^\phi G_m + be^{2\phi}\partial\eta + \partial(be^{2\phi}\eta). \tag{A.11}$$

as well as its antiholomorphic counterpart  $\tilde{\mathcal{X}}$ . These are operators which have unit charge under  $U(1)_{\text{picture}}$ .

In this work, we consider the type IIB theory in 10d Minkowski space. For this back-

ground, the matter CFT consists of ten free noncompact bosons  $X^\mu$  and ten free Majorana fermions  $\psi^\mu, \tilde{\psi}^\mu$  with  $\mu = 0, \dots, 9$ . The elementary fields obey

$$X^\mu(z, \bar{z})X^\nu(w, \bar{w}) \sim -\frac{\alpha'}{2}\eta^{\mu\nu} \log |z - w|^2, \quad \psi^\mu(z)\psi^\nu(w) \sim \frac{\eta^{\mu\nu}}{z - w}, \quad (\text{A.12})$$

where  $\eta^{\mu\nu} = \text{diag}(-1, +1, \dots, +1)$  is the Minkowski metric in mostly plus signature. The stress tensor and supercurrent take the respective forms

$$\begin{aligned} T_m &= -\frac{1}{\alpha'}\partial X_\mu\partial X^\mu - \frac{1}{2}\psi_\mu\partial\psi^\mu, \\ G_m &= i\sqrt{\frac{2}{\alpha'}}\psi_\mu\partial X^\mu. \end{aligned} \quad (\text{A.13})$$

The Hilbert space of the free fermion decomposes into different sectors based on the periodicities of  $\psi^\mu$  and  $\tilde{\psi}^\mu$  on the cylinder, with the NS sector corresponding to antiperiodic boundary conditions and the R sector to periodic boundary conditions. Operators in the NS sector correspond to products of derivative of  $\psi^\mu$ , while operators in the R sector include contributions from a pair of conjugate Weyl spinors  $S^\alpha$  and  $S_\alpha$ . Since the ghost field  $\phi$  is periodic, its Hilbert space admits a similar decomposition, with  $e^{n\phi}$  in the NS sector and  $e^{\frac{1}{2}n\phi}$  in the R sector for  $n \in \mathbb{Z}$ . By pairing these operators with the matter fields, one can construct operators with matching worldsheet and spacetime statistics. This corresponds to taking the R-sector ground states  $e^{-\frac{1}{2}\phi}S^\alpha$  and  $e^{+\frac{1}{2}\phi}S_\alpha$  to both be Grassmann odd and GSO even. We also have that the NS sector ground state  $e^{-\phi}\psi^\mu$  is Grassmann even. Fixing the conventions for these operators then fully specifies the worldsheet statistics of all of the remaining operators in the theory. A brief list of several operators and their properties in Figure A.1.

Operator	Weight	GSO	Worldsheet parity	$U(1)_{\text{ghost}}$	$U(1)_{\text{pic}}$
$b$	2	+	-	-1	0
$c$	-1	+	-	+1	0
$\xi$	2	+	-	-1	+1
$\eta$	-1	+	-	+1	-1
$e^{(n-\frac{1}{2})\phi}S^\alpha$	$\frac{1}{2}(n-1)(n+2)$	$(-)^n$	$(-)^{n+1}$	0	$n - \frac{1}{2}$
$e^{(n+\frac{1}{2})\phi}S_\alpha$	$\frac{1}{2}n(n+3)$	$(-)^n$	$(-)^{n+1}$	0	$n + \frac{1}{2}$
$e^{(n-1)\phi}\psi^\mu$	$1 - \frac{1}{2}n^2$	$(-)^n$	$(-)^n$	0	$n$
$\partial X^\mu$	1	+	+	0	0

**Figure A.1:** Properties of the basic holomorphic operators in the free worldsheet theory, where  $n \in \mathbb{Z}$ .

The type IIB string also has 10d  $\mathcal{N} = (2, 0)$  target space supersymmetry generated by 32 chiral supercharges,  $\widehat{Q}_{(-\frac{1}{2})}^\alpha$  and  $\widehat{\widetilde{Q}}_{(-\frac{1}{2})}^\alpha$ , where the hat indicates a worldsheet operator. In the  $(-\frac{1}{2})$ -picture they are given by

$$\widehat{Q}_{(-\frac{1}{2})}^\alpha \equiv \oint \frac{dz}{2\pi i} \frac{1}{\alpha'^{1/4}} e^{-\frac{1}{2}\phi} S^\alpha(z), \quad (\text{A.14})$$

and similarly for  $\widehat{\widetilde{Q}}_{(-\frac{1}{2})}^\alpha$ . We also work with the supercharges in the  $(+\frac{1}{2})$ -picture as given by

$$\widehat{Q}_{(+\frac{1}{2})}^\alpha \equiv - \oint \frac{dz}{2\pi i} \frac{1}{\alpha'^{3/4}} (\gamma_\mu)^{\alpha\beta} i\partial X^\mu e^{+\frac{1}{2}\phi} S_\beta(z), \quad (\text{A.15})$$

where  $\gamma^\mu$  are the gamma matrices. Together they satisfy the super-Poincaré algebra

$$\begin{aligned} \{\widehat{Q}_{(-\frac{1}{2})}^\alpha, \widehat{Q}_{(+\frac{1}{2})}^\beta\} &= -\frac{1}{2}(\gamma_\mu)^{\alpha\beta} P_{(0)}^\mu, \\ \{\widetilde{\widehat{Q}}_{(-\frac{1}{2})}^\alpha, \widetilde{\widehat{Q}}_{(+\frac{1}{2})}^\beta\} &= -\frac{1}{2}(\gamma_\mu)^{\alpha\beta} \widetilde{P}_{(0)}^\mu, \\ \{\widehat{Q}_{(\pm\frac{1}{2})}^\alpha, \widetilde{\widehat{Q}}_{(\mp\frac{1}{2})}^\beta\} &= 0, \end{aligned} \tag{A.16}$$

where  $P_{(0)}^\mu$  and  $\widetilde{P}_{(0)}^\mu$  generate target space translations as

$$P_{(0)}^\mu \equiv \oint \frac{dz}{2\pi i} \frac{2}{\alpha'} i\partial X^\mu(z). \tag{A.17}$$

Note that in a noncompact target space  $P_{(0)}^\mu$  and  $\widetilde{P}_{(0)}^\mu$  act identically on momentum eigenstates as  $P^\mu e^{ip\cdot X} = p^\mu e^{ip\cdot X}$ .

### A.1.3 ASYMPTOTIC CLOSED STRING STATES

The asymptotic closed string states correspond to on-shell closed string fields  $\Psi_c \in \mathcal{H}_c$ , as defined in [35], which obey the Siegel gauge constraints  $b_0\Psi_c = \widetilde{b}_0\Psi_c = 0$ . Of particular interest are the massless closed strings, which comprise the 128 states of the supergraviton multiplet. The bosonic states arise from the NSNS and RR sectors. In the NSNS sector, we work with the BRST representative

$$V_{\text{NSNS}}^{(-1,-1)} = g_c \widetilde{c}\widetilde{c} \varepsilon_{\mu\nu}(p) e^{-\phi} \psi^\mu e^{-\widetilde{\phi}} \widetilde{\psi}^\nu e^{ip\cdot X}, \quad p^2 = 0, \tag{A.18}$$

where  $g_c$  is the closed string coupling. The polarization tensor  $\varepsilon_{\mu\nu}$  obeys

$$\varepsilon_{\mu\nu}(p)p^\mu = \varepsilon_{\mu\nu}(p)p^\nu = 0, \quad \varepsilon_{\mu\nu}(p)\varepsilon^{\mu\nu}(p) = 1, \quad (\text{A.19})$$

where the first condition ensures that the vertex operator is BRST-closed, and the second corresponds to the canonical normalization of one-particle states. The polarization tensor decomposes into irreducible representations of the  $SO(8)$  little group as

$$\varepsilon_{\mu\nu} = h_{\mu\nu} + b_{\mu\nu} + e_{\mu\nu} \quad (\text{A.20})$$

corresponding to a symmetric, traceless tensor (the graviton), an antisymmetric tensor (the Kalb-Ramond B-field), and a scalar (the dilaton  $\delta\tau_2$ ).

In the RR sector, there is a unique choice of BRST representative given by

$$V_{\text{RR}}^{(-\frac{1}{2}, -\frac{1}{2})} = g_c c\tilde{c} f_{\alpha\beta} e^{-\frac{1}{2}\phi} S^\alpha e^{-\frac{1}{2}\tilde{\phi}} \tilde{S}^\beta e^{ip\cdot X}, \quad p^2 = 0, \quad (\text{A.21})$$

where the polarization tensor  $f_{\alpha\beta} = f_{\alpha\beta}(p)$  obeys

$$f_{\alpha\beta}(p)\not{p}^{\beta\gamma} = f_{\alpha\beta}(p)\not{p}^{\alpha\gamma} = 0, \quad \not{p} \equiv p_\mu \gamma^\mu. \quad (\text{A.22})$$

As a bispinor,  $f_{\alpha\beta}$  decomposes into odd-rank forms according to

$$f_{\alpha\beta}^{(r)}(p) = \frac{i}{r!} F_{\mu_1 \dots \mu_r}^{(r)}(p) (\gamma^{\mu_1 \dots \mu_r})_{\alpha\beta}, \quad (\text{A.23})$$

where  $F^{(r)}$  is related to  $F^{(10-r)}$  by Hodge duality, with the 5-form  $F^{(5)}$  naturally being



self-dual. For these coefficients, the transversality constraints (A.22) reduce to

$$p_{[\nu} F_{\mu_1 \dots \mu_r]}^{(r)}(p) = 0. \quad (\text{A.24})$$

The  $F_{\mu_1 \dots \mu_r}^{(r)}$  thus serve as field strengths associated to the RR gauge potentials, which consist of a 4-form, a 2-form, and a scalar (the axion  $\delta\tau_1$ ).

The axion-dilaton  $\delta\tau$ , which plays a dominant role in the analysis, is specified by the vertex operator

$$V_{\delta\tau(p)} = \frac{1}{\sqrt{2}} (V_{\delta\tau_1(p)} + iV_{\delta\tau_2(p)}) . \quad (\text{A.25})$$

The dilaton vertex operator corresponds to (A.18) with the polarization tensor<sup>1</sup>

$$e_{\mu\nu}(p) = \frac{1}{\sqrt{8}} (\eta_{\mu\nu} - \ell_\mu p_\nu - \ell_\nu p_\mu), \quad \ell^2 = 0, \quad \ell \cdot p = 1, \quad (\text{A.28})$$

which relies on the introduction of a spacelike vector  $\ell^\mu = \ell^\mu(p)$ . The axion vertex operator  $V_{\delta\tau_2}$  corresponds to (A.21). Lorentz invariance and supersymmetry fixes its polariza-

---

<sup>1</sup>Being a scalar, the dilaton should have a polarization tensor with only a single degree of freedom. The freedom to choose  $\ell^\mu$ , which superficially contradicts this statement, is merely an artifact from our choice of BRST representative. In particular,  $\ell$  is expected to drop out of any on-shell amplitudes calculated using (A.28). It can also be removed once and for all by adding to (A.18) a BRST-exact term

$$g_c c \tilde{c} \left( (\ell_\mu p_\nu + \ell_\nu p_\mu) e^{-\phi} \psi^\mu e^{-\tilde{\phi}} \tilde{\psi}^\nu + (e^{-2\phi} \partial \xi \tilde{\eta} + e^{-2\tilde{\phi}} \bar{\partial} \tilde{\xi} \tilde{\eta}) \right) e^{ip \cdot X}, \quad (\text{A.26})$$

in which case the scalar nature of the dilaton is manifest in the vertex operator

$$g_c c \tilde{c} \left( e^{-\phi} \psi^\mu e^{-\tilde{\phi}} \tilde{\psi}_\mu + e^{-2\phi} \partial \xi \tilde{\eta} + e^{-2\tilde{\phi}} \bar{\partial} \tilde{\xi} \tilde{\eta} \right) e^{ip \cdot X}. \quad (\text{A.27})$$

Both this vertex operator and (A.18) should produce identical on-shell amplitudes, although intermediate diagrams will in general differ from one another. In practice, we shall stick with the latter since it is easier to use in our computations.

tion tensor to

$$f_{\alpha\beta}^{(0)}(p) = -\frac{\not{p}_{\alpha\beta}}{\sqrt{32\alpha'}}. \quad (\text{A.29})$$

Note that the vertex operator for  $\delta\bar{\tau}$  takes a similar form, with the factor multiplying the NSNS vertex operator replaced by  $i \rightarrow -i$ .

Next consider the fermions, which are constructed from states in the NSR and RNS sectors. Here, we shall work with BRST representatives of the form

$$\begin{aligned} V_{\text{NSR}}^{(-1, -\frac{1}{2})} &= g_c \tilde{c} \tilde{u}_{\mu\alpha} e^{-\phi} \psi^\mu e^{-\frac{1}{2}\tilde{\phi}} \tilde{S}^\alpha e^{ip \cdot X} \\ V_{\text{RNS}}^{(-\frac{1}{2}, -1)} &= g_c \tilde{c} \tilde{v}_{\mu\alpha} e^{-\frac{1}{2}\phi} S^\alpha e^{-\tilde{\phi}} \tilde{\psi}^\mu e^{ip \cdot X} \end{aligned} \quad (\text{A.30})$$

with  $p^2 = 0$ , and where the polarization tensors satisfy

$$p^\mu u_\mu(p) = u_\mu(p) \not{p} = 0, \quad (\text{A.31})$$

and similarly for  $v_{\mu\alpha}$ . Each admits a decomposition into  $SO(8)$  representations of the form

$$u_{\mu\alpha}(p) = (\gamma_\mu)_{\alpha\beta} \lambda^\beta(p) + \psi_{\mu\alpha}(p), \quad \psi(p) = 0, \quad (\text{A.32})$$

which obey (A.31)

$$\not{p} \lambda(p) = 0, \quad \gamma^{\mu\nu\rho} p_\nu \psi_{i\rho}(p) = 0. \quad (\text{A.33})$$

These are the momentum-space Dirac and Rarita-Schwinger equations, respectively. In other words, the RNS and NSR states comprise two massless spin 1/2 fermions  $\lambda_i$  (the dilatini), and two massless spin 3/2 fermions  $\psi_i$  (the gravitini).

In this work, we shall consider a certain complex combination of the dilatino,  $\lambda$ , with associated vertex operator

$$V_{\lambda(p)}^{(-\frac{3}{2})} = \frac{g_c}{\sqrt{2}} (\gamma_\mu)_{\alpha\beta} \lambda^\beta(p) c\tilde{c} \left( e^{-\frac{1}{2}\phi} S^\alpha e^{-\tilde{\phi}} \tilde{\psi}^\mu + i e^{-\phi} \psi^\mu e^{-\frac{1}{2}\tilde{\phi}} \tilde{S}^\alpha \right) e^{ip \cdot X}. \quad (\text{A.34})$$

which is related to that of  $\delta\tau$  by a single application of  $\widehat{Q}_-$ .

#### A.1.4 PICTURE-RAISED VERTEX OPERATORS

By taking the PCOs coincident with the vertex operators, one can define their raised counterparts. The picture  $(0, -1)$  NSNS vertex operator is given by

$$\begin{aligned} V_{\text{NSNS}}^{(0,-1)}(z, \bar{z}) &= \lim_{p \rightarrow z} \mathcal{X}(p) V_{\text{NSNS}}^{(-1,-1)}(z, \bar{z}) \\ &= g_c \varepsilon_{\mu\nu} \left( \sqrt{\frac{2}{\alpha'}} c i \partial X^\mu + \sqrt{\frac{\alpha'}{2}} c p \cdot \psi \psi^\mu + \eta e^\phi \psi^\mu \right) \tilde{c} e^{-\tilde{\phi}} \tilde{\psi}^\nu e^{ip \cdot X}(z, \bar{z}). \end{aligned} \quad (\text{A.35})$$

Similarly, the picture  $(0, 0)$  NSNS vertex operator reads

$$\begin{aligned} V_{\text{NSNS}}^{(0,0)} &= \lim_{p \rightarrow z} \lim_{\bar{p} \rightarrow \bar{z}} \mathcal{X}(p) \tilde{\mathcal{X}}(\bar{p}) V_{\text{NSNS}}^{(-1,-1)}(z, \bar{z}) \\ &= g_c \varepsilon_{\mu\nu} \left( \sqrt{\frac{2}{\alpha'}} c i \partial X^\mu + \sqrt{\frac{\alpha'}{2}} c p \cdot \psi \psi^\mu + \eta e^\phi \psi^\mu \right) \\ &\quad \times \left( \sqrt{\frac{2}{\alpha'}} \tilde{c} i \bar{\partial} X^\nu + \sqrt{\frac{\alpha'}{2}} \tilde{c} p \cdot \tilde{\psi} \tilde{\psi}^\nu + \tilde{\eta} e^{\tilde{\phi}} \tilde{\psi}^\beta \right) e^{ip \cdot X}(z, \bar{z}). \end{aligned} \quad (\text{A.36})$$

The picture  $(+\frac{1}{2}, -\frac{1}{2})$  RR vertex operator is

$$\begin{aligned} V_{\text{RR}}^{(\frac{1}{2}, -\frac{1}{2})}(z, \bar{z}) &= \lim_{p \rightarrow z} \mathcal{X}(p) V_{\text{RR}}^{(-\frac{1}{2}, -\frac{1}{2})}(z, \bar{z}) \\ &= g_c f_{\alpha\beta} (\gamma^\mu)^{\alpha\gamma} \left( \frac{1}{\sqrt{\alpha'}} c i \partial X_\mu e^{\frac{1}{2}\phi} S_\gamma \right) \tilde{c} e^{-\frac{1}{2}\tilde{\phi}} \tilde{S}^\beta e^{ip \cdot X}(z, \bar{z}) + \dots, \end{aligned} \quad (\text{A.37})$$

where we have neglected terms that contain the momentum or the ghost structure  $e^{\frac{1}{2}\phi}\eta$ .

Using these, it is natural to define the picture-raised axion-dilaton vertex operators

$$\begin{aligned} V_{\delta\tau(p)}^{(-1)} &= \frac{1}{\sqrt{2}} \left( V_{\delta\tau_1(p)}^{(0,-1)} + iV_{\delta\tau_2(p)}^{(-\frac{1}{2},-\frac{1}{2})} \right), \\ V_{\delta\tau(p)}^{(0)} &= \frac{1}{\sqrt{2}} \left( V_{\delta\tau_1(p)}^{(0,0)} + iV_{\delta\tau_2(p)}^{(+\frac{1}{2},-\frac{1}{2})} \right). \end{aligned} \tag{A.38}$$

### A.1.5 D-INSTANTON BOUNDARY CONDITIONS

The single D-instanton solution is characterized by a family of BRST-invariant boundary conditions parametrized by ten bosonic moduli  $x^\mu$  and sixteen fermionic moduli  $\theta_\alpha$ . For simplicity, we restrict to the subset satisfying  $\theta_\alpha = 0$ , since those with nonzero  $\theta_\alpha$  can be described in terms of massless R-sector boundary deformations. To be concrete, take the worldsheet to be the disc  $D^2$  represented by the upper half plane  $\text{Im}(z) > 0$  with boundary parametrized by  $u = \text{Re}(z)$ . Compatibility with BRST invariance implies that the ghosts obey the boundary conditions

$$\begin{aligned} b(u) &= \tilde{b}(u), & c(u) &= \tilde{c}(u), \\ \eta(u) &= \tilde{\eta}(u), & \xi(u) &= \tilde{\xi}(u), & \phi(u) &= \tilde{\phi}(u). \end{aligned} \tag{A.39}$$

In the matter sector, the D-instanton imposes Dirichlet boundary conditions in all ten (Euclidean) spacetime directions such that

$$\partial X^\mu(u) = -\bar{\partial} X^\mu(u), \quad \psi^\mu(u) = -\tilde{\psi}^\mu(u). \tag{A.40}$$

This implies that there is a family of boundary conditions with  $\theta_\alpha = 0$  parametrized by  $x^\mu \in \mathbb{R}^{10}$  given by

$$X^\mu(u) = x^\mu. \quad (\text{A.41})$$

Furthermore, consistency of the boundary conditions for  $\psi^\mu$  in (A.40) with the  $\psi^\mu S^\alpha$  OPE (A.52) imply that the spin fields necessarily obey

$$e^{-\frac{1}{2}\phi} S^\alpha(u) = i s e^{-\frac{1}{2}\tilde{\phi}} \tilde{S}^\alpha(u), \quad s = \pm 1, \quad (\text{A.42})$$

where the factor of  $i$  arises from Wick rotation to Euclidean signature. We shall take  $s = +1$  to correspond with the D-instanton, and  $s = -1$  with the anti-D-instanton. Note that this choice is merely a matter of convention in backgrounds with a vanishing RR zero-form potential.

In general, the D-instanton boundary conditions  $(x^\mu, \theta_\alpha)$  preserve half of the target space supersymmetries. The associated preserved supercharges are given by

$$\hat{Q}_{(\pm\frac{1}{2}),+}^\alpha = \hat{Q}_{(\pm\frac{1}{2})}^\alpha + i\tilde{\hat{Q}}_{(\pm\frac{1}{2})}^\alpha. \quad (\text{A.43})$$

It is convenient to organize the remaining supercharges into

$$\hat{Q}_{(\pm\frac{1}{2}),-}^\alpha = \hat{Q}_{(\pm\frac{1}{2})}^\alpha - i\tilde{\hat{Q}}_{(\pm\frac{1}{2})}^\alpha. \quad (\text{A.44})$$

With respect to this basis, the super-Poincaré algebra takes the form

$$\begin{aligned}
\left\{ \widehat{Q}_{(\pm\frac{1}{2}),+}^\alpha, \widehat{Q}_{(\mp\frac{1}{2}),-}^\alpha \right\} &= -(\gamma_\mu)^{\alpha\beta} (P_{(0)}^\mu + \widetilde{P}_{(0)}^\mu), \\
\left\{ \widehat{Q}_{(\pm\frac{1}{2}),+}^\alpha, \widehat{Q}_{(\pm\frac{1}{2}),+}^\alpha \right\} &= 0, \\
\left\{ \widehat{Q}_{(\pm\frac{1}{2}),-}^\alpha, \widehat{Q}_{(\pm\frac{1}{2}),-}^\alpha \right\} &= 0.
\end{aligned} \tag{A.45}$$

### A.1.6 D-INSTANTON SCATTERING AMPLITUDES

Consider the scattering amplitude of  $n_c$  closed strings in a general D-instanton background. In general, this involves several disconnected worldsheet diagrams whose insertions include the closed string vertex operators  $V_i^c$  corresponding to the asymptotic states, as well as several open string vertex operators  $V_j^o$  coming from deformations of the D-instanton boundary conditions. The contribution from a given connected topology takes the form

$$A^{g,b}[V_1^c, \dots, V_{n_c}^c; V_1^o, \dots, V_{n_o}^o] = \int_{\mathcal{M}} \Omega[V_1^c, \dots, V_{n_c}^c; V_1^o, \dots, V_{n_o}^o], \tag{A.46}$$

where  $\mathcal{M}$  is the moduli space of bordered Riemann surfaces  $\Sigma_{g,b}$  with  $g$  handles and  $b$  boundaries,  $n_c$  bulk punctures, and  $n_o$  boundary punctures. It can be parameterized by  $m = -3\chi(\Sigma_{g,b}) + 2n_c + n_o$  real worldsheet moduli  $t^k \in \mathbb{R}$ . The integrand is given by a  $k$ -dimensional form

$$\Omega = \left\langle \bigwedge_{k=1}^m \mathcal{B}_{t_k} dt^k \prod_{l=1}^{N_p} \mathcal{X}(y_l) \prod_{i=1}^{n_c} V_i^c(z_i, \bar{z}_i) \prod_{j=1}^{n_o} V_j^o(z_j) \right\rangle_{\text{BC}}^{\Sigma_{g,b}}, \tag{A.47}$$

which takes the form of a correlation function on  $\Sigma_{g,b}$  with the vertex operators inserted at arbitrary moduli dependent points  $z_i = z_i(t)$ . The boundary conditions on the world-sheet fields, denoted by BC, correspond to a particular position in D-instanton moduli space. In order to saturate the picture anomaly, there are  $N_p$  PCO insertions at  $y_l = y_l(t)$ , where

$$\begin{aligned}
N_p = & -\chi(\Sigma_{g,b}) \\
& + 2n_{\text{NSNS}}^c + n_{\text{RR}}^c + \frac{3}{2}n_{\text{RNS}}^c + \frac{3}{2}n_{\text{NSR}}^c \\
& + 2n_{\text{NS}}^o + \frac{1}{2}n_{\text{R}}^o.
\end{aligned} \tag{A.48}$$

Here,  $n^c$  and  $n^o$  denote the number of closed and open string vertex operators, respectively, with the subscript referring to the NS/R sectors.

In general, the punctured Riemann surface can be defined as a union of local patches separated by a set of circles  $C_a$  and semi-circles  $S_b$ . The local coordinates in neighboring patches are required to agree on their overlap  $C_a$  or  $S_b$ , where they take the form  $z_a = z_a(t)$  and  $z_b = z_b(t)$ , respectively. The  $b$ -ghost insertions are then defined with respect to this parameterization as

$$\begin{aligned}
B_{t^k} = & \sum_{C_a} \left( \oint_a \frac{dz}{2\pi i} \frac{\partial z_a}{\partial t^k} b(z) - \oint_a \frac{d\bar{z}}{2\pi i} \frac{\partial \bar{z}_a}{\partial t^k} \tilde{b}(\bar{z}) \right) \\
& + \sum_b \left( \int_{S_b} \frac{dz}{\pi i} \frac{\partial z_b}{\partial t^k} b(z) - \sum_b \int_{S_b} \frac{d\bar{z}}{\pi i} \frac{\partial \bar{z}_b}{\partial t^k} \tilde{b}(\bar{z}) \right).
\end{aligned} \tag{A.49}$$

In order for  $\Omega$  to be a well-defined form on the fiber bundle of local coordinates *and* PCO locations over  $\mathcal{M}$ , these insertions must be modified to

$$\mathcal{B}_{t^k} = B_{t^k} + \sum_{l=1}^{N_p} \frac{1}{\mathcal{X}(y_l)} \frac{\partial y_l}{\partial t^k} \partial \xi(y_l). \tag{A.50}$$

### A.1.7 OPEs AND CORRELATION FUNCTIONS

In this part of the appendix, we collect various OPEs relevant for the disc amplitudes considered in this work:

$$\begin{aligned}
e^{-\phi}\psi^\mu(z)e^{-\frac{1}{2}\phi}S^\alpha(w) &\sim -\frac{(\gamma^\mu)^{\alpha\beta}}{\sqrt{2}(z-w)}e^{-\frac{1}{2}\phi}S_\beta(w), \\
e^{-\phi}\psi^\mu(z)e^{-\frac{1}{2}\phi}S_\alpha(w) &\sim -\frac{(\gamma^\mu)_{\alpha\beta}}{\sqrt{2}(z-w)}e^{-\frac{1}{2}\phi}S^\beta(w), \\
e^{-\frac{1}{2}\phi}S^\alpha(z)e^{-\frac{1}{2}\phi}S^\beta(w) &\sim \frac{(\gamma_\mu)^{\alpha\beta}}{\sqrt{2}(z-w)}e^{-\phi}\psi^\mu(w), \\
e^{-\frac{3}{2}\phi}S_\alpha(z)e^{-\frac{1}{2}\phi}S^\beta(w) &\sim \frac{\delta_\alpha^\beta}{(z-w)^2}e^{-2\phi}(w) - \frac{3}{2(z-w)}e^{-2\phi}\partial\phi(w) \\
&\quad - \frac{(\gamma_{\mu\nu})_\alpha^\beta}{2(z-w)}e^{-2\phi}\psi^\mu\psi^\nu(w), \\
\psi^\mu\psi^\nu(z)e^{-\phi}\psi^\rho(w) &\sim \frac{\eta^{\nu\rho}\delta_\sigma^\mu - \eta^{\mu\rho}\delta_\sigma^\nu}{z-w}e^{-\phi}\psi^\sigma(w), \\
\psi^\mu\psi^\nu(z)e^{-\frac{1}{2}\phi}S^\alpha(w) &\sim -\frac{1}{2}\frac{(\gamma^{\mu\nu})_\alpha^\beta}{z-w}e^{-\frac{1}{2}\phi}S^\beta(w).
\end{aligned} \tag{A.51}$$

These OPEs subsequently determine various correlators, such as the 3-point function

$$\left\langle e^{-\phi}\psi^\mu(z_1)e^{-\frac{1}{2}\phi}S^\alpha(z_2)e^{-\frac{1}{2}\phi}S^\beta(z_3) \right\rangle_{\text{chiral}}^{S^2} = -\frac{(\gamma^\mu)^{\alpha\beta}}{\sqrt{2}z_{12}z_{13}z_{23}}, \tag{A.52}$$

as well as the 4-point function

$$\begin{aligned}
&\left\langle e^{-\frac{1}{2}\phi}S^{\alpha_1}(z_1)e^{-\frac{1}{2}\phi}S^{\alpha_2}(z_2)e^{-\frac{1}{2}\phi}S^{\alpha_3}(z_3)e^{-\frac{1}{2}\phi}S^{\alpha_4}(z_4) \right\rangle_{\text{chiral}}^{S^2} \\
&= -\frac{(\gamma_\mu)^{\alpha_1\alpha_2}(\gamma^\mu)^{\alpha_3\alpha_4}}{2z_{12}z_{23}z_{24}z_{34}} + \frac{(\gamma_\mu)^{\alpha_1\alpha_3}(\gamma^\mu)^{\alpha_2\alpha_4}}{2z_{13}z_{32}z_{34}z_{24}} - \frac{(\gamma_\mu)^{\alpha_1\alpha_4}(\gamma^\mu)^{\alpha_2\alpha_3}}{2z_{14}z_{42}z_{43}z_{23}}.
\end{aligned} \tag{A.53}$$



## A.2 MODULAR FORMS AND $SL(2, \mathbb{Z})$ COVARIANCE

In this appendix, we collect various results for the vertices appearing in the low-energy expansion of the quantum effective action of type IIB string theory. Their coefficients transform under the  $SL(2, \mathbb{Z})$  duality group as non-holomorphic forms of weight  $(w, \tilde{w})$ , i.e.

$$f^{(w, \tilde{w})} \left( \frac{a\tau + b}{c\tau + d} \right) = (c\tau + d)^w (c\bar{\tau} + d)^{\tilde{w}} f^{(w, \tilde{w})}(\tau), \quad a, b, c, d \in \mathbb{Z}, \quad ad - bc = 1. \quad (\text{A.54})$$

We shall also need the (holomorphic) modular covariant derivative on the upper-half  $\tau$ -plane,

$$\mathcal{D}_w = i\tau_2 \partial_\tau + \frac{w}{2}, \quad (\text{A.55})$$

which takes non-holomorphic forms of weight  $(w, \tilde{w})$  to those of weight  $(w + 1, \tilde{w} - 1)$ .

We first consider the  $\frac{1}{2}$ -BPS  $R^4$  and  $\frac{1}{4}$ -BPS  $D^4 R^4$  vertices. Their coefficients take the form of modular functions, i.e. non-holomorphic modular forms of weight  $(0, 0)$ , which satisfy a homogenous Laplace equation on the upper half plane

$$\left( \tau_2^2 \partial_\tau \partial_{\bar{\tau}} - \frac{1}{4} s(s-1) \right) f(\tau, \bar{\tau}) = 0, \quad s \in \mathbb{C}, \quad (\text{A.56})$$

subject to the boundary condition  $f(\tau, \bar{\tau}) = \mathcal{O}(\tau_2^p)$  for  $p \in \mathbb{R}$ . Its solution is given by the

non-holomorphic Eisenstein series

$$\begin{aligned}
E_s(\tau, \bar{\tau}) &= \sum_{(m,n) \neq (0,0)} \frac{\tau_2^s}{|m + n\tau|^{2s}} \\
&= 2\zeta(2s)\tau_2^s + 2\sqrt{\pi} \frac{\Gamma(s-1/2)\zeta(2s-1)}{\Gamma(s)} \tau_2^{1-s} \\
&\quad + \frac{4\pi^s}{\Gamma(s)} \tau_2^{1/2} \sum_{n \neq 0} |n|^{s-\frac{1}{2}} \sigma_{1-2s}(|n|) e^{2\pi i n \tau_1} K_{s-\frac{1}{2}}(2\pi |n| \tau_2),
\end{aligned} \tag{A.57}$$

where  $K_\alpha(z)$  is the K-Bessel function, and  $\sigma_z(n)$  is the divisor function

$$\sigma_z(n) = \sum_{d|n} d^{2z}, \quad \sigma_{-z}(n) = n^{-z} \sigma_z(n). \tag{A.58}$$

In the weak-coupling limit,  $E_s$  admits an expansion in  $\tau_2^{-1}$  given by

$$\begin{aligned}
E_s(\tau, \bar{\tau}) &= 2\zeta(2s)\tau_2^s + 2\sqrt{\pi} \frac{\Gamma(s-1/2)\zeta(2s-1)}{\Gamma(s)} \tau_2^{1-s} \\
&\quad + (e^{2\pi i \tau} + e^{-2\pi i \tau}) \left( \frac{2\pi^s}{\Gamma(s)} + \frac{s(s-1)}{2\Gamma(s)} \tau_2^{-1} + O(\tau_2^{-2}) \right) + O(e^{-4\pi \tau_2}).
\end{aligned} \tag{A.59}$$

The  $R^4$  and  $D^4 R^4$  coefficients  $f_0$  and  $f_4$  correspond to  $s = 3/2$  and  $s = 5/2$ , respectively,

$$f_0 = \frac{1}{26} E_{\frac{3}{2}}(\tau, \bar{\tau}), \quad f_4 = \frac{1}{211} E_{\frac{5}{2}}(\tau, \bar{\tau}). \tag{A.60}$$

The coefficient of the  $\frac{1}{8}$ -BPS  $D^6 R^4$  interaction meanwhile satisfies an inhomogeneous Laplace equation of the form

$$(\tau_2^2 \partial_\tau \partial_{\bar{\tau}} - 12) \mathcal{E}_3(\tau, \bar{\tau}) = -E_{\frac{3}{2}}(\tau, \bar{\tau})^2, \tag{A.61}$$

together with the weak-coupling boundary condition  $f_6(\tau, \bar{\tau}) = \mathcal{O}(\tau_2^3)$  as  $\tau_2 \rightarrow \infty$ . Its solution takes the form of a modular function that can be written in the weak-coupling limit ( $\tau_2 \rightarrow \infty$ ) as [58]

$$\begin{aligned} \mathcal{E}_3(\tau, \bar{\tau}) &= \frac{2\zeta(3)^2}{3}\tau_2^3 + \frac{4\zeta(2)\zeta(3)}{3}\tau_2 + \frac{8\zeta(2)^2}{5}\tau_2^{-1} + \frac{4\zeta(6)}{28}\tau_2^{-3} \\ &+ (e^{2\pi i\tau} + e^{-2\pi i\tau})(8\zeta(3)\tau_2^{\frac{1}{2}} + \mathcal{O}(1)) - e^{-4\pi\tau_2} (2\tau_2^{-2} + \mathcal{O}(\tau_2^{-3})) \\ &+ \mathcal{O}(e^{-6\pi\tau_2}). \end{aligned} \quad (\text{A.62})$$

Under our conventions, the  $D^6 R^4$  coefficient appearing in the main text is given by

$$f_6 = \frac{1}{2^{12}} \mathcal{E}_3(\tau, \bar{\tau}). \quad (\text{A.63})$$

In our discussion on higher-point amplitudes, we will also need the coefficients of the  $N$ -point MRV vertices, which transform as weight  $(N - 4, 4 - N)$  non-holomorphic modular forms. To describe such forms, we introduce the generalized Eisenstein series  $E_s^{(w)}$  as given by

$$\begin{aligned} E_s^{(w)}(\tau, \bar{\tau}) &= \sum_{(m,n) \neq (0,0)} \left( \frac{m + n\bar{\tau}}{m + n\tau} \right)^w \frac{\tau_2^s}{|m + n\tau|^{2s}} \\ &= \frac{2^w \Gamma(s)}{\Gamma(s + w)} \mathcal{D}_{w-1} \cdots \mathcal{D}_0 E_s(\tau, \bar{\tau}). \end{aligned} \quad (\text{A.64})$$

Following [49], the  $\delta\tau^2 R^4$  and  $\delta\tau^2 D^4 R^4$  coefficients are proportional to

$$r_0^{(6)} = \frac{15}{2^8} E_{\frac{3}{2}}^{(2)}(\tau, \bar{\tau}), \quad r_4^{(6)} = \frac{35}{2^{13}} E_{\frac{5}{2}}^{(2)}(\tau, \bar{\tau}), \quad (\text{A.65})$$

where the overall choice of normalization does not factor into our analysis in the main text.

It was shown in [49] that the coefficients multiplying  $\delta\tau^2 D_i^6 R^4$ , with the associated kinematic structures  $\mathcal{O}_{6,i}^{(3)}$  in (1.99) and (1.101), satisfy inhomogeneous Laplace equations of the form

$$\begin{aligned} (\tau_2^2 \partial_\tau \partial_{\bar{\tau}} - 10) \mathcal{E}_{2,1} &= -\frac{15}{2} \left( E_{\frac{3}{2}}^{(0)} E_{\frac{3}{2}}^{(2)} + \frac{3}{5} E_{\frac{3}{2}}^{(1)} E_{\frac{3}{2}}^{(1)} \right), \\ (\tau_2^2 \partial_\tau \partial_{\bar{\tau}} - 10) \mathcal{E}_{2,2} &= -\frac{5}{2} c_1 \left( E_{\frac{3}{2}}^{(0)} E_{\frac{3}{2}}^{(2)} - E_{\frac{3}{2}}^{(1)} E_{\frac{3}{2}}^{(1)} \right), \end{aligned} \tag{A.66}$$

where  $c_1$  is not determined by supersymmetry and  $SL(2, \mathbb{Z})$ -covariance alone. Their solutions can be written in terms of the  $D^6 R^4$  coefficient as

$$\begin{aligned} \mathcal{E}_{2,1} &= 4\mathcal{D}_1 \mathcal{D}_0 \mathcal{E}_3, \\ \mathcal{E}_{2,2} &= \frac{c_1}{5} \left( \mathcal{E}_{2,1} - \frac{1}{2} E_{\frac{3}{2}}^{(1)} E_{\frac{3}{2}}^{(1)} \right). \end{aligned} \tag{A.67}$$

In our conventions, the  $\delta\tau^2 D_i^6 R^4$  coefficients  $r_{6,i}^{(6)}$  are proportional to

$$r_{6,1}^{(6)} = \frac{1}{2^{12}} \mathcal{E}_{2,1}(\tau, \bar{\tau}), \quad r_{6,2}^{(6)} = \frac{1}{2^{12}} \mathcal{E}_{2,2}(\tau, \bar{\tau}), \tag{A.68}$$

where only the relative factors between these and the lower-order coefficients is of relevance.

### A.3 ANNULUS 1-POINT DIAGRAM

In this section we compute the annulus amplitude with a single  $\delta\tau$  insertion. Similar to the empty topologies, this diagram is also expected to vanish in the on-shell approach due to supersymmetry, which we demonstrate explicitly.

The annulus  $A^2$  with modulus  $t \in (0, \infty)$  can be parametrized by the strip with coordi-

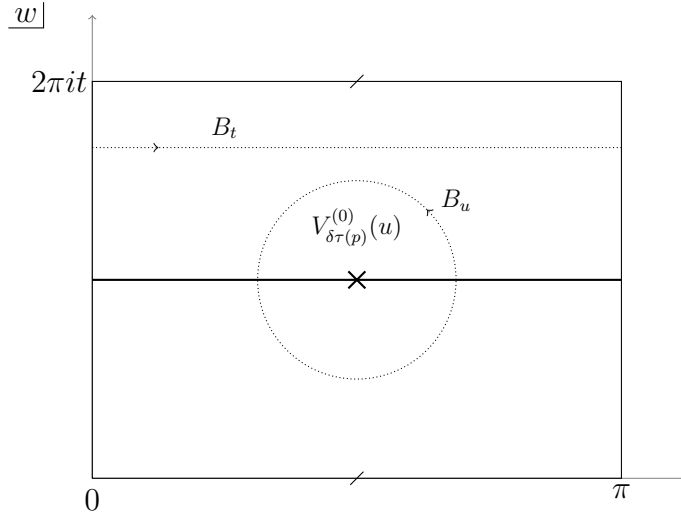


**Figure A.2:** The annulus  $A^2(t)$  represented by a rectangle  $w \in [0, \pi] \times [0, 2\pi it]$  with opposite sides  $w \simeq w + 2\pi it$  identified. There is a single closed string puncture at  $w = u$  for  $u \in \mathbb{R}$ , which has been drawn off the real axis for clarity. The  $b$  ghost contour  $B_u$  surrounds the (picture zero) integrated vertex operator  $V_{\delta\tau(p)}^{(0)}$ , while  $B_t$  runs along a horizontal line segment.

nate  $w$  satisfying  $0 \leq \text{Re}(w) \leq \pi$  with the identification  $w \simeq w + 2\pi it$ . Alternatively, it can be described in terms of the torus  $T^2$  with modulus  $it$  under the identification  $w \simeq -\bar{w}$ . We take both boundaries to lie on the same D-instanton. The residual conformal symmetry  $S^1 \times \mathbb{Z}_2$  acts by periodic translations  $\text{Im}(w) \mapsto \text{Im}(w) + v$  for  $v \in (0, 2\pi)$  and reflections  $\text{Re}(w) \rightarrow \pi - \text{Re}(w)$  that exchange the two boundaries. The annulus admits four spin structures corresponding to the choice of boundary conditions for the fermionic fields as well as their periodicity under  $w \mapsto w + 2\pi it$ . It is convenient to label the spin structures in terms of those on the torus, with  $\nu = 1$  denoting the odd spin structure and  $\nu = 2, 3, 4$  the even spin structures.

Now consider the annulus with a single closed string puncture. We use the residual conformal symmetry to fix its location to  $w = u$  with  $0 \leq u \leq \pi$ . The  $\mathbb{Z}_2$  reflection symmetry can be accounted for multiplying the amplitude by a factor of  $\frac{1}{2}$ . We implement

the type IIB GSO projection by inserting  $\frac{1}{2}(-1)^\nu$  into the annulus correlator and summing over spin structures  $\nu$ . The amplitude requires a single PCO for an RR insertion and two PCOs for an NSNS insertion, which we take to be coincident with the vertex operators., such that they are in the  $(+\frac{1}{2}, -\frac{1}{2})$ - and  $(0, 0)$ -pictures, respectively. With these preliminaries in mind, the amplitude takes the form

$$A_{\delta\tau}^{A^2} = \frac{1}{4} \sum_{\nu=1}^4 (-1)^\nu \int_0^\infty dt \int_0^\pi du \langle B_t B_u V_{\delta\tau(p)}(u) \rangle_{x^\mu=0}^{A^2(t),\nu}, \quad (\text{A.69})$$

where as usual the choice of picture is kept implicit. Here, the  $b$  contours associated to the moduli  $u, t$  are given by

$$\begin{aligned} B_u &= \frac{1}{2\pi i} \oint_{C_u} \left( dw b(w) - d\bar{w} \tilde{b}(\bar{w}) \right), \\ B_t &= \int_S \left( dw b(w) + d\bar{w} \tilde{b}(\bar{w}) \right), \end{aligned} \quad (\text{A.70})$$

where  $C_u$  is a counterclockwise contour surrounding  $V_{\delta\tau(p)}(u)$ , and  $S$  is a line segment at some fixed vertical position that runs horizontally from  $\text{Re}(w) = 0$  to  $\text{Re}(w) = \pi$ .

Both the NSNS and RR vertex operators take the form  $c\tilde{c}e^{q\phi}e^{-q\tilde{\phi}}\mathcal{O}_{\delta\tau_{1/2}(p)}$  modulo extra operators which have vanishing correlator, where  $\mathcal{O}_{\delta\tau_{1/2}(p)}$  is a conformal primary in the RR/NSNS sector of the matter SCFT corresponding to the axion/dilaton. It follows that the contribution of the  $b, c$  ghosts is

$$\langle B_t B_u c\tilde{c}(u) \rangle_{bc}^{A^2(t),\nu} = 2\pi i \eta(it)^2. \quad (\text{A.71})$$

Similarly, the contribution of the  $\phi, \eta, \xi$  system is

$$\left\langle e^{q\phi} e^{-q\tilde{\phi}}(u) \right\rangle_{\phi\eta\xi}^{A^2(t), \nu} = \frac{\eta(it)}{\vartheta_\nu(2qu|it)} \left( \frac{\vartheta_1(2u|it)}{\vartheta_1'(it)} \right)^{q^2}, \quad (\text{A.72})$$

where  $\vartheta_\nu(w|\tau)$  are the Jacobi theta functions with characteristics, with  $\vartheta_1(w|\tau)$  being the unique odd function in  $w$ , and  $\vartheta_\nu(\tau) \equiv \vartheta_\nu(0|\tau)$ . Up to an overall phase, the contribution of  $\delta\tau_{1/2}$  to the amplitude thus reduces to an integrated correlator in the matter CFT given by

$$\frac{\pi}{2} \sum_{\nu=1}^4 (-1)^{\nu+1} \int_0^\infty dt \frac{\eta(it)^3}{\vartheta_1'(it)^{q^2}} \int_0^\pi du \frac{\vartheta_1(2u|it)^{q^2}}{\vartheta_\nu(2qu|it)} \left\langle \mathcal{O}_{\delta\tau_{1/2}(p)}(u) \right\rangle_{X^\mu \psi^\nu, x^\mu=0}^{A^2(t), \nu}. \quad (\text{A.73})$$

First consider the annulus 1-point amplitude for the dilaton. We strip off the matter part of the vertex operator  $V_{\delta\tau_2(p)}$  in picture  $(0, 0)$ , which contributes to the amplitude as

$$\mathcal{O}_{\delta\tau_2(p)}(u) = e_{\mu\nu}(p) (i\partial X^\mu + \frac{1}{2}p \cdot \psi \psi^\mu) (i\bar{\partial} X^\nu + \frac{1}{2}p \cdot \tilde{\psi} \tilde{\psi}^\nu) e^{ip \cdot X}(u). \quad (\text{A.74})$$

Using the doubling trick on the annulus, we can trade all of antiholomorphic operators at  $\bar{w} = u$  with their holomorphic counterparts at the reflected point  $-\bar{w} = -u$  on the torus  $T^2$  with complex modulus  $it$ . By Lorentz invariance, the four-fermion correlator can only involve kinematic structures of the form  $p^2 e_{\mu\nu}(p) \eta^{\mu\nu}$  or  $e_{\mu\nu}(p) p^\mu p^\nu$ , which vanish due to the mass-shell and transversality constraints, respectively. The mixed correlators involving both  $\psi^\mu$  and  $\partial X^\mu$  vanish since the fermion fields have nothing to contract with.

The only remaining term involves both copies of  $\partial X^\mu$ , contributing

$$\left\langle e_{\mu\nu} \partial X^\mu \bar{\partial} X^\nu e^{ip \cdot X}(u) \right\rangle_{X^\mu \psi^\mu, x^\mu=0}^{A^2(t), \nu} \propto \frac{\vartheta_\nu(it)^5}{\eta(it)^{15}} \frac{\partial^2}{\partial u^2} \log \vartheta_1(2u|it). \quad (\text{A.75})$$

In the above expression, we have evaluated the torus correlator in the matter CFT, which in particular receives a contribution  $[\vartheta_\nu(it)/\eta(it)]^5$  from the path integral over  $\psi^\mu$ .

Next consider the annulus 1-point amplitude for the axion. In the  $(+\frac{1}{2}, -\frac{1}{2})$  picture, the matter field content of  $\mathcal{O}_{\delta\tau_1(p)}$  consists of  $(\psi\gamma^\mu)^\alpha{}_\beta S_\alpha \tilde{S}^\beta \partial X_\mu e^{ip \cdot X}$ . It follows that the correlator appearing in the moduli integrand for each spin structure is proportional to  $p^2$ , which vanishes by the mass-shell constraint, and so the amplitude is zero.

Since the axion correlator vanishes identically, the annulus amplitude reduces to the contribution of the NSNS matter fields (A.75). Using (A.73), we find

$$A_{\delta\tau}^{A^2} \propto \sum_{\nu=1}^4 (-1)^\nu \int_0^\infty dt \frac{\vartheta_\nu(it)^4}{\eta(it)^{12}} \int_0^\pi du \frac{\partial^2}{\partial u^2} \vartheta_1(2u|it) = 0, \quad (\text{A.76})$$

which vanishes by the quartic Jacobi identity  $\vartheta_2^4 - \vartheta_3^4 + \vartheta_4^4 = 0$ .

#### A.4 OPEN STRING BACKGROUND INDEPENDENCE AND SEN GAUGE

As discussed in Section 2.1.5, in order to integrate over the massless bosonic open string fields  $\phi^\mu$ , we perform a field redefinition trading the  $\phi^\mu$  for the bosonic moduli  $x^\mu$  (2.13). The existence of such a field redefinition relies on the fact that  $W_f[\phi^\mu, \theta_\alpha, \zeta^2, \Psi_c]$  vanishes upon setting the other fields to zero, i.e. it does not contain a potential for  $\phi^\mu$ . Although this result is anticipated from open string background independence, it is by no means



obvious in the SFT framework.<sup>2</sup>

In this appendix, we shall explicitly demonstrate the vanishing of such terms in the massless open string effective action. In particular, we set our sights on the tree-level quartic coupling appearing in  $W_f$ , whose contribution is fixed by Lorentz invariance to take the form

$$\frac{1}{4}g_{\text{tree}}(\phi^2)^2 \subset W_f[\phi^\mu, \theta_\alpha, \zeta^2, \Psi_c]. \quad (\text{A.77})$$

In the standard perturbative framework, we know that  $g_{\text{tree}}$  enters into the 4-point amplitude as

$$A_{\phi^\mu \phi^\nu \phi^\sigma \phi^\rho}^{D^2} = 2g_{\text{tree}} S^{\mu\nu\sigma\rho}, \quad S^{\mu\nu\sigma\rho} = \eta^{\mu\nu} \eta^{\sigma\rho} + \eta^{\mu\sigma} \eta^{\nu\rho} + \eta^{\mu\rho} \eta^{\sigma\nu}. \quad (\text{A.78})$$

In the EFT analysis, this amplitude receives contributions from the elementary 4-point Feynman vertex together with a set of Feynman diagrams consisting of 3-point Feynman vertices  $A_{\phi^\mu \phi^\nu \psi}^{D^2}$  for two  $\phi^\mu$  fields and one massive field  $\psi \in \Psi_o^f$ , stitched together by an open string propagator  $P_\psi$ , i.e.

$$A_{\phi^\mu \phi^\nu \phi^\sigma \phi^\rho}^{D^2} = A_{\phi^\mu \phi^\nu \phi^\sigma \phi^\rho}^{D^2} \Big|_{\text{vertex}} + \sum_{\psi \in \Psi_o^f} \left( A_{\phi^\mu \phi^\nu \psi}^{D^2} P_\psi A_{\psi \phi^\sigma \phi^\rho}^{D^2} + 5 \text{ permutations of } \mu, \nu, \sigma, \rho \right) \Big|_{\text{propagator}}. \quad (\text{A.79})$$

From the perspective of the moduli space integration, the first term on the RHS of (A.80) contributes to the “vertex region” of the amplitude, and the terms in the sum to the “propagator region.” The 6 permutations of the Lorentz indices reflects the decomposition of the propagator region into three disconnected components, each with two boundaries.

---

<sup>2</sup>We stress that  $\phi^\mu$  is not the same as a moduli deformation of  $x^\mu$ , and so the fact that the potential vanishes is not simply a consequence of conformal perturbation theory.

By a judicious choice of 3-point vertex, we can completely integrate out all of the massive open strings with nonzero weight. This leaves the ghost zero mode  $\varkappa^1$ , for which the amplitude becomes

$$A_{\phi^\mu \phi^\nu \phi^\sigma \phi^\rho}^{D^2} = A_{\phi^\mu \phi^\nu \phi^\sigma \phi^\rho}^{D^2} \Big|_{\text{vertex}} + \left( V_{\phi^\mu \phi^\nu \varkappa^1}^{D^2} P_{\varkappa^1} V_{\varkappa^1 \phi^\sigma \phi^\rho}^{D^2} + 5 \text{ permutations of } \mu, \nu, \sigma, \rho \right) \Big|_{\text{propagator}}. \quad (\text{A.80})$$

Our goal is thus to show that this expression vanishes.<sup>3</sup>

### 3-POINT VERTEX

In the following sections, we review the construction of the 3-point and 4-point Feynman vertices so that this appendix is self-contained. In order to define the elementary 3-point Feynman vertex for NS-sector string fields, we need to specify a set of local coordinate charts around the punctures as well as the location of the PCO. As before, we take the disc to be parameterized by global coordinate  $z$  in the UHP. We shall employ the same set of coordinate maps as in [29] and the main text, with

$$f_0(w_0) = \frac{2w_0}{2\alpha + w_0}, \quad f_1(w_1) = \frac{2\alpha + w_1}{2\alpha - w_1}, \quad f_\infty(w_\infty) = \frac{w_\infty - 2\alpha}{2w_\infty}, \quad (\text{A.81})$$

---

<sup>3</sup>The 4-point amplitude has been previously confirmed to vanish, albeit for a choice of vertices where the ghost zero mode does not contribute. [68, 69]

where  $w_{z_a}$  labels the local coordinate for the patch surrounding the open string puncture at  $z = z_a$ . Recall that such transition maps have inverses given by

$$w_0(z) = \frac{2\alpha z}{2-z}, \quad w_1(z) = \frac{2\alpha(z-1)}{z+1}, \quad w_\infty(z) = \frac{2\alpha}{1-2z}. \quad (\text{A.82})$$

With this choice of coordinates, we take the PCO to be located at the permutation-invariant point  $z = p_{000}$  with

$$p_{000} = e^{\pm \frac{i\pi}{3}}. \quad (\text{A.83})$$

In practice, we take the SFT parameter  $\alpha$  to be arbitrarily large so that the massive open string modes other than  $\varkappa^1$  do not contribute to the effective vertex.<sup>4</sup> Using our choice of local coordinates and PCO location, its 3-point Feynman vertex is given by the amplitude

$$A_{\phi^\mu \phi^\nu \varkappa^1}^{D^2} = \left\langle \mathcal{X}(p_{000}) ce^{-\phi} \psi^\mu(0) ce^{-\phi} \psi^\nu(1) c \partial ce^{-2\phi} \partial \xi(\infty) \right\rangle^{D^2}. \quad (\text{A.84})$$

By direct computation, we find

$$A_{\phi^\mu \phi^\nu \varkappa^1}^{D^2} = \eta^{\mu\nu} \frac{1+p_{000}}{1-p_{000}}, \quad (\text{A.85})$$

and so the contribution of  $\varkappa^1$  to the propagator region of the 4-point amplitude in (A.80)

is

$$S^{\mu\nu\sigma\rho} \left( \frac{1+p_{000}}{1-p_{000}} \right)^2, \quad (\text{A.86})$$

---

<sup>4</sup>We have also repeated the calculation of this appendix at finite  $\alpha$ , in which case all of the massive open string fields contribute, with the same conclusion (A.102), but will not present its lengthy details here.

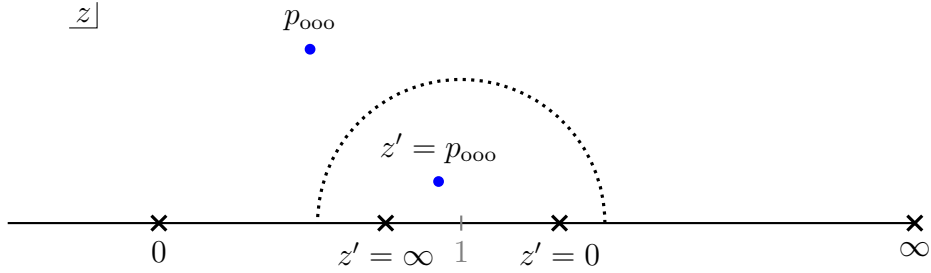


**Figure A.3:** Plumbing configuration of the 4-point propagator region for a finite choice of the SFT parameter  $\alpha$ . Vertex operator insertions are marked with black crosses, while PCO insertions are marked with blue dots.

where we have used the ghost propagator  $P_{z^1} = 1/2$ .

#### 4-POINT VERTEX

In order to define the 4-point vertex, we must first introduce the family of worldsheet configurations corresponding to two 3-point vertices joined together by an open string propagator. That is to say that the range of integration for the vertex region is given by the complement of the propagator region. The aforementioned configurations consist of two discs, parametrized by global coordinates  $z, z'$  in the UHP, sewn together by plumbing maps involving the local coordinates in (A.82). Since the 3-point vertex is defined by summing over permutations of identical open string fields, we need only consider a single plumbing configuration, e.g. (see Figure A.3)

$$w_1(z)w_1(z') = -q, \quad 0 < q < 1. \quad (\text{A.87})$$

We subsequently perform an  $SL(2, \mathbb{R})$  transformation that maps three of the punctures on the  $z$ -disc to  $0, 1, \infty$ . This transformation maps the fourth puncture to some function  $x(q)$  of the gluing parameter  $q$ , which can be identified with the modulus of the 4-punctured disc. Similarly, the PCO locations are mapped to  $p_1(q), p_2(q)$ , which depend explicitly on the gluing parameter and hence implicitly on the modulus. Depending on the  $SL(2, \mathbb{R})$  transformation,  $x(q)$  is mapped to one of three disconnected regions, conventionally referred to as the  $s, t, u$ -channel contributions to the disc 4-point amplitude. Up to order  $\mathcal{O}(\alpha^{-4})$ , the propagator region consists of the components

$$\begin{aligned}
s\text{-channel} : \quad & x \in (-\alpha^{-2}, \alpha^{-2}), \\
t\text{-channel} : \quad & x \in (1 - \alpha^{-2}, 1 + \alpha^{-2}), \\
u\text{-channel} : \quad & x \in (-\infty, -\alpha^2) \cup (\alpha^2, \infty).
\end{aligned} \tag{A.88}$$

For instance, in the  $s$ -channel the fourth puncture is arranged to be located at

$$x = x_s(q), \quad x_s(q) = \frac{q}{\alpha^2} + O(\alpha^{-4}), \tag{A.89}$$

while the two PCOs are located at

$$\begin{aligned}
p_1 = p_{1s}(q), \quad p_{1s}(q) &= p_{\text{ooo}} - \frac{p_{\text{ooo}}q}{2\alpha^2} + O(\alpha^{-4}), \\
p_2 = p_{2s}(q), \quad p_{2s}(q) &= \frac{p_{\text{ooo}} - 1}{p_{\text{ooo}}} + \frac{q}{2p_{\text{ooo}}\alpha^2} + O(\alpha^{-4}).
\end{aligned} \tag{A.90}$$

Similarly, in the  $t$ -channel, the fourth puncture is located at

$$x = x_t(q), \quad x_t(q) = 1 - \frac{q}{\alpha^2} + O(\alpha^{-4}), \tag{A.91}$$

and the PCOs reside at

$$\begin{aligned}
p_1 &= p_{1t}(q), & p_{1t}(q) &= 1 - \frac{p_{\text{ooo}}q}{\alpha^2(p_{\text{ooo}} - 1)} + \mathcal{O}(\alpha^{-4}), \\
p_2 &= p_{2t}(q), & p_{2t}(q) &= p_{\text{ooo}} - \frac{p_{\text{ooo}}q}{2\alpha^2} + \mathcal{O}(\alpha^{-4}).
\end{aligned}
\tag{A.92}$$

Strictly speaking, the range  $0 < q < 1$  only covers half of the  $s, t, u$  regions, and so we must also consider the same  $SL(2, \mathbb{R})$  transformations under  $q \rightarrow -q$ .

We now return to the construction of the 4-point elementary vertex. Using Lorentz invariance, we can write the contribution of the vertex region as<sup>5</sup>

$$A_{\phi^\mu \phi^\nu \phi^\sigma \phi^\rho}^{D^2} \Big|_{\text{vertex}} = 3 \left[ \int_{\alpha^{-2}}^{1-\alpha^{-2}} \Omega_x dx + \text{VI}_s + \text{VI}_t \right].
\tag{A.93}$$

Let us briefly unpack this expression. The first term takes the form of an integrated correlator with integrand

$$\Omega_x = \frac{1}{24} \sum_{\text{perm of } \mu, \nu, \sigma, \rho} \left\langle \mathcal{B}_x \mathcal{X}(p_1) \mathcal{X}(p_2) ce^{-\phi} \psi^\mu(0) ce^{-\phi} \psi^\nu(x) ce^{-\phi} \psi^\sigma(1) ce^{-\phi} \psi^\rho(\infty) \right\rangle^{D^2}.
\tag{A.94}$$

By averaging over the 24 permutations of the spacetime Lorentz indices in (A.94), we can restrict the vertex region to lie between the  $s$ - and  $t$ -channels, i.e.  $x_s(1) < x < x_t(1)$ , where  $x_s(q)$  and  $x_t(q)$  are the local coordinates covering half of the  $s$ - and  $t$ -channel regions, as defined in (A.89) and (A.91). We have chosen the PCOs to reside at fixed loca-

---

<sup>5</sup>In principle, we must specify a set of local coordinates around the open string punctures together as well as the two PCO locations which are necessarily compatible with those of the 3-point vertex. However, since the 4-point vertex involves only on-shell fields, it is insensitive to the choice of coordinate maps.

tions

$$p_1 = p_{\text{ooo}} - \frac{p_{\text{ooo}}}{2\alpha^2}, \quad p_2 = 1 + \frac{p_{\text{ooo}}}{\alpha^2(1 - p_{\text{ooo}})}, \quad (\text{A.95})$$

which are precisely  $p_{1s}(q = 1)$  and  $p_{1t}(q = 1)$ , respectively. This ensures that the location of one PCO agrees on the boundary between the  $s$ -channel region and the vertex region, and similarly for PCO 2 with the  $t$ -channel. Note that this choice of PCO locations differs with that of the 4-point vertex of the main text. Finally,  $\mathcal{B}_x dx$  is the Beltrami differential associated to the modulus  $x$ . For two PCOs on the disc, it generically takes the form

$$\mathcal{B}_x = \int_x \frac{dz}{2\pi i} b(z) + \frac{1}{\mathcal{X}(p_1)} \frac{\partial p_1}{\partial x} \partial \xi(p_1) + \frac{1}{\mathcal{X}(p_2)} \frac{\partial p_2}{\partial x} \partial \xi(p_2), \quad (\text{A.96})$$

where recall that  $1/\mathcal{X}(p)$  should be understood as a formal operator which removes the corresponding PCO  $\mathcal{X}(p)$ . However, we have chosen PCO locations in (A.95) that do not depend on the moduli, and so the  $\partial \xi$  terms in the above expression drop out.

Following a straightforward application of Wick contractions, we find

$$\begin{aligned} \Omega_x &= \frac{1}{3} S^{\mu\nu\sigma\rho} \left[ \frac{F_0(p_1, p_2)}{x^2} + \frac{F_1(p_1, p_2)}{(1-x)^2} + F_\infty(p_1, p_2) \right], \\ F_0(p_1, p_2) &= -C_{D^2} \frac{p_1 p_2 (p_1 + p_2 - 2)}{(p_1 - p_2)^2}, \\ F_1(p_1, p_2) &= C_{D^2} \frac{(p_1 - 1)(p_2 - 1)(p_1 + p_2)}{(p_1 - p_2)^2}, \\ F_\infty(p_1, p_2) &= C_{D^2} \frac{p_1(2p_2 - 1) - p_2}{(p_1 - p_2)^2}. \end{aligned} \quad (\text{A.97})$$

Integrating this expression gives a contribution that is subleading in  $\alpha$ , namely

$$\int_{\alpha^{-2}}^{1-\alpha^{-2}} \Omega_x dx = \mathcal{O}(\alpha^{-2}). \quad (\text{A.98})$$

At each of the boundaries between the propagator and vertex regions there is a single PCO whose location assumes some value  $p$  on one side and  $p'$  on the other. This issue of non-agreement can be fixed following [63], where one closes the gap by integrating along the PCO direction. This amounts to integrating  $\partial\xi$  in (A.96), leading to  $\xi(p) - \xi(p')$ . For the vertex under consideration, we must perform such a vertical integration at the  $s$ -channel boundary, which contributes as

$$\begin{aligned}
\text{VI}_s &= \frac{1}{24} \sum_{\text{perm of } \mu, \nu, \sigma, \rho} \langle \mathcal{X}(p_1) \left( \xi(p_{1t}(q=1)) - \xi(p_{2s}(q=1)) \right) \rangle \\
&\quad \times \langle ce^{-\phi}\psi^\mu(0) ce^{-\phi}\psi^\nu(x) ce^{-\phi}\psi^\sigma(1) ce^{-\phi}\psi^\rho(\infty) \rangle^{D^2} \\
&= -\frac{1}{3} C_{D^2} S^{\mu\nu\sigma\rho} \frac{1 + p_{\text{ooo}}}{(1 - p_{\text{ooo}})^2} + \mathcal{O}(\alpha^{-2}),
\end{aligned} \tag{A.99}$$

as well as the  $t$ -channel boundary, which contributes as

$$\begin{aligned}
\text{VI}_t &= \frac{1}{24} \sum_{\text{perm of } \mu, \nu, \sigma, \rho} \langle \left( \xi(p_{1s}(q=1)) - \xi(p_{2t}(q=1)) \right) \mathcal{X}(p_2) \rangle \\
&\quad \times \langle ce^{-\phi}\psi^\mu(0) ce^{-\phi}\psi^\nu(x) ce^{-\phi}\psi^\sigma(1) ce^{-\phi}\psi^\rho(\infty) \rangle^{D^2} \\
&= -\frac{1}{3} C_{D^2} S^{\mu\nu\sigma\rho} \frac{p_{\text{ooo}}(1 + p_{\text{ooo}})}{(1 - p_{\text{ooo}})^2} + \mathcal{O}(\alpha^{-2}).
\end{aligned} \tag{A.100}$$

From this it follows that the vertex region contributes as

$$A_{\phi^\mu\phi^\nu\phi^\sigma\phi^\rho}^{D^2} \Big|_{\text{vertex}} = -C_{D^2} S^{\mu\nu\sigma\rho} \left( \frac{1 + p_{\text{ooo}}}{1 - p_{\text{ooo}}} \right)^2. \tag{A.101}$$

Comparing this with (A.86), we find that the vertex region exactly cancels that of the



propagator region to give

$$A_{\phi^\mu \phi^\nu \phi^\sigma \phi^\rho}^{D^2} = 0, \tag{A.102}$$

and so the 4-point vertex in the massless open string effective action vanishes, as promised.

# References

- [1] D. Friedan, E. J. Martinec, and S. H. Shenker, *Conformal Invariance, Supersymmetry and String Theory*, *Nucl. Phys. B* **271** (1986) 93–165.
- [2] M. B. Green, J. H. Schwarz, and E. Witten, *SUPERSTRING THEORY. VOL. 1: INTRODUCTION*. Cambridge Monographs on Mathematical Physics. 7, 1988.
- [3] J. Polchinski, *String theory. Vol. 1: An introduction to the bosonic string*. Cambridge Monographs on Mathematical Physics. Cambridge University Press, 12, 2007.
- [4] J. Polchinski, *Combinatorics of boundaries in string theory*, *Phys. Rev.* **D50** (1994) R6041–R6045, [[hep-th/9407031](#)].
- [5] K. Becker, M. Becker, and A. Strominger, *Five-branes, membranes and nonperturbative string theory*, *Nucl. Phys. B* **456** (1995) 130–152, [[hep-th/9507158](#)].
- [6] S. Kachru, R. Kallosh, A. D. Linde, and S. P. Trivedi, *De Sitter vacua in string theory*, *Phys. Rev. D* **68** (2003) 046005, [[hep-th/0301240](#)].
- [7] M. B. Green and M. Gutperle, *Effects of D instantons*, *Nucl. Phys.* **B498** (1997) 195–227, [[hep-th/9701093](#)].
- [8] M. B. Green and P. Vanhove, *D instantons, strings and M theory*, *Phys. Lett. B* **408** (1997) 122–134, [[hep-th/9704145](#)].
- [9] E. Kiritsis and B. Pioline, *On  $R^{*4}$  threshold corrections in IIB string theory and  $(p, q)$  string instantons*, *Nucl. Phys. B* **508** (1997) 509–534, [[hep-th/9707018](#)].
- [10] B. Pioline and E. Kiritsis, *U duality and D-brane combinatorics*, *Phys. Lett. B* **418** (1998) 61–69, [[hep-th/9710078](#)].
- [11] M. Billo, M. Frau, I. Pesando, F. Fucito, A. Lerda, and A. Liccardo, *Classical gauge instantons from open strings*, *JHEP* **02** (2003) 045, [[hep-th/0211250](#)].
- [12] M. Billo, M. Frau, I. Pesando, and A. Lerda,  *$N = 1/2$  gauge theory and its instanton moduli space from open strings in RR background*, *JHEP* **05** (2004) 023, [[hep-th/0402160](#)].

- [13] M. Billo, *Instanton Calculus With R-R Background And Topological Strings*, *Fortsch. Phys.* **55** (2007) 561–566, [[hep-th/0701072](#)].
- [14] R. Argurio, M. Bertolini, G. Ferretti, A. Lerda, and C. Petersson, *Stringy instantons at orbifold singularities*, *JHEP* **06** (2007) 067, [[arXiv:0704.0262](#)].
- [15] M. Billo, M. Frau, I. Pesando, P. Di Vecchia, A. Lerda, and R. Marotta, *Instantons in  $N=2$  magnetized D-brane worlds*, *JHEP* **10** (2007) 091, [[arXiv:0708.3806](#)].
- [16] M. Billo, M. Frau, I. Pesando, P. Di Vecchia, A. Lerda, and R. Marotta, *Instanton effects in  $N=1$  brane models and the Kahler metric of twisted matter*, *JHEP* **12** (2007) 051, [[arXiv:0709.0245](#)].
- [17] M. Billo, L. Ferro, M. Frau, F. Fucito, A. Lerda, and J. F. Morales, *Non-perturbative effective interactions from fluxes*, *JHEP* **12** (2008) 102, [[arXiv:0807.4098](#)].
- [18] M. Billo, L. Ferro, M. Frau, F. Fucito, A. Lerda, and J. F. Morales, *Flux interactions on D-branes and instantons*, *JHEP* **10** (2008) 112, [[arXiv:0807.1666](#)].
- [19] M. Billo, L. Ferro, M. Frau, L. Gallot, A. Lerda, and I. Pesando, *Exotic instanton counting and heterotic/type I-prime duality*, *JHEP* **07** (2009) 092, [[arXiv:0905.4586](#)].
- [20] M. Billo, M. Frau, F. Fucito, A. Lerda, J. F. Morales, and R. Poghossian, *Stringy instanton corrections to  $N=2$  gauge couplings*, *JHEP* **05** (2010) 107, [[arXiv:1002.4322](#)].
- [21] M. Billo, L. Gallot, A. Lerda, and I. Pesando, *F-theoretic versus microscopic description of a conformal  $N=2$  SYM theory*, *JHEP* **11** (2010) 041, [[arXiv:1008.5240](#)].
- [22] H. Ghorbani, D. Musso, and A. Lerda, *Stringy instanton effects in  $N=2$  gauge theories*, *JHEP* **03** (2011) 052, [[arXiv:1012.1122](#)].
- [23] S. Alexandrov, D. Persson, and B. Pioline, *Fivebrane instantons, topological wave functions and hypermultiplet moduli spaces*, *JHEP* **03** (2011) 111, [[arXiv:1010.5792](#)].
- [24] B. Balthazar, V. A. Rodriguez, and X. Yin, *ZZ Instantons and the Non-Perturbative Dual of  $c = 1$  String Theory*, [arXiv:1907.07688](#).
- [25] B. Balthazar, V. A. Rodriguez, and X. Yin, *Multi-Instanton Calculus in  $c = 1$  String Theory*, [arXiv:1912.07170](#).

- [26] B. Balthazar, V. A. Rodriguez, and X. Yin, *The S-Matrix of 2D Type 0B String Theory Part 1: Perturbation Theory Revisited*, [arXiv:2201.05621](#).
- [27] B. Balthazar, V. A. Rodriguez, and X. Yin, *The S-Matrix of 2D Type 0B String Theory Part 2: D-Instanton Effects*, [arXiv:2204.01747](#).
- [28] A. Sen, *Fixing an Ambiguity in Two Dimensional String Theory Using String Field Theory*, *JHEP* **03** (2020) 005, [[arXiv:1908.02782](#)].
- [29] A. Sen, *D-instanton Perturbation Theory*, *JHEP* **08** (2020) 075, [[arXiv:2002.04043](#)].
- [30] A. Sen, *D-instantons, String Field Theory and Two Dimensional String Theory*, [arXiv:2012.11624](#).
- [31] A. Sen, *Normalization of D-instanton Amplitudes*, [arXiv:2101.08566](#).
- [32] A. Sen, *Normalization of Type IIB D-instanton Amplitudes*, [arXiv:2104.11109](#).
- [33] A. Sen, *Muti-instanton Amplitudes in Type IIB String Theory*, [arXiv:2104.15110](#).
- [34] S. Farough Moosavian, A. Sen, and M. Verma, *Superstring Field Theory with Open and Closed Strings*, *JHEP* **01** (2020) 183, [[arXiv:1907.10632](#)].
- [35] C. de Lacroix, H. Erbin, S. P. Kashyap, A. Sen, and M. Verma, *Closed Superstring Field Theory and its Applications*, *Int. J. Mod. Phys. A* **32** (2017), no. 28n29 1730021, [[arXiv:1703.06410](#)].
- [36] S. Alexandrov, A. Sen, and B. Stefański, *D-instantons in Type IIA string theory on Calabi-Yau threefolds*, *JHEP* **11** (2021) 018, [[arXiv:2108.04265](#)].
- [37] S. Alexandrov, A. Sen, and B. Stefański, *Euclidean D-branes in type IIB string theory on Calabi-Yau threefolds*, *JHEP* **12** (2021) 044, [[arXiv:2110.06949](#)].
- [38] D. Berenstein and R. G. Leigh, *Superstring perturbation theory and Ramond-Ramond backgrounds*, *Phys. Rev. D* **60** (1999) 106002, [[hep-th/9904104](#)].
- [39] D. Berenstein and R. G. Leigh, *Quantization of superstrings in Ramond-Ramond backgrounds*, *Phys. Rev. D* **63** (2001) 026004, [[hep-th/9910145](#)].
- [40] M. Cho, S. Collier, and X. Yin, *Strings in Ramond-Ramond Backgrounds from the Neveu-Schwarz-Ramond Formalism*, *JHEP* **12** (2020) 123, [[arXiv:1811.00032](#)].
- [41] N. Ishibashi, H. Kawai, Y. Kitazawa, and A. Tsuchiya, *A Large N reduced model as superstring*, *Nucl. Phys. B* **498** (1997) 467–491, [[hep-th/9612115](#)].

- [42] M. B. Green and M. Gutperle, *D Particle bound states and the D instanton measure*, *JHEP* **01** (1998) 005, [[hep-th/9711107](#)].
- [43] P. Yi, *Witten index and threshold bound states of D-branes*, *Nucl. Phys. B* **505** (1997) 307–318, [[hep-th/9704098](#)].
- [44] S. Sethi and M. Stern, *D-brane bound states redux*, *Commun. Math. Phys.* **194** (1998) 675–705, [[hep-th/9705046](#)].
- [45] G. W. Moore, N. Nekrasov, and S. Shatashvili, *D particle bound states and generalized instantons*, *Commun. Math. Phys.* **209** (2000) 77–95, [[hep-th/9803265](#)].
- [46] H. Elvang and Y.-t. Huang, *Scattering Amplitudes*, [arXiv:1308.1697](#).
- [47] M. B. Green and S. Sethi, *Supersymmetry constraints on type IIB supergravity*, *Phys. Rev. D* **59** (1999) 046006, [[hep-th/9808061](#)].
- [48] Y. Wang and X. Yin, *Constraining Higher Derivative Supergravity with Scattering Amplitudes*, *Phys. Rev. D* **92** (2015), no. 4 041701, [[arXiv:1502.03810](#)].
- [49] M. B. Green and C. Wen, *Modular Forms and  $SL(2, \mathbb{Z})$ -covariance of type IIB superstring theory*, *JHEP* **06** (2019) 087, [[arXiv:1904.13394](#)].
- [50] M. B. Green and P. Vanhove, *Duality and higher derivative terms in M theory*, *JHEP* **01** (2006) 093, [[hep-th/0510027](#)].
- [51] R. H. Boels and D. O’Connell, *Simple superamplitudes in higher dimensions*, *JHEP* **06** (2012) 163, [[arXiv:1201.2653](#)].
- [52] J. Polchinski, *String theory. Vol. 2: Superstring theory and beyond*. Cambridge Monographs on Mathematical Physics. Cambridge University Press, 12, 2007.
- [53] R. H. Boels, *Maximal R-symmetry violating amplitudes in type IIB superstring theory*, *Phys. Rev. Lett.* **109** (2012) 081602, [[arXiv:1204.4208](#)].
- [54] W.-M. Chen, Y.-t. Huang, and C. Wen, *From  $U(1)$  to  $E_8$ : soft theorems in supergravity amplitudes*, *JHEP* **03** (2015) 150, [[arXiv:1412.1811](#)].
- [55] Y. Wang and X. Yin, *Supervertices and Non-renormalization Conditions in Maximal Supergravity Theories*, [arXiv:1505.05861](#).
- [56] M. Bianchi, A. L. Guerrieri, Y.-t. Huang, C.-J. Lee, and C. Wen, *Exploring soft constraints on effective actions*, *JHEP* **10** (2016) 036, [[arXiv:1605.08697](#)].

- [57] J. Polchinski, *Dirichlet Branes and Ramond-Ramond charges*, *Phys. Rev. Lett.* **75** (1995) 4724–4727, [[hep-th/9510017](#)].
- [58] M. B. Green, S. D. Miller, and P. Vanhove,  *$SL(2, \mathbb{Z})$ -invariance and  $D$ -instanton contributions to the  $D^6 R^4$  interaction*, *Commun. Num. Theor. Phys.* **09** (2015) 307–344, [[arXiv:1404.2192](#)].
- [59] A. Guerrieri, J. Penedones, and P. Vieira, *Where Is String Theory in the Space of Scattering Amplitudes?*, *Phys. Rev. Lett.* **127** (2021), no. 8 081601, [[arXiv:2102.02847](#)].
- [60] R. Gopakumar, E. Perlmutter, S. S. Pufu, and X. Yin, *Snowmass White Paper: Bootstrapping String Theory*, [arXiv:2202.07163](#).
- [61] A. Sen, *String Field Theory as World-sheet UV Regulator*, *JHEP* **10** (2019) 119, [[arXiv:1902.00263](#)].
- [62] D. S. Eniceicu, R. Mahajan, P. Maity, C. Murdia, and A. Sen, *The ZZ annulus one-point function in non-critical string theory: A string field theory analysis*, *JHEP* **12** (2022) 151, [[arXiv:2210.11473](#)].
- [63] A. Sen and E. Witten, *Filling the gaps with PCO's*, *JHEP* **09** (2015) 004, [[arXiv:1504.00609](#)].
- [64] A. Sen, *On the Background Independence of String Field Theory*, *Nucl. Phys. B* **345** (1990) 551–583.
- [65] A. Sen and B. Zwiebach, *Quantum background independence of closed string field theory*, *Nucl. Phys. B* **423** (1994) 580–630, [[hep-th/9311009](#)].
- [66] A. Sen, *Background Independence of Closed Superstring Field Theory*, *JHEP* **02** (2018) 155, [[arXiv:1711.08468](#)].
- [67] A. Sen, *Tachyon condensation on the brane anti-brane system*, *JHEP* **08** (1998) 012, [[hep-th/9805170](#)].
- [68] C. Maccaferri and A. Merlano, *Localization of effective actions in open superstring field theory*, *JHEP* **03** (2018) 112, [[arXiv:1801.07607](#)].
- [69] C. Maccaferri and A. Merlano, *Localization of effective actions in open superstring field theory: small Hilbert space*, *JHEP* **06** (2019) 101, [[arXiv:1905.04958](#)].

**T**HIS THESIS WAS TYPESET using L<sup>A</sup>T<sub>E</sub>X, originally developed by Leslie Lamport and based on Donald Knuth's T<sub>E</sub>X. The body text is set in 11 point Egenolff-Berner Garamond, a revival of Claude Garamont's humanist typeface. The above illustration, *Science Experiment 02*, was created by Ben Schlitter and released under **CC BY-NC-ND 3.0**. A template that can be used to format a PhD dissertation with this look & feel has been released under the permissive AGPL license, and can be found online at [github.com/suchow/Dissertate](https://github.com/suchow/Dissertate) or from its lead author, Jordan Suchow, at [suchow@post.harvard.edu](mailto:suchow@post.harvard.edu).